Tracing terrestrial salt cycling using chlorine and bromine

Michael Anthony Short

November 2017

A thesis submitted for the degree of Doctor of Philosophy of The Australian National University

Declaration of originality

I declare that this thesis has not been used toward the award of any other degree of any institution, and to the best of my knowledge and belief, this thesis does not contain any material previously published or written by another person except where due reference is made in the text.

……

Michael A. Short

Farewell D.C. ‘Bear’ McPhail

During the review of this thesis, Bear McPhail tragically passed away while on holiday in his much-loved, Great White North. Bear was an incredible family man, scientist and personality. His passionate and cheerful manner were infectious, and everyone who was fortunate enough to know him will forever cherish the influence he had in their lives.

Bear was also the most dedicated and selfless educator I have ever met – whether academically, as an undergraduate and graduate lecturer/supervisor/course-coordinator/spokesman, or as a hockey coach (and once a year he was both for a groundwater fieldtrip). Bear’s passing is a tragic loss to the students he mentored over the years and to those students who will now miss the opportunity to sit in his lecture theatre or share a glass of wine with him.

You will be greatly missed, Bear!

Bear, front and centre, with undergraduate groundwater students during the 2013 fieldtrip to the Lower Murrumbidgee.

Acknowledgements

During my Ph.D. candidature, I had two main supervisors: Bear McPhail and Brad Pillans. Bear acted as my primary supervisor, and provided me with invaluable advice, feedback, discussions, friendship and staff meetings that helped shape the thesis that follows. For this, I will always be grateful and will always remember you. Brad also provided me with invaluable feedback throughout my research, especially thanks to his unrivalled knowledge of the Lake George Basin and the geology of the Canberra region. He also graciously took up the reigns as my primary supervisor after Bear's tragic passing, despite the shock of this great personal loss. In addition to my main supervisors, the other members of my supervisory panel, Patrick De Deckker, Steve Eggins and Tony Dosseto, provided me helpful advice and feedback throughout my candidature, especially guidance during my mid-term assessment.

I have been lucky enough to be involved with guiding and being guided by five talented undergraduate students, John Daly, Diana Cato-Smith, Aero Leplastrier, Rob Sargent and Annie Dolan, during my time at RSES. They graciously provided me with their cheap labour and company for varying (mostly negligible) amounts of reward. I can only hope that they find happiness and success in whatever they chose to pursue, and that we cross paths again in the future.

In addition to those mentioned above, who I have interacted with for significant parts of my candidature, I have also had the pleasure of being assisted by numerous other people for specific sections of this research. These people are acknowledged below, in order of the chapter that they were involved with.

Chapter 2 acknowledgements

Kyle Horner was the brains behind the core idea of Chapter 2. I was lucky enough to have been allowed to add my own (hopefully helpful) flavour to it. Emily Hilder and Dario Arrua at the Australian Centre for Research on Separation, University of Tasmania provided me with free use of their modern ion chromatography system and technical knowledge of anion analysis. This was crucial in obtaining the chloride and bromide compositions used in this chapter.

Chapter 3 acknowledgements

There is no doubt that Chapter 3 would not have been possible without all of those who are involved with maintaining and improving the National Atmospheric Deposition Program. The NADP is a truly unique and valuable environmental monitoring network that continues to provide data freely to anyone who asks for it. I would particularly like to thank Chris Lehmann of the Illinois State Water Survey, who was my initial point of contact within the NADP and continued to provide useful advice (and more data) throughout this section of my research.

I would also like to give special thanks to Patrice de Caritat, whose lecture on statistical methods for geochemistry sparked the idea of applying the imputation routine to the wet deposition dataset. He subsequently helped to turn that work into a published journal article that Patrice, Bear and I can all be proud of.

Chapter 5 acknowledgements

A significant part of Chapter 5 would not have been possible without the assistance of the friendly locals of the Lake George region. The Osborne and Keatley families provided access to their land to collect water samples and years of knowledge about the region, staff of the Winderadeen Homestead and Bungendore Post Office

allowed me to install a rain collector on their property, and the Palerang Council provided access to the Bungendore Alluvium monitoring bores and technical reports.

Chapter 5 also relied heavily on the expertise of technical staff to obtain geochemical results. This includes Linda McMorrow (ICP-AES and IC) and Les Kinsley (ICP-MS), John McDonald (ICP-AES and ICP-MS), Hilary Stuart-Williams (stable water isotopes), Rhys Gwynn (stable halogen isotopes), Shaun Frape (stable halogen isotopes) and Keith Fifield (chlorine-36). They all provided me with their time and knowledge for which I am very thankful.

I would also like to thank Rhys Gwynn and Shaun Frape, of the University of Waterloo Department, and Randy Stotler, of the University of Kansas, who all made me feel welcome (and find a fresh appreciation of my fluency in Australian English) during my overseas trip to Ontario and Nebraska.

Funding acknowledgements

The Australian Government provided funding to this research in the form of an Australian Postgraduate Award, which funded my lavish student lifestyle, and two Australian Research Council Linkage Grants LP140100911 and LP0989358, which funded the Lake George (Chapters 4 and 5) and Lower Murrumbidgee (Chapter 2) projects, respectively. The Research School of Earth Sciences provided funding in the form of a supplementary scholarship and travel funding for my trips to Hobart, Newcastle, Waterloo and Rome. I was provided with further assistance for my trip to Waterloo and Rome by the Mervyn and Katalin Paterson Fellowship. The Geological Society of Australia and International Association of GeoChemistry provided funding in the form of separate Ph.D. research awards that assisted with purchasing analytical equipment and isotopic analyses, respectively.

Abstract

Understanding and quantifying terrestrial salt cycling is central to scientific fields such as sedimentary geology, mineral exploration, water resources, palaeontology, atmospheric chemistry and limnology. Dissolved chlorine and bromine concentrations have been utilised for decades as individual tracers or as a ratio to trace geochemical processes in saline environments. The stable isotope variations of these two elements have also been found to be useful for understanding and quantifying geochemical processes. However, both hydrogeochemical techniques could benefit from being applied in new environments and the collection of further data on a local and continental scale, as well as developing quantitative methods to provide further value to their use. This thesis presents findings based on theoretical analysis, large-scale monitoring and a targeted field investigation to improve the understanding of how chlorine and bromine can be utilised as tracers of terrestrial salt cycling.

Firstly, bench-top salt dissolution experiments were used to verify a previously established quantitative mixing model that utilises chloride/bromide ratios to correct chloride- or bromide-based tracer methods for other chloride sources. The results show that the model can predict the percentage of alternate salt sources accurately after analytical and endmember uncertainties are considered. The results are used to extend the understanding of the uncertainties and sensitivities of the mixing models, providing scientists with a guide to which environments and scenarios the mixing model would be most appropriate. The mixing model correction provides a useful and cheap method for scientists to improve their use of chloride- or bromide-based tracer techniques in catchment studies.

Secondly, a continental-scale dataset of wet deposition compositions spanning six and half years was analysed to identify spatial and temporal trends in chloride/bromide ratios. A recently developed imputation algorithm was applied to estimate the high proportion of censored bromide values, as well as the other eight analytes, based on the multivariate relationships of nine analytes. Chloride/bromide ratios of wet deposition decrease with distance inland following a logarithmic regression. The observations provide further confidence in the findings presented in previous studies that have shown that chloride/bromide ratios systematically decrease with increasing distance from the coast.

Lastly, chlorine and bromine tracer techniques were applied in a case study of the Lake George Basin, NSW, to trace modern salt cycling proximal to a saline lake, and to investigate how hydrogeochemical signatures can elucidate palaeohydrologic processes. The Lake George Basin was chosen as the field site because of its long, near-continuous sequence of Cenozoic lake sediments, and its complex salt cycling regime. The chlorine- and bromine-based tracer methods, in combination with other geochemical information, have provided a better understanding of the modern salt cycling regime within the catchment, and have also provided useful constraints on the timing of the recession of the mega-lake that existed in the basin during the last glacial maximum. This study also illustrated the utility of chlorine- and bromine-based tracer methods to delineate salt cycling processes in saline lake environments.

Table of contents

List of figures

List of tables

"You must be patient in investigation, accurate in measurement, cautious in accepting results, content to stand one in a long series who, for the good of humanity, are striving to interpret the laws of Nature."

–Henry C. Russell, 1885, President's address to the annual general meeting of the Royal Society of New South Wales

Introduction

1. Rationale

Earth's near-surface cycling of salt and dissolved solutes (from herein referred to collectively as salt cycling) has important implications for several disciplines of the earth and environmental sciences (e.g., sedimentary geology, mineral exploration, atmospheric chemistry, water resources, oceanography, etc.). Of relevance to the research presented in this thesis, observing, quantifying and predicting salt cycling processes is key in water resources studies for understanding and regulating the concentration of elements that may be beneficial or detrimental to human health [e.g., *Ghassemi et al.*, 1995; *Lollar*, 2014 and references therein], and in palaeoenvironmental studies where the distribution of some elements can be used to infer processes that occurred in the distant (or not-so-distant) past [e.g., *Cerling*, 2014; *Mackenzie*, 2014 and references therein].

Hydrogeochemical methods such as tracing dissolved ionic species and interpreting variations in stable isotope ratios can be utilised to quantify and interpret salt cycling processes between Earth's hydrosphere, lithosphere and atmosphere [*Appelo and Postma*, 2005; *Deocampo and Jones*, 2014; *Vengosh*, 2014]. Dissolved chlorine and bromine concentrations (predominantly in the form of halides: chloride and bromide, respectively) have been utilised for many decades as individual tracers or together as a ratio to trace geochemical processes in saline environments (e.g., salt accumulation, solute transport and evaporite dissolution/precipitation [*Davis et al.*, 1998]). More recently, the stable isotope variations of these two elements have also been found to be useful for quantifying and interpreting geochemical processes (e.g., solute transport, geochemical provenancing, evaporite dissolution/precipitation and oxidation reactions [*Eggenkamp*, 2014]). However, their applications are limited

because we need to understand better how chloride and bromide concentrations and isotopes vary on local and regional spatial and short- to long-term temporal scales, plus to develop more robust quantitative methods of interpretation and prediction. A combination of experimental, mathematical modelling and field studies is used in this thesis to enhance our current understanding.

The Lake George Basin, NSW (Figure 1), is chosen as the field site for this research for two reasons. Firstly, the Lake George Basin contains one of the longest, near-continuous sequences of Cenozoic lake sediments in Australia [*Abell*, 1985; *Macphail et al.*, 2015; *Macphail et al.*, 2016; *McEwan Mason*, 1991]. Consequently, numerous researchers have studied the basin over the last century, and many parts of its geologic history have been uncovered. Thus, many processes that would be unknown in other settings are well-constrained at Lake George. Secondly, the Lake George Basin is known to have a complex salt cycling regime, where salt, which is estimated to have accumulated over the last two million years, diffuses through its low-permeability lakebed sediments as well as being dispersed by wind erosion during dry periods [*Jacobson et al.*, 1991]. As such, the Lake George Basin represents a unique opportunity to investigate salt cycling and solute transport processes in a small endorheic basin using novel geochemical techniques, especially those that use chlorine and bromine geochemistry.

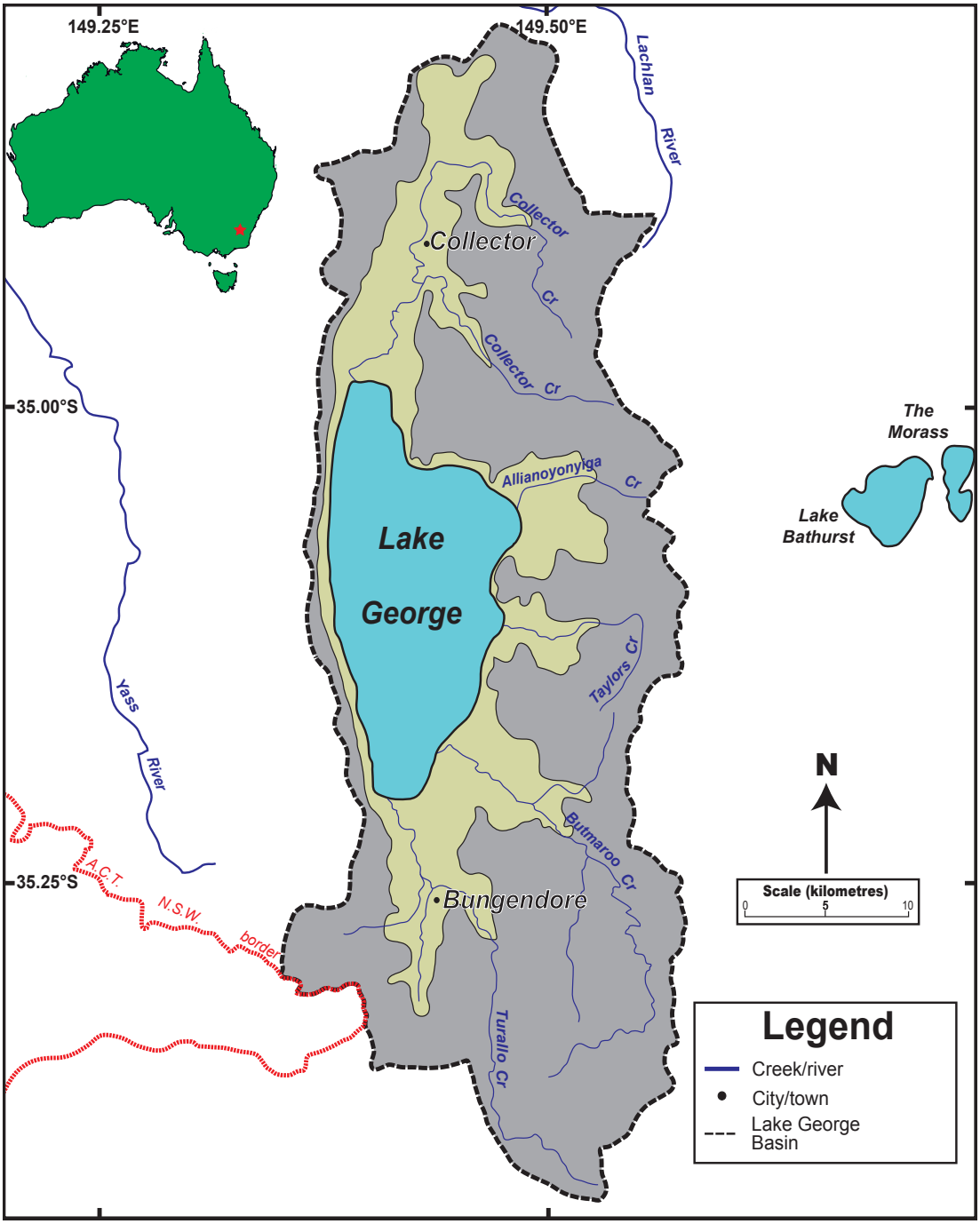

Figure 1: Location map of the Lake George Basin with respect to Australia (insert).

2. Aims

The research aims of this thesis are to:

1. improve the understanding of how chloride/bromide ratios can be quantitatively and semi-quantitatively used to investigate global and regional salt cycling;
2. identify continental-scale trends in atmospheric halide deposition;
3. improve the understanding of how stable halogen isotope ratios can be utilised to trace salt cycling in saline lake environments; and
4. delineate and quantify salt cycling processes around the Lake George Basin.

3. Objectives

The above aims are addressed using the following methods:

1. reviewing the literature review to establish the current knowledge of the geochemistry of chlorine, bromine and stable halogen isotopes in natural waters, and Australian saline lakes;
2. assess the uncertainties and sensitivities of using chloride/bromide ratios as a quantitative tool in catchment hydrology;
3. investigate the continental-scale variation of chloride/bromide ratios in atmospheric deposition; and
4. apply chloride/bromide ratios and stable halogen isotope ratios to a saline lake basin to demonstrate the utility of the above techniques and understanding.

4. Thesis structure

This thesis is comprised of a compilation of stand-alone thesis chapters, some of which have been submitted or accepted manuscripts of which I am either the primary author of or to which I made a significant contribution. Chapters that contain inputs

from co-authors are preceded by a foreword declaring my contribution and the contribution made by each of the co-authors.

4.1. Chapter 1: Chlorine and bromine hydrogeochemistry

This chapter provides the background and scientific rationale for the research undertaken during my Ph.D. candidacy, and to identify research gaps that I have aimed to address in this thesis. It is a summary of the current scientific knowledge regarding chlorine and bromine geochemistry in natural waters with a focus on how new stable isotope techniques are improving our understanding of the hydrogeochemistry of these two elements, including the physical and chemical processes that affect their concentrations, ratios and isotope compositions.

4.2. Chapter 2: Chloride and bromide sources in water: Quantitative model use and uncertainty

Chapter 2 is included because the model and uncertainties discussed in the manuscript have made a significant contribution to how scientists will use chloride/bromide ratios in catchment hydrology studies. This chapter also presents the key concepts of the use of chloride/bromide ratios that are later utilised in Chapters 3 and 5.

It is based on a journal article that was produced as a co-author with Kyle Horner and Bear McPhail. The article was published in *Journal of Hydrology* in early-2017 [*Horner et al.*, 2017]. The initial development of the article was work undertaken by Kyle Horner during his Ph.D. candidacy, where he developed the idea and mathematical model for new equations to use the chloride/bromide ratio quantitatively. I made a significant contribution to this work by assisting with the development of simple bench-top experiments to verify the model, undertaking the experiments, analysing the

experimental samples, and providing the interpretation and discussion about uncertainties associated with the model, based on analytical methods and end member compositions.

4.3. Chapter 3: Continental-scale variation in chloride/bromide ratios of wet deposition

Chapter 3 is included because it makes a significant contribution to the scientific understanding of how chloride and bromide are transported into terrestrial catchments, on regional to continental scales. It builds upon the work presented in Chapter 2 that discussed current limitations in researchers understanding of end member chloride/bromide compositions.

It is based on a journal article that I have produced as the senior author with Patrice de Caritat and Bear McPhail. The article was published in *Science of the Total Environment* online in early-2017 [*Short et al.*, 2017].

This chapter presents North American wet deposition chloride/bromide ratio data that have recently been collected by the National Atmospheric Deposition Program (NADP). The findings of the analysis presented in the manuscript have helped to improve the understanding of the global cycling of chlorine and bromine. The findings are of importance for how hydrologists can better use the chloride/bromide ratio to assist with land and water resource investigations, and for how atmospheric chemists account for halogen sources and sinks in global models. The study also utilised new statistical methods in a novel way to overcome shortcomings in the dataset.

4.4. Chapter 4: The Lake George Basin

Chapter 4 includes detailed description of the field site investigated in Chapter 5, Lake George, and identifies salt cycling processes that are known and unknown to occur

at this field site. It provides a summary of the geographic setting, geology, hydrology, climate and salt cycling processes of the Lake George Basin.

It also introduces the key concepts regarding the development of saline lakes and general processes that are important in salt cycling in these environments. This section has been included to clearly demonstrate the unique geochemical processes that occur in these unique geochemical environments and the importance of research in this field to the wider science community.

4.5. Chapter 5: Tracing salt cycling in the Lake George Basin

Chapter 5 is a synthesis of the work I have undertaken throughout my Ph.D. candidacy and demonstrates the developed techniques and new geochemical understandings to a unique field site. It builds on the findings of the previous chapters, and presents the findings of field sampling from the Lake George Basin over two and a half years, where chloride/bromide ratios and stable halogen isotope ratios were used, in combination with other major ion geochemistry techniques, to better understand the rates and pathways of salt cycling within the Lake George Basin.

4.6. Appendices

The appendices contain supplemental data that support the content of the thesis. They include tables of data that are not referred to directly in the body of the thesis but are worthy of recording for future reference.

Chapter 1: Chlorine and bromine hydrogeochemistry

Chlorine and bromine are ubiquitous in Earth's natural waters and are widely studied because of their importance in biogeochemical cycling, utility as applied and environmental tracers, and occurrence in common contaminants. Chloride and bromide (Cl^- and Br^-), the most common form of Cl and Br in the near-surface environment, are two of the most conservative ions found in aqueous environments owing to their high solubility in water, weak affinity for mineral surfaces, and very low concentrations in common rock-forming minerals [*Davis et al.*, 1998; *Flury and Papritz*, 1993]. As a result, Cl^- and Br^- are useful to hydrogeochemists in three main ways: (1) Cl^- is one of the most commonly used environmental tracers in hydrology for investigating groundwater recharge, groundwater flow and groundwater-surface water interactions [e.g., *Allison et al.*, 1994; *Healy*, 2010; *Scanlon et al.*, 2002]; (2) Br^- is a useful applied tracer because of its low toxicity and low natural abundance, in addition to its high solubility and near-conservative behaviour [e.g., *Davis et al.*, 1998; *Flury and Papritz*, 1993]; and (3) the ratio of Cl^- and Br^- is a popular parameter for tracing hydrogeochemical evolution of water sources [e.g., *Bloch and Schnerb*, 1953; *McCaffrey et al.*, 1987], groundwater and surface water salinisation mechanisms [e.g., *Alcalá and Custodio*, 2008b; *Bennetts et al.*, 2006; *Cartwright et al.*, 2006; *Herczeg and Leaney*, 2011; *Macumber*, 1991] and identifying pollution sources [e.g., *Dailey et al.*, 2014; *Davis et al.*, 1998; *Katz et al.*, 2011].

Stable chlorine and bromine isotope compositions are also now utilised thanks to advances in mass spectrometry to further refine our understanding of the biogeochemical cycles of these two elements, for enhancing their utility as chemical tracers, and as forensic tools for investigating water contamination. The initial investigations into stable chlorine isotope variations ($\delta^{37}Cl$) were focused on dissolved Cl^- in porewaters [e.g., *Desaulniers et al.*, 1986; *Kaufmann et al.*, 1984]. However, the

stable isotope composition of Cl^- has now been used as an environmental tracer for investigating many hydrogeochemical processes (e.g., diffusion, evaporite dissolution/precipitation, solute mixing, salinisation mechanisms and chemical evolution/cycling [e.g., *Eastoe et al.*, 2007; *Eggenkamp et al.*, 1995; *Groen et al.*, 2000; *Li et al.*, 2012; *Rebeix et al.*, 2014; *Richard et al.*, 2011; *Sie and Frape*, 2002; *Yamanaka et al.*, 2014; *Zhang et al.*, 2007]).

1. Chlorine and bromine in natural waters

Chlorine and bromine are both members of Group 17 of the periodic table (i.e., the halogens) along with fluorine and iodine, which are also found in aqueous environments. The halogens are characterised by their very high electronegativity, which is due to their outer electron shell being only one electron short of a noble gas configuration. Chlorine has an atomic number of 17, an atomic mass of ~35.5, one main and six minor oxidation states (–1 and 0, +1, +3, +4, +5, +7, respectively) [*Haynes*, 2015], an estimated upper continental crust concentration of ~370 μg g^{-1} [*Rudnick and Gao*, 2014], an estimated oceanic crust concentration of 20 – 2,800 μg g^{-1} [*Jambon et al.*, 1995], and a mean seawater abundance of 19,400 μg g^{-1} [*Millero*, 2014]. Bromine, by contrast, has an atomic number of 35, an atomic mass of ~79.9, five main oxidation states (–1, +1, +3, +5, +7) [*Haynes*, 2015], an estimated upper continental crust concentration of ~1.6 μg g^{-1} [*Rudnick and Gao*, 2014], an estimated oceanic crust concentration of 0.1 – 1.3 μg g^{-1} [*Jambon et al.*, 1995], and a mean seawater abundance of 67 μg g^{-1} [*Millero*, 2014]. Chlorine and bromine are enriched in Earth's hydrosphere relative to their crustal abundance (by factors of up to 970 and 670, respectively) because they are volatile and prefer to exist predominantly as highly soluble halides [*Graedel and Keene*, 1996].

1.1. Chloride/bromide ratios

The key geochemical differences of Cl^- and Br^- can provide researchers with vital qualitative and quantitative information relating to geochemical reactions in catchments and basins. Consequently, the ratio of dissolved Cl^- and Br^-, as a molar or mass ratio (from herein mass ratios are adopted; $[Cl^-/Br^-]_{molar} = 2.254 \times [Cl^-/Br^-]_{mass}$), has become a widely quantitative and semi-quantitative parameter in the field of hydrogeochemistry [e.g., *Alcalá and Custodio*, 2008b; *Cartwright et al.*, 2006; *Davis et al.*, 2004; *Davis et al.*, 1998; *Edmunds*, 1996; *Herczeg and Edmunds*, 1999] and sedimentary (evaporite) geochemistry [e.g., *Cendón et al.*, 2004; *Holser*, 1966; *Holser*, 1970; *McCaffrey et al.*, 1987; *Taberner et al.*, 2000; *Valyashko*, 1956]. In the context of saline environments, Cl^-/Br^- ratios have utility for identifying evaporite dissolution/precipitation, quantifying salt additions/losses and delineating salt sources.

Seawater, the primary reservoir for Cl^- and Br^-, has a relatively uniform Cl^-/Br^- ratio of approximately 288 [*Millero*, 2014], and a similar ratio is typically observed in coastal rainfall. However, chemical fractionation at the ocean surface during marine aerosol development causes oceanic aerosols of variable sizes to have Cl^-/Br^- ratios deviating from the mean ocean water ratio, and studies have found that Br^- tends to be enriched in the smaller aerosols [*Zhou et al.*, 1990]. A possible explanation for this is the observation that halide ions have a tendency to cluster near the air-water interface and that this tendency increases with an ion's polarisability [*Jungwirth and Tobias*, 2002]. The approximately 30% higher polarisability of Br^- than that of Cl^- means that Br^- is likely to be found in greater proportions in smaller oceanic aerosol particles because of their greater surface area to volume ratio [*Davis et al.*, 2004]. As a result, it is hypothesised that the Cl^-/Br^- ratio of atmospheric aerosols will decrease with distance inland and with increasing elevation because of washout effects and the ability of

smaller aerosols to be transported over greater distances and elevations [*Davis et al.*, 2004]. The few available rainwater and groundwater data from continental and countrywide studies tend to find that inland Cl^-/Br^- ratios are lower than that of seawater, which supports this hypothesis [e.g., *Alcalá and Custodio*, 2008b; *Crosbie et al.*, 2012; *Davis et al.*, 2004; *Davis et al.*, 1998].

Halite (NaCl) has a high Cl^-/Br^- ratio because of the exclusion of all but trace quantities of Br^- from the crystal lattice [*Holser*, 1970] and the much higher solubility of Br^- [*Davis et al.*, 2004; *Davis et al.*, 1998]. Bulk halite has been observed to have a Cl^-/Br^- ratio range of approximately 2 000 – 10 000 [*Davis et al.*, 2004; *Davis et al.*, 1998], and individual crystals can be found with ratios as high as 100 000 [*Davis et al.*, 1998]. It is only once potassium begins to replace sodium in the crystal lattice of evaporites during brine evaporation (i.e., formation of sylvite and carnallite), that bromine is readily incorporated and Cl^-/Br^- ratios of precipitates begin to fall to 400 [*Alcalá and Custodio*, 2008b; *Taberner et al.*, 2000]. During the precipitation of evaporite minerals, bromine is enriched in the residual brine, and Cl^-/Br^- ratios have been found to fall as low as 30 – 80 [*Birkle et al.*, 2009; *McCaffrey et al.*, 1987; *Taberner et al.*, 2000]. These chemical fractionation characteristics of Cl^- and Br^- make Cl^-/Br^- ratios an excellent parameter to utilise in environments where evaporite dissolution/precipitation and subsequent brine evolution are expected, making this technique especially attractive in salt lake environments, of either marine or non-marine origin [*Eugster and Jones*, 1979; *Holser*, 1970; *Macumber*, 1991].

Anthropogenic pollution sources have also been found to contain varying Cl^-/Br^- ratios [e.g., *Cendón et al.*, 2015; *Davis et al.*, 2004; *Davis et al.*, 1998; *Sollars et al.*, 1982; *Vengosh and Pankratov*, 1998]. Sewage effluent typically has an elevated Cl^-/Br^- ratio (approximately 400 – 900) because of the widespread domestic use of table salt

[*Vengosh and Pankratov*, 1998]. In contrast, urban runoff can have a wide range of Cl^-/Br^- ratios. In the United Kingdom, *Sollars et al.* [1982] found that during winter months, urban runoff had a high mean Cl^-/Br^- ratio (approximately 1200) because of the use of de-icing salt on roadways. However, during the summer months, runoff had a lower mean Cl^-/Br^- ratio of approximately 20, which was interpreted to be caused by the dissolution of Br^- containing additives in dust expelled from the exhausts of cars fuelled by leaded petrol. The effect of car exhaust aerosols on the Cl^-/Br^- ratio of urban runoff is likely to have diminished in the decades since the phasing-out of leaded petrol in the 1980s, like reductions in lead pollution on roadways [e.g., *MacKinnon et al.*, 2011; *Wang et al.*, 2006]. However, road de-icing salts are still widely used in countries that experience heavy snow, and Cl^-/Br^- ratios are commonly used to identify where the quality of surface water and groundwater may be impacted by this activity [e.g., *Dailey et al.*, 2014]. In agricultural soils and water, a potentially large source of anthropogenic Br can be introduced by Br-containing fertiliser and pesticide, the degradation of which releases Br^- into the environment [*Flury and Papritz*, 1993].

2. Stable halogen isotope geochemistry

Chlorine has two stable isotopes: the more abundant ^{35}Cl (75.76%) and the less abundant ^{37}Cl (24.24%) [*Berglund and Wieser*, 2011]. Bromine also has two stable isotopes that have a relatively even natural distribution: ^{79}Br (50.69%) and ^{81}Br (49.31%) [*Berglund and Wieser*, 2011]. With the rapid development of analytical methods for analysing stable isotope ratios over the last half-century, researchers have been able to assess the isotopic variations of natural materials for many of the elements. These methods have become particularly popular in the earth and environmental sciences because they are useful for elucidating many physical and biogeochemical

processes that chemical composition alone cannot identify (see *Eiler et al.* [2014] for a recent review of the state-of-the-science). Notation for describing stable halogen isotope ratio variations follows the standard delta convention used for other stable isotopes, where variations are reported as per mil (‰) deviations from a standard:

$$\delta^{37}Cl = \left(\frac{\left({}^{37}Cl / {}^{35}Cl \right)_{sample}}{\left({}^{37}Cl / {}^{35}Cl \right)_{SMOC}} - 1 \right) \times 1000 \qquad (1)$$

and:

$$\delta^{81}Br = \left(\frac{\left({}^{81}Br / {}^{79}Br \right)_{sample}}{\left({}^{81}Br / {}^{79}Br \right)_{SMOB}} - 1 \right) \times 1000 \qquad (2)$$

where SMOC and SMOB denote the commonly used natural reference standards for stable halogen isotope compositions: Standard Mean Ocean Chloride and Standard Mean Ocean Bromide, respectively [*Eggenkamp*, 2014; *Jochum and Enzweiler*, 2014]. Both standards are not officially assigned; however, studies have found ocean water to be adequately homogenous with respect to its stable chlorine isotope ratio [*Godon et al.*, 2004; *Kaufmann et al.*, 1984]. Seawater also represents a cheap and convenient natural reference material that is easily obtained and shared amongst laboratories. A large-scale intercomparison study of seawater is yet to be undertaken for stable bromine isotopes; however, seawater is considered an appropriate standard because its oceanic residence time (~130 Ma) is even greater than Cl^- (~84 Ma) [*Eggenkamp*, 2014; *Eggenkamp and Coleman*, 2000]. A recent study presenting data for five seawaters had an overall range of <0.1 ‰ [*Du et al.*, 2013], which is similar to the analytical precision of many Br isotope laboratories.

Variations in $\delta^{37}Cl$ values in nature have been found to be caused by fluid mixing [e.g., *Beekman et al.*, 2011; *Groen et al.*, 2000; *Shouakar-Stash et al.*, 2007], molecular diffusion [e.g., *Appelo and Postma*, 2005; *Desaulniers et al.*, 1986; *Lavastre et al.*,

2005] and evaporite dissolution/precipitation [e.g., *Eastoe et al.*, 1999; *Eastoe et al.*, 2007; *Eggenkamp et al.*, 1995]. *Kaufmann et al.* [1984] hypothesised that stable chlorine isotopes were likely to be fractionated by molecular diffusion because kinetic effects should cause the lighter ^{35}Cl to diffuse at a faster rate than ^{37}Cl. Once analytical methods advanced to the point that variations in $\delta^{37}Cl$ were discernible beyond analytical uncertainty, molecular diffusion through low-permeability glacial deposits in northern America was the first instance of theoretical fractionation modelling being supported by field data [e.g., *Desaulniers et al.*, 1986]. *Desaulniers et al.* [1986] provided evidence to support the hypothesis that Cl^- in underlying saline formation water was migrating upwards through the glacial tills by showing that ^{35}Cl was enriched relative to ^{37}Cl with decreasing depth. This study confirmed that in environments where diffusive transport of solutes occurs, stable chlorine isotopes are very effective tracers because of the conservative nature of Cl^-. Since the discovery of fractionation during diffusion, stable chlorine isotopes have become widely used to identify and quantify solute transport through low-permeability units, and are particularly popular in studies assessing the suitability of sites for nuclear waste storage [e.g., *Lavastre et al.*, 2005; *Mazurek et al.*, 2011; *Rebeix et al.*, 2014].

Soon after the discovery that stable chlorine isotope abundances were not homogeneous in nature, researchers began work to define fractionation factors for evaporite mineral formation. The first study published with data from laboratory-based fractionation experiments was *Eggenkamp et al.* [1995], where fractionation factors between brine and Cl^- bearing evaporite minerals were determined. This study found that early and late stage evaporites exhibit varying fractionation factors such that early stage evaporites (e.g., halite) have positive fractionation factors (i.e., ^{37}Cl is precipitated preferentially) and *vice versa* for late stage evaporites (e.g., sylvite and bischofite). The

values of the laboratory-determined fractionation factors were supported by geochemical data from an evaporite sequence core containing both early and late stage evaporite minerals (e.g., halite, bischofite, carnallite and kainite). Since the work of *Eggenkamp et al.* [1995], numerous studies have been published highlighting the variations of stable chlorine isotopes in evaporite deposits [e.g., *Eastoe et al.*, 2001; *Eastoe et al.*, 2007; *García-Veigas et al.*, 2009; *Peryt et al.*, 2005].

Luo et al. [2014] published a recent study revisiting chlorine isotope fractionation during evaporite formation because of the perception that corrections were required to improve the methodology (i.e., allowing complete evaporation of experiments before sampling) of *Eggenkamp et al.* [1995] and *Eastoe et al.* [1999]. *Luo et al.* [2014] found that at all stages of evaporite formation, fractionation factors between brine and precipitate were positive. This result contradicts the work of *Eggenkamp et al.* [1995] and *Eastoe et al.* [1999] but is consistent with field data from other studies of evaporite sequences [e.g., *Eastoe et al.*, 2007; *Luo et al.*, 2012], where late stage evaporites display $\delta^{37}Cl$ values that are much lower than early stage evaporites. *Eggenkamp et al.* [2016] recently presented an experimental study that measured the $\delta^{37}Cl$ and $\delta^{81}Br$ variations of numerous Cl^- and Br^- salts from saturated solutions. The authors concluded that the fractionation factor was solely dependent on the cation of the precipitating salt but could not identify a mechanism for the large differences. These contrasting experimental results, and subsequent communication between researchers [i.e., *Eggenkamp*, 2015; *Luo et al.*, 2015], highlight that the field of chlorine stable isotope geochemistry is still in its infancy and specific fractionation processes still need to be understood [*Eggenkamp et al.*, 2016; *Kharaka and Hanor*, 2014]. Furthermore, these lab-based experimental studies do not incorporate the large-scale, both spatial and temporal, processes that lead to the formation of natural evaporite deposits (e.g., steady-

state *vs.* transient hydrologic systems, variable solute sources, basin restriction and if total desiccation is achieved). The current estimated range of $\delta^{37}Cl$ values in natural samples is approximately –8.0 – +8.0 ‰ [*Shouakar-Stash*, 2008].

The study of stable bromine isotope variations in the earth sciences is in its infancy and only a handful of studies have been published so far [e.g., *Boschetti et al.*, 2011; *Cameron and Lippert Jr*, 1955; *Eggenkamp and Coleman*, 2000; 2009; *Frape et al.*, 2007; *Gelman and Halicz*, 2011; *Shouakar-Stash*, 2008; *Shouakar-Stash et al.*, 2007; *Shouakar-Stash et al.*, 2005b; *Stotler et al.*, 2010; *Xiao et al.*, 1993; *Zakon et al.*, 2014]. Field investigations of brines and evaporites have typically used $\delta^{81}Br$ compositions in conjunction with $\delta^{37}Cl$ because of the expected similarities between the two. However, *Eggenkamp and Coleman* [2000] found that stable halogen isotopes fractionated in different directions in oilfield brine samples, with $\delta^{37}Cl$ values ranging from –0.27 to –4.96 ‰ SMOC had $\delta^{81}Br$ values ranging from +0.08 to +1.27 ‰. Although the authors could not explain the observed differences, it led them to conclude that the combined use of stable chlorine and bromine isotopes could provide a complementary insight into solute pathways and brine evolution. This conclusion was further supported by *Shouakar-Stash et al.* [2005b] who found distinct $\delta^{37}Cl$ and $\delta^{81}Br$ signatures of brine from three Canadian basins. Later, *Shouakar-Stash et al.* [2007] reported the $\delta^{37}Cl$ and $\delta^{81}Br$ compositions of brine, brackish and fresh water from the across the Siberian Platform. The authors found that each of the water types had distinct isotopic signatures but found it difficult to explain the differences, except for mixing between different water types.

Molecular diffusion is also expected to be a mechanism of stable bromine isotope fractionation in natural systems [*Eggenkamp and Coleman*, 2000; 2009]. Fractionation of stable bromine isotopes during diffusion would be expected to be less than chlorine

because the mass difference between stable bromine isotopes is approximately half the difference of chlorine isotopes (2.5% and 5%, respectively). Researchers have investigated the diffusion of stable bromine isotopes in molten bromine compounds ($PbBr_2$ and $ZnBr_2$) in the middle of the twentieth century [e.g., *Cameron et al.*, 1956; *Lundén and Lodding*, 1960]. However, it was not until a recent study by *Eggenkamp and Coleman* [2000] that estimates of stable bromine isotope diffusivities (*D*) were reported for experiments undertaken with conditions similar to those found in near-surface hydrologic systems. The authors used polyacrylamide gel with varying concentrations of NaBr (50 – 160 g L^{-1}) and temperatures (2 – 80 °C) to replicate Br^- diffusion through a low-permeability geological formation. The reported range of isotopic fractionation factors for stable bromine isotopes (D_{79}/D_{81}) was 1.00064 – 1.00098, which is half the range of fractionation factors the authors found for stable chlorine isotopes (D_{35}/D_{37}) under the same experimental conditions (1.00128 – 1.00192). However, stable bromine isotope fractionation during diffusion has not yet been confirmed during field studies.

Variations in $\delta^{81}Br$ fractionation factors have been experimentally determined for precipitating Br^- salts from saturated solutions [*Eggenkamp et al.*, 2016]. Like $\delta^{37}Cl$ fractionation factors determined from the same study, $\delta^{81}Br$ fractionation factor variations during mineral precipitation are dependant of the cation of the salt. However, it was found that $\delta^{81}Br$ fractionation factors during mineral precipitation were very small, and were unlikely to cause large differences between salt and brines [*Eggenkamp et al.*, 2016]. The current estimated range of $\delta^{81}Br$ variations observed in natural systems is –0.80 – +3.35 ‰ [*Shouakar-Stash*, 2008]. Unfortunately, most field studies have found it difficult to attribute observed $\delta^{81}Br$ compositions to specific processes [e.g., *Boschetti et al.*, 2011; *Eggenkamp and Coleman*, 2000; *Frape et al.*, 2007;

Shouakar-Stash, 2008; *Shouakar-Stash et al.*, 2007; *Stotler et al.*, 2010], emphasising the need for more targeted field studies of specific processes.

The research presented in this thesis aims to address some of the knowledge gaps associated with the use of chlorine and bromine to trace salt cycling. Specifically, this thesis will address some of the uncertainties associated with using chlorine and bromine to quantify salt cycling, and use recent datasets to investigate the spatial and temporal variability of the input of these elements into catchments on a regional and continental scale. Furthermore, chlorine and bromine tracer techniques are applied to an Australian saline lake (i.e., Lake George Basin) in order to demonstrate their utility in improving the understanding of salt cycling and transport in natural environments. The measurement of stable halogen isotope compositions at Lake George represents one of the first (for chlorine) and only (for bromine) field datasets in Australia, which should provide valuable information about their utility for investigating salt cycling in Australia's unique environment.

Chapter 2: Chloride and bromide sources in water: Quantitative model use and uncertainty

Foreword

The following chapter is based on an article that was published in *Journal of Hydrology* in early-2017 [*Horner et al.*, 2017]. The article is titled 'Chloride and bromide sources in water: Quantitative model use and uncertainty' with the following authorship: Horner, K.N., Short, M.A. and McPhail, D.C.

Much of the work presented in the manuscript was undertaken by Kyle Horner during his Ph.D. candidacy at the Australian National University [*Horner*, 2013]. The idea for the paper was his and he was the primary author of the sections relating to the concept background (Section 1), model development (Section 2) and constraining chloride/bromide ratio tracer studies (Section 5). My contribution was to help design the bench-top halite dissolution experiments, and then undertake geochemical analyses of the experimental samples (Section 3). I was also the primary contributor to sections on the model sensitivity (Sections 4.1 and 4.2) and initial composition uncertainty (Section 4.3). Bear McPhail helped to review the model development and experimental results, provided guidance on the manuscript structure and content, and assisted with editing.

1. Introduction

Chloride (Cl^-) is a widely-used geochemical tracer for characterising the origin, movement, and discharge of surface water, porewater, and groundwater. Dissolved Cl^- is used because of its ubiquity, ease of sampling and analysis, low concentration in common rock-forming minerals, and near-conservative behaviour in the environment [*Davis et al.*, 1998]. A number of chloride-based tracer techniques have been developed, such as: vertical Cl^- profiling in the vadose zone to estimate recharge rates [e.g., *Cook et al.*, 1989; *Scanlon et al.*, 2007; *Tyler et al.*, 1996; *Zhu et al.*, 2003]; Cl^- delineation in streams and aquifers to trace contaminant migration [e.g., *Gasser et al.*, 2010; *Perera et al.*, 2013; *Shaw et al.*, 2012; *Stigter et al.*, 2011]; and, $R^{36}Cl$ surveys along flow paths to calculate flow rates, residence times, and recharge variability [e.g., *Bird et al.*, 1989; *Cartwright et al.*, 2006; *Love et al.*, 2000; *Scheiber et al.*, 2015; *Stone and Edmunds*, 2016].

These techniques are underpinned by the assumption that dissolved Cl^- behaves conservatively in the environment, with no unaccounted Cl^- sources or sinks affecting its concentration. Therefore, changes in a solution's Cl^- concentration as a result of dissolution/precipitation of natural salts (e.g., evaporites) or anthropogenic salts (e.g., fertilisers or deicing agents), or mixing of waters of different Cl^- concentrations (e.g., via stream confluence, preferential flow, vertical leakage, or seawater intrusion) present sources of error in chloride-based tracer techniques unless such Cl^- inputs/outputs are identified and compensated for in calculations [*Davis et al.*, 1998; *Love et al.*, 2000; *Scanlon*, 2000].

When mineral dissolution or water mixing is suspected and end-member compositions are known, mass-balance calculations can be used to compensate for

changes in Cl^-, removing this source of error [e.g., *Alcalá and Custodio*, 2008b]. However, in natural environments (especially arid climates), fluid mixing and salt dissolution often coincide with evapotranspiration (ET). In such cases, multiple processes act concurrently to change dissolved Cl^- concentrations, complicating mass balance calculations. As the extent of evapotranspiration and the timing of salt dissolution are often unknown, they cannot readily be compensated for in the mass balance calculations.

Instead, differentiating the effects of such processes requires measurement of additional parameters to confirm the cause of observed Cl^- concentration changes. While this has been accomplished by other workers using a combination of stable and radioisotopes [e.g., *Love et al.*, 2000] or major and trace cations [e.g., *Johnson et al.*, 2015], dissolved bromide (Br^-) offers an alternative and potentially more cost effective alternative to these methods to not only identify but to quantify the extent of such processes.

Cl^- and Br^- behave in a similar manner in the environment as they are both halide ions. Distinct differences in their natural abundances in surface water, groundwater, and minerals make the Cl^- and Br^- ratio (the Cl^-/Br^- ratio) a useful and versatile environmental tracer [e.g., *Bennetts et al.*, 2006; *Cartwright et al.*, 2006; *Davis et al.*, 1998; *Herczeg et al.*, 2001; *Johnson et al.*, 2015; *McInnis et al.*, 2013; *Petrides et al.*, 2006; *Vengosh and Pankratov*, 1998].

Cl^-/Br^- ratios are most effective as tracers when end-members have strongly contrasting compositions. Relative to natural waters, halite typically has a very high Cl^-/Br^- ratio due to the exclusion of all but trace quantities of Br [*Siemann and Schramm*, 2000]. Similarly, leakage of waste water from urban or industrial sources or leaching of deicing salts into streams or aquifers can be identified by localised deviations of Cl^-/Br

ratios [*Dailey et al.*, 2014; *Johnson et al.*, 2015; *Katz et al.*, 2011; *McArthur et al.*, 2012; *Mullaney et al.*, 2009].

In this chapter, a series of equations are derived to quantitatively use Cl^-/Br^- ratios quantitatively to correct the dissolved Cl^- concentration in a water for inputs from mineral dissolution and/or binary water mixing, and to demonstrate that the equations can be applied to waters also modified by evapotranspiration. The equations can be used to determine the proportional Cl^- contributions from each end-member to a solution providing there has been no precipitation of chloride-bearing minerals and the Cl^-/Br^- ratio of each end-member is known. The validity and sensitivity of the equations are evaluated via bench-top experiments simulating a common environmental process: halite dissolution in a near-surface environment subject to concurrent evapotranspiration. In addition, we discuss the sensitivity of the equations to end-member compositions and analytical uncertainty, and provide an example illustrating how use of the equations can reduce uncertainty when using Cl^--based tracer techniques to evaluate recharge rates and groundwater age.

1.1. Cl^-/Br^- ratios in the environment

Bulk Cl^-/Br^- ratios from 1900 to more than 8700 have been reported for Cl^- salt beds and domes around the world [*Alcalá and Custodio*, 2008b; *Cartwright et al.*, 2004; *Davis et al.*, 1998]. Sequential mineral dissolution/precipitation cycles can result in Cl^-/Br^- ratios in individual salt crystals exceeding 100 000 as Br^- is progressively excluded from minerals such as halite [*Siemann and Schramm*, 2000]. There may also be a large amount of heterogeneity in Cl^-/Br^- ratios of halite samples due to the distribution and abundance of fluid (i.e. brine) inclusions, which can be enriched in Br^- [e.g., *Moretto*, 1988] and cause bulk halite (i.e. solid phase plus inclusions) compositions to be markedly different from the solid phase compositions.

Seawater, in contrast, has a mean Cl^-/Br^- ratio from 284 – 293 [*Berner and Berner*, 1996; *Eggenkamp*, 2014; *McCaffrey et al.*, 1987; *Quinby-Hunt and Turehian*, 1983]. Marine aerosols are the primary sources of solutes in coastal rainfall and precipitation often has ocean-like ion/ion ratios [*Appelo and Postma*, 2005]. As a result, many low-salinity coastal aquifers exhibit Cl^-/Br^- ratios similar to seawater due to recharge by rainwater [*Alcalá and Custodio*, 2008b; *Davis et al.*, 1998]. However, this is not always the case, as illustrated in a recent study presented in *Cendón et al.* [2014], where shallow, coastal groundwater Cl^-/Br^- ratios were found to be markedly elevated (>400 by mass for some samples) relative to seawater despite the aquifer having little anthropogenic inputs or contact with evaporite minerals.

As atmospheric moisture moves inland, differential rain-out of Cl^- and Br^- and dissolution of continentally-derived sediments, agricultural products, and smoke from fires or fossil fuel combustion can modify rainfall Cl^- and Br^- concentrations [*Alcalá and Custodio*, 2008b; *Davis et al.*, 2004; *Davis et al.*, 1998; *Keywood et al.*, 1997]. Typically, there is a proportional increase in Br^- and inland rainwater tends to have lower Cl^-/Br^- ratios than seawater, although dissolution of aeolian salts can increase meteoric Cl^-/Br^- ratios [*Davis et al.*, 1998].

Following rainfall, concentrations of dissolved Cl^- and Br^- can be further modified via anthropogenic impacts (e.g., fertiliser and deicing salt dissolution), fluid mixing (e.g., stream confluence), and mineral dissolution at the land surface or in the unsaturated zone [e.g., *Cartwright et al.*, 2009; *Davis et al.*, 1998; *Kaushal et al.*, 2005; *Kelly et al.*, 2008; *Vengosh and Pankratov*, 1998]. Cl^-/Br^- ratios between 10 and 100 000 have been measured in surface water and groundwater around the world, illustrating the marked impacts these processes can have on Cl^-/Br^- ratios throughout the water cycle [e.g., *Alcalá and Custodio*, 2008b; *Cartwright et al.*, 2009; *Herczeg et al.*, 2001].

Biogeochemical processes in the unsaturated zone such as plant uptake and clay sorption, as well as anion exchange on clays and organic matter, have been shown to have a strong effect on soil water and groundwater composition [*Edwards and Webb*, 2009; *Scanlon et al.*, 2009]; however, Cl^- and Br^- are not affected strongly. For instance, Clifford et al. [2011] illustrated the preferred sorption order for anions to activated alumina (a soil analogue) to be:

$$OH^- > H_2AsO_4^- > F^- > SO_4^{2-} >> HCO_3^- > Cl^- > NO_3^- > Br^-$$

As preferentially-sorbed ions such as fluoride, sulfate, and bicarbonate are often present in surface water and groundwater, anion sorption will not have a significant effect on Cl^- and Br^- concentrations in many natural systems.

1.2. Impacts of concurrent mixing/dissolution and evapotranspiration on Cl^-/Br^-

Binary mixing and mineral dissolution will modify both dissolved Cl^- and Br^- in proportion to the quantity of each end member in the final admixture. Accordingly, as demonstrated by *Alcalá and Custodio* [2008b], Cl^-/Br^- ratios offer an inexpensive and straightforward method to identify and quantify dissolved Cl^- inputs where ET is not suspected to be signficant. However, ET often cannot be discounted and, as qualitative discussions of Cl^-/Br^- ratios show [e.g., *Davis et al.*, 1998; *Lenahan et al.*, 2011], failure to account for it will introduce error when interpreting dissolved Cl^-/Br^- ratios. The significance of this error is demonstrated in Table 1, which summarises the quantity of halite (mass $Cl^-/Br^- = 5\,000$) required to raise the Cl^-/Br^- ratio of a hypothetical coastal rainwater ($Cl^- = 10$ mg kg^{-1}, mass $Cl^-/Br^- = 290$) to a final ratio of 500 at progressive stages of ET.

Table 1: Solute concentrations of an initial solution at progressive stages of evapotranspiration (ET), the amount of Cl^- and Br^- from halite dissolution (mg kg^{-1} solution) required to raise the Cl^-/Br^- ratio of a unit mass (1 kg) of the concentrated solution from 290 to 500 (Cl_I = 10 mg kg^{-1}; R_H = 5 000), and the proportion of halite-derived Cl^- and Br^- in the final solution (mass %).

	Initial Solution (R_I = 290)		Halite Added (R_H = 5000)		Final Solution (R_F = 500)	
ET (%)	Cl_I mg kg^{-1}	Br_I mg kg^{-1}	Cl_H mg kg^{-1}	Br_H mg kg^{-1}	Cl_H (%)	Br_H (%)
0	10.00	0.0345	8.046	0.0016	44.6	4.5
10	11.11	0.0383	8.940	0.0018	44.6	4.5
25	13.33	0.0460	10.73	0.0021	44.6	4.5
50	20.00	0.0690	16.09	0.0032	44.6	4.5
75	40.00	0.1379	32.18	0.0064	44.6	4.5
90	99.99	0.3448	80.45	0.0161	44.6	4.5
95	200.0	0.6895	160.9	0.0322	44.6	4.5
99	999.0	3.445	803.8	0.1608	44.6	4.5
99	1996	6.883	1606	0.3212	44.6	4.5

The timing of dissolution or mixing processes and the extent of ET undergone by an environmental water sample are often unknown, so to avoid problems resulting from volume changes the results in Table 1 are presented as concentrations (solute mass per kilogram of evapoconcentrated solution) rather than as total mass (or volume). This is also an advantage because chemical compositions are the data available to investigators. As shown in Table 1, dissolved Cl^-/Br^- ratios in the evapoconcentrated solution remain constant if the solution is not sufficiently concentrated for Cl^-- and/or Br^--bearing minerals to precipitate. If mineral saturation is reached, Cl^-/Br^- ratios would change as dissolved Cl^- and Br^- partition into the solid phase [e.g., *Siemann and Schramm*, 2000].

Below saturation, however, ET ‘entrenches’ the Cl^-/Br^- ratio of a solution. That is, with increasing ET, greater masses of halite (or other halide-bearing minerals) are required to increase the Cl^-/Br^- ratio proportionally to a unit mass or volume of the evapoconcentrated solution. Thus, the absolute quantity of halite required to increase

the Cl^-/Br^- ratio of a given mass of solution by a fixed amount is dependent upon the initial solution composition, the extent of ET, and the timing of halite dissolution.

Crucially, the relative quantities (wt. %) of Cl^- and Br^- in the final solution contributed by halite dissolution are constant, regardless of the degree of evapotranspiration (Table 1). Instead, the relative quantities depend upon the differences in the Cl^-/Br^- ratios of the end-members: the initial solution (R_I); halite (R_H); and, the final solution (R_F).

This leads to three important observations. First, where evaporation or transpiration occur the absolute quantity of dissolved halite cannot readily be inferred through a qualitative review of Cl^-/Br^- ratios. Second, small changes in dissolved Cl^-/Br^- ratios can signify large proportional Cl^- contributions via mineral dissolution or binary mixing if the end members have strongly contrasting Cl^-/Br^- ratios. For the case of the hypothetical solution in Table 1, 44.6 wt.% of the final dissolved Cl^- load is derived from halite dissolution but the Cl^-/Br^- ratio only increased by 210 in all instances. Third, it is possible to use Cl^-/Br^- ratios to calculate the proportion of dissolved Cl^- from each end-member in a chloride salt solution or binary water mixture, providing no Cl^-- and Br^--containing salts have precipitated. These calculations can be applied to correct dissolved Cl^- concentrations for external inputs, reducing uncertainty in many Cl^--based tracer calculations.

2. Dissolved Cl^- correction factors

The Cl^-/Br^- ratio of a solution or mineral is defined as:

$$R = \frac{Cl^-}{Br^-} \quad (3)$$

where Cl^- and Br^- are expressed in the same concentration units. If the mass of water remains constant as the Cl^-/ Br^- ratio in the solution changes from an initial value (R_I) to a final value (R_F) due to, for example, dissolution of a chloride salt such as halite, then:

$$R_F = \frac{Cl_I + Cl_H}{Br_I + Br_H} \tag{4}$$

where Cl_I and Br_I are the initial concentrations and Cl_H and Br_H are the contributions of Cl^- and Br^- from halite dissolution. Assuming congruent dissolution, Cl_H and Br_H are constrained by the Cl^-/ Br^- ratio of halite (R_H):

$$R_H = \frac{Cl_H}{Br_H} \tag{5}$$

Using these relationships δCl_H, the proportion of dissolved Cl^- resulting from halite dissolution (here expressed as a percentage), can be calculated:

$$\delta Cl_H = \frac{Cl_H}{Cl_I + Cl_H} \times 100 = \frac{R_H(R_F - R_I)}{R_F(R_H - R_I)} \times 100 \tag{6}$$

Once the proportion of dissolved Cl^- contributed to the final solution from mineral dissolution is known it can be compensated for and the quantity of dissolved Cl^- from the initial solution can be readily determined:

$$\delta Cl_I = 100\% - \delta Cl_H = \frac{R_I(R_H - R_F)}{R_F(R_H - R_I)} \times 100 \tag{7}$$

Multiplying the final dissolved Cl^- concentration by δCl_I will return a corrected Cl^- concentration suitable for use in chloride-based tracer calculations.

The proportions of Br^- from halite dissolution and the bromide correction factor can be determined in the same manner:

$$\delta Br_H = \frac{(R_F - R_I)}{(R_H - R_I)} \times 100 \quad (8)$$

$$\delta Br_I = \frac{(R_H - R_F)}{(R_H - R_I)} \times 100 \quad (9)$$

Molar Cl^-/Br^- ratios should be used to determine a molar correction factor, while mass Cl^-/Br^- ratios should be used to determine a mass correction factor. Once calculated, the correction factor can be applied to analytical results to correct dissolved Cl^- or Br^- concentrations for contributions from halite dissolution, allowing chloride-based tracer techniques to be used in regions where salt dissolution and ET have concurrently or sequentially modified a solution's composition.

2.1. Binary mixing

Equation (6) and Equation (7) can also be used to calculate the proportion of dissolved Cl^- in a mixture contributed from two waters with different Cl^-/Br^- ratios. By replacing the halite terms in Equation (6) and Equation (7) with R_A, the Cl^-/Br^- ratio of an added solution, binary mixing equations can be formulated and the proportional contributions of both end members can be determined (Equations (10) and (11)). Once the relative contributions of Cl^- in the final solution are determined, a mass-balance approach can be used to calculate the mixing fraction of the end members.

$$\delta Cl_A = \frac{R_A(R_F - R_I)}{R_F(R_A - R_I)} \times 100 \quad (10)$$

$$\delta Cl_I = \frac{R_I(R_A - R_I)}{R_F(R_A - R_I)} \times 100 \quad (11)$$

3. Experimental and analytical methods

A series of bench-top experiments were conducted to validate the mathematical model and to assess the sensitivity of the model to heterogeneous halite compositions and analytical uncertainty. We accomplished this by dissolving three different halite samples with contrasting Cl^-/Br^- ratios into a series of solutions with initial Cl^- and Br^- concentrations and Cl^-/Br^- mass ratios within the range commonly reported for natural environments.

The three halite samples used in the experiments were: Saxa Pink Himalayan table salt (Cerebos Australia Ltd., Australia); Lake Deborah 'bubble salt' (WA Salt Group, Australia); and, Searles Lake halite (California, USA; The Australian National University museum collection, ID 37341).

3.1. Halite dissolution experiment

Cl^- and Br^- concentrations were determined using a Dionex ICS-5000 Reagent-Free ion chromatograph (IC; Thermo Scientific, USA) at the Australian Centre for Research on Separation Science (ACROSS) laboratories of the University of Tasmania, Australia. The IC was run using a gradient potassium hydroxide elution with an IonPac AS-19 analytical column and suppressed conductivity detection. Analytical precision, determined by replicate analysis of samples and calibration standards, was better than 5% for all Cl^- and Br^- analyses.

The Cl^-/Br^- ratio of each halite sample was determined prior to the batch experiments by dissolving three aliquots of each halite sample in ultra-pure water (18.2 MΩ cm^{-1} at 25°C Milli-Q; Merck Millipore, Germany) and filtering through 0.2 μm nylon syringe filters. Cl^-/Br^- ratios in the Saxa Pink Himalayan (SPH), Lake Deborah (LD) and Searles Lake (SL) halite sample replicates are shown in Table 2.

Table 2: Measured mass Cl^-/Br^- ratios for halite aliquots used in experiments.

	Searles Lake	Lake Deborah	Saxa Pink Himalyan
Replicate A	27 100 ± 2 700	44 400 ± 4400	15 400 ± 1 500
Replicate B	22 200 ± 2 200	42 200 ± 4200	30 000 ± 3 000
Replicate C	20 000 ± 2 000	54 400 ± 5400	15 000 ± 1 500

Batch experiments were then conducted simulating halite dissolution into a low-salinity water (0% ET, Cl_I = 49.9 mg kg^{-1}; Br_I = 0.26 mg kg^{-1}; mass R_I = 193) and in higher-salinity water representing progressive stages of evapoconcentration (50, 75, 90 and 99 wt.% evaporated, Table 3). The 99 wt.% stock (Cl_I = 4940.8 mg kg^{-1}; Br_I = 24.56 mg kg^{-1}; mass R_I = 201) was made using analytical grade NaCl (Merck Pty. Ltd. 'AnalaR' 99.5% NaCl; batch number 36158) and laboratory grade sodium bromide ('Unilab' 99.5% NaBr; Ajax Finechem Pty. Ltd. batch number F1K217) dissolved in ultrapure water. The remaining initial solutions for each stage of evapoconcentration were prepared from the maximum salinity stock (99 wt.%) by serial dilution with ultrapure water to the required salinity. Once the initial solutions were prepared, a series of solutions were generated for each halite sample by dissolving approximately 50 mg (accurately weighed) of halite into a separate aliquot of each initial solution (Table 3).

Table 3: Initial solution composition, mass of added halite, final solution composition, and measured and calculated δCl_H values for batch experiments.

Sample % ET	Solution (g)	Cl_I (mg kg^{-1})	Br_I (mg kg^{-1})	R_I (mass)	Halite added (mg)	Cl_F (mg kg^{-1})	Br_F (mg kg^{-1})	R_F (mass)	Measured δCl_H (wt. %)	Calculated δCl_H (wt. %) Replicate A	Replicate B	Replicate C
Searles Lake halite												
0.0	99.7	49.9 ± 2.5	0.259 ± 0.013	193 ± 19	48.7	310 ± 16	0.243 ± 0.012	1 280 ± 130	83.9 ± 1.6	85.5 ± 3.0	85.7 ± 3.0	85.7 ± 3.0
49.4	99.2	102 ± 5	0.511 ± 0.026	200 ± 20	52.2	273 ± 14	0.495 ± 0.025	552 ± 55	62.7 ± 3.7	64.2 ± 7.4	64.3 ± 7.4	64.4 ± 7.4
74.6	100.0	197 ± 10	0.982 ± 0.049	201 ± 20	51.3	494 ± 25	0.909 ± 0.046	543 ± 54	60.1 ± 4.0	63.5 ± 7.5	63.6 ± 7.5	63.6 ± 7.6
89.8	100.3	507 ± 25	2.49 ± 0.13	204 ± 20	56.5	816 ± 41	2.36 ± 0.12	346 ± 35	37.9 ± 6.2	41.4 ± 12.0	41.4 ± 12.0	41.5 ± 12.0
99.0	100.0	4 940 ± 250	24.6 ± 1.2	201 ± 20	48.4	5230 ± 260	25.0 ± 1.3	209 ± 21	5.6 ± 9.5	3.9 ± 19.6	3.9 ± 19.6	3.9 ± 19.6
Lake Deborah 'Bubble' salt												
0.0	100.1	49.9 ± 2.5	0.259 ± 0.013	193 ± 19	52.0	343 ± 17	0.217 ± 0.011	1 580 ± 160	85.5 ± 1.5	88.2 ± 2.5	88.2 ± 2.5	88.1 ± 2.5
49.4	100.0	102 ± 5	0.511 ± 0.026	200 ± 20	50.3	370 ± 19	0.442 ± 0.022	837 ± 84	72.4 ± 2.8	76.4 ± 4.8	76.5 ± 4.8	76.4 ± 4.8
74.6	100.0	197 ± 10	0.982 ± 0.049	201 ± 20	48.6	486 ± 24	0.844 ± 0.042	576 ± 58	59.5 ± 4.1	65.4 ± 7.1	65.4 ± 7.1	65.3 ± 7.1
89.8	100.1	507 ± 25	2.49 ± 0.13	204 ± 20	63.2	884 ± 44	2.36 ± 0.12	375 ± 38	42.7 ± 5.7	45.8 ± 11.0	45.8 ± 11.0	45.8 ± 11.0
99.0	100.1	4 940 ± 250	24.6 ± 1.2	201 ± 20	57.6	5 500 ± 280	24.6 ± 1.2	224 ± 22	10.2 ± 9.0	10.3 ± 18.2	10.3 ± 18.2	10.3 ± 18.2
Saxa Pink Himalayan												
0.0	103.8	49.9 ± 2.5	0.259 ± 0.013	193 ± 19	48.2	335 ± 17	0.230 ± 0.012	1 460 ± 150	85.1 ± 1.5	87.9 ± 2.7	87.3 ± 2.7	87.9 ± 2.6
49.4	103.0	102 ± 5	0.511 ± 0.026	200 ± 20	45.1	402 ± 20	0.433 ± 0.022	928 ± 93	74.6 ± 2.5	79.5 ± 4.4	79.0 ± 4.4	79.5 ± 4.4
74.6	104.0	197 ± 10	0.982 ± 0.049	201 ± 20	53.4	510 ± 26	0.863 ± 0.043	591 ± 59	61.4 ± 3.9	66.9 ± 7.0	66.4 ± 6.9	66.9 ± 7.0
89.8	103.9	507 ± 25	2.49 ± 0.13	204 ± 20	57.1	866 ± 43	2.48 ± 0.12	349 ± 35	41.5 ± 5.9	42.1 ± 12.0	41.8 ± 11.9	42.1 ± 12.0
99.0	104.0	4 940 ± 250	24.6 ± 1.2	201 ± 20	47.3	5 480 ± 270	24.1 ± 1.2	227 ± 23	9.9 ± 9.0	11.6 ± 18.1	11.5 ± 18.0	11.6 ± 18.1

3.2. Data evaluation

Halite contributions to dissolved Cl^- loads in the final solutions were first determined directly by subtracting the initial Cl^- concentration from the final concentration (measured δCl_H). Initial and final Cl^-/Br^- ratio results from the experiments were then used as input values for the mathematical model, and halite contributions to dissolved Cl^- loads in the final solutions were calculated (calculated δCl_H).

As the mathematical models developed here require input of a single Cl^-/Br^- ratio, sensitivity of the models to natural variability in the halite samples' composition results were assessed by calculating δCl_H using the values for each halite replicate (A, B, C; Table 2). The measured and calculated results were then compared (Table 3).

Uncertainties for measured δCl_H values were calculated using the uncertainties package for the Python programming language (version 2.4.6.1 [*Lebigot*, 2014]), and are based on an analytical precision of ±5% for measured halide concentrations. The uncertainty of results produced by the mathematical model due to the analytical precision of input parameters is discussed further in Section 4.1.

4. Results and discussion

The results show very good agreement, with all calculated δCl_H values varying by only 0 – 6% from the measured δCl_H values (Figure 2), indistinguishable when compared to the uncertainties associated with both the measured and calculated δCl_H values. Triplicates of the calculated δCl_H values (Table 3), calculated using the three

reported values of R_H for each halite sample (Table 2), also show good agreement, with all calculated values falling well within the range of their associated uncertainty.

The results demonstrate that the mathematical model is a robust tool for determining the proportional contributions of dissolved Cl^- and Br^- from halite dissolution with concurrent evapotranspiration.

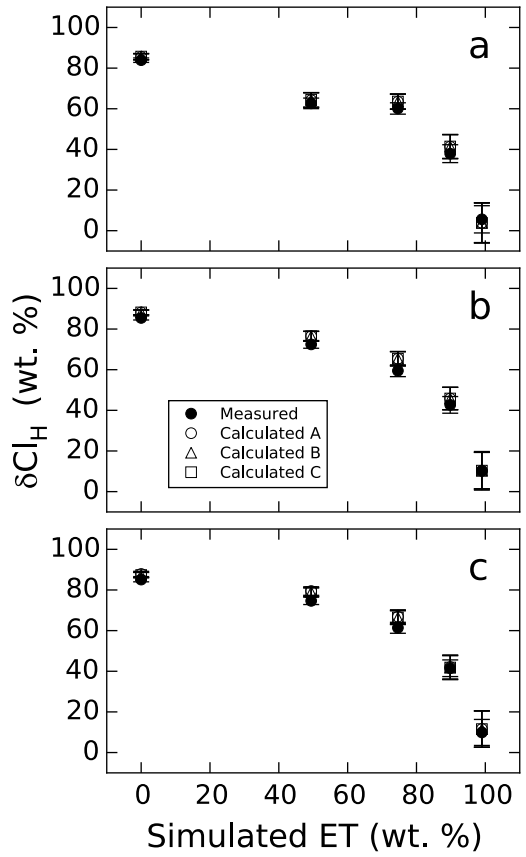

Figure 2: Calculated and measured δCl_H at different stages of evapotranspiration for (a) Searles Lake (SL); (b) Lake Deborah (LD); and (c) Saxa Pink Himalayan (SPH) halite dissolution experiments. Values calculated using replicate halite analyses (Table 2).

4.1. Mathematical model sensitivity analysis

The sensitivity of the mathematical model to contrasts in Cl^-/Br^- ratios between the initial solution and dissolving halite was evaluated numerically. Simulations were run by calculating the progressive evolution of Cl^-/Br^- ratios when adding halite with

differing Cl^-/Br^- ratios to a series of solutions with uniform initial compositions. The simulations assessed Cl^-/Br^- ratio contrasts between 2× (i.e., R_H twice R_I) to 50× (Figure 3).

To compare results between simulations, data were normalised to the proportion of halite dissolved. This was achieved by calculating a ratio of the actual change in Cl^-/Br^- ratio (R_F-R_I) to the maximum possible change for a given simulation (R_H-R_I), and denoted as δR_H, to serve as a proxy for halite dissolution (Figure 3a).

Figure 3a shows that the δCl_H value has a strong dependence on the magnitude of the Cl^-/Br^- contrast. During dissolution of halite with a low Cl^-/Br^- contrast (2×) the δCl_H of the solution evolves in a close-to-linear manner, while the trend becomes increasingly hyperbolic with increasing Cl^-/Br^- contrasts. For the low-contrast Cl^-/Br^- system, halite-derived Cl^- becomes the dominant (>50%) source of dissolved Cl^- when the Cl^-/Br^- ratio has changed by more than 33% of the maximum possible. For the highest-contrast Cl^-/Br^- systems (50×), halite-derived Cl^- is the dominant source of dissolved Cl^- after Cl^-/Br^- ratios change by 2% percent of the maximum possible.

For a real-world system where a low-salinity water (mass Cl^-/Br^- = 250) is modified by dissolution of halite with mass Cl^-/Br^- of 5 000, halite-derived Cl^- would dominate the solution once the solution's Cl^-/Br^- ratio exceeded 487.5. This again illustrates the substantial contributions halite dissolution can make to dissolved Cl^- loads without markedly changing a solution's Cl^-/Br^- ratio.

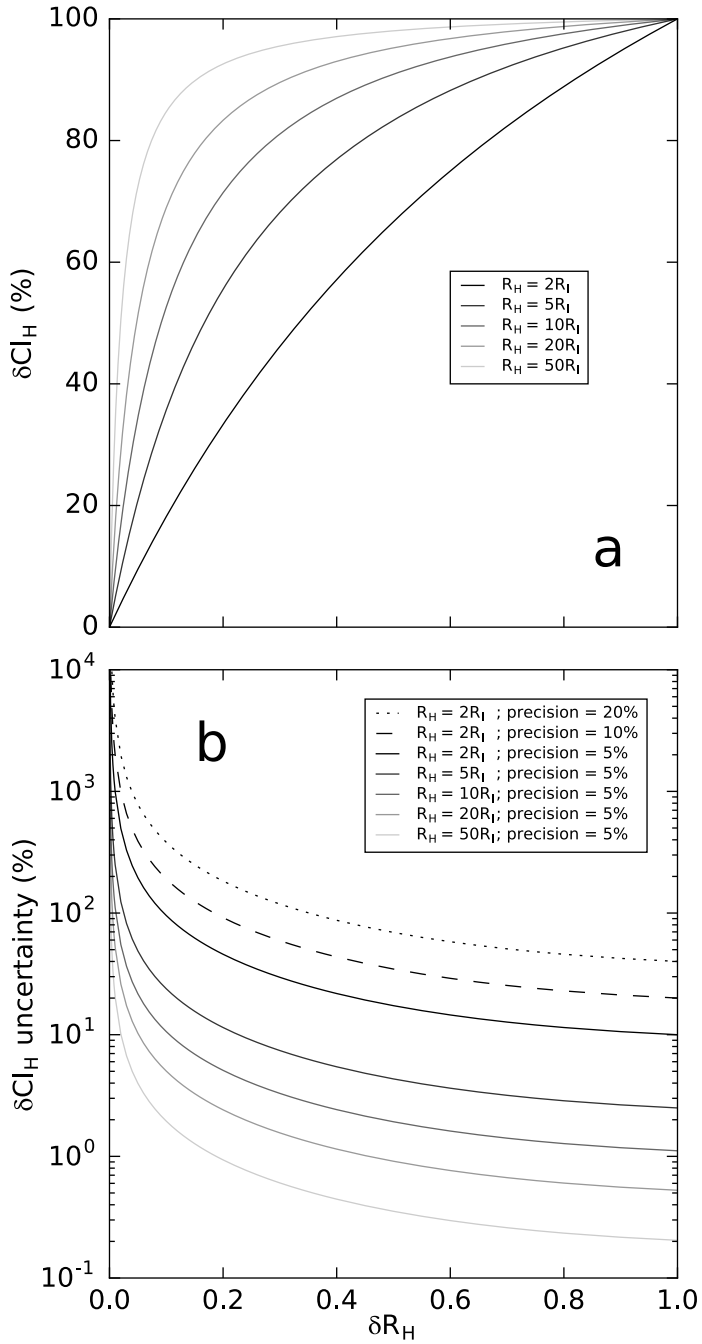

Figure 3: (a) Calculated proportions of halite-derived Cl^- relative to total dissolved chloride (δCl_H), as a function halite dissolute extent $(R_F\text{-}R_I)/(R_H\text{-}R_I)$. (b) Uncertainty associated with calculated δCl_H values for ranges of analytical precision and R_H values.

For the various Cl^-/Br^- contrasts depicted in Figure 3a, differences in calculated δCl_H are greatest at low halite dissolution extents but the magnitude of the difference decreases with an increasing difference between R_H and R_I. Thus, the sensitivity of

Equation (7) to uncertainty in R_H values decreases with increasing contrast in the Cl^-/Br^- ratio of the initial solution and the dissolving halite. The results for the Saxa Pink Himalayan salt dissolution experiment demonstrate this clearly. Due to the large discrepancy between the halite sample and the initial solution, a δCl_H difference of only 0.6 – 0.7% was calculated despite the two-fold range of R_H in the dissolving halite (Table 3).

As halite Cl^-/Br^- ratios are commonly >10× those of surface water and groundwater, the sensitivity analysis demonstrates that uncertainty or heterogeneity in the Cl^-/Br^- ratio of dissolving halite would only produce an error of a few percent in calculated δCl_H. Therefore, in natural systems where the Cl^-/Br^- ratio of dissolving halite can be inferred to be much higher than the initial solution, δCl_H can be estimated without knowing the precise Cl^-/Br^- ratio of the dissolving halite.

At each step of the simulations described above, the uncertainty associated with a given δCl_H value was also calculated (Figure 3b). The uncertainty, as a percentage of the calculated δCl_H value, is reported as the uncertainty based on an analytical precision of ±5% for both Cl^- and Br^-, and was calculated using the Python error propagation package, *uncertainties*. The plot shown in Figure 3b visually demonstrates three main points. First, at a given δR_H, the uncertainty of calculated δCl_H values decreases in the form of an inverse power law that is proportional to the difference between R_H and R_I (i.e., an increasing difference between R_H and R_I results in increasingly smaller uncertainties). Second, the uncertainty of calculated δCl_H values decrease in the form of an inverse power law that is proportional to δR_H (i.e., higher δR_H values result in increasingly smaller uncertainties). Third, at a given value of δR_H, the uncertainty of calculated δCl_H values decreases such that a doubling of analytical precision of Cl^- and Br^- measurements results in a doubling of the calculation uncertainty. The second point

is highlighted by the results the salt dissolution experiments (Figure 2): for the low-salinity samples (i.e., no ET) the added salt results in δR_H values of 0.026 – 0.086 and uncertainties of ±1 – 3% of the calculated δCl_H values. By contrast, the same amount of dissolved salt results in relatively small δR_H values of <0.002 for the high-salinity samples (i.e., ET = 99 wt.%) and greater uncertainties of ±77 – 254% of the calculated δCl_H values. The combination of experimental results (Figure 2) and simulated examples (Figure 3) provide guidance on which situations will result in more robust results after application of the equations derived here.

4.2. Initial composition uncertainty

Uncertainty in the initial dissolved Cl^-/Br^- ratio of the initial solution is likely to be a significant source of error when applying the mathematical model to field data. For some investigations, the initial water source may be surface water (i.e., creeks, rivers or lakes) or groundwater from adjacent formations. In these situations, constraining the initial Cl^-/Br^- ratio should be straightforward (e.g., sampling upstream waters or bores screened in adjacent aquifers). However, in many catchments (especially arid and semi-arid catchments) direct recharge from precipitation is a major source of water. In the absence of precipitation chemistry data, many studies quote the seawater ratio as an approximation for water entering a catchment when assessing observed Cl^-/Br^- ratios of groundwater [e.g., *Cartwright et al.*, 2013; *Dogramaci et al.*, 2012; *Hofmann and Cartwright*, 2013; *Kim et al.*, 2003; *Skrzypek et al.*, 2013]. This assumption may be particularly tempting for coastal catchments where sea spray could reasonably be assumed to be the major source of solutes [*Short et al.*, 2017]. However, findings from several studies around the world suggest that complex reactions occurring during the production of marine aerosols may alter the Cl^-/Br^- ratio significantly from the seawater ratio [e.g., *Ayers et al.*, 1999; *Bloch et al.*, 1966; *Duce et al.*, 1965; *Zhou et al.*, 1990].

Limited data for Cl^-/Br^- ratios in precipitation (including snow) from around the world demonstrate the widely varying Cl^-/Br^- ratios that may be found in local precipitation (Figure 4) [*Alcalá and Custodio*, 2008b; *Bloch et al.*, 1966; *Cawse*, 1987; *Crosbie et al.*, 2012; *Duce et al.*, 1965; *Harriss and Williams*, 1969; *Jacobi et al.*, 2012; *Liljestrand and Morgan*, 1981; *C Neal et al.*, 1990; *M Neal et al.*, 2007; *Short et al.*, 2017; *Simpson et al.*, 2005].

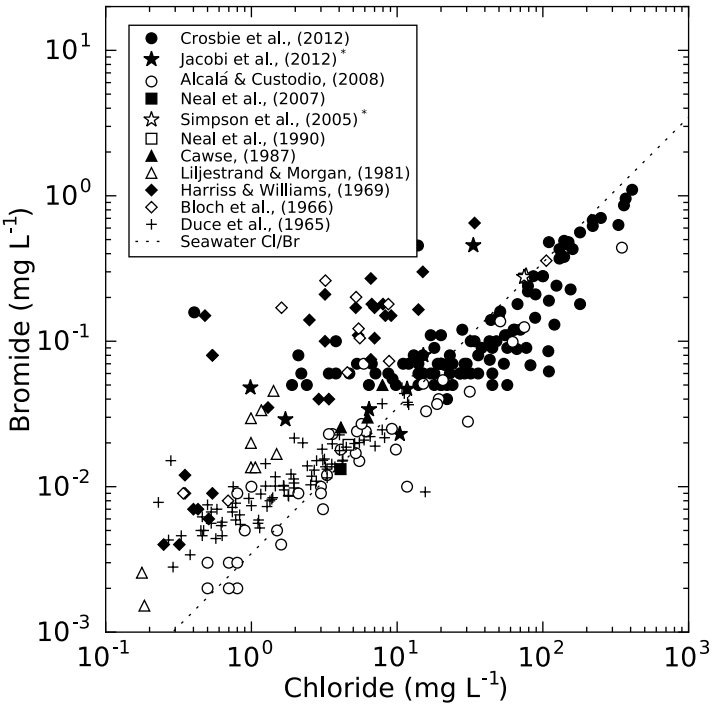

Figure 4: Global variability of reported Cl^-/Br^- mass ratios for rain (stars) and snow (circles). Data sources shown in the figure.

A useful example to demonstrate the potential for error when assuming a seawater Cl^-/Br^- ratio for precipitation is given by data from Cape Grim in Tasmania, Australia. The Cape Grim Baseline Air Pollution Station has been used to monitor atmospheric pollution for more than four decades and is considered to be unaffected by major pollution sources because of its location on the isolated northwest coast of Tasmania [*Ayers et al.*, 1999; *Ayers and Gras*, 1983]. In addition to sampling atmospheric gases, the site has also been used for collecting precipitation samples for major and minor ion

analysis [e.g., *Ayers and Ivey*, 1988; *Crosbie et al.*, 2012], and investigating the composition of marine aerosols [e.g., *Ayers et al.*, 1999]. Precipitation sampled at this location is primarily comprised of moisture and solutes from the Southern Ocean [*Ayers et al.*, 1999; *Ayers and Ivey*, 1988]. *Ayers et al.* [1999] used data from Cape Grim to support an autocatalytic model for loss of Cl^- and Br^- from marine aerosols. The authors found that Cl^- loss from marine aerosols (relative to seawater) was at most a few percent while Br^- loss averaged 30 – 50% annually.

More recently, *Crosbie et al.* [2012] reported precipitation composition for Cape Grim for the period May 2007 to December 2011, although March 2010 through to December 2011 was the only period when continuous Cl^- and Br^- data were available. During this period, the precipitation amount-weighted average Cl^-/Br^- mass ratio was 355 and Cl^-/Br^- ratios of individual monthly samples ranged from 229 to 1140. Therefore, if an assumed initial Cl^-/Br^- ratio of 290 (i.e., seawater) was used at Cape Grim to calculate a Cl^- correction factor for a groundwater sample that resembles local precipitation (i.e., $R_F = 355$), it would be erroneously concluded that 19.4% of Cl^- in the groundwater sample is contributed from sources other than precipitation (assuming a R_H of 5 000). This demonstrates that the Cl^- correction factor (Equation (7)) should only be applied when the Cl^-/Br^- ratio of the recharge water is confidently known.

4.3. Uncertainty in Cl^-/Br^- ratios

When determining the uncertainty in a ratio calculated from two parameters with individual uncertainties, error propagation results in the calculated ratio (R) having a greater error than the numerator or denominator. The relative error of a ratio is determined by:

$$\frac{\Delta R}{R} = \sqrt{\left(\frac{\Delta Cl}{Cl}\right)^2 + \left(\frac{\Delta Br}{Br}\right)^2} \qquad (12)$$

where Δ denotes the absolute uncertainty of the indicated parameter [*Ellison and Williams*, 2012; *Farrance and Frenkel*, 2012]. For example, the relative analytical uncertainty for measurements presented here is ±5% for both Cl^- and Br^-, and the relative uncertainty in the calculated Cl^-/Br^- ratio is ±7.1%.

Left-censoring of solute concentrations (i.e., where solute concentrations are less than the quantitation limit of the analytical method) present a practical limit to the determination of Cl^-/Br^- ratios. At solute concentrations at or slightly great than the quantitation limit, Cl^-/Br^- ratios can be determined by analytical factors such as baseline noise and signal interferences increase uncertainty, requiring calculation of an expanded uncertainty interval if sufficient information is available [*Ellison and Williams*, 2012]. Such expanded uncertainty intervals propagate into calculated ratios, increasing the error for any ratio where either the numerator or denominator is near the quantitation limit.

In most natural systems Cl^- is more abundant than Br^- and, therefore, the accurate measurement of dissolved Br^- may be the limiting factor in calculating Cl^-/Br^- ratios. Where insufficient analytical data are available to calculate an expanded uncertainty interval for solute concentrations near the quantitation limit, it is not recommended that quantitative interpretation of Cl^-/Br^- ratios be attempted.

5. Constraining uncertainty in Cl^--based tracer calculations

Potential Cl^- contributions by unknown or unquantified processes are a frequently-cited source of uncertainty for Cl^--based tracer techniques. Even in cases

where these processes are recognised, the method chosen to correct Cl^- concentrations can greatly influence the tracer calculations.

For example, work by *Bentley et al.* [1986], *Torgersen et al.* [1991], and *Love et al.* [2000] uses a trio of ^{36}Cl-based age models to estimate apparent groundwater ages along transects through the eastern [*Bentley et al.*, 1986] and western [*Love et al.*, 2000] Great Artesian Basin (GAB) in Australia (Figure 5). As groundwater residence times in the GAB can exceed one million years, a long-lived radioisotope is required for groundwater age calculations.

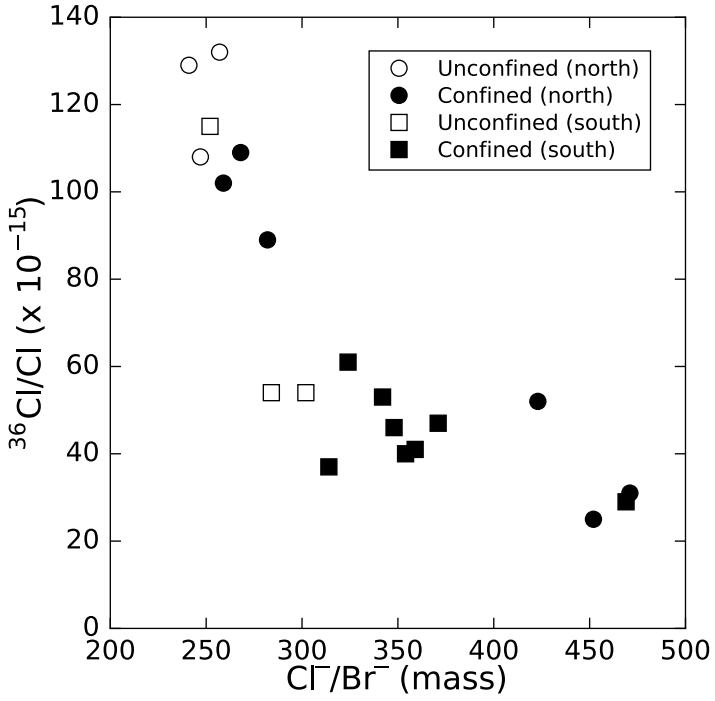

Figure 5: $^{36}Cl/Cl$ versus mass Cl^-/Br^- mass ratio for northern and southern transect groundwater samples from unconfined and confined aquifers reported by *Love et al.* [2000].

^{36}Cl has a half-life of 3.01×10^5 years, making it a viable tracer in the GAB. ^{36}Cl concentrations or the $^{36}Cl/Cl$ ratio along a hydraulic gradient can be used to estimate groundwater ages on timescales of up to 1.5×10^6 years provided that sources and sinks of ^{36}Cl and Cl^- can be accounted for. However, as explained in *Bentley et al.* [1986] and

Love et al. [2000], it is difficult to determine the initial $^{36}Cl/Cl$ ratio in recharge water when using ^{36}Cl age dating techniques in the GAB.

These difficulties are evident from the variable $^{36}Cl/Cl$, dissolved Cl^-, and Cl^-/Br^- ratios along the GAB transects (Table 4). For one eastern transect, *Bentley et al.* [1986] identifies interlayer leakage and introduction of Cl^- from underlying formations as a possible mechanism which may cause such variability. Along two western transects, *Love et al.* [2000] noted that Cl^-/Br^- results for groundwater samples are consistent with initial evapoconcentration of infiltrating rain water (Cl_I = 2 mg L^{-1}) to between 250 and 500 mg L^{-1} and subsequent modification by dissolution of halite. However, *Love et al.* [2000] discounted halite as a significant source of Cl^- due to low (<1 000) Cl^-/Br^- ratios in groundwater samples and the absence of evaporite deposits in the study area.

As demonstrated in Table 1 and Section 4, though, where ET and potential halite sources coincide, low Cl^-/Br^- ratios cannot be considered prima facie evidence that halite dissolution is not a significant Cl^- source. Although the final concentration of dissolved Cl^- in groundwater samples along the GAB transects is determined by the extent of evapotranspiration, halite dissolution may still be a significant source of the dissolved Cl^- being concentrated. It also does not necessarily need to be a halite source that has caused the changes to the groundwater compositions. This trend could also be attributed to mixing with another water source with an elevated Cl^-/Br^- ratio.

Indeed, despite the spatially variability along the *Love et al.* [2000] transects, an inverse relationship between $^{36}Cl/Cl$ and Cl^-/Br^- ratios is present (Figure 5), suggesting that the observed decrease in $^{36}Cl/Cl$ along the transects may not be entirely attributable to ^{36}Cl decay.

Table 4 Calculated maximum halite contributions to dissolved Cl^- concentrations and modelled groundwater ages along *Love et al.* [2000] transects through the western Great Artesian Basin. Initial Cl^-/Br^- ratios taken from first sample collected along each transect. Locations are shown in *Love et al.* [2000]. δCl_H calculated assuming Cl_H = 5 000.

Bore number	Name	Distance (km)	TDS (mg L^{-1})	$^{36}Cl/Cl$ ($\times 10^{-15}$)	Cl^- (mg L^{-1})	Br^- (mg L^{-1})	Cl^-/Br^- (mass)	δCl_H (%)	Eqn. (13) (ka)	Eqn. (14) (ka)
North Transect										
574400015	Lambina Homestead	47	2334	129 ± 8	866	3.6	241	0.0%		
574400003	Warrungadinna	61	2916	132 ± 10	1130	4.4	257	8.3%		
574400004	Lambina Soak	71	2954	108 ± 7	1110	4.5	247	3.3%		
584300025	Marys Well 3	129	2039	102 ± 8	674	2.6	259	9.5%	58	60
584300026	Murdarinna 2	145	1923	109 ± 10	644	2.4	268	13.6%	47	14
594300017	Midway Bore	154	1899	89 ± 4	621	2.2	282	19.5%	160	84
594200001	Oodnadatta Town Bore 1	203	1902	52 ± 5	676	1.6	423	56.7%	380	150
604200021	Watson Creek 2	246	2623	25 ± 3	1040	2.3	452	61.6%	550	498
614200004	Duckhole 2	261	2228	31 ± 4	848	1.8	471	64.4%	540	361
South Transect										
574100007	CB Bore	6	1470	115 ± 8	530	2.1	252	0.0%		
574100014	Ross Bore	33	4035	54 ± 6	1620	5.7	284	15.0%		
574100049	Evelyn Downs Homestead	43	4087	54 ± 5	1420	4.7	302	22.0%		
584100053	Woodys Bore Windmill	67	5642	47 ± 5	2410	6.5	371	42.7%		
584100050	Robyns Bore 2	80	5596	41 ± 4	2440	6.8	359	39.7%	46	365
584100011	Ricky Bore 2	89	4997	37 ± 3	2070	6.6	314	26.1%	110	480
594100003	Paulines Bore	95	4452	40 ± 4	1700	4.8	354	38.4%	230	384
594100017	Nicks Bore	114	3960	46 ± 5	1460	4.2	348	36.6%	280	322
594100013	Leos Bore	136	3442	53 ± 5	1130	3.3	342	35.2%	320	261
594100006	Fergys Bore	141	2751	61 ± 1.2	940	2.9	324	29.6%	330	218
604100037	Lagoon Hill Drill Hole 15	183	2451	29 ± 3	937	2	469	61.7%	710	419

As Figure 5 illustrates, the proportion of ^{36}Cl systematically decreases as Cl^-/Br^- ratios increase along both transects. This indicates spatially or temporally variable Cl^- input may have occurred from one or more sources with elevated Cl^-/Br^- ratios and depleted $^{36}Cl/Cl$ ratios relative to recharge water. As vertical leakage has been discounted as a significant process along the western transects by *Love et al.* [2000], the trend in Figure 5 may be the result of diffusion of Cl^- and Br^- from the saline aquitard overlying the aquifer (with $^{36}Cl/Cl$ ratios reflecting secular equilibrium conditions), or the result of dissolution of temporally-variable quantities of wind-borne halite during recharge (with similarly depleted $^{36}Cl/Cl$ ratios).

Although determining which of these two scenarios is most probable is beyond the scope of this chapter, the potential impact of this input on measured Cl^- concentrations can be constrained using Equation (7). If the low Cl^-/Br^- ratio of groundwater at the start of the transect can be considered indicative of recharge water compositions prior to modification by halite dissolution, calculations (Table 4) show that halite dissolution could account for up to 64.4% of total dissolved Cl^- reported by *Love et al.* [2000].

This is important because the three $^{36}Cl/Cl$-based age models (e.g., Section 5.5 of *Love et al.* [2000]) applied in the GAB studies are founded on differing assumptions about the extent of dissolved Cl^- inputs, and use different approaches to correct $^{36}Cl/Cl$ ratios for these inputs. The first model assumes no Cl^- addition and $^{36}Cl/Cl$ ratios are taken at face value. The second model relies solely on ^{36}Cl concentrations, with no dependence on dissolved chloride concentrations or correction for external input. Only the third model (Equation (13)) corrects for chloride inputs, and therefore represents a scenario where dissolution of halite and evapotranspiration coincide during recharge.

$$t = -\frac{1}{\lambda_{36}} \ln \frac{Cl_m}{Cl_{ET}} \frac{(R - R_{se})}{(R_0 - R_{se})} \quad (13)$$

Here, λ_{36} is the decay constant for ^{36}Cl, Cl_m is the chloride concentration measured in a groundwater sample, Cl_{ET} is the estimated chloride concentration "governed by ET only and free of subsurface Cl addition", R is the $^{36}Cl/Cl$ ratio measured in groundwater samples along the transects, R_{se} is the $^{36}Cl/Cl$ ratio at secular equilibrium, and R_0 is the initial $^{36}Cl/Cl$ value.

The ages calculated by the three models used by *Bentley et al.* [1986] and [*Love et al.*, 2000] exhibit no systematic relationship and differ in magnitude by two to ten times for a given water sample. Therefore, for the GAB transects, groundwater age estimates are significantly influenced by the choice of age model. A temporal variability in halite dissolution is suggested by the ^{36}Cl and Cl^-/Br^- relationship in Figure 5. Accordingly, Equation (13) may best represent conditions along the western transects through the GAB while results from the other ^{36}Cl age models should be interpreted with a grain of salt. Furthermore, *Park et al.* [2002] noted the limitations of ^{36}Cl-based groundwater age determinations in saline environments: *"In models of simple flow regimes the ^{36}Cl method fails to predict groundwater age accurately where groundwater chlorinity exceeds ~75 – 150 mg kg^{-1}."*

When applying Equation (13), *Love et al.* [2000] set Cl_{ET} as the lowest dissolved Cl^- concentrations measured in the confined portion of each aquifer transect. One may alternatively calculate the Cl_{ET} term on a sample-by-sample using Cl^-/Br^- ratios to correct for possible halite inputs ($Cl_{ET} = \delta Cl_I \times Cl_m$). Groundwater ages for each sample along a given transect can then be recalculated (Equation (14)) by setting the lowest Cl^-/Br^- ratio (which happens to be the first sample) on each transect as the initial recharge condition (Table 4).

$$t = -\frac{1}{\lambda_{36}} \ln \frac{Cl_m (R - R_{se})}{Cl_I (R_0 - R_{se})} \quad (14)$$

As shown in Table 4, even when Cl^- input is identified, the choice of correction technique can result in significant discrepancies in tracer-based calculations. In this case, differences in corrected Cl^- values between Equations (13) and Equation (14) yield up to an eight-fold difference in estimated groundwater ages. Although no one method is suitable for every application, the equations presented here can be used to rapidly assess the potential extent of such inputs, and constrain the uncertainty they may introduce when using Cl^--based tracer techniques.

6. Conclusions

There may be increased uncertainty in the results from chloride-based geochemical tracer techniques if Cl^- contributions *via* mineral dissolution or mixing is not identified and quantified. In this chapter it was demonstrated that, under a range of conditions, Cl^-/Br^- ratios can be used effectively to differentiate between the inputs from various dissolved Cl^- and Br^- sources to a water undersaturated with respect to halide-bearing salts if the proportions of dissolved Cl^- and Br^- contributed by salt dissolution are considered rather than the absolute quantity. The resultant mathematical models provide a rapid method to identify and correct for the spatial or temporal variability of common dissolved Cl^- sources.

The equations presented here permit the differentiation of a solution's dissolved Cl^- concentration into the component inputs from processes such as mineral dissolution and/or binary mixing. This enables rapid calculation of correction factors (δCl_I) for total dissolved Cl^- concentrations which can be applied without a priori knowledge of the extent of evaporation, transpiration, mixing, or salt dissolution. Furthermore, accurate

δCl_I values may be determined in the absence of robust information on halite composition if the discrepancy between the Cl^-/Br^- ratios of the initial solution and dissolving halite can be inferred to be large (>10×), as is commonly observed in natural systems.

Given the prevalence of chloride-based tracer techniques and the range of environments where evaporation, transpiration, and salt dissolution occur, dissolved Br^- concentrations should routinely be measured to enable correction of dissolved Cl^- concentrations for external inputs using the methods presented here.

Chapter 3: Continental-scale variation in chloride/bromide ratios of wet deposition

Foreword

The following chapter is based on an article published in *Science of the Total Environment* [*Short et al.*, 2017]. Thus, there is some repetition in the introduction of this chapter and the rest of this thesis.

Most the work presented in the manuscript is my own. Patrice de Caritat provided the initial motivation and assistance with running the imputation algorithm with the wet deposition data. He also provided guidance with manuscript content and structure. Bear McPhail helped to review the imputation results, provided guidance on the manuscript structure and content, and assisted with editing.

1. Introduction

The cycling of chlorine (Cl) and bromine (Br) at the Earth's near-surface is central to the interests of atmospheric chemists and catchment hydrologists (e.g., climate variability, acid rain, water movement, carbon and nitrogen cycles, and pollutant cycling). Chlorine has an atomic number of 17, an atomic mass of ~35.5, one main and six minor oxidation states (–1 and 0, +1, +3, +4, +5, +7, respectively) [*Haynes*, 2015], an estimated upper continental crust concentration of ~370 μg g^{-1} [*Rudnick and Gao*, 2014], an estimated oceanic crust concentration of 20 – 2 800 μg g^{-1} [*Jambon et al.*, 1995], and a mean seawater abundance of 19 400 μg g^{-1} [*Millero*, 2014]. Bromine, by contrast, has an atomic number of 35, an atomic mass of ~79.9, five main oxidation states (–1, +1, +3, +5, +7) [*Haynes*, 2015], an estimated upper continental crust concentration of ~1.6 μg g^{-1} [*Rudnick and Gao*, 2014], an estimated oceanic crust concentration of 0.1 – 1.3 μg g^{-1} [*Jambon et al.*, 1995], and a mean seawater abundance of 67 μg g^{-1} [*Millero*, 2014]. Chlorine and bromine are enriched in Earth's hydrosphere relative to their crustal abundance by factors of up to 52 and 42, respectively, because they are highly volatile and exist predominantly as the highly soluble halides, chloride (Cl^-) and bromide (Br^-) [*Graedel and Keene*, 1996]. The ubiquity and near-conservative character of Cl^- and Br^- in the hydrosphere has meant that catchment hydrologists and aqueous geochemists have developed methods to utilise them as naturally occurring tracers of water and solute movement [*Davis et al.*, 1998; *Edmunds*, 1996; *Herczeg and Edmunds*, 1999]. The Cl^-/Br^- ratio – we have adopted mass-ratios unless explicitly stated otherwise; molar-ratios are a factor of 2.25 higher – has been found to be particularly useful because a wide range of values are observed in nature as a result of differences in the physico-chemical properties, redox behaviour, and natural abundance of the individual elements [*Davis et al.*, 1998]. As a result, scientists are able to utilise

variations in Cl^-/Br^- values of natural substances to throw light on various natural and anthropogenic processes such as delineating water flow, solute transport, mineral dissolution/precipitation and identifying pollution sources [*Davis et al.*, 1998; *Flury and Papritz*, 1993]. Furthermore, this ratio is also used to identify activation of reactive halogens, which efficiently destroy ozone molecules, in snowpack, sea ice and aerosols during ozone depletion events in the spring polar boundary layer of the Arctic and Antarctic [*Saiz-Lopez and von Glasow*, 2012; *Simpson et al.*, 2007; *von Glasow and Crutzen*, 2014].

Chlorine and bromine are two of the more reactive elements in the atmosphere despite occurring in only trace amounts (3.4×10^{-3} μg g^{-1} and 2.0×10^{-5} μg g^{-1}, respectively) [*Seinfeld and Pandis*, 2006]. Atmospheric halogen species (e.g., chlorofluorocarbons, halogen oxides and methyl halides) including those containing Cl and Br, are highly destructive to ozone molecules in the stratosphere [*Molina and Rowland*, 1974]. Halocarbons emitted through anthropogenic activity contribute to ozone destruction [*von Glasow and Crutzen*, 2014]; consequently, there have been numerous scientific studies undertaken to understand atmospheric halogen chemistry [e.g., *Daniel et al.*, 1999; *Keene et al.*, 1999; *McElroy et al.*, 1986; *Montzka et al.*, 1999; *von Glasow and Crutzen*, 2014] and there have been international actions (e.g., the 1987 Montreal Protocol) to minimise anthropogenic emissions of destructive chemicals [e.g., *Haas*, 1991]. As a result of the increased interest in the impacts of anthropogenic Cl and Br, these elements have also been found to be key components of natural elemental cycles of other more abundant atmospheric constituents such as nitrogen (N), carbon (C) and sulfur (S) [*von Glasow and Crutzen*, 2014].

A common natural source of Cl and Br to catchments and atmosphere is sea-salt aerosol (SSA) produced by breaking waves and bursting bubbles at the surface of

Earth's oceans [*Berner and Berner*, 1996; *Carroll*, 1962; *Sander et al.*, 2003; *von Glasow and Crutzen*, 2014]. Following SSA production, chemical reactions on the surface of SSA can result in the emission of gaseous Cl and Br species into the atmosphere [*Sander et al.*, 2003; *Vogt et al.*, 1996]. These reactions also alter the Cl^-/Br^- ratio of SSA relative to that of the ocean because they preferentially emit/retain one element over the other depending on SSA particle size and the presence of other gases [*Davis et al.*, 2004; *Sander et al.*, 2003; *Vogt et al.*, 1996]. For example, autocatalytic reactions that involve these halides have been observed to result in a greater loss of Br relative to Cl in super-micrometre-sized SSA particles [*Sander et al.*, 2003]. In contrast, Br can be enriched in sub-micrometre-sized SSA particles resulting in Cl^-/Br^- ratios that are lower than seawater [*Sander et al.*, 2003; *Virkkula et al.*, 1999]. The mechanism for Br enrichment in smaller SSA particles is unclear but *Davis et al.* [2004] hypothesised that it may be due to differences in polarisabilities of Cl and Br that have the potential to result in Br being enriched in smaller particles during aerosol production [*Jungwirth and Tobias*, 2002; *Virkkula et al.*, 1999; *Zhou et al.*, 1990].

The processes that modify Cl^-/Br^- ratios of SSA are also of interest to catchment hydrologists because many of the common applications for using the Cl^-/Br^- ratio as a hydrological or geochemical tracer require a robust knowledge of the composition of atmospheric solute sources. In many catchments, especially in arid and semi-arid environments, a major source of solutes is atmospheric deposition (e.g., wet and dry deposition) [e.g., *Appelo and Postma*, 2005; *Blackburn and McLeod*, 1983; *Carroll*, 1962; *Feth*, 1981; *Herczeg et al.*, 2001; *Herczeg and Edmunds*, 1999; *Nimz*, 1998; *Stallard and Edmond*, 1981]. However, the very low concentration of Br^- in atmospheric deposition (commonly below analytical detection limits that range from 50 to 5 $\mu g\ L^{-1}$) [e.g., *Crosbie et al.*, 2012; *Dogramaci et al.*, 2012; *NADP*, 2013] is a major

hindrance, which has resulted in very few regions having well-constrained Cl^-/Br^- ratios of atmospheric deposition. There are three noteworthy exceptions: 1) the Plynlimon region of Wales [e.g., *C Neal et al.*, 1990; *M Neal et al.*, 2007] where Cl^- and Br^- concentrations of precipitation have been used to identify solute sources in groundwater and streamflow, and as part of method comparisons; 2) Spain [e.g., *Alcalá and Custodio*, 2008a; *Alcalá and Custodio*, 2008b], where Cl^- and Br^- concentrations of atmospheric deposition have helped to delineate Cl^- sources and salinisation mechanisms in groundwater; and, 3) a small compilation (n = 168) of Cl^-/Br^- ratios of North American precipitation [*Davis et al.*, 1998] that cover various time-scales and collection methods, which was used to speculate about possible mechanisms for continental variations.

As an alternative to direct measurement of atmospheric deposition compositions, *Davis et al.* [2004] presented findings based on a survey of low-salinity groundwater (i.e., $Cl^- < 10$ mg L^{-1}) from sites across the United States. They found that Cl^-/Br^- ratios of low-salinity groundwater rapidly decreased from values similar to seawater at coastal locations (i.e., ~288) [*Millero*, 2014] to approximately 50 at sites located >1,000 km inland. The authors hypothesised that these observations were due to either a decreasing contribution of sea-salt aerosol (SSA) with distance inland and an increasing contribution of tropospheric aerosol (i.e., a ratio of ~50), or differences in the Cl^-/Br^- ratios of different sized SSA particles and the ability of different sized SSA particles to be transported inland from the coast [*Davis et al.*, 2004 and references therein]. Although the former is a plausible hypothesis, the large-scale variations of Cl^-/Br^- ratios of atmospheric deposition are likely to be a result of a complex combination of physical transport (i.e., weather patterns), atmospheric chemistry (i.e., aerosol surface reactions)

and additional natural (i.e., wild fires, biological emissions) or anthropogenic (i.e., fuel combustion, industrial emissions) sources.

Despite the increasing amount of available data for atmospheric deposition, Cl^- and Br^- compositions and general understanding of the chemistry of atmospheric Cl and Br, a continental-scale assessment of atmospheric deposition has not been possible because of a lack of spatially and temporally extensive datasets. In this study, findings are presented that are based on six and a half years of wet deposition compositional data collected at over 280 sites across North America. Like many previous datasets, there is a large proportion of Br^- censoring due to many samples having concentrations below detection levels, and we overcome this limitation by using the statistically robust compositional data technique of expectation maximisation to predict the likely spatial variation of these two ions in wet deposition across North America. The results of this study are important for interpreting catchment salt sources and constraining sources/sinks of atmospheric Cl and Br.

2. Data source

Data used in this study were supplied by the National Atmospheric Deposition Program (NADP). The NADP is a collaborative atmospheric deposition monitoring program run by various government and non-government agencies, universities, and private companies across the Americas [*Lamb and Van Bowersox*, 2000]. Data used in this study are for wet deposition samples collected by the NADP's National Trends Network (NADP/NTN) for the period June 2009 (when Br^- was added by the NADP as a routine analyte) through December 2015. The NADP/NTN includes weekly wet deposition collection sites located at 286 sites (Figure 6) across the USA (279), Canada (5), Puerto Rico (1), the Virgin Islands (1), plus one in Argentina, which was not

included in this study. The geographic information, data, photographs, etc. for the individual sampling sites can be sourced from the NADP's website (http://nadp.sws.uiuc.edu/data/sites/list/?net=NTN).

Between June 2009 and December 2015, data were reported for a total of 56 347 composite weekly samples that are considered valid (i.e., results of each routine analyte was reported, no contamination was noted, and rainfall amounts were recorded). The samples were collected using automated wet-only deposition samplers [*Dossett and Bowersox*, 1999], which remain closed to the atmosphere in the absence of precipitation and open after activation of a precipitation sensor. The number of weekly samples at individual sites ranged from 1 to 306, which was dependent on when sampling at a site was initiated/concluded, if precipitation occurred during the sampling period, and if contamination was suspected. Samples used in this study were analysed for Br^-, Cl^-, calcium (Ca), potassium (K), magnesium (Mg), sodium (Na), ammonium (NH_4^+), nitrate (NO_3^-) and sulfate (SO_4^{2-}). The detection limits for each of the analytes (Table 5) varied through the dataset depending on whether a sample was diluted prior to analysis and instrument performance. Bromide had the greatest censoring at 78.3% (Table 5), with all other analytes having a low proportion of censoring (i.e., ranging from Mg at 4.7% to SO_4^{2-} at <0.1%). The percentage of censored Cl^-/Br^- ratios (i.e., samples where Cl^- and/or Br^- are below detection levels) in the NADP dataset was also 78.3%.

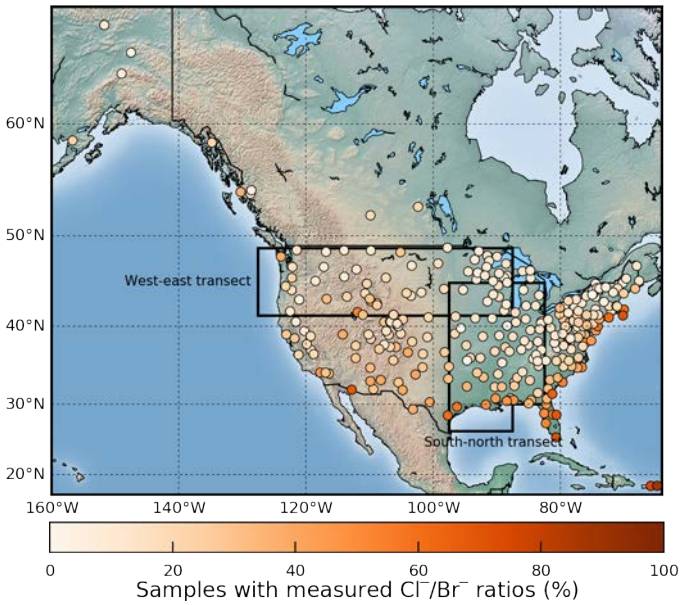

Figure 6: Location map of NADP/NTN sites included in this study. Symbol colours indicate the percentage of weekly wet deposition samples at each site with measured Cl^-/Br^- ratios. Polygons delineate the transects used in *Guelle et al.* [2001] and *Davis et al.* [2004].

Table 5: Number, percentage of censored samples for each analyte and Cl^-/Br^- ratios of weekly wet deposition, and detection limit range and mode (i.e., most common detection limit) at NADP/NTN sites. Total number of valid samples was 56 347.

Analyte	Censored samples (n)	Censoring rate (%)	Detection limit range (µg L^{-1})	Detection limit mode (µg L^{-1})
Br^-	44 118	78.3	5 – 33	5
Cl^-/Br^-	44 129	78.3	–	–
Mg	2 637	4.7	1 – 54	9
NH_4^+	2 057	3.7	6 – 190	16
Ca	1 578	2.8	4 – 165	27
Na	990	1.8	1 – 26	6
K	618	1.1	1 – 14	3
Cl^-	167	0.3	3 – 48	9
NO_3^-	82	0.1	5 – 94	5
SO_4^{2-}	4	<0.1	5 – 58	–

The data supplied by NADP are considered reliable because the NADP undergo regular scrutiny of their sampling methods and quality assurance of analytical methods used at their laboratory (Central Analytical Laboratory at the Illinois State Water Survey, Champaign, USA). Internal NADP quality assurance reviews [e.g., *Gartman*, 2014] have found that their data comply with reported targets for analytical precision,

reproducibility and blank concentrations [*NADP*, 2016]. External audits by the US Geological Survey have concluded that data collated as part of the NADP/NTN, "continue to be of sufficient quality for the analysis of spatial distributions and time trends of chemical constituents in wet deposition across the United States" [*Wetherbee and Martin*, 2014; *Wetherbee et al.*, 2014]. Recent NADP data (i.e., analyte concentrations and precipitation measurements) also show no significant biases when compared to the Canadian Air and Precipitation Monitoring Network, which have co-located samplers at three sites [*Wetherbee et al.*, 2010]. Readers are directed to the *Publications* page of the NADP's website (http://nadp.sws.uiuc.edu/lib/) for more information on the QA/QC procedures and the performance of the NADP's laboratory and field sampling methods, and *Gartman* [2014] for more information regarding the analytical techniques used at the Central Analytical Laboratory.

The geographic information and the mean and median wet deposition compositions for each site are presented in Appendix I.

3. Statistical methods

Censored Cl^- and Br^- concentrations of the wet deposition data were imputed using the *multRepl* and *lrEM* functions of the recently developed *R* statistics package, *zCompositions* (version 1.0.3 [*Palarea-Albaladejo and Martín-Fernández*, 2015]). The routines are named *multRepl* and *lrEM* because the former uses simple multiplicative replacement to imputed values, whereas the latter uses a log-ratio expectation-maximisation technique. The parameters used for the imputation of the NADP data are presented in Table 6.

Table 6: Input parameters used in this study to implement the *lrEM* and *multRepl* functions of the *zCompositions* R package (see text).

Function argument	*lrEM*	*multRepl*	Input
delta	default (0.65)	default (0.65)	-
rob	Yes	No	TRUE
ini.cov	Yes	No	complete.obs
tolerance	Yes	No	0.1
max.iter	Yes	No	50
rlm.maxit	Yes	No	150

The *multRepl* routine imputes censored values by simple multiplicative replacement of the reported detection limit. The default setting for the *multRepl* routine is to impute censored values at 0.65 times the reported detection limit. The *lrEM* routine imputes censored values with their expected values based on the covariance structure of the dataset after log-ratio transformation [e.g., *Aitchison*, 1982; *Pawlowsky-Glahn and Buccianti*, 2011]. This routine allows for the option of implementing MM-estimation (i.e., a maximum likelihood algorithm) for a robust, computationally efficient method [e.g., *Yohai*, 1987] of imputing censored values. This option was selected so that outliers in the NADP data had minimal impact on the results. To seed the algorithm under robust estimation conditions, an initial estimate of the covariance structure is required. The two options for this initial estimate are: 1) 'complete.obs', which uses the subset of the samples with no censored values for any analyte (11 496 samples for the NADP dataset); or 2) 'multRepl', which uses the *multRepl* (i.e., multiplicative replacement) routine to produce an initial estimate based on simple multiplicative replacement of the censored values. We use the results of the 'complete.obs' option because it is more reasonable to use measured values than using a fixed arbitrary proportion of the detection limit for the initial estimates (i.e., the 'multRepl' initial estimate method). Furthermore, the mean difference between imputed values calculated by the two methods was only 2.0% for Br^- and <0.1% for Cl^-. To satisfy the requirement of the algorithm that at least one analyte had measured values for all

samples, we removed the four samples from the NADP dataset that had censored SO_4^{2-} concentrations. Where only one measured analyte exists for a sample (i.e., SO_4^{2-}) the *lrEM* routine reverts to a simple multiplicative replacement with a default delta value of 0.65.

4. Results and discussion

4.1. Measured data

Measured Cl^- and Br^- concentrations, and Cl^-/Br^- ratios of wet deposition samples were inversely correlated with increasing distance inland (i.e., orthogonal distance) from the coast (Figure 7). This is consistent with numerous other studies that have found that the salinity of atmospheric deposition typically decreases away from coastal regions, especially the concentrations of seawater-derived ions (i.e., Cl^-, Br^-, K, Na and Mg) because of SSA 'washout' [*Carroll*, 1962; *Guelle et al.*, 2001; *Hutton*, 1976; *Junge and Werby*, 1958; *Keywood et al.*, 1997; *Vet et al.*, 2014]. The NADP data were also consistent with the small North American precipitation dataset that was presented *Davis et al.* [1998], the generalised envelope of which is shown in Figure 7.

The rate of censoring of Cl^-/Br^- ratios also had an inverse correlation with increasing distance inland from coast (Figure 6). The percentage of samples with censored Cl^-/Br^- ratios at sites <200 km from the nearest coastline was 68.1%, compared to 83.1% at sites >1 000 km from the nearest coastline. This observation is unsurprising given the generally low concentration of all analytes in wet deposition samples combined with the rapid decrease of the overall salinity of samples with increased distance inland. The spatial pattern is clear despite using orthogonal distance (i.e., does not account for topography or prevailing weather patterns), even though it might be expected to introduce noise.

The strong influence of SSA is further highlighted when measured Cl^- and Br^- concentrations of wet deposition are plotted (Figure 7). There are two distinct groups of samples on this plot. The first group includes the samples with Cl^- concentrations <1 mg L^{-1} and a wide range of Br^- concentrations (approximately 0.001 – 0.5 mg L^{-1}). The Cl^- and Br^- concentrations of these samples show no distinct bivariate relationship and they have Cl^-/Br^- ratios with a range of approximately 300 to <1. The sample locations in this first group are mainly >1 000 km inland; however, there are still many samples from sites located <200 km from the coast (Figure 7). The second distinct group on the Cl^- *vs.* Br^- plot is comprised of samples with Cl^- concentrations of >1 mg L^{-1} and the same range of Br^- concentrations as the first group (i.e., approximately 0.001 – 0.5 mg L^{-1}). Unlike the first group of samples, however, the Cl^- and Br^- concentrations of this second group generally had a distinct bivariate relationship, which is close to the seawater 288:1 ratio (Figure 7). The majority of samples in this group were collected from sites <200 km from the coast, and there were only a handful of samples from sites located further inland.

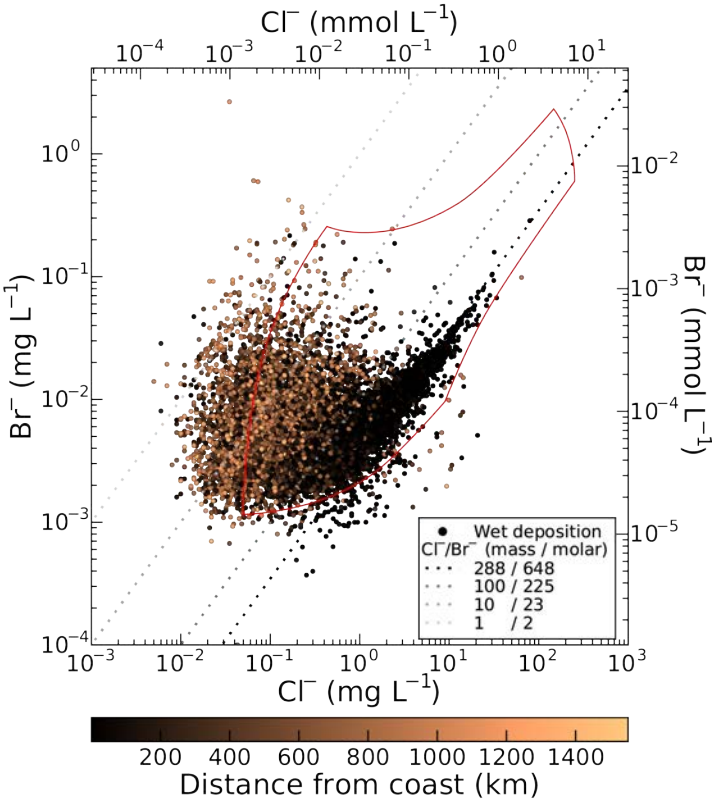

Figure 7: Measured Cl^- and Br^- concentrations (mass and molar) of weekly wet deposition samples collected at the 286 NADP/NTN sites between June 2009 and December 2015. Symbol colours indicate the orthogonal distance of the sample site from the nearest coastline. Lines of equal Cl^-/Br^- ratios are included for reference (dotted lines), including the seawater ratio (black dotted line). The red polygon delineates the generalised envelope that *Davis et al.* [1998] presented for their compilation of North American precipitation. Imputed values are not included.

These two features are also seen in the other seawater-derived ions/elements (Figure 8). Samples with higher ion or element concentrations tend to plot along the line of the seawater-like ratios, whereas samples with lower ion or element concentrations typically had no discernible bivariate relationship. Furthermore, a similar trend is observed for the geographic locations of the samples in these groups (i.e., samples displaying seawater-type ratios were generally collected <200 km from the coast and more inland samples deviate from it). The behaviours of Na and Cl^- were exceptions to this because they tend to act much more conservatively (i.e., there is much less

deviation from the seawater ratio) relative to the other seawater-derived ions across all sites. However, samples with low Na and Cl^- concentrations still deviate from the seawater-type ratio, albeit to much lesser degree compared to the other seawater-derived ions or elements.

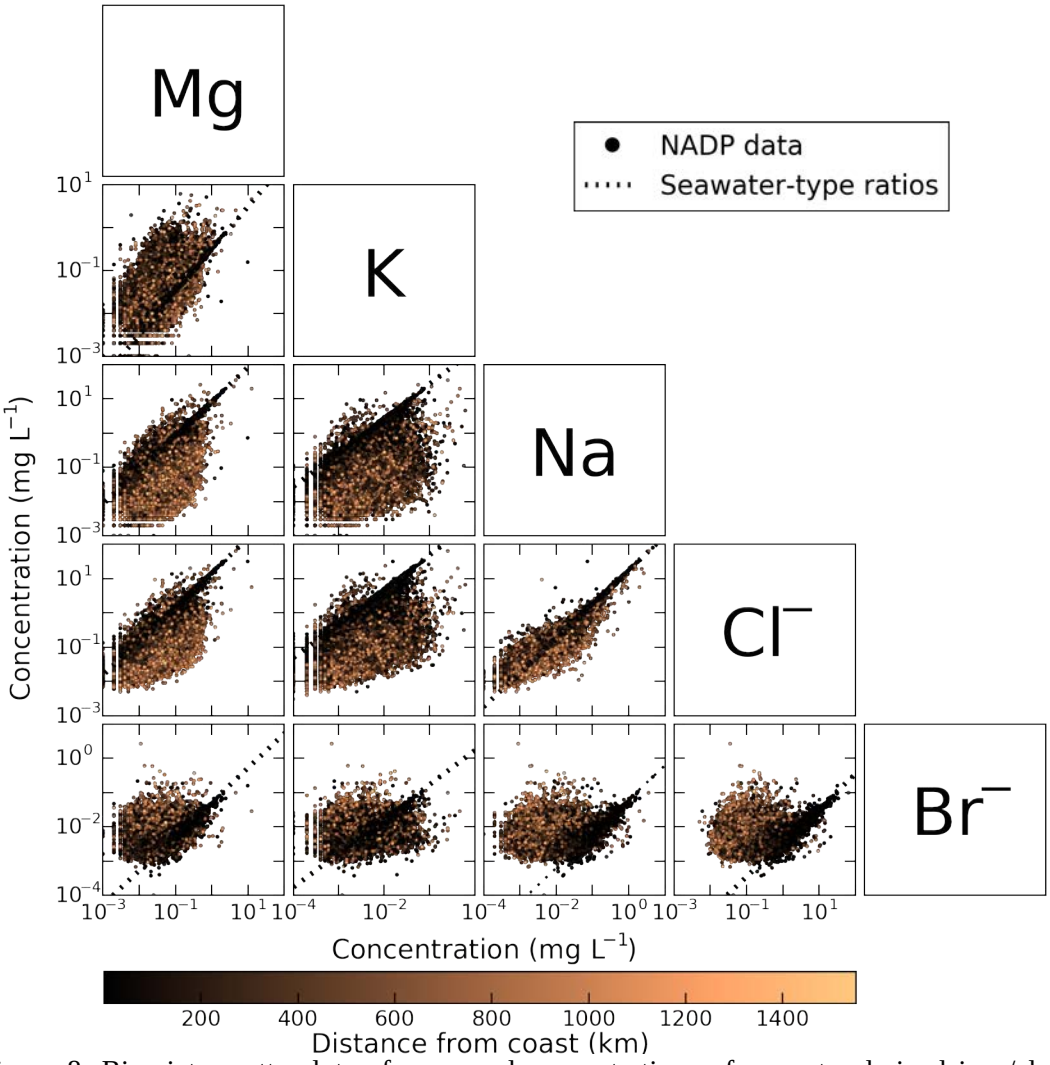

Figure 8: Bivariate scatterplots of measured concentrations of seawater-derived ions/elements for weekly wet deposition samples collected at the 286 NADP/NTN sites from June 2009 through December 2015. Black dashed lines represent the seawater ratios of ion/element pairs. Symbol colours indicate the orthogonal distance of the sample site from the nearest coastline. Imputed values are not included.

4.2. Imputation

Two sets of imputed data were produced using the *lrEM* and *multRepl* routines described above. Censored values were imputed for all analytes, not just Br^-, as a result

156 samples had imputed Cl^- and Br^- values. Hereafter, only the *lrEM* results are used because the *multRepl* results suffered from shortcomings, such as producing an artificially high frequency of Br^- concentrations of exactly 0.65 times the most common detection limit of 5 μg L^{-1}. An example artificial feature can be seen in Figure 9 where there is a clustering of Br^- concentrations at 5 μg L^{-1}, which have been produced because there was only one measured analyte for these samples or the *lrEM* routine failed to produce a stable result. The second shortcoming of the *multRepl* routine is that it uses an arbitrary multiplier rather than utilising the covariance relationships of the full available dataset. In addition, and even with the shortcomings, the *multRepl* results were broadly consistent with those calculated with the *lrEM* routine (even if the delta value was varied from 0.01 and 0.95; results not shown). We acknowledge that it is difficult to quantitatively assess the accuracy of the imputed values because only data with much less censoring (i.e., obtained with improved lower limits of detection), which are not yet available, will be able to show any underlying biases in the imputation method.

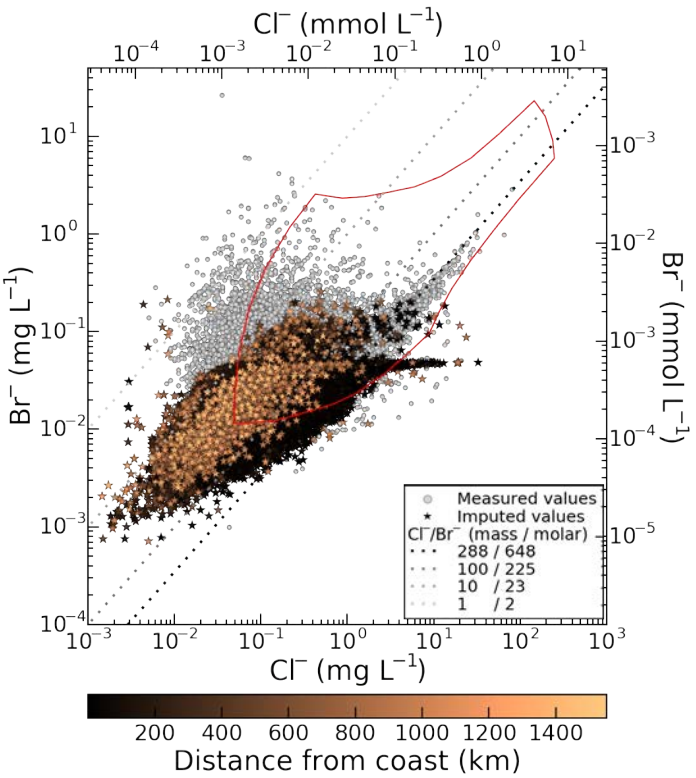

Figure 9: Measured (grey symbols) and imputed (solid symbols) weekly Cl^- and Br^- concentrations (mass and molar) of wet deposition collected at the 286 NADP/NTN sites between June 2009 through December 2015. Imputed values were calculated using the *lrEM* routine of the *zCompositions* package. Symbol colours indicate the orthogonal distance of the sample site from the nearest coastline. Lines of equal Cl^-/Br^- ratios are included for reference (dotted lines), including the seawater ratio (black dotted line).

4.3. Spatial trends

From here on, Cl^- and Br^- compositions of wet deposition are presented as wet deposition rates (i.e., kg ha^{-1}) instead of concentrations, and Cl^-/Br^- ratios are presented as deposition ratios (i.e., kg ha^{-1}/ kg ha^{-1}) not concentration ratios. This conversion was performed to account for precipitation amounts when discussing the statistical features of the dataset, which is not possible when using wet deposition concentrations because individual samples are given equal weighting even though they represent widely varying precipitation amounts (i.e., 0.25 – 366 mm $week^{-1}$). The deposition rates were

calculated using reported precipitation depths or, in the absence of depths, total sample mass and sampler intake diameter.

Mean Cl^-/Br^- ratios of wet deposition show a distinct spatial pattern when plotted against distance from the coast (Figure 10). The Cl^-/Br^- ratios of wet deposition at coastal sites (i.e., <100 km) are close to the seawater ratio but rapidly decrease with increasing distance from the coast. Further inland, Cl^-/Br^- ratios continue to decrease with distance inland but at a reduced rate. Logarithmic regressions produced the best fit to the mean Cl^-/Br^- ratios, and were fitted separately to both the measured-only values and the combined measured/imputed values. The coefficients for the regressions and r-squared values are listed in Table 7. The shape of the regression curves is similar for the measured-only values and the combined values; however, the regression based on measured-only values consistently produces Cl^-/Br^- ratios that are lower than those of the combined values (Figure 10). This is likely to be a result of bias from higher Br^- concentrations in the measured-only values (i.e., detectable concentrations), which leads to a bias from lower Cl^-/Br^- ratios. This observation provides confidence in our rationale for, and results from, the imputation because it suggests that the elevated measured concentrations exert a greater influence on calculated mean weekly compositions than the much lower censored values. However, it also indicates that the absolute values obtained by imputation techniques have produced values that are offset from the measured data and cannot currently be verified. Thus, the imputed data and regression should be used with caution and under the full understanding of their limitations until further data are available.

The *lrEM* imputation also produced compositions that are consistent with the data presented the low-salinity groundwater data in *Davis et al.* [2004], and the SSA deposition in *Guelle et al.* [2001] (Figure 11). Along the west-east transect (Figure 11a),

mean Cl^-/Br^- ratios of wet deposition decrease rapidly from values similar to seawater between 125°W and 115°W longitude, and then continue to decrease more slowly eastward until 87°W. Cl^-/Br^- ratios of low-salinity groundwater are also similar to seawater on the western side of the transect and decrease with distance east, albeit at a less rapid rate than the wet deposition compositions. Along the south-north transect (Figure 11b), the decrease in Cl^-/Br^- ratios with increasing distance is more consistent and follows a power-law trend. This pattern is matched by the decrease in sea-salt deposition reported in *Guelle et al.* [2001] and the shape of the trends are similar to the low-salinity groundwater data reported in *Davis et al.* [2004]. However, similar to the west-east transect, the rate of decrease in Cl^-/Br^- ratios of low-salinity groundwater is reduced relative to that of wet deposition and SSA deposition. A possible cause for the variation in the rates of decrease across the two transects is differences in precipitation patterns. Along the west-east transect, most of the precipitation, and subsequent 'washout' of larger SSA particles, occurs close to the western margin of the transect near the Cascade Range [*NOAA*, 2015]. In contrast, decrease in precipitation across the south-north transect is much more gradual and may account for lower rate in decrease in Cl^-/Br^- ratios of wet deposition.

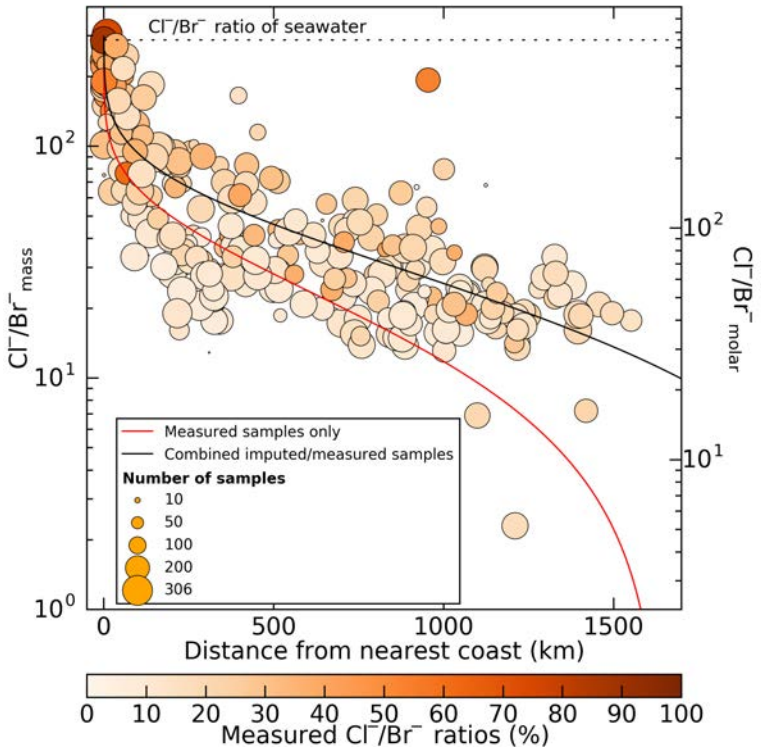

Figure 10: Mean weekly Cl^-/Br^- ratios of wet deposition calculated using a combination of measured and imputed (*lrEM*) values with distance from the nearest coastline. Circle colours and sizes indicate the percentage of measured Cl^-/Br^- ratios of wet deposition and number of weekly samples used to calculate the mean at each site, respectively. Lines represent best fits of values (in the form $y = a\ln(x) + b$); coefficients reported in Table 7 for the mean wet deposition data: the solid black line is the regression for the combined measured/imputed dataset (i.e., the plotted data), and the solid red line is for the measured-only data. The Cl^-/Br^- ratio of seawater is included for reference (horizontal dotted line).

Table 7: Coefficients and r-squared values for the logarithmic regressions (in the form $y = a\ln(x) + b$) fitted to the mean Cl^-/Br^- ratios of wet deposition in Figure 10.

Dataset	*a*	*b*	r-squared
Measured-only values	–23.55 ± 1.18	174.5 ± 5.7	0.588
Combined values (*lrEM*)	–29.52 ± 1.21	229.5 ± 6.9	0.676

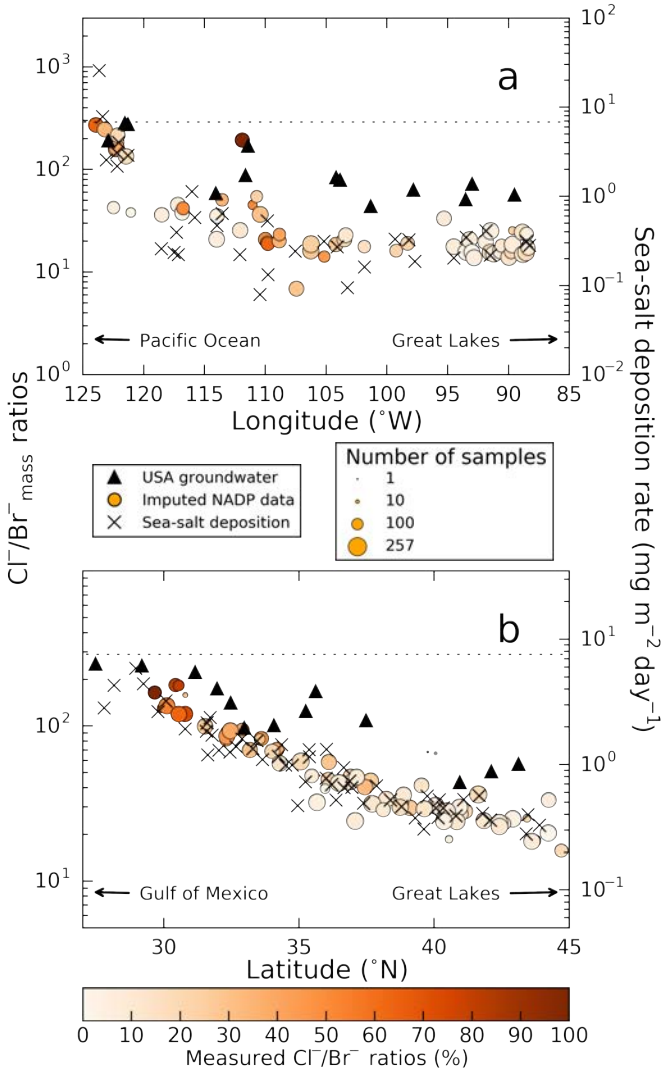

Figure 11: Variations in Cl^-/Br^- ratios of low-salinity groundwater (triangles) reported in *Davis et al.* [2004] and mean Cl^-/Br^- ratios of weekly wet deposition (including imputed values) presented in this study (circles) along the west-east (a) and south-north (b) transects shown in Figure 6. Cl^-/Br^- ratios are plotted with the sea-salt deposition rates (crosses) calculated by *Guelle et al.* [2001]. Circle colours and sizes indicate the percentage of measured (i.e., not imputed) Cl^-/Br^- ratios of wet deposition and number of weekly samples used to calculate the mean at each site, respectively. The Cl^-/Br^- ratio of seawater is included for reference (horizontal dotted line).

Although the pattern of variation of Cl^-/Br^- ratios was similar for wet deposition and low-salinity groundwater along both transects, the absolute values of imputed Cl^-/Br^- ratios of wet deposition are consistently less than the low-salinity groundwater

reported in *Davis et al.* [2004]. There are several possible explanations for the difference. One is that there may be a potential bias from the imputation methods as discussed previously, which may have produced artificially high Br^- concentrations, hence lower Cl^-/Br^- ratios. However, when imputed Br^- concentrations only are plotted against distance (data not shown), values do not appear to be biased towards higher values. A second explanation is anthropogenic contamination. For instance, sewage effluent, which has been found to have elevated Cl^-/Br^- ratios (i.e., intermediate between seawater and halite) because of the use of halite, in the form of table salt in cooking, and its subsequent discharge into sewage systems and potentially the environment [*Davis et al.*, 1998; *Katz et al.*, 2011; *Panno et al.*, 2006; *Vengosh and Pankratov*, 1998]. Although this is a possibility, the groundwater samples presented in *Davis et al.* [2004] were pre-screened to remove samples that displayed signs of anthropogenic contamination, such as elevated salinities and nutrient concentrations. Therefore, we do not believe that *Davis et al.* [2004] low-salinity groundwater data is displaying signs of sewage contamination. A third is that groundwater compositions may also be affected by solutes introduced by dry deposition [e.g., *Tyler et al.*, 1996], which the wet deposition samplers of the NADP and the data presented in *Guelle et al.* [2001] were specifically designed to exclude. Dry deposition, such as aeolian dust, commonly consists of aggregates of silicate minerals, organic matter and evaporite minerals such as halite (i.e., NaCl) [e.g., *Shiga et al.*, 2011; *Tyler et al.*, 1996], which have Cl^-/Br^- ratios much greater than seawater (typically >5000) because of the exclusion of all but trace amounts of Br^- from their crystal lattice [*Davis et al.*, 1998]. Thus, even a small contribution of dust to the solute load of the low-salinity groundwater would result in elevated Cl^-/Br^- ratios relative to wet deposition. Although the NADP data are collected such that dry deposition is avoided as much as possible, it

is near-impossible to completely exclude some dry deposition additions to the samples. Thus, non-sea-salt (NSS) Ca, Mg and K (as proxies for mineral contributions) are likely to provide a semi-quantitative assessment of dust contribution. We examined this possibility by calculating the NSS proportions of these elements, all relative to Na as a reference ion, of mean wet deposition at the NADP sites. Proportions of NSS Ca, Mg and K all increase with distance inland, suggesting that an increasing dust contribution is a plausible explanation. Furthermore, groundwater has been hypothesised to contain varying proportions of solutes derived from dry deposition in many regions based on isotopic and ion ratio data [*Appelo and Postma*, 2005; *Herczeg and Edmunds*, 1999; *Nimz*, 1998], and is likely to be responsible for some of the observed difference.

A map depicts the mean weekly wet deposition results (Figure 12), highlighting the spatial pattern in Cl^-/Br^- ratios of wet deposition. There is a distinct 'coastal rim' on the map where sites <100 km of the coast have elevated Cl^-/Br^- ratios that are similar to seawater. In contrast, the Cl^-/Br^- ratios of inland sites are greatly reduced and tend to decrease with increasing distance inland. Localised elevated Cl^-/Br^- ratios of wet deposition proximal to the Great Salt Lake appear to show a contribution of aeolian-derived solutes. A site at Logan (site UT01), which is proximal to the Great Salt Lake, Utah, has a much greater mean Cl^-/Br^- ratio (193) relative to other sites in this region. For example, the Murphy Ridge site (site UT08), located ~80 km east-southeast of the Logan site, and the Craters of the Moon National Monument site (site ID03), located ~240 km northwest of Logan, have mean Cl^-/Br^- ratios of 45 and 51, respectively. The Great Salt Lake is known for its economic deposits of halite on the surface of its lakebed [*Jones et al.*, 2009], and it has also been observed to emit large quantities of aeolian dust into the atmosphere of the local region [e.g., *Hahnenberger and Nicoll*, 2012]. As discussed previously, dust that includes even a small amount of halite in its

composition has the potential to increase the Cl^-/Br^- ratio of low-salinity water such as wet deposition because of the very high Cl^-/Br^- ratios found in halite. By applying the simple mixing/dissolution equation presented in *Horner et al.* [2017], and assuming a halite Cl^-/Br^- ratio of 1900 – 8700 [e.g., *Horner et al.*, 2017] and 'true' Logan wet deposition Cl^-/Br^- ratio of 48 (i.e., the mean of UT08 and ID03), it is possible that dust from the lakebed could account for 76 – 77% of dissolved Cl^- observed in wet deposition at Logan.

Large emissions of dust from inland salt lakes have also been observed in other regions such as North America [e.g., *Reynolds et al.*, 2007; *Zlotnik et al.*, 2012], Australia [e.g., *Blackburn and McLeod*, 1983; *Prospero et al.*, 2002; *Shiga et al.*, 2011], Africa [e.g., *Prospero et al.*, 2002], Asia [e.g., *Liu et al.*, 2011] and South America [e.g., *Prospero et al.*, 2002]. Thus, similar solute contributions to wet deposition can reasonably occur in these regions.

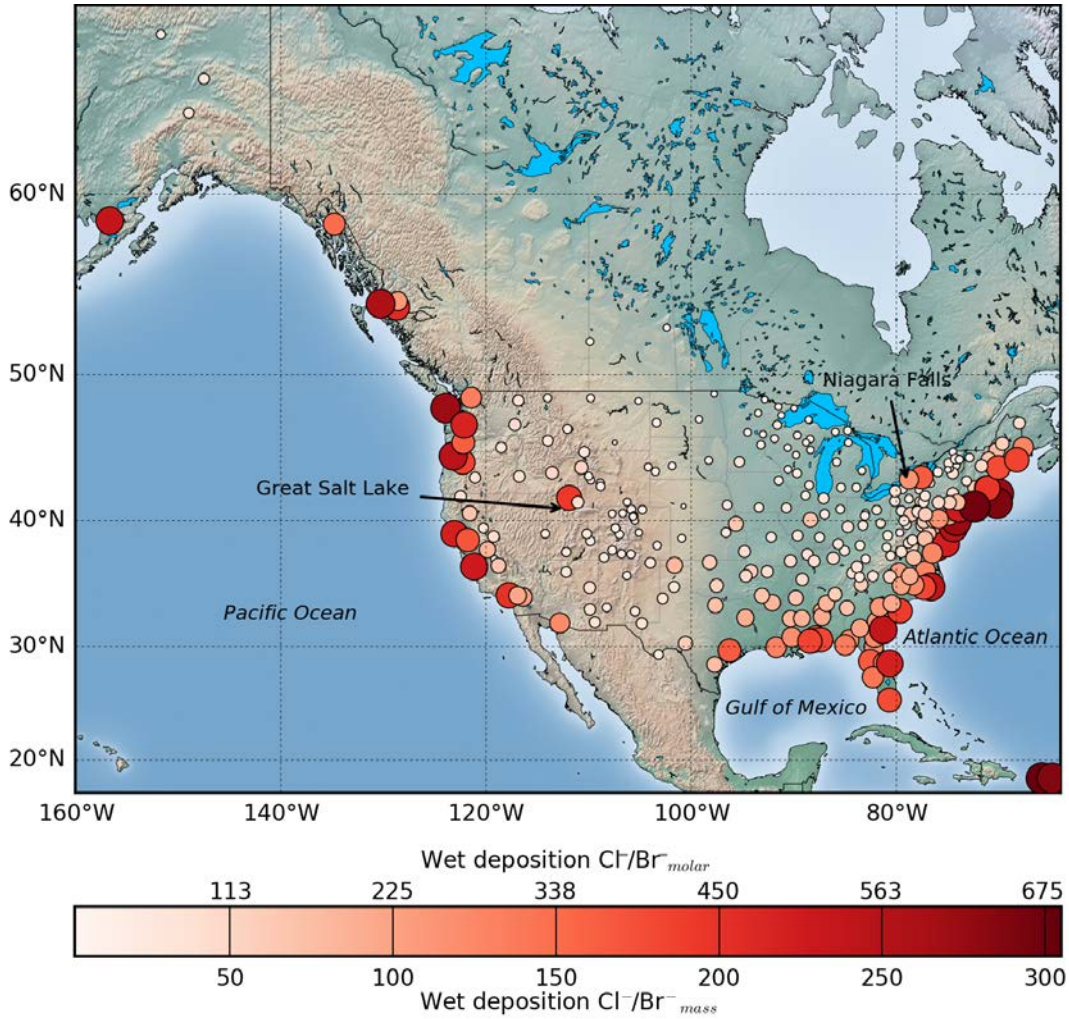

Figure 12: Dot map of mean weekly Cl^-/Br^- ratios of wet deposition calculated for NADP/NTN collection sites. Mean values include imputed and measured values. Symbol colours and sizes are proportional to mean Cl^-/Br^- ratios.

Aerosols emitted by spray droplets from the large, perennial Niagara Falls also appear to contribute to solute loads of local wet deposition, based on the high mean ratios of the two NADP sites that are closest to the falls (Figure 12). The Rochester (site NY43) and Amherst (site NY92) sites have mean Cl^-/Br^- ratios of 166 and 115, respectively. In contrast, the Chautauqua site (site NY10), located ~90 km southwest of Amherst, and Aurora Research Farm site (site NY08), located ~90 km southeast of Rochester, have mean Cl^-/Br^- ratios of 26 and 21, respectively. No literature currently exists regarding Niagara Falls as a potential source of atmospheric solutes to the surrounding region; however, Cl^- and Br^- concentrations of the Great Lakes surface

water, collected by researchers who have previously investigated pollution sources to the Great Lakes, display an increase in the Cl^-/Br^- ratio and Cl^- concentration along the surface flow path of the lakes [*Tiffany et al.*, 1969]. From upstream to downstream, the observed mean Cl^-/Br^- ratios of the lakes were 120 (Lake Superior; n = 12), 330 (Lake Michigan; n = 15), 280 (Lake Huron; n = 6), 670 (Lake Erie; n = 14) and 510 (Lake Ontario; n = 8). Niagara Falls lie between Lake Erie and Lake Ontario, which have the highest Cl^-/Br^- ratios of the Great Lakes. Widespread use of road salt (halite) during the winter months is a known pollution source and is likely to be responsible for the overall increase in salinity and Cl^-/Br^- ratios in the Great Lakes [e.g., *Eyles and Meriano*, 2010; *Eyles et al.*, 2013; *Tiffany et al.*, 1969]. The road salt is transported by surface runoff into the catchments surrounding the Great Lakes, as well as many of the catchments across the northern USA and much of Canada, and is subsequently discharged into the Great Lakes and emitted as soluble aerosol particles by the water falls. As a result, the mean Cl^-/Br^- ratios of wet deposition proximal to Niagara Falls appear to be affected by road salt pollution *via* spray droplets from the falls.

The logarithmic regressions discussed in section 4.3 (Figure 10 and Table 7) were recalculated with the three anomalous sites removed to evaluate the affect they have on the general spatial trend. However, the resulting coefficient changed only slightly (i.e., by less than the reported errors) for both the measured-only and combined datasets.

4.4. Enrichment factors

Enrichment factors (EF) were determined for Cl^- and Br^-, relative to their ratios to Na in seawater, in order to investigate the differences in behaviour of the two ions (e.g., preferential enrichment or depletion of one species over the other). The EFs are calculated by:

$$EF_X = \frac{(R_X)_{WD}}{(R_X)_{SW}} \qquad (15)$$

where *X* denotes either Cl^- or Br^-, and R_X is the X/Na ratio of wet deposition (*WD)* and seawater (*SW),* respectively. Mean EFs were determined for each site (Figure 13) using the mean weekly Cl^- or Br^- wet deposition rates (i.e. kg ha^{-1}), which include *lrEM*-imputed data.

The calculated EFs indicate that the variation in Cl^-/Br^- ratios of wet deposition appear to be mostly due to an enrichment in Br^- relative to Cl^-; inland sites have EF_{Br}- up to 10 compared with a mean EF_{Cl}- of ~0.8. The opposing directions of enrichment/depletion (i.e., EF_{Br}->1 and EF_{Cl}-<1) also help to increase the inland variation in Cl^-/Br^- ratios of wet deposition.

Enrichment of Br^- is consistent with the hypothesis of *Davis et al.* [2004], i.e., decreasing Cl^-/Br^- ratios with inland distance for low-salinity groundwater is likely to be caused by smaller SSA particles, which have been found to be more enriched in Br^- relative to Cl^- [e.g., *Sander et al.*, 2003; *Virkkula et al.*, 1999], being transported further inland than larger particles. However, as mentioned earlier, there are other potential processes that may affect the ratios (e.g., weather patterns, chemical cycling, and additional natural or anthropogenic sources). It is not possible to distinguish the individual effects with the currently available data.

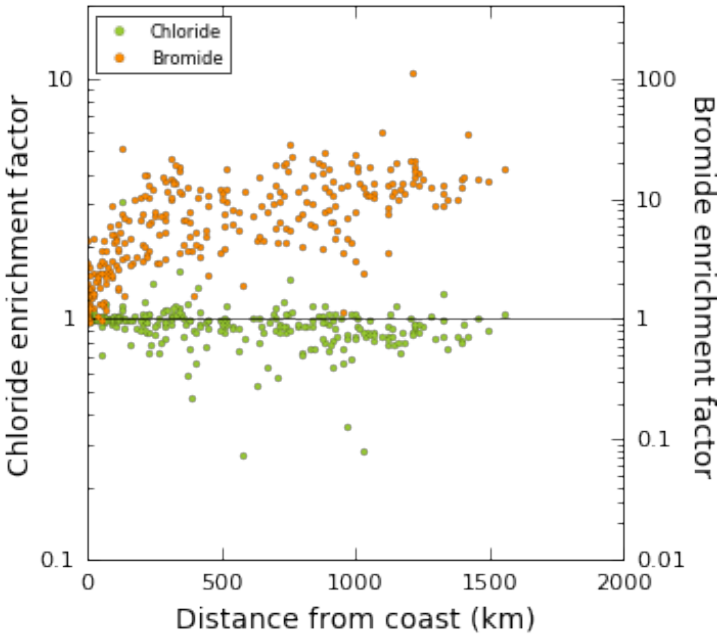

Figure 13: Enrichment factors (relative to seawater) for mean Cl^- and Br^- compositions of wet deposition (including imputed data) of NADP sites with distance from the coast.

4.5. Temporal patterns

The imputed (*lrEM*) results were also grouped seasonally and by distance (<200, 200 – 1,000 and >1,000 km from a coastline) to investigate temporal differences in weekly Cl^- and Br^- wet deposition rates, and Cl^-/Br^- ratios of weekly wet deposition samples (Figure 14). The means of all seasonal subsets for each of the three distance ranges were significantly different from each other (i.e., $p<0.05$ using unequal variances *t*-tests) except for winter and autumn weekly Cl^- wet deposition rates for the distance intervals of <200 and 200 – 1,000 km (i.e., no significant differences; $p>0.05$). Weekly Cl^- and Br^- wet deposition rates were observed to have similar temporal patterns (Figure 14a and Figure 14b), namely that wet deposition rates were typically more elevated during the spring and summer months, and lower during the autumn and winter months. However, the difference between seasons of greatest and lowest wet deposition was greater for weekly Br^- wet deposition rates than it was for Cl^-. Weekly Br^- wet deposition rates varied throughout the year by factors of 1.6, 2.5 and 7.1, compared to

weekly Cl^- wet deposition rates, which varied throughout the year by factors of 1.5, 1.6 and 4.5 for the distance ranges <200, 200 – 1 000 and >1 000 km, respectively. These results also indicate that the seasonality is more pronounced with increasing distance inland. Because of the observed variation in magnitude of the seasonality of Cl^- and Br^- wet deposition, Cl^-/Br^- ratios of weekly wet deposition also displayed seasonality (Figure 14c). The Cl^-/Br^- ratios of wet deposition were greatest during the winter months and lowest during the summer months. Unlike Cl^- and Br^- wet deposition rates, the absolute variation in Cl^-/Br^- ratios of wet deposition decreased with distance inland from the coast, with Cl^-/Br^- ratios of wet deposition varying throughout the year by factors of 2.1, 1.9 and 1.6 for the distance ranges <200, 200–1 000 and >1 000 km, respectively.

A possible explanation for the elevated deposition rates of Cl^- and especially Br^- is through transport and re-deposition of atmospheric halogen species activated during 'bromine explosion' events during the polar spring, where photochemical reactions activate particulate Br species, and to a lesser degree Cl, at the surface of snow, ice and water in polar regions during the spring [*Biegalski et al.*, 1997]. *Biegalski et al.* [1997] found that Br concentrations in aerosol collected at a site north of Lake Huron exhibited a high during March, and used back trajectory modelling to identify the source air as coming from the Arctic. Thus, the elevated wet deposition of Br^- during the spring and summer, and to a lesser degree increase in wet deposition of Cl^-, at inland sites may represent long-range transport of halogen species produced in the Arctic boundary layer. Other potential sources that could explain the greater increase in the wet deposition of Br^- compared to Cl^- in the spring and summer months could be emissions of methyl bromide by wildfires, emissions from pesticide use during growing season (under a Critical Use Exemption because of restrictions of the Montreal Protocol) or

through natural emissions from salt lakes and marshes [*EPA*, 2016; *Manö and Andreae*, 1994; *Rhew et al.*, 2014; *Stutz et al.*, 2002].

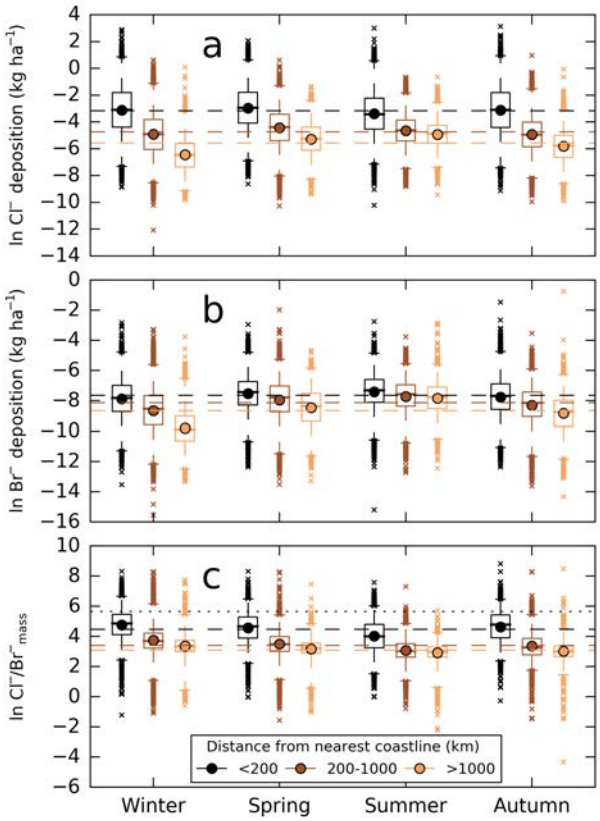

Figure 14: Box and whisker plots of seasonal variation of weekly wet deposition rates of Cl^- (a) and Br^- (b), and mean weekly Cl^-/Br^- ratios of wet deposition (c) at the 286 NADP/NTN sites between June 2009 through December 2015. Data include imputed (*lrEM*) values. Symbol colours indicate the distance of the sample site from the nearest coastline, horizontal dashed lines indicate annual means, and the horizontal black dotted line indicates the seawater ratio (c only). Box ranges are from the 1st to the 3rd quartile and whisker ranges are from the 1st to the 99th percentile.

4.6. Environmental implications

The spatial patterns presented here will provide catchment scientists with a much greater understanding of the likely Cl^-/Br^- ratio of wet deposition for different regions across the USA. The logarithmic regression presented in Figure 10 and coefficients reported in Table 7 provide a useful tool to estimate of Cl^-/Br^- ratios of wet deposition

at a given distance from the coast in the absence of site-specific data. The Great Lakes region provides a useful example of where this information can be utilised. As discussed previously, it has long been established that runoff containing dissolved road salt is contributing to increasing salinity in the lakes. If a mean Cl^-/Br^- ratio of Lake Ontario was assumed to be 49 (obtained using a distance of 450 km in the logarithmic regression fitted to the combined dataset; Table 7) then it can be seen that road salt pollution has resulted in a ten-fold increase Lake Ontario's Cl^-/Br^- ratio (~510). These end-member values can then be used in modelling to predict the total solute load contributed by road salt pollution in this region. For example, if the above ratios are assumed, along with a generalised road salt Cl^-/Br^- ratio range of 1900 – 8700 [e.g., *Horner et al.*, 2017], a simple Cl^-/Br^- ratio mixing calculation presented in *Horner et al.* [2017] estimates that approximately 90 – 92% of Cl^- dissolved in Lake Ontario exists as a result of road salt pollution.

These findings will also have implications for catchments that are located near coastlines that are highly responsive to sea-level variations (i.e., those with shallowly sloping coastal bathymetry). Given that the majority of Earth's groundwater is found to have recharge ages that are pre-modern (i.e., >50 years) and commonly >10 000 years in semi-arid and arid regions [e.g., *Cook and Herczeg*, 1999; *Gleeson et al.*, 2015; *Phillips*, 2013], it is likely that Cl^-/Br^- ratios of groundwater in such catchments will be a mixture of water recharged during times when the catchment was near and far from a coastline. In well-mixed systems, this may limit the quantitative use of Cl^-/Br^- ratios for investigating solute budgets over long timescales because of difficulty in assessing variations in the timing and fluxes of incoming solutes. However, in poorly-mixed systems, Cl^-/Br^- ratios of groundwater may be able to be used effectively with other groundwater tracers to investigate palaeohydrological processes.

The spatial patterns in Cl^-/Br^- ratios of wet deposition are significant for more than just the application of Cl^-/Br^- ratios in North American catchments because similar spatial variations of the rate of sea-salt deposition have been observed [e.g., *Ballance and Duncan*, 1985; *Mahalinganathan et al.*, 2012] or predicted [e.g., *Fan and Toon*, 2011; *Vet et al.*, 2014] over other Earth landmasses. Therefore, it is likely that the spatial variations in Cl^-/Br^- ratios of wet deposition observed across North America is repeated over other continents. The absolute change in the Cl^-/Br^- ratio atmospheric deposition for the other continents will have their own unique spatial and temporal patterns depending on regional weather patterns, atmospheric chemistry, and site-specific landscape features or industrial areas that have the potential to act as a source of Cl^-- or Br^--bearing aerosol to the lower atmosphere.

5. Conclusions

We have presented findings of the first continental-scale assessment of the spatial variations in Cl^-/Br^- ratios of wet deposition. Our results rely, in part, on imputing censored data, due to many Br^- concentrations reported as below detection; however, the Cl^-/Br^- ratios of wet deposition across North America decrease systematically from values similar to seawater near the coast to values of more than a factor of 20 less than the seawater ratio at inland sites. These observations are consistent with a previous survey of the variations in Cl^-/Br^- ratios of low-salinity groundwater [*Davis et al.*, 2004] and a small compilation for precipitation across the USA [*Davis et al.*, 1998], suggesting that the composition of these ions/elements in groundwater are strongly associated with wet deposition but may also include a component of aeolian solutes at inland sites. The variations seem to be closely associated with variations in SSA deposition rates and the atmospheric physico-chemical processes that affect Br

compositions in SSA during production and inland transport. However, seasonal variations that act to increase Br^- wet deposition more than Cl^- at inland sites suggest that the variations may also be partly caused by Br^- contributions from other source than SSA, such as Artic air-masses, wildfires, natural emissions or pesticide applications.

Our findings should serve as a caution to scientists who utilise this ratio to investigate catchment hydrogeochemical processes, mainly because catchments located further than ~100 km from a coastline are likely to be receiving atmospheric deposition that has a Cl^-/Br^- ratio that is considerably less than the seawater ratio. In the absence of site-specific data, in North America, the regression:

$$\left(\frac{Cl^-}{Br^-}\right)_{wet\ deposition} = -29.52 \times \ln(km) + 229.5 \qquad (16)$$

can be used to estimate the mean Cl^-/Br^- ratios of wet deposition. Distance, *km*, used in Equation (16) is the orthogonal distance from the coast.

The increase in available data being accumulated for Cl^- and Br^- concentrations of atmospheric deposition by the NADP will continue to extend our knowledge of changes in Cl^-/Br^- ratios and increase the ability to use this ratio quantitatively in North American catchments. Furthermore, new techniques such as stable halogen isotope ratios (i.e., $\delta^{37}Cl$ and $\delta^{81}Br$), which have been used to identify solute sources in a range of environments [e.g., *Eggenkamp*, 2014], may help to identify the processes that are contributing to the spatial variations in Cl^-/Br^- ratios of atmospheric deposition.

Chapter 4: The Lake George Basin

The aim of this chapter is to provide readers with a thorough background about the unique geologic, hydrologic and palaeoenvironmental processes of the Lake George Basin, which make it attractive for applying chlorine and bromine tracer techniques to better understanding its salt cycling history. The chapter begins with descriptions of the environmental features of saline lakes, such as Lake George, that make them important for understanding terrestrial salt cycling.

1. Saline lakes

Saline lakes are landscape features that occur on all of Earth's continents and they play a crucial role in biogeochemical cycling and salinity regulation in the environments in which they appear [*Deocampo and Jones*, 2014; *Rosen*, 1994]. The hydrogeochemistry of saline lakes is of interest to earth and environmental scientists because it can throw light on the meteorological (i.e., rainfall, evaporation and weather patterns), geological (i.e., tectonic, hydrothermal and sedimentary environments), biological (i.e., land cover and production), and hydrological (i.e., surface and subsurface) conditions and histories of their local and regional environments. In the context of coastal saline lakes, hydrogeochemical compositions can assist with determining the timing and duration of coastal inundation, sea-level variation, and tectonic movement by assessment of evaporite mineral assemblages [e.g., *Warren*, 2010; 2014]. However, the hydrogeochemistry of coastal saline lakes is dominated by the ionic composition of seawater, which makes it difficult to discern information about alternate solute sources or subtle geochemical processes. In contrast, the hydrogeochemistry of continental saline lakes is much more sensitive to variations in drainage lithology, biology, atmospheric inputs (i.e., wet and dry deposition) and hydrothermal activity [*Deocampo and Jones*, 2014; *Warren*, 2010]. This sensitivity to

the local environments enables continental saline lakes to act as natural laboratories where researchers can gain valuable information about geologic and climatic processes [*Eugster and Jones*, 1979].

In the following sections, continental saline lakes – particularly Australian saline lakes – are focussed on because of the field site investigated in later chapters of this thesis.

1.1. Australian saline lakes

The landscape of Australia's arid and semi-arid interior is typified by the occurrence of numerous large inland saline lake systems. Some of the most notable Australian saline lake provinces are those located within the 'Wheatbelt' of Western Australia, the large endorheic basins of central Australia, and the central Murray-Darling Basin [*Bowler*, 1981]. However, many other significant saline lake systems occur across the arid interior of mainland Australia, and even in the cooler climate of Tasmania [e.g., *De Deckker and Williams*, 1982]. These large, mostly dry, lakes have been known for decades to be important for numerous palaeoenvironmental [*Torgersen et al.*, 1986], economic [*Mernagh*, 2013; *Williams*, 1981], hydrogeological [*Macumber*, 1991], ecological [*De Deckker*, 1983] and cultural [*Williams*, 2002] reasons. Research into Australia's saline lakes reached a peak during the 1980s and 1990s when the Salt Lakes, Evaporites and Aeolian Deposits (SLEADS) project was active at the Australian National University [*Chivas and Bowler*, 1986]. The researchers involved in this project published work that is still being used today as a benchmark by international researchers for expanding the conceptual and quantitative understanding of the geological, meteorological and ecological evolution of saline lakes [e.g., *Burrough et al.*, 2009; *Deocampo and Jones*, 2014; *Kohfeld et al.*, 2013; *Sim et al.*, 2006].

A recent investigation by Geoscience Australia into Australia's saline lakes has again highlighted their mineral resource and economic value for deposits such as potash, halite, boron, lithium and uranium [*Mernagh*, 2013; *Mernagh et al.*, 2016]. Moreover, this recent work has made it clear that research into Australia's saline lakes could benefit greatly from further research using modern techniques. One key recommendation in *Mernagh* [2013] was to work towards a better understanding of the hydrogeochemical processes that occur within and proximal to saline lakes. The authors noted that this aspect was one of the key components for properly understanding the potential resource significance of these lakes. In addition to resource significance, it has been found that constraining hydrogeochemical pathways around saline lakes is vital for understanding how saline lakes affect nearby land and water resources [e.g., *Bowler*, 1986; *Deocampo and Jones*, 2014; *Lyons et al.*, 1995; *Macumber*, 1991; *Rosen*, 1994].

1.2. Hydrogeochemical development of saline lakes

The development of saline lakes is primarily controlled by three key geomorphologic and climatic features, as defined in *Deocampo and Jones* [2014]. Firstly, outflow from saline lake basins is typically absent or severely restricted, such that evaporation is the primary means of discharge. This condition is typically observed in areas of current or past tectonic or volcanic activity (e.g., Lake Eyre, Lake George, Caspian Sea, Dead Sea and Great Salt Lake) where established drainage systems are altered or impeded by significant landscape alterations. Secondly, evaporation typically exceeds inflow from rainfall, streams and groundwater for at least half of the year. This condition is observed in the semi-/arid interiors of many of the large continents (e.g., Australia, Asia and the Americas). Thirdly, sufficient inflow into saline lake basins by rivers or groundwater should be able to maintain a surface water body, at least intermittently. Consequently, saline lakes rarely occur in the extremely arid interiors of

deserts because very low annual rainfall and recharge cannot sustain any permanent, or even ephemeral, water bodies. *Bowler* [1981] also noted that the ratio of a basin's catchment area to its lake area (Ac/Al) is a strong determinant of whether or not a saline lake will contain water (Figure 15). Bowler related the Ac/Al ratio to a climate function (*FC*), which is defined by:

$$FC = \frac{0.8E - P}{Pf} + 1 \qquad (17)$$

where E is annual pan evaporation (L, e.g., mm; converted to open-water evaporation using a generalised factor of 0.8), P is annual precipitation (L, e.g., mm) and f is the basin's runoff coefficient (i.e., the proportion of rain that reaches the lake as runoff). The hydrologic threshold in Figure 15 is defined as a lake in steady state – lakes that fall to the left of the line are permanent lakes and lakes that fall on the right of the line are dry lakes. Lakes with higher Ac/Al ratios tend to be permanent water bodies under a range of different climatic conditions except in very arid regions. As the Ac/Al ratio of a lake decreases, permanent surface water can only be maintained under increasingly humid conditions. Figure 15 illustrates this relationship with reference to several of Australia's saline lakes.

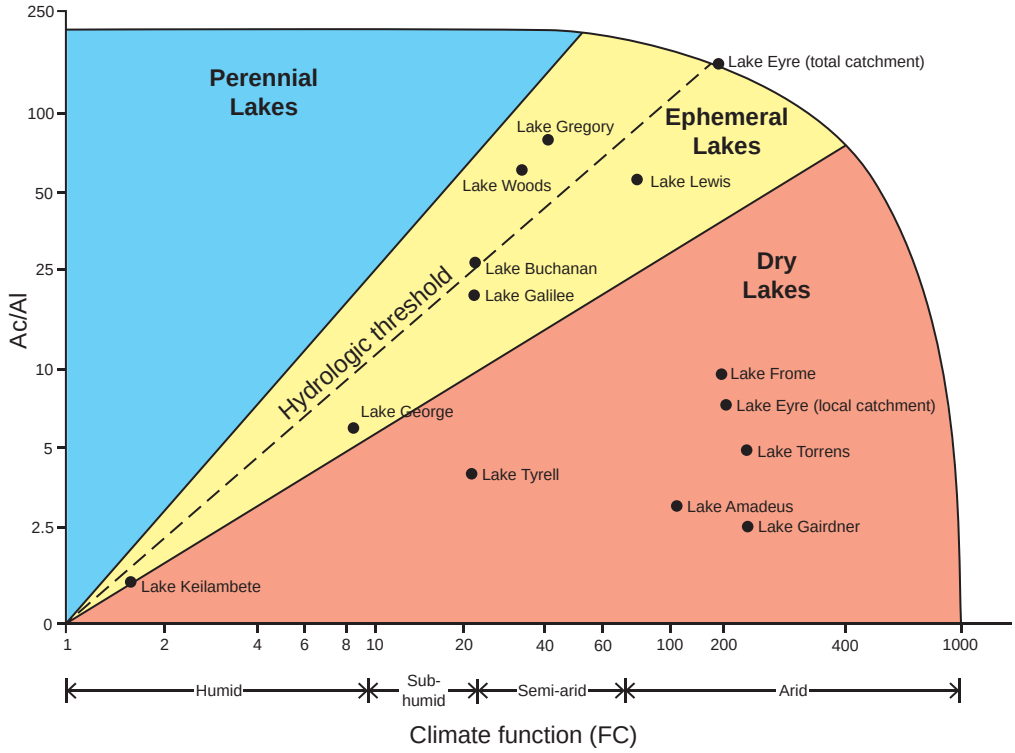

Figure 15: Relationship between the ratio of catchment area to lake area (Ac/Al), climate function and hydrologic conditions. Reproduced and modified from *Mernagh* [2013].

Saline lake basins can receive solutes from a wide range of different sources such as atmospheric deposition, surface water inflow, groundwater inflow or hydrothermal activity (Figure 16). The absence or presence of sources, and the variations in source geochemistry, gives each saline lake system a very distinct geochemical signature and evolutionary pathway [*Deocampo and Jones*, 2014]. Of the pathways depicted in Figure 16, atmospheric deposition and mineral weathering are the dominant solute sources [*Deocampo and Jones*, 2014]. Atmospheric deposition (i.e., precipitation and aerosols) contributes a large proportion of total salinity in many catchments [*Blackburn and McLeod*, 1983; *Crosbie et al.*, 2012; *Deocampo and Jones*, 2014; *Junge and Werby*, 1958]. Solutes derived from the atmosphere are not only deposited directly on to the lake surface, but are also carried by discharging streams and groundwater. Continental rainfall typically exhibits seawater-type ion signatures (e.g., Na^+/Cl^- = 0.56, Cl^-/Br^- = 288 by mass [*Millero*, 2014]) because marine aerosols are the primary contributor to the

solute composition of precipitation [e.g., *Blackburn and McLeod*, 1983; *Junge and Werby*, 1958]. However, continental chemical signatures derived from dust may be dominant in atmospheric deposition in regions proximal to sources such as saline lakes or deserts, and regions far from coastlines [*Junge and Werby*, 1958; *Shiga et al.*, 2011].

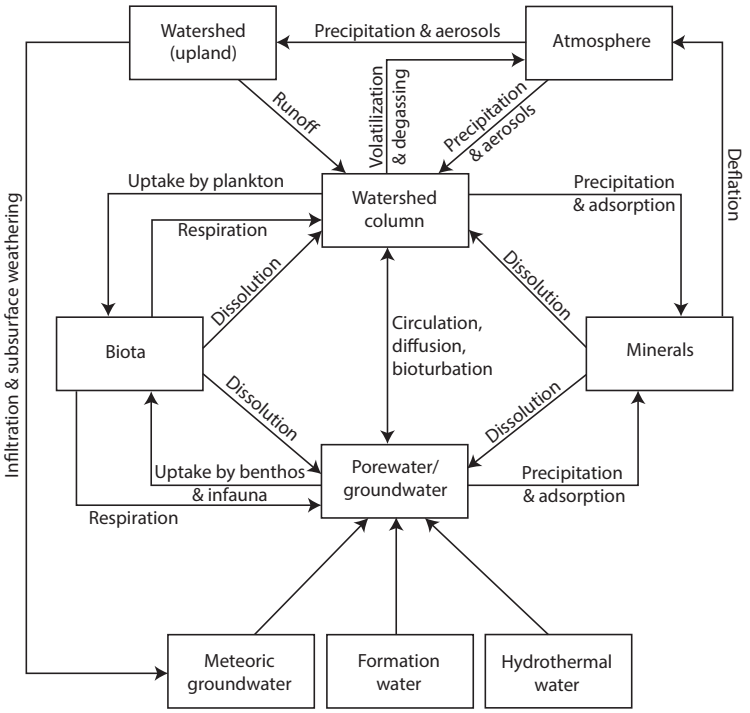

Figure 16: Schematic of the potential solute sources and pathways in a saline lake system. Reproduced from *Deocampo and Jones* [2014].

The other dominant source of solutes to saline lake basins is mineral weathering. This solute source can be an even more dominant source than atmospheric deposition depending on the susceptibility of the catchment lithology to weathering and the residence times of surface water and groundwater [*Deocampo and Jones*, 2014]. Mineral weathering contributes solutes of widely varying compositions due to variations in catchment lithology. This process is primarily responsible for the wide range of water types found in saline lake basins [*Deocampo and Jones*, 2014; *Eugster and Jones*, 1979]. The major ions contributed by mineral weathering are commonly the

alkali and alkaline-earth metals (Na^+, K^+, Mg^{2+} and Ca^{2+}), bicarbonate/carbonate and silica [*Appelo and Postma*, 2005].

Like most hydrologic systems, the composition of saline lake basins is dominated by only a few major ions including Na^+, K^+, Ca^{2+}, Mg^{2+}, Cl^-, SO_4^{2-}, HCO_3^-, CO_3^{2-} and SiO_2 [*Deocampo and Jones*, 2014]; however, the relative abundance of these solutes can be significantly altered by processes such as evaporation, biological activity and mineral dissolution/precipitation (Figure 16). Evaporation acts to concentrate ions in the residual water and may cause various evaporite minerals to precipitate at different stages of evapoconcentration [*Deocampo and Jones*, 2014; *Eugster and Jones*, 1979]. Alkaline-earth carbonates, such as calcite and aragonite, are the first minerals to precipitate, followed by sulfates, sodium carbonates and chlorides. However, different evolutionary pathways, known as 'chemical divides', are followed depending on the initial water composition [*Eugster and Jones*, 1979]. Figure 17 illustrates an idealised case of brine evaporation in a closed-system (loosely analogous to a terminal lake) showing brine composition and precipitation products of different water types. The distinct chemical divides during brine evolution produce diagnostic mineral assemblages in saline lake evaporite deposits, which can enable researchers to determine past and present solute sources to saline lakes [*Deocampo and Jones*, 2014; *Eugster and Jones*, 1979].

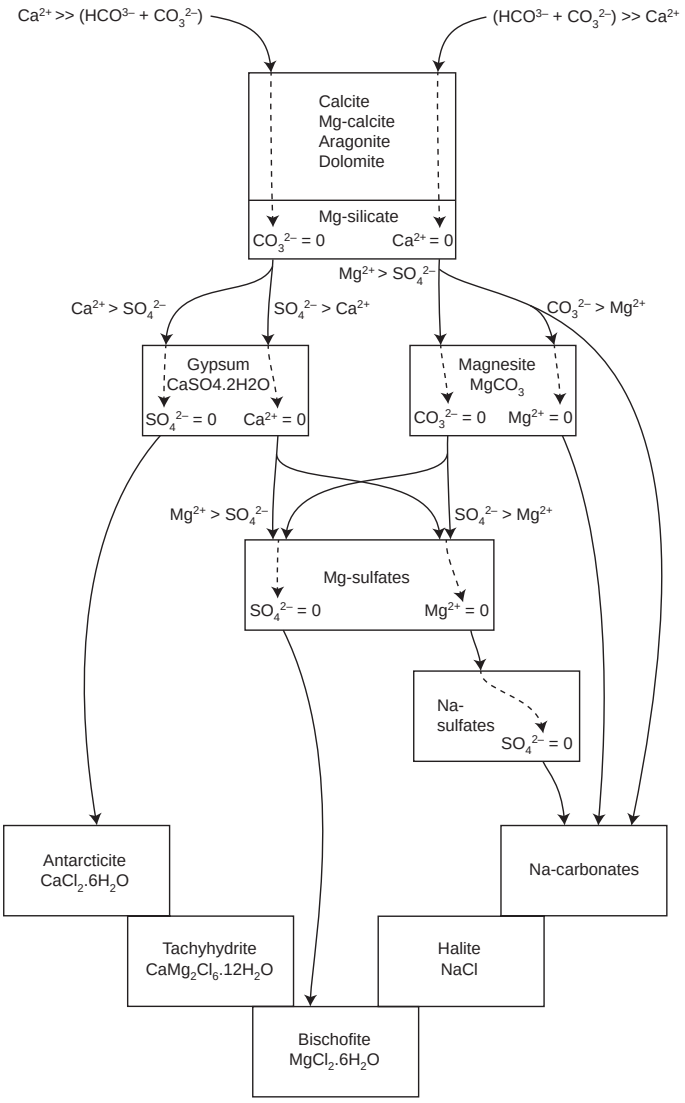

Figure 17: Flow chart of idealised brine evolution and mineral precipitation during evaporation (evapoconcentration increases downward) for different water types in a closed system. Brine composition is depicted by the flow lines and precipitates are depicted by cylinders. Solute concentrations are in equivalents and CO_3 refers to total carbonate species in solution. Reproduced from *Deocampo and Jones* [2014].

A major limitation of the idealised brine evolution depicted in Figure 17 is that it does not account for interactions with groundwater, surface water or biological activity during evapoconcentration [*Deocampo and Jones*, 2014]. Of these processes, interactions with groundwater is one of the most relevant for Australian saline lakes [*Mernagh*, 2013; *Rosen*, 1994]. *Rosen* [1994] described the key configurations between saline lakes and groundwater (Figure 18). The first configuration is a dry lake that has

little or no exchange with the underlying groundwater system (Figure 18a). This type of lake is known a ‘through-flow playa’ because it is likely to occur in basins where groundwater is discharged to adjacent basins. The second configuration is known as a ‘recharge playa’ because the lakebed acts as a localised recharge zone when it contains water (Figure 18b). The third and fourth configurations are known as ‘discharge playas’ because the lake surface acts as a local groundwater discharge zone, where water is lost by evaporation from within the lakebed sediments (Figure 18c) or from surface water (Figure 18d).

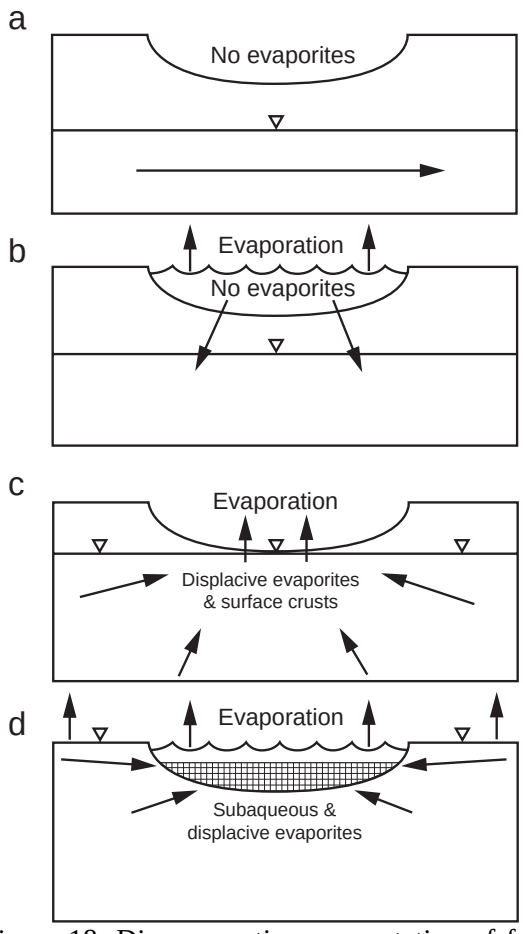

Figure 18: Diagrammatic representation of four generalised saline lake – groundwater relationship configurations: (a) ‘through-flow playa’; (b) a ‘recharge playa’; (c) a ‘discharge playa’ without permanent surface water; and (d) a ‘recharge playa’ with permanent surface water. Reproduced from *Rosen* [1994].

2. The Lake George Basin

The Lake George Basin is an endorheic basin with a catchment area of approximately 950 km^2 located ~40 km northeast of Canberra, Australia (Figure 19). The basin is delineated to the east by the Great Dividing Range and to the west by the Lake George Fault escarpment. To the north and south, the basin is delineated by low saddles in the topography, which consist of artificial drainage lines and swampy lagoonal areas [*Abell,* 1985]. The basin contains the two small townships of Collector and Bungendore, which are situated to the north and south of Lake George, respectively. These towns, and surrounding industries (agriculture and viticulture), are heavily reliant on groundwater because of the lack of sustainable potable surface water resources in the basin.

The Lake George Basin has been the focus of scientific studies since its discovery by European settlers in 1820, and has included research related to its geology [e.g., *Abell,* 1985; *Macphail et al.*, 2015; *Macphail et al.*, 2016; *Taylor*, 1907]; hydrology [e.g., *Burton*, 1972; *Burton and Wilson*, 1973; *Jacobson et al.*, 1991; *Jacobson and Schuett*, 1979; *Noakes*, 1951; *Russell*, 1886]; and the palaeoenvironmental conditions of the region [e.g., *Churchill et al.*, 1978; *Fitzsimmons and Barrows*, 2010; *Macphail et al.*, 2015; *Macphail et al.*, 2016; *Singh and Geissler*, 1985; *Singh et al.*, 1981]. These studies have all shown that Lake George has immense potential for scientific discovery. Henry Russell, government astronomer, made the following observation on the value of Lake George as an unique environment for scientific investigation in his 1877 text on the climate of New South Wales [*Russell,* 1877, p. 182]:

> *"… the history of Lake George is instructive, situated as it is in the mountains, with a well-defined catchment area, and no*

outlet. It forms a sort of rain-gauge, and should afford valuable information."

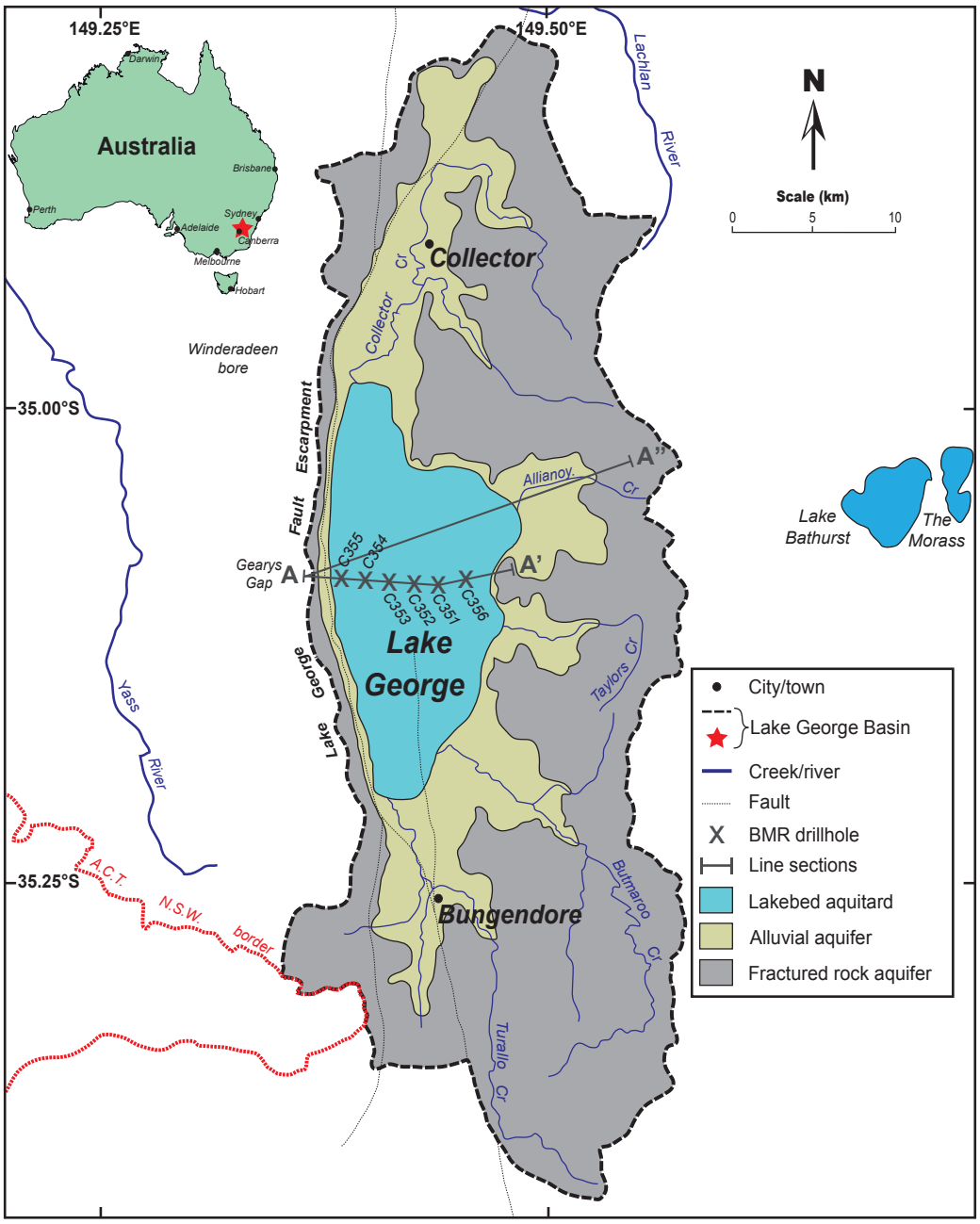

Figure 19: Location map of the Lake George Basin with respect to Australia (insert). See Figure 20 and Figure 26 for geologic cross section A-A' and hydrogeologic cross section A-A'', respectively.

2.1. Geology

The Lake George Basin is a tectonically formed half-graben, which was shaped by faulting during the Pliocene [*Macphail et al.*, 2015; *Macphail et al.*, 2016] – possibly as a result of the rejuvenation of Late Palaeozoic faults [*Abell*, 1985]. The basin's basement geology consists of marine turbidite sediments of Middle to Upper Ordovician age, which are overlain unconformably by Late Silurian acid volcanics and intruded by Siluro-Devonian granite. The units were then folded, faulted and weakly metamorphosed by a series of Palaeozoic earth movements, giving a strong north-south trend to the basement geology (Table 8 and Figure 20 from *Abell* [1985]).

Table 8: Stratigraphy of the Lake George Basin. Adapted from *Taylor* [1907], *Abell* [1985], *McEwan Mason* [1991], *MacPhail et al.* [2015] and *MacPhail et al.* [2016].

<table>
<tr><th>Formation</th><th>Lithology</th><th>Facies</th><th colspan="2">Age</th><th>Palaeo-hydrology</th><th>Hydraulic properties</th><th>Vegetation</th></tr>
<tr><td>Bungendore Formation</td><td>Clay/silt</td><td>Lacustrine</td><td>Pleistocene</td><td rowspan="3">Cenozoic</td><td>Closed catchment</td><td>Aquitard</td><td rowspan="2">Open forest and grassland</td></tr>
<tr><td>Ondyong Point Formation

Top of</td><td>Clay/ silt/ sand

deep</td><td>Fluvio-lacustrine

weathering</td><td>Late-Pliocene to early-Pleistocene
profile</td><td>Transitional: open – closed</td><td rowspan="2">Aquitard/ poor aquifer</td></tr>
<tr><td>Gearys Gap Formation</td><td>Gravel/ sand/ silty clay</td><td>Fluvial</td><td>Early-Pliocene</td><td>Open catchment</td><td>Gravel aquifer</td><td>Rainforest</td></tr>
<tr><td>Intrusions</td><td>Acid and basic volcanics</td><td rowspan="2">Bedrock</td><td>Silurian to Devonian</td><td rowspan="2">Palaeozoic</td><td rowspan="2">???</td><td rowspan="2">Fractured rock aquifer</td><td rowspan="2">???</td></tr>
<tr><td>Pittman Formation</td><td>Phyllite/ quartzite</td><td>Late-Ordovician</td></tr>
</table>

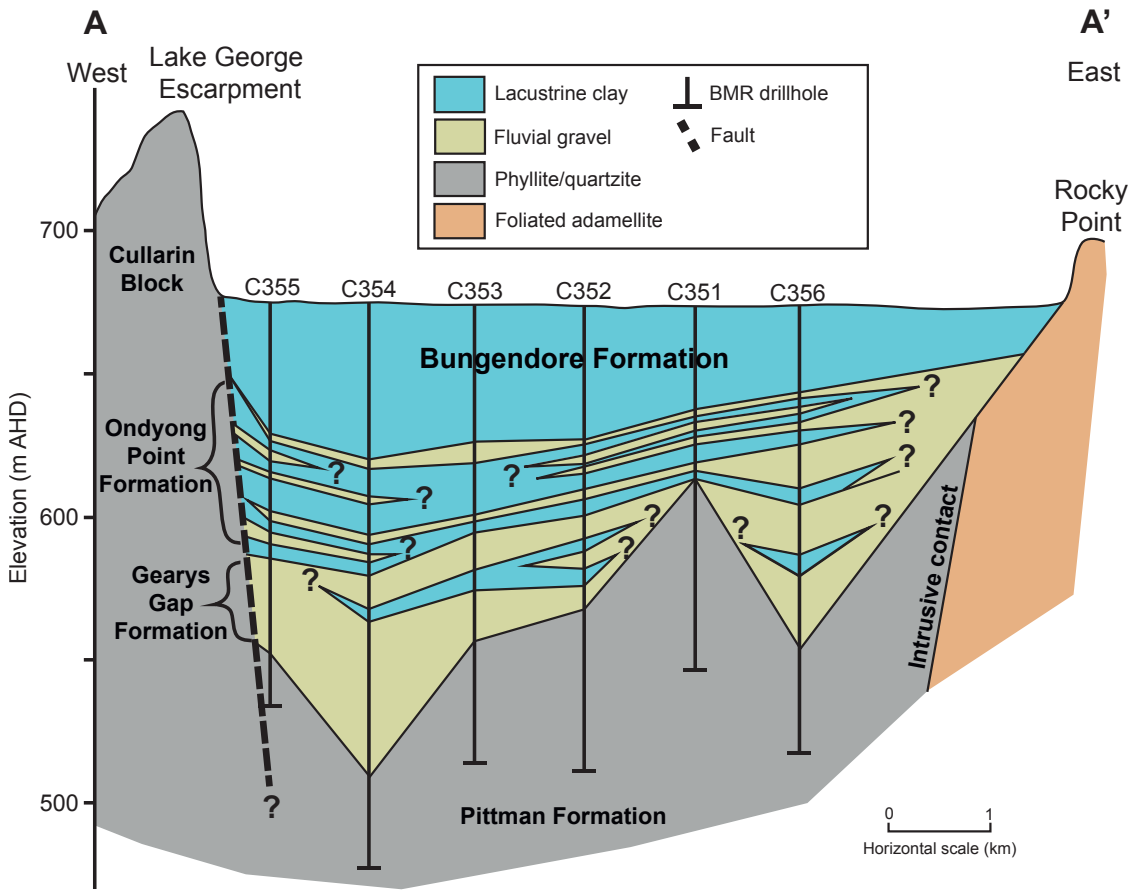

Figure 20: Geologic cross section of the line section A-A" in Figure 19. Reproduced from *Abell* [1985].

Lake George's lakebed consists of ~165 m (at its deepest known point) of fluvio-lacustrine sediment (Figure 20) that has been deposited since the early-Pliocene [*Macphail et al.*, 2015; *Macphail et al.*, 2016]. The Cenozoic sequence is divided into three stratigraphic units:

1. the Gearys Gap Formation, which is the oldest of the Cenozoic sequence, is estimated to be early-Pliocene in age at its base [*Abell*, 1985; *Macphail et al.*, 2015; *Macphail et al.*, 2016; *McEwan Mason*, 1991], and consists of deeply weathered fluvial gravel and sand. The fluvial lithology associated with the Gearys Gap Formation was deposited while the basin was part of a large

westward flowing drainage system. Palaeochannels of the old drainage system have been interpreted beneath the lakebed [*Abell*, 1985].

2. The Ondyong Point Formation, which is in the middle of the Cenozoic sequence, has been dated to be late-Pliocene in age at its base [*Abell*, 1985; *Macphail et al.*, 2015; *Macphail et al.*, 2016], and consists of fluvial sands and lacustrine clay and silt. The sediments of the Ondyong Point Formation were deposited unconformably on top of a deep weathering profile and are associated with closed drainage conditions [*Abell*, 1985; *Macphail et al.*, 2015; *Macphail et al.*, 2016].
3. The Bungendore Formation, which is the youngest of the Cenozoic sequence, is dated to be late-Pleistocene in age at its base [*McEwan Mason*, 1991], and consists of lacustrine clay and silt. The sediments of the Bungendore Formation were deposited conformably on top of the Ondyong Point Formation and are associated with a closed drainage system.

There are also Quaternary sediments in the basin that include colluvium along the base of hill slopes and the Lake George Fault escarpment, and lacustrine strandlines and aeolian deposits around the lake margin [*Mason*, 1995].

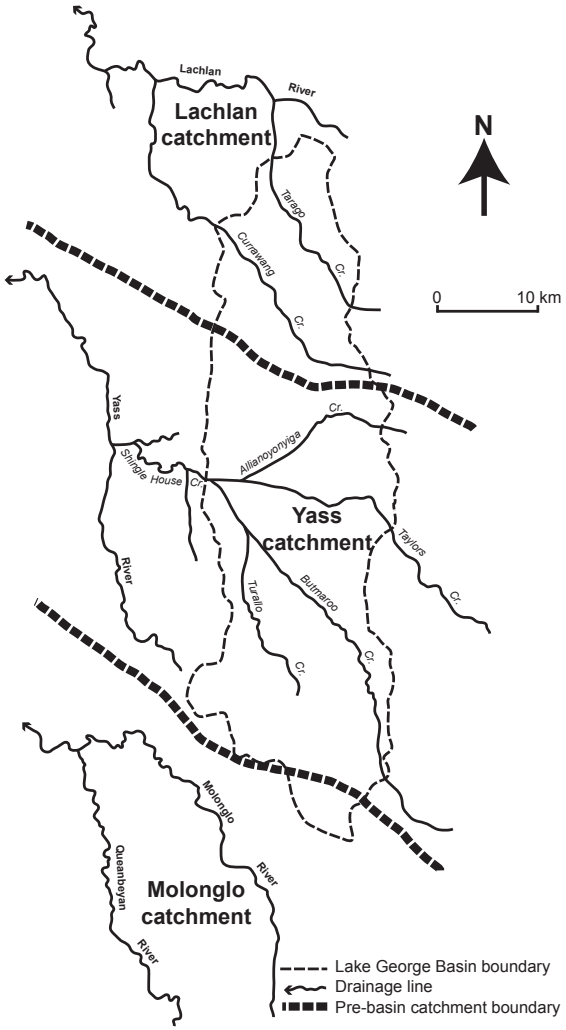

Figure 21: Hypothesised palaeo-drainage network of the Lake George Basin prior to uplift of the Lake George fault. Reproduced from *Abell* [1985].

2.2. Climate

The present-day climate of the region is temperate with warm summers and no distinct wet season (denoted as *Cfb* by the Köppen climate classification in *Peel et al.* [2007]), and dry-subhumid according to the region's aridity index of 0.51 (the ratio of mean annual precipitation and potential evapotranspiration, e.g., *Middleton and Thomas* [1997]). However, this aridity index is on the margin of being semi-arid (i.e., aridity index <0.5), and normal variation (i.e., one standard deviation) in annual precipitation

and potential evapotranspiration (PET) means that the basin's year-to-year aridity index has a range of 0.43 – 0.59.

The range of mean maximum daily temperatures (Figure 22a) for the basin is from 12.2°C (July) to 29.2°C (January), and the range of mean minimum daily temperature is from 0.0°C (July) to 13.3°C (February). Temperatures are estimated for the basin (Figure 22) using the mean of daily temperature measurements recorded at the Australian Bureau of Meteorology (BoM) weather stations located at Goulburn airport (34.81°S, 149.73°E; data from 1991 in *BoM* [2015]) and Canberra airport (35.31°S, 149.20°E, data from 2009 in *BoM* [2015]).

Monthly rainfall is distributed relatively uniformly throughout the year (Figure 22b) and ranges from 41 ± 35 mm (May) to 71 ± 34 mm (November). Mean annual rainfall, based on the last 30 years of rainfall data, is estimated to be 666 ± 145 mm. Precipitation for the basin is estimated using the mean of the precipitation recorded at the BoM rain gauges (Figure 19) located at the Bungendore Post Office (35.24°S, 149.45°E; date from 1890 in *BoM* [2015]), Bungendore Gidleigh (35.31°S, 149.47°E; data for 1886 – 2011 in *BoM* [2015]), Bungendore Lockhart (35.33°S, 149.50°E; data for 2006 – 2012 in *BoM* [2015]), Collector Lerida (34.88°S, 149.36°E; data for 1961 – 2012 in *BoM* [2015]) and Collector Winderadeen (34.94°S, 149.43°E; data from 1976 in *BoM* [2015]).

Annual PET for the basin, based on the four years of available data, is estimated to be 1310 ± 121 mm. The BoM have also published estimates of areal mean actual evapotranspiration rates, which are estimated based on PET and existing rainfall conditions of a given region. The Lake George Basin and surrounding regions are estimated to have a mean actual evapotranspiration rate of 550 – 600 mm $year^{-1}$. Potential evapotranspiration for the basin is estimated using the mean of the daily PET

calculated for the Canberra (data from 2009) and Goulburn (data from 2009) airports [*BoM*, 2015]. Potential evapotranspiration is calculated using the Penman-Monteith equation [e.g., *Allen et al.*, 1998] by staff at BoM based on meteorological data from their weather stations. Mean daily PET (Figure 22c) for the basin ranges from 1.2 ± 0.1 mm (June) to 6.3 ± 0.7 mm (January).

Mean daily pan evaporation (Figure 22d) for the basin varies from 1.2 ± 0.2 mm (June) to 7.1 ± 1.1 mm (January). Annual pan evaporation for the basin, based on the current 30-year mean, is estimated to be 1437 ± 158 mm. Annual open-water evaporation, which is estimated using a pan coefficient of 0.89 [*McMahon et al.*, 2013] because of the differences in energy balance between an evaporation pan and a lake [e.g., *Lim et al.*, 2013], for Lake George is estimated to be 1,278 ± 140 mm. Evaporation rates for the basin are obtained using the mean of daily Class A pan evaporation measurements recorded at BoM pan evaporation stations at Canberra Forestry (35.30°S, 149.10°E; data for 1957 – 1980 in *BoM* [2015]), Canberra airport (data for 1967 – 2013 in *BoM* [2015]), Canberra city (35.27°S, 149.12°E; data for 1974 – 1988 in [*BoM*, 2015]) and Goulburn TAFE (34.75°S, 149.70°E; data from 1971 in *BoM* [2015]).

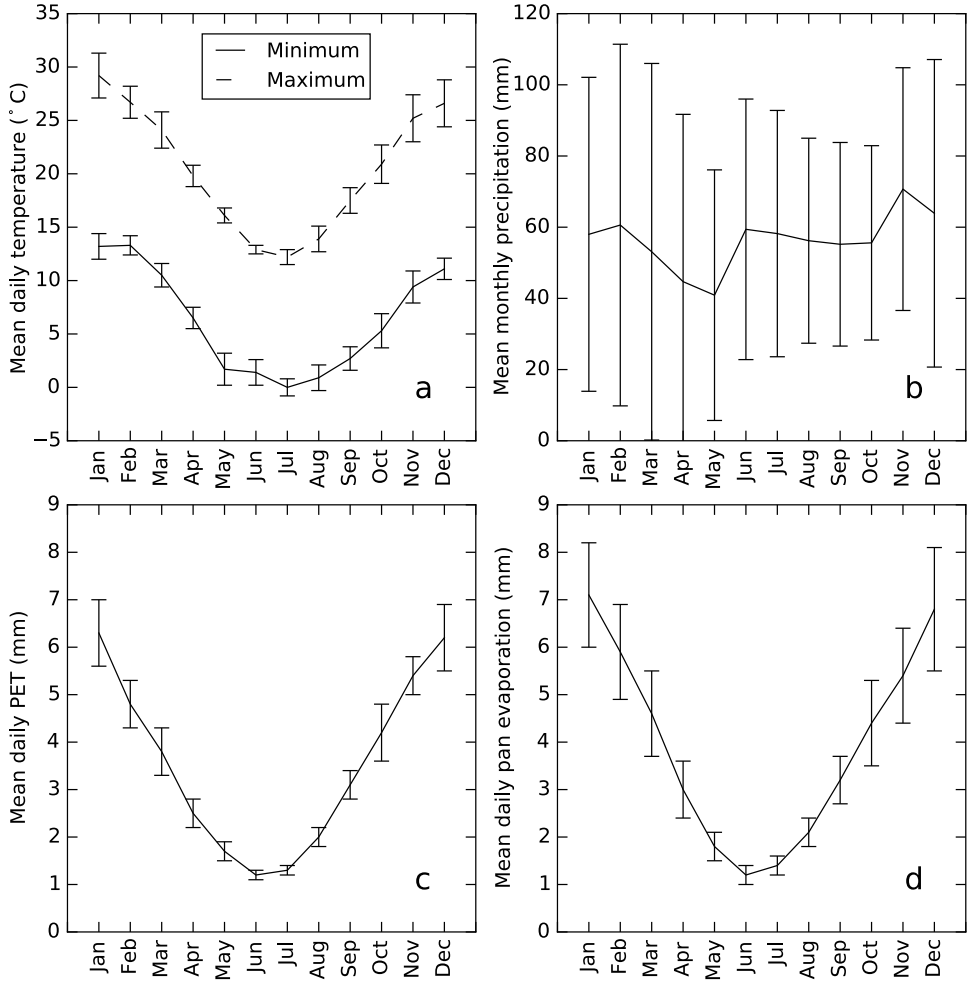

Figure 22: Mean daily maximum and minimum temperatures (a); mean monthly precipitation (b), mean daily potential evapotranspiration (c); and mean daily Class-A pan evaporation (d) for each month for the Lake George Basin. Uncertainty intervals indicate one standard deviation. All data from *BoM* [2015].

As illustrated by the wind roses in Figure 23, wind direction and speed across the lake varies during night- and day-time hours. During night-time hours, the prevailing wind is an east southeasterly with typical speeds of 0 – 5 m s^{-1}. During daytime hours, the prevailing wind is west northwesterly and typically stronger (5 – 10 m s^{-1}). The strong, persistent daytime winds experienced at Lake George, and the diurnal nature of the wind, has led the development of the Capital Wind Farm located on the eastern slopes of the basin. Wind speeds and directions in the Lake George Basin were recorded at the Icon Water weather station [pers. comm., 2015, *T. Purves*, Senior Engineer, Icon

Water] at Rocky Point (Figure 19) from February 2006 until the site was decommissioned in August 2015.

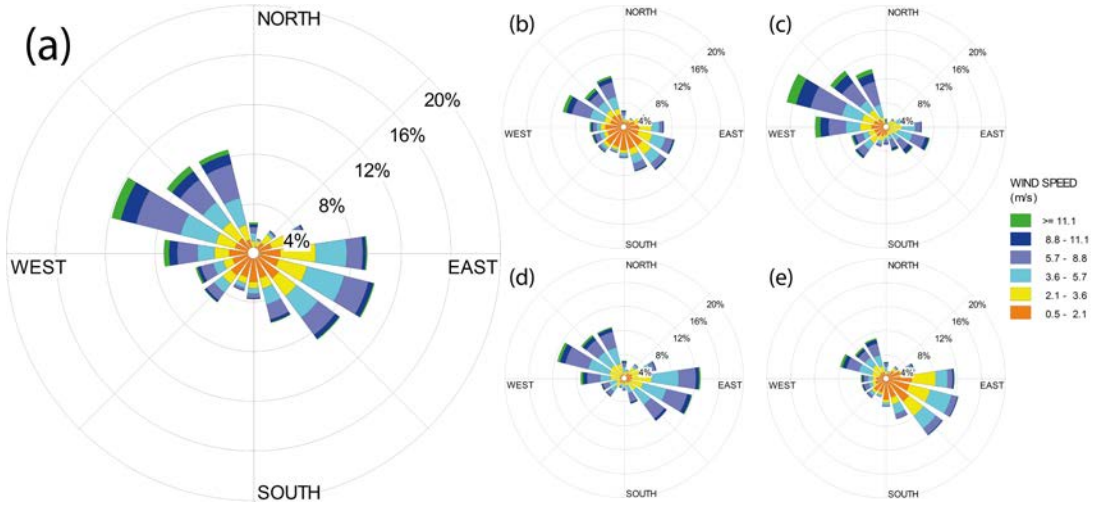

Figure 23: Wind roses showing the frequency, direction and speed of mean hourly wind recorded at the Rocky Point Icon Water monitoring station since February 2006 (n=67,872). Subplots show wind roses for all data (a) and time intervals 04:00-08:00 (b), 10:00-14:00 (c), 16:00-20:00 (d) and 22:00-02:00 (e).

2.3. Hydrology

At the centre of the Lake George Basin lies Lake George, also known as Weereewa, meaning 'bad water' in the language of the local indigenous people [*Singh and Geissler*, 1985]. When full (i.e., the modern arbitrary boundary marked on maps corresponding to a surface elevation of 680 m AHD), the lake is the largest natural inland water body in New South Wales, occupying 16% (156 km^2) of the Lake George Basin. The lake is the focus of drainage for five main sub-catchments (Figure 19): Collector/Currawang Creek in the north (catchment area of 262 km^3), Allianoyonyiga Creek in the northeast (catchment area of 89 km^3), Taylors Creek in the east (catchment area of 58 km^3), Butmaroo Creek in the southeast (catchment area of 176 km^3) and Turallo Creek to the south (catchment area of 188 km^3). Runoff is also directed from the fault escarpment towards the lake by a series of small creeks (catchment area of 21 km^3). Butmaroo Creek and Collector Creek contain near-perennial surface water,

whereas Allianoyonyiga Creek, Taylors Creek and Turallo Creek are ephemeral and only flow after heavy rainfall [*Jacobson et al.*, 1991; *Jacobson and Schuett*, 1979].

The Lake George hydrograph is one of the longest records of its type in the world [*Churchill et al.*, 1978; *Jacobson and Schuett*, 1979]. Figure 24 is a compilation (this study) of Lake George water level records including the initial inferred and observed water levels recorded by Henry C. Russell between 1820 and 1886 [*Russell*, 1886], Australian Bureau of Mineral Resources [*Burton and Wilson*, 1973; *Jacobson et al.*, 1991; *Jacobson and Schuett*, 1979; *Noakes*, 1951], recent Icon Water measurements [pers. comm., 2015, *T. Purves*, Senior Engineer, Icon Water], and the measurements collected as part of this research. Long-term rainfall records, extending back to 1857, from in and around the Lake George Basin (Goulburn rainfall is used to reconstruct rainfall between 1870 and 1885) also enable previous long-term rainfall trends for the region to be investigated. The values of the black dashed line in Figure 24 are calculated as the cumulative deviation of each year's annual rainfall from the overall mean. The slope of the black dashed line in Figure 24, rather than the absolute value, illustrates the long-term rainfall trend for the basin. Put simply, negative slopes indicate consecutive years of below mean rainfall (e.g., 1900 through 1950, and 2000 to present) and *vice versa* for positive slopes (e.g., 1950 through 2000).

In addition to the rainfall record, Class A pan evaporation has been recorded in Canberra and Goulburn for the last 40 years [*BoM*, 2015]. The pan evaporation, calculated using the same method as the rainfall trend, is plotted as the grey dashed line on Figure 24. When compared to the hydrograph, the long-term lake level trends are primarily controlled by short- and long-term rainfall and evaporation trends.

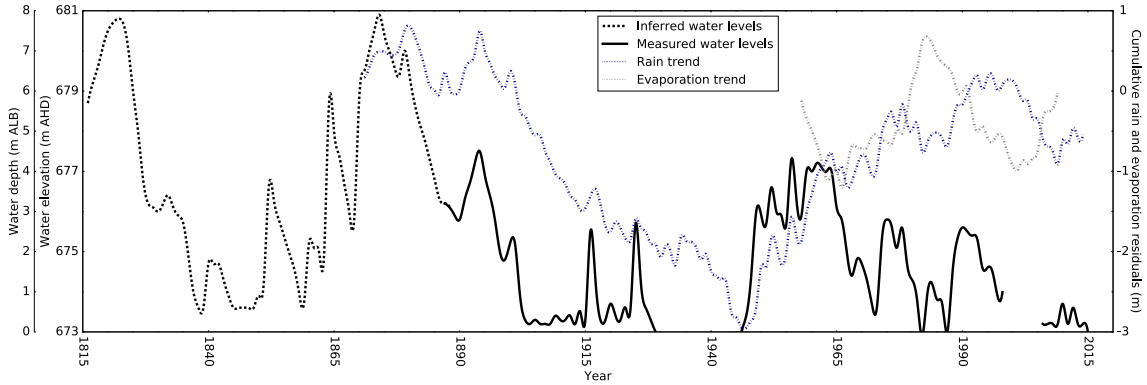

Figure 24: Water level fluctuations (solid and dashed black lines), cumulative rainfall residual (dashed blue line) and cumulative pan evaporation residual (dashed grey line) of Lake George from 1820, 1871 and 1958, respectively.

The very flat bathymetry of Lake George is another major control on its fluctuating water levels. At low lake stages (670 – 675 m AHD water levels), small changes in lake volume (on the order of annual creek runoff variations) induce relatively large changes in surface area compared to higher stages (Figure 25). These variations in lake surface area greatly increase evaporation from the lake surface. This phenomenon is most evident on the lake hydrograph (Figure 24) during the periods 1873 – 1903 and 1946 – 1972 when consecutive years of above mean rainfall, and presumably greater runoff, caused a rapid rise in lake stage, which was then followed by rapid reductions in lake stage because of increased evaporation from a greater lake surface.

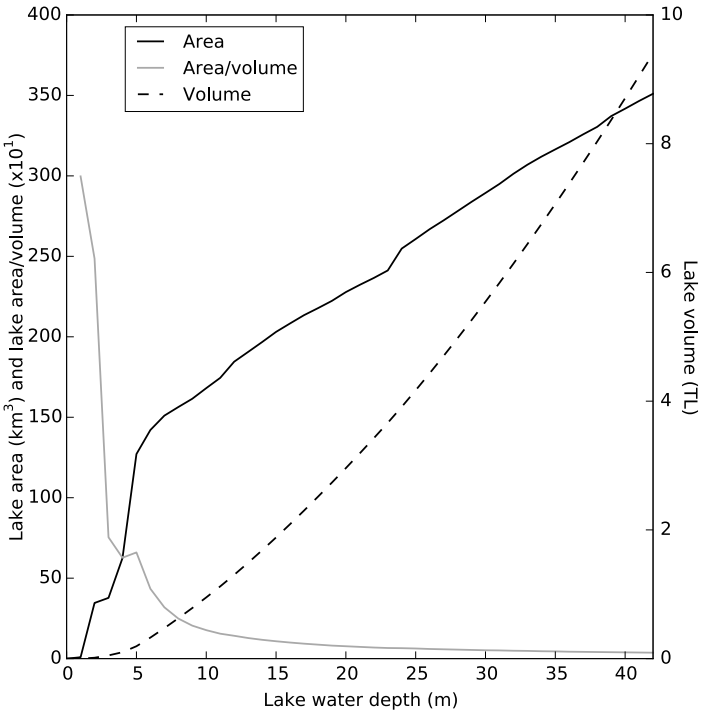

Figure 25: Lake George's area, volume and area/volume ratio with varying water depth. Bathymetry data was sourced from the shuttle radar data for the region [*USGS*, 2012].

The long records of hydrometeorological data for the basin and surrounding region enable some components of the basin's water budget to be estimated (Figure 26). Rainfall for the basin is estimated using daily precipitation measurement from six rain gauges located within or proximal to the basin (Section 2.2). Evaporation directly from the lake and PET over land surfaces is estimated using corrected pan evaporation and calculated PET data, respectively. *Jacobson and Schuett* [1979] estimated mean annual creek discharge to Lake George to be approximately 50 GL. Accurate estimates for creek discharge are not available in the Lake George Basin because only one (Butmaroo Creek) out of the five main creeks is gauged, and the gauge is located 15 km away from the lake boundary. Groundwater recharge for the basin has been estimated as 1 – 8% of annual rainfall (7 – 53 mm $year^{-1}$; ~6 – 51 GL $year^{-1}$) based on chloride mass-balance calculations and values from similar catchments in the region [*Beavis*, 2011; *Hydroilex*, 2005]. Current groundwater abstraction in the basin is estimated to be 700 – 1 100 ML

year^{-1} from the aquifer in alluvial embayments marginal to the lake, and is abstracted for Bungendore's town water supply and regional agricultural/viticultural use [*Beavis*, 2011; *Hydroilex*, 2005]. Based on a remote sensing analysis, *Beavis* [2011] estimated that farm dam storage for the basin is approximately 38.5 ML km^{-2} (37 GL for the basin), and the surface area covered by these dams represents 0.35% (3.3 km^2) of the catchment area. However, this estimate has not been verified by alternate means, and is likely to contain a significant amount of uncertainty.

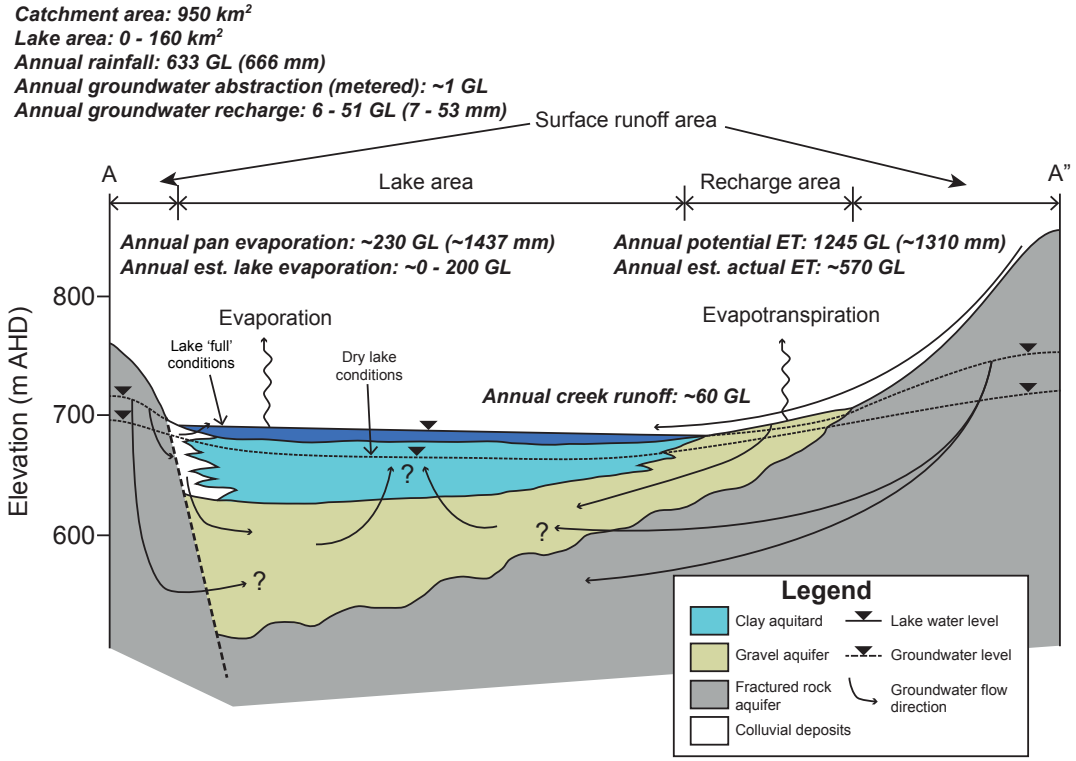

Figure 26: Schematic water balance and hydrogeologic conceptual model of the Lake George Basin. Amounts represent annual volumes/depths. Modified from *Jacobson et al.* [1991]. See text for data sources.

The current conceptual understanding of the Lake George Basin groundwater system consists of four main components (Figure 19 and Figure 26) described in *Abell* [1985] and *Jacobson et al.* [1991]:

1. a surficial clay aquitard (the Bungendore Formation and large parts of the upper Ondyong Point Formation), which makes up the first 20 – 50 m of sediment

below the lakebed. The aquitard acts as a seal separating the lake's surface water from the underlying gravel aquifers. However, positive pressure in the aquifers below the aquitard, caused by the basin's topography being up to 200 m above the lakebed, suggests that the lakebed may be a groundwater discharge zone for the basin;

2. alluvial aquifers (the lower Ondyong Point Formation and Gearys Gap Formation), which extend from the alluvial embayments of the basin's creeks to beneath the lakebed. The alluvial aquifers are unconfined marginal to the lake and become confined by the Bungendore Formation beneath the lakebed. Clay layers of the Ondyong Point Formation may form localised confining units in some areas of the alluvial embayments. The alluvial aquifers are likely to be recharged by rainfall and creek infiltration at the alluvial embayments and may also receive water from the underlying fractured rock aquifer. Water levels in regional bores indicate that groundwater flow in the alluvial aquifers is from the hills surrounding Lake George towards the centre of the lake (Figure 27);
3. piedmont deposit aquifers at the base of the Lake George Fault escarpment, which consist of colluvial and alluvial deposits. Water yields from these deposits can be highly variable and they are likely to be highly heterogeneous. Groundwater abstracted from water yielding zones of these deposits is typically very fresh indicating a short transit time after recharge from precipitation and creek infiltration from the fault escarpment. However, it is unclear if the Lake George fault itself acts as conduit for flow or impedes it at greater depths; and
4. a regionally extensive fractured rock aquifer (the Pittman Formation), which underlies the entire basin. Groundwater levels observed at regional bores indicate that groundwater flow in the fractured rock aquifer, like the alluvial

aquifers, is from the surrounding hills towards the centre of the lake. However, it is unknown whether there is significant exchange between the fractured rock and alluvial aquifers. It is also unclear if the basin acts a closed basin in the subsurface because current data are unable to provide evidence of flow into or out of adjacent catchments.

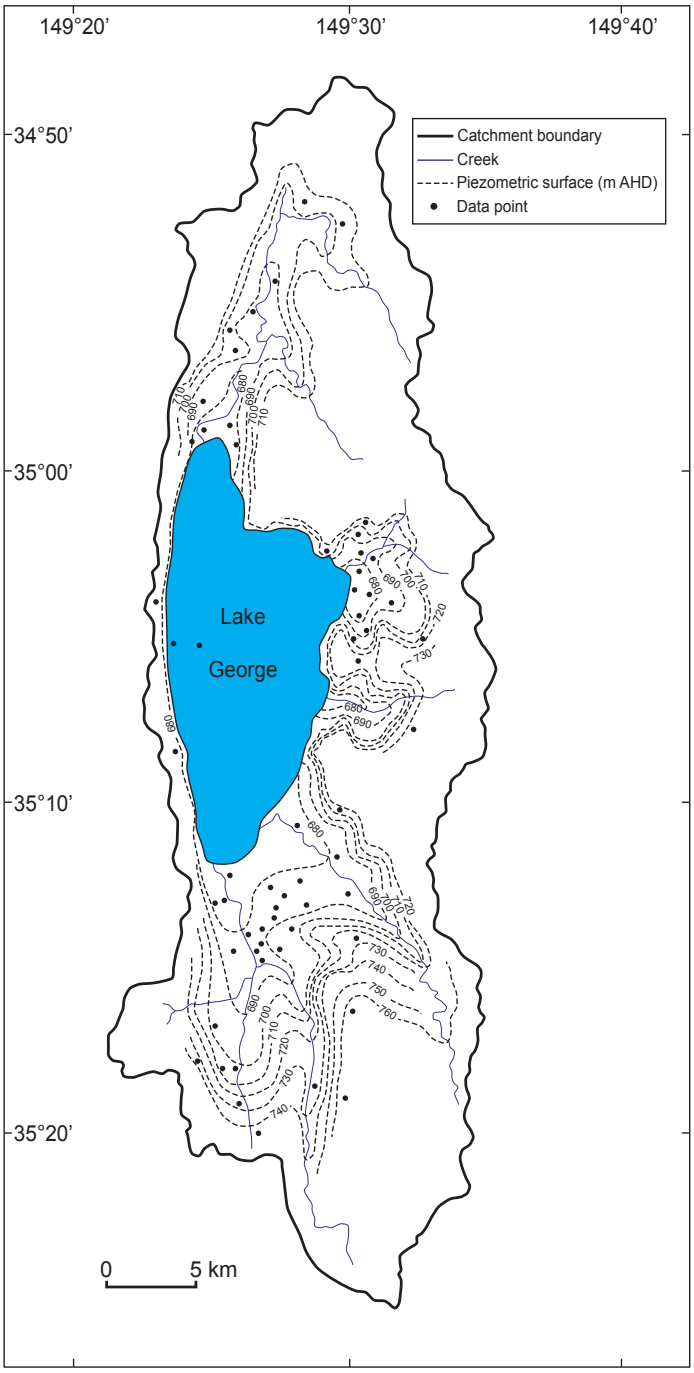

Figure 27: Potentiometric surface map of the alluvial sediments in the Lake George Basin. Reproduced and modified from *Jacobson et al.* [1991].

2.4. Hydrogeochemical pathways

The hydrogeochemical evolution of the Lake George Basin was investigated by researchers from the Australian Bureau of Mineral Resources (BMR) during a dry phase

of the lake in the 1980s [summarised in *Abell*, 1985]. The dry lakebed enabled the BMR scientists to retrieve core samples from the middle of the lake and determine the chemistry of the underlying porewater. Unfortunately, there have been no further investigations of the basin's hydrogeochemistry since the early study.

Jacobson et al. [1991] classified five different water types within the basin:

1. rainwater and recently recharged groundwater that is fresh with HCO_3^- or Cl^-, and Na^+ as the predominant anions and cations, respectively;
2. creek water is typically fresh to brackish with HCO_3^- or Cl^-, and Na^+ or Mg^{2+} as the predominant anions and cations, respectively. The freshest creek waters have total dissolved solids (TDS) of 100 – 300 mg L^{-1} and are typically HCO_3^-–Cl^-–Na^+–Mg^{2+} type waters. The fresh to brackish creek waters (300 – 1,500 mg L^{-1}) are typically Cl^-–HCO_3^-–Mg^{2+}–Na^+ type waters, and the more saline creek waters (>1,500 mg L^{-1}) are typically Cl^-–Na^+ type;
3. shallow groundwaters are fresh to brackish with TDS in the range of 150 – 2 000 mg L^{-1}. Groundwater with TDS less than 200 mg L^{-1} is typically HCO_3^-–Na^+–Mg^{2+}–Ca^{2+} type water. Groundwater evolves to HCO_3^-–Cl^-–Na^+–Mg^{2+}–Ca^{2+} type waters in the TDS range of 200 – 400 mg L^{-1} and to Cl^-–HCO_3^-–Na^+–Mg^{2+}–Ca^{2+} type waters at a TDS above 400 mg L^{-1}. Groundwater within the alluvial sediments beneath the lake is brackish (~3 – 6 g L^{-1} TDS) and is Cl^-–Na^+ type water;
4. lake water has the widest TDS range of 1 – 45 g L^{-1} and remain Cl^-–Na^+ type waters over most that range but also contain appreciable amounts of Mg^{2+} and HCO_3^- when brackish, and SO_4^{2-} when more saline; and
5. lakebed porewaters are brackish to saline and have Cl^-–Na^+ type waters with little variation.

Jacobson et al. [1991] also developed a conceptual model of the hydrogeochemical pathways during wet and dry lake periods. During wet periods, solutes are transported to the lake by direct rainfall and runoff from the surrounding sub-catchments. These solutes are subsequently concentrated as the lake begins to dry, and they begin to infiltrate into lakebed clay where they are restricted by the low permeability of the lakebed sediments. During both wet and dry periods, groundwater is transported from the recharge zones in the more elevated areas of the basin towards the lake. Along the groundwater flow paths, mineral dissolution contributes Na^+, K^+, Mg^{2+} (although data do not exist to confirm which mineral species contribute these ions), Ca^{2+} and SiO_2 to the water and transpiration acts to concentrate these solutes. Solutes are also transported into the aquifer beneath the lake by diffusion from the saline lakebed porewater. According to the playa classifications described by [*Rosen*, 1994] (Section 1.2 of this Chapter), Lake George could be classified intermittently as either a 'through-flow playa' (i.e., under conditions where the water level falls below the ground surface and water a solutes move downwards through the lakebed; Figure 18a) or a 'discharge playa' (under conditions of a near-permanent lake; Figure 18c).

One process that was not discussed at length by *Jacobson et al.* [1991] is wind erosion of thin salt crusts on the lake surface during dry periods. Wind erosion from the lake by the strong persistent westerly winds (discussed in Section 2.2 of this chapter) occurs during periods when the lake evaporates to dryness. There are no large inputs of groundwater to the lake surface, so thick salt crusts are unable to form but thin salt crusts are deposited during the final stage of evaporation [*Jacobson et al.*, 1991]. This thin salt crust is subsequently eroded by wind erosion, which has been documented by some of the scientists who have studied the lake [e.g., *Abell*, 1985; *Jacobson et al.*, 1991; *Jennings*, 1981]. The dust is likely to be composed primarily of clay particles

from the top of the Bungendore Formation and a minor proportion of evaporites that are deposited during the drying out of the lake. The photograph in Figure 28, showing a dust cloud just south of Rocky Point in January 2014, is a recent example of wind erosion from the surface of Lake George after the lake dried completely in November 2013.

Figure 28: Photograph of wind erosion from surface of Lake George looking south of Rocky Point (Figure 19) on 6 January 2014.

One of the most significant aspects of the hydrogeochemical cycling within the Lake George Basin is the large amount of dissolved salt stored within the lakebed (the Bungendore Formation). *Jacobson et al.* [1991] observed a concentration gradient in porewater solutes from two of the BMR cores from the Bungendore Formation (Figure 29). The TDS of the porewater is similar to saline lake surface water at low levels (20 – 30 g L^{-1}) but rapidly increases with depth to a maximum of 30 – 40 g L^{-1} at approximately 10 – 12 m below the lake surface. An almost linear decrease in TDS is then observed from a depth of 12 to 50 m, which is the lower boundary of the

Bungendore Formation. *Jacobson et al.* [1991] hypothesised that the linear decrease in TDS was likely to be caused by molecular diffusion through the low permeability sediments of the Bungendore Formation because of very low porewater advection. The lower salinity near the surface is believed to be due to dilution by superimposed brackish lake water and displacement of the diffusion profile downward. The hypothesis of diffusion through the Bungendore Formation is supported by fluid pressures and densities observed for the porewater within this formation. An imbalance in fluid pressure and density at depths less than 10 – 12 m suggests that there is a potential for downward fluid flow. However, a balance between fluid pressure and density below this depth suggests that fluid flow is minimal at depths below 12 m. Therefore, diffusion is likely to be the primary process transporting solutes downward beyond this depth. A solute mass-balance calculated by *Jacobson et al.* [1991] indicated that continual diffusion and salt accumulation within the Bungendore Formation has resulted in the accumulation of a total salt mass of approximately 100 Mt, and this may have taken place over the last two million years based on current diffusion rates. However, the estimates of *Jacobson et al.* [1991] only incorporate porewater concentrations that extend to the base of the Bungendore Formation and do not account for salt stored within the low-permeability sediments of the upper Ondyong Formation or the underlying aquifer. Therefore, the salt accumulation estimate of *Jacobson et al.* [1991] is likely to contain considerable uncertainty.

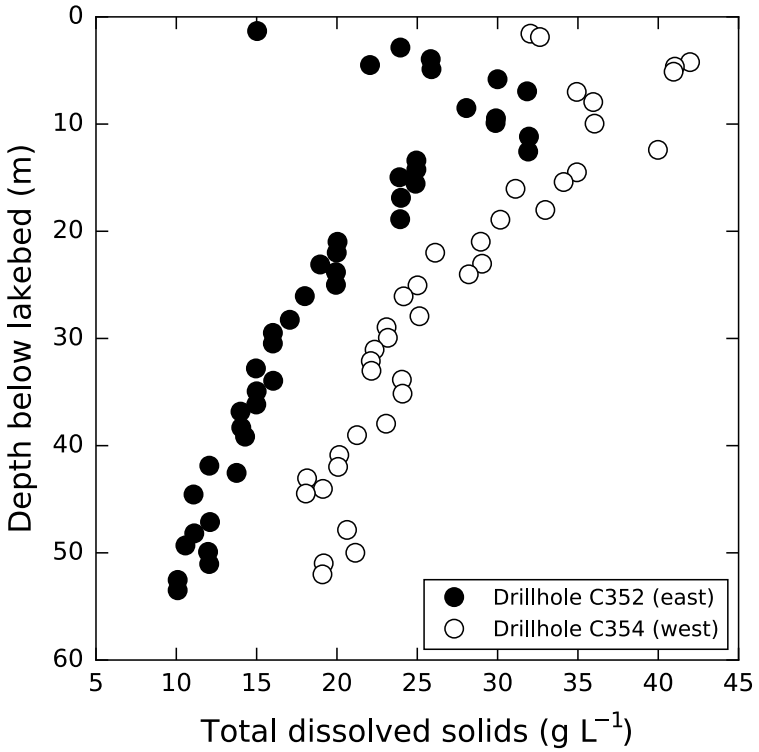

Figure 29: Profiles of total dissolved solids concentration with depth below the lakebed in porewater of cores C352 and C354 (locations shown in Figure 19 and Figure 20). Data from *Jacobson et al.* [1991].

Chapter 5: Tracing salt cycling in the Lake George Basin

This chapter presents the results and findings of applying various hydrogeochemical techniques, dominated by chlorine- and bromine-based ones, to uncover new knowledge about salt cycling at an Australian field site. The Lake George Basin was chosen because of its rich geological, hydrologic, hydrogeochemical and palaeoenvironmental record (Chapter 4), and it is currently the focus of an interdisciplinary scientific study to reinterpret and build on previous investigations to understand landscape evolution, changes in palaeoenvironments and human occupation history [e.g., *Macphail et al.*, 2015; *Macphail et al.*, 2016]. These make it especially worthy of application of the methods and principles discussed in previous chapters and to further demonstrate the utility of chlorine and bromine as tracers of terrestrial salt cycling.

1. Introduction

Lake George is a brackish to saline lake located in southeast Australia that has a rich hydrological history of fluctuating water levels. Recent water level fluctuations have been directly measured since the late nineteenth century and inferred back to the early nineteenth century from anecdotal records of local pastoralists (Figure 24; Chapter 4) [*Burton*, 1972; *Burton and Wilson*, 1973; *Jacobson et al.*, 1991; *Jacobson and Schuett*, 1979; *Noakes*, 1951; *Russell*, 1886]. During that period, the lake rapidly filled and emptied several times to a maximum depth of ~8 m, which led to speculation amongst local residents regarding the source and fate of the water [e.g., unlikely subterranean connections to lakes in New Zealand, China or South America; *Barrow*, 2012]. However, researchers have found that the lake's water budget is easily explained by a balance of rainfall, evaporation and creek runoff within the catchment [*Burton*, 1972; *Burton and Wilson*, 1973; *Jacobson et al.*, 1991; *Jacobson and Schuett*, 1979].

This sensitivity of the lake to climatic forcings, in particular rainfall, was noted by the New South Wales government astronomer, Henry Russell, in the late-nineteenth century when he wrote in his seminal work on the climate of New South Wales, "…the history of Lake George is instructive, situated as it is in the mountains, with a well-defined catchment area, and no outlet. It forms a sort of rain-gauge, and should afford valuable information" [*Russell*, 1877, p. 182]. In fact, the lake's sensitivity to short- and medium-term variations in rainfall (Figure 24, Chapter 4) has been used as a hydroclimate proxy to compare to reconstructed River Murray flows [*Gallant and Gergis*, 2011].

In addition to recently recorded water level fluctuations, geomorphological features within Lake George basin [e.g., strandlines; *Coventry*, 1976; *Coventry and Walker*, 1977; *Fitzsimmons and Barrows*, 2010], and palaeontological features of the lakebed sediments [e.g., ostracods; *De Deckker*, 1982; *Singh and Geissler*, 1985; *Singh et al.*, 1981] also provide evidence of even greater high stands of the lake, of up to ~36 m above the current lakebed, during the Holocene. *Coventry* [1976] produced an estimated hydrograph of Lake George since the end of the last glacial maximum (LGM; ~20 – 30 ka BP) based on relative age sequencing, and radiocarbon dating of charcoal within the strandline deposits. The reconstructed hydrograph suggests that water level of Lake George was ~36 m above the lakebed at the end of the LGM. Following the LGM, the water level of Lake George progressively decreased over the next ~6 ka, possibly to dryness. *Coventry* [1976] also found that geomorphological features of the basin indicated that there were four periods of ~1 ka each between 3 – 15 ka BP when the lake had water levels between approximately 12 – 26 m. *Fitzsimmons and Barrows* [2010] also produced an estimate of previous water levels from 15 ka BP to present based on optically stimulated luminescence (OSL) dating of shoreline sediments. The

authors found that the lake had three 'permanent lake' phases when the water level was 15 – 18 m, interspersed with periods of lower water levels with unknown depths. The reconstructed hydrograph is presented in Figure 30.

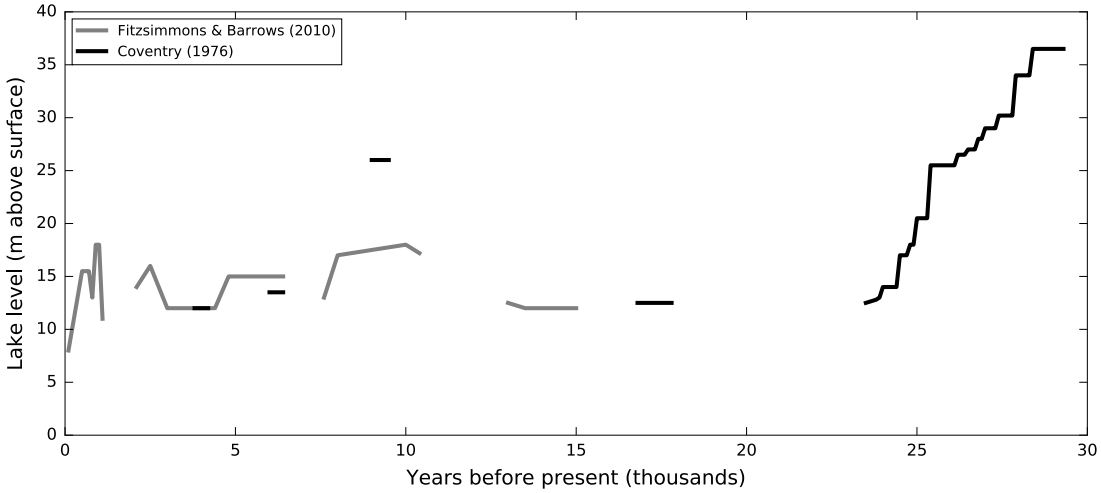

Figure 30: Lake George water levels since the last glacial maximum as estimated by *Coventry* [1976] and *Fitzsimmons and Barrows* [2010].

These previous studies have focussed on geomorphological and palaeontological evidence of past water level fluctuation as a means of uncovering information about the palaeo-environmental conditions of southeast Australia. However, *Jacobson et al.* [1991] focused on the Lake George basin groundwater system and hydrogeochemical evolution, which provided insight into the local salt cycling and transport. This aspect is also important to understanding the nature of Lake George during water level fluctuations and is worthy of further investigation using modern environmental tracer methods. The aim of this study is to better constrain salt and solute cycling within the Lake George basin to identify hydrogeochemical features that may provide insight into the palaeoenvironmental conditions of the basin. In addition, the results are used to assess any possible connection between the saline lakebed porewater and proximal freshwater aquifer that is utilised as a town water supply. This aim was addressed by applying various hydrogeochemical tracing techniques, mainly chlorine- and bromine-

based tracer ones. This study also provides a further demonstration of the utility of these methods and principles in a unique environment.

2. Environmental tracers

Environmental tracers are any measurable property that is naturally occurring (e.g., dissolved constituents, isotope compositions and physicochemical parameters) or was not intentionally introduced into the environment for the purpose of tracing environmental processes (e.g., industrial gases and anthropogenic isotopes)[*Cook*, 2015]. Researchers in the fields of hydrology and geochemistry have utilised environmental tracer techniques for several decades as a means of uncovering information on environmental processes that are hard to measure by other methods or to provide additional lines of evidence [e.g., *Clark and Fritz*, 1997; *Cook and Herczeg*, 1999; *Kendall and McDonnell*, 1998]. In this study, concentrations of dissolved chloride and bromide, stable isotope ratios of chlorine and water, and chlorine-36 compositions of waters from the Lake George Basin are utilised to delineate solute and water movement, and to uncover the palaeohydrologic evolution of Lake George.

2.1. Chloride and bromide

See Section 1 of Chapter 1.

2.2. Stable Halogen isotopes

See Section 2 of Chapter 1.

2.3. Stable water isotopes

The stable isotopic composition of the water molecule (δ^2H and $\delta^{18}O$) has been one of the most widely used tracers in hydrology since the mid-twentieth century [e.g., *Craig*, 1961; *Epstein and Mayeda*, 1953]. The stable water isotope compositions are

useful in hydrologic studies because both hydrogen and oxygen partake in very few geochemical reactions at ambient temperatures and are only modified during phase changes of water [i.e., evaporation, condensation, freezing and sublimation; *Clark and Fritz*, 1997]. The pioneering work of *Craig* [1961] showed that the δ^2H and $\delta^{18}O$ composition of global precipitation, when plotted as δ^2H against $\delta^{18}O$, delineate a global meteoric water line (GMWL). The equation for the GMWL is defined by a linear least square regression where the slope and intercept are approximately 8 and 10, respectively [*Gat and Gonfiantini*, 1981].

On a local scale, the relationship between δ^2H and $\delta^{18}O$ of precipitation can deviate from the slope and deuterium excess of the GMWL depending on climatic conditions [*Gat and Gonfiantini*, 1981]. Precipitation in relatively cool climate, high latitude, high altitude and inland areas will have more depleted isotopic compositions (i.e., values will plot lower on the LMWL), and vice versa for warm climate, low latitude, low altitude and coastal areas [*Gat and Gonfiantini*, 1981]. The slope of the LMWL is generally found to be close to 8 in most regions [*Clark and Fritz*, 1997; *Gat and Gonfiantini*, 1981]. However, smaller slopes can be observed in arid regions where raindrops regularly undergo evaporation during rainfall [*Clark and Fritz*, 1997].

The isotopic fractionation of stable water isotopes during evaporation also imparts distinct δ^2H and $\delta^{18}O$ signatures on the residual water. This is a particularly useful behaviour in catchments containing open water bodies (e.g., lakes, dams and rivers) or where soil water undergoes evaporation before being recharged to aquifers [*Kendall and McDonnell*, 1998 and references therein]. In systems that can loosely be considered closed (e.g., evaporation ponds or terminal lakes), the isotopic composition of evaporating water bodies will plot along a ‘local evaporation line’ (LEL) at successive stages of evaporation (Figure 31) [*Clark and Fritz*, 1997; *Gat and Gonfiantini*, 1981;

Kendall and McDonnell, 1998]. Evaporation under humid conditions will result in a greater slope for the LEL and vice versa for evaporation in arid regions [*Gat and Gonfiantini*, 1981]. This application is especially useful for identifying evaporation as a salinisation mechanism in systems such as salt lakes [e.g., *Currell et al.*, 2010; *Friedman et al.*, 1976].

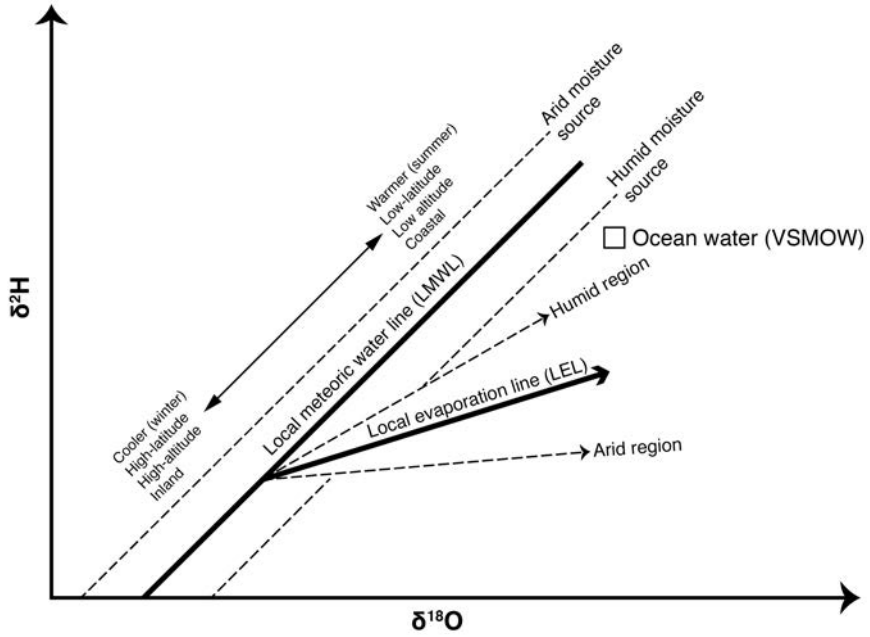

Figure 31: Diagram of the generalised processes that affect the stable water isotope composition of precipitation.

3. Site description

See Chapter 4.

4. Methods

4.1. Sampling

Rain, creek water, lake water, groundwater and lakebed porewater samples were collected between August 2013 and July 2015. Rain was collected as approximately

monthly composite samples in samplers located at three sites around the Lake George Basin (denoted as BRW, RPRW and WRW; Figure 32 and Figure 33). The rain sampler design was modified from that used by the International Atomic Energy Agency [*Gröning et al.*, 2012] that minimises the water's interaction with the atmosphere without the need to add a layer of paraffin oil. The collection funnel was open to the atmosphere at all times during collection, which means that solute loads in the rain samples were a combination of wet (i.e., rain and hail) and dry deposition (i.e., dust and aerosol). Sample weights were recorded after collection and converted into precipitation depths based on funnel diameters. Creek water (denoted as ACSW, BCSW, CCSW, TCSW and TuCSW; Figure 32 and Figure 33) and lake water (denoted as LGSW; Figure 32) samples were collected directly from water sources using a HDPE beaker rinsed at least three times with the water to be sampled. Groundwater samples were collected from a series of town water supply monitoring piezometers (denoted as 100 – 105, and AS/AD, BS/BD, C, D, E, FS/FD, G, KS/KD, LS/LD and M; Figure 32 and Figure 33), domestic and stock wells (Keatley's, Dominic's, Harry's, Winderadeen and Osborne bores; Figure 32 and Figure 33), and a shallow (~1.5 m) piezometer installed in the lakebed sediments (named 'Russell's bore' in this study; Figure 32) using a combination of a Bennett sample pump (Bennett Sample Pumps, USA), QED MicroPurge bladder pump (QED Environmental Systems, USA), plastic bailer and installed impeller pumps. All groundwater piezometers and bores were pumped until stable (±5%) physicochemical parameters (i.e., temperature, electrical conductivity, pH and dissolved oxygen) were recorded in three consecutive 15-minute intervals.

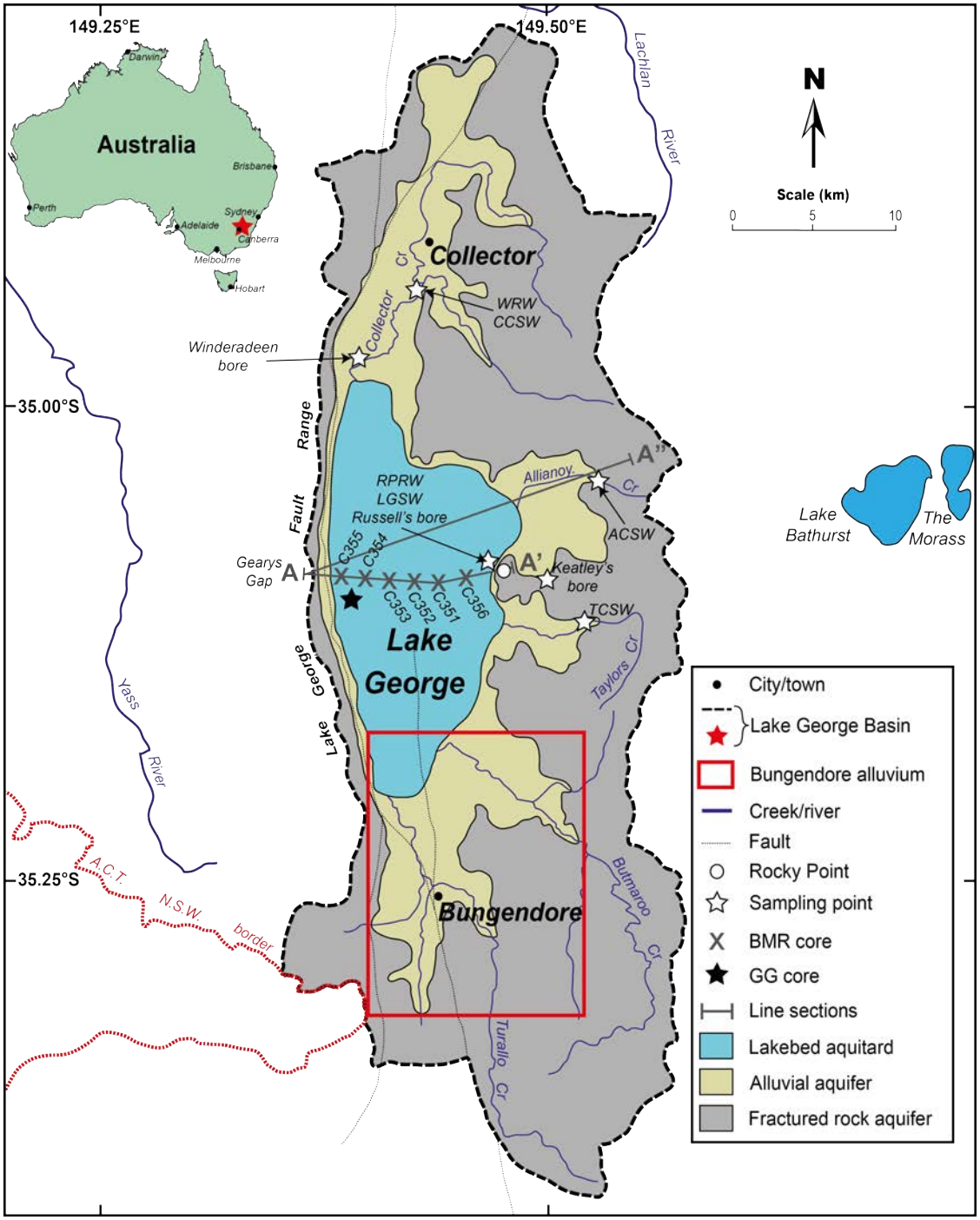

Figure 32: Location map of Lake George, sampling locations and line-sections for the cross-sections presented in Figure 20 and Figure 26 (both in Chapter 4). The red box delineates the location map presented in Figure 33.

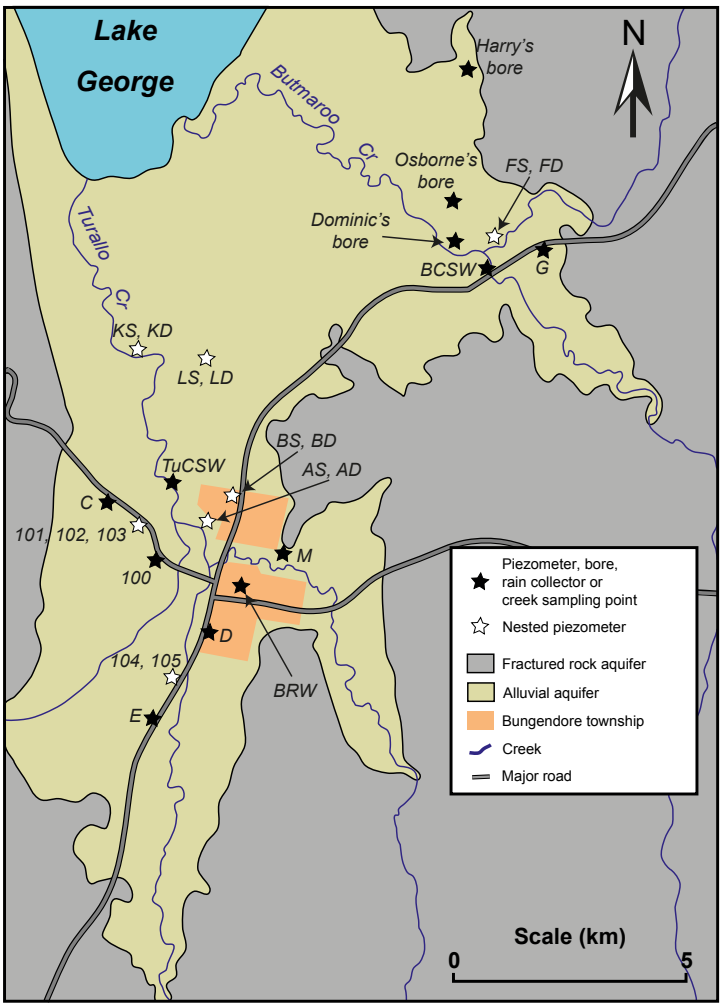

Figure 33: Location map of Bungendore township with sampling locations. See Figure 32 for the location relative to the wider Lake George Basin.

Once collected, all water samples were filtered using 0.2 μm nylon membrane filters and split into sub-samples: one for physicochemical measurements, two 30 – 125 mL HDPE bottles for anion analysis and elemental analysis (the latter was acidified to a pH of <2 using ultrapure HNO_3), one 15 mL HDPE bottle for stable water isotope analysis, and 0.1 – 2 L HDPE bottles/containers for stable chlorine isotope analysis (volumes were dependent on expected Cl^- contents). A sub-sample of rain was also collected for spectrophotometric ammonium analysis using the Nessler method [e.g., *Galvão et al.*, 2013] with a Hach portable spectrophotometer (model DR 2800; Hach Company, USA). Sub-samples of creek water, lake water and groundwater were

collected for alkalinity titrations to a methyl orange endpoint (pH ~4) with 103 mM HCl using a Hach digital titrator (Hach Company, USA). Alkalinity was not determined for rain samples because of very low alkalinity and sample volume constraints. Instead, the alkalinity of rain samples was estimated using the geochemical modelling program PHREEQC (version 3 with the MinTEQ database version 2 [*Parkhurst and Appelo*, 2013]) only where the samples had the majority of remaining dissolved species were determined (i.e., NH_4^+, Cl^-, SO_4^{2-}, NO_3^-, PO_4^{3-}, F^-, Br^-, Na, Ca, Mg and K). A sub-sample of each groundwater sample was collected for spectrophotometric sulfide analysis in the field using the methyl blue method [e.g., *Lindsay and Baedecker*, 1993] with a Hach portable spectrophotometer (model DR 2800; Hach Company, USA). All water samples were stored in the dark at ~4°C between sampling and laboratory analysis.

Samples of interstitial salts in the Bungendore Formation were obtained for stable halogen isotope ratio analysis by sampling archived cores stored in the Geoscience Australia National Offshore Petroleum Data and Core Repository archive in Canberra, Australia. The cores were collected during the large geological study of the Lake George Basin in the 1980s discussed earlier (Chapter 4). The samples were originally saturated with water but have subsequently dried after three decades of storage. However, *in situ* major ion and element concentrations of porewater were obtained and were reported for squeezed core samples from two of the cores (C352 and C354; see Figure 20 and Figure 32) directly after collection [*Jacobson et al.*, 1991]. During this study, ~200 g of dried core samples (~10 cm sections) were collected at 5 – 10 m intervals from the top section (i.e., 0 – 60 m; Bungendore Formation and upper Ondyong Point Formation) of cores C351, C352, C353, C354, C355 (Figure 20 and Figure 32). The samples were gently crushed in a tungsten carbide mill and mixed in a

ratio of approximately 40 g ultrapure water to 30 g of crushed sediment. The sediment slurries were then mixed on an orbital shaker for 24 hours, centrifuged and supernatants filtered through 0.2 μm nylon syringe filters into HDPE bottles. The crush/leach extracts were obtained to undertake stable chlorine isotope analysis; however, anion analyses were also carried out on each sample to ensure that Cl^-/Br^- ratios were similar to present-day porewater (see below) in order to indicate complete re-dissolution of Cl^-. A small selection of samples was also analysed for stable bromine isotope ratios but the results were ambiguous and are not reported here (see Appendix II). Crush/leach samples were stored in the dark at ~4°C between sampling and laboratory analysis.

In November 2015, a sediment core was collected from the surface of Lake George using sonic drilling methods during a dry phase (Gearys Gap core; Figure 32). Core sections 1.5 m long were extracted to a depth of 77.3 m below ground surface using sonic drilling methods. Drilling water was not used for depths <50 m; however, drilling water was used at depths >50 m. The drilling water was pushed down the outside of the casing and was spiked with D_2O to detect any potential contamination from the drilling water. Cores were sealed *in situ* in plastic (Lexan) liners capped with LDPE covers. The capped liners were then inserted into cardboard tubes and the ends covered with opaque adhesive tape, which were then stored in a refrigerated room at ~4 °C until splitting and sampling. Sediment samples (3-5 cm long) were collected from one half of the core, vacuum sealed in plastic bags to prevent any evaporation, weighed and stored in a refrigerator at ~4°C. Weights ranged from approximately 80 – 130 g.

When ready to extract the water, the samples in the sealed bags were reweighed and found to be within the precision of the measurements (i.e., <0.2 g). Water was extracted from the sediment samples using hydraulic presses (Enerpac; Wisconsin, USA) at Geoscience Australia. The vacuum-sealed bags were opened and the sediment

placed into stainless steel vessels fitted with a paper filter and drain hole. The samples were then covered with washed and dried Teflon disks and the whole assembly placed into the presses. After pressing residual air space out of the sample vessels, 15 mL sterile plastic syringes were inserted into the drain hole to collect the extracted water, minimising any contact with the atmosphere. The clay-rich sediments have very low permeability, so the water extraction typically took several hours and sometimes overnight. Water volumes ranged from approximately 5 mL to more than 15 mL, in which case a new, additional syringe was inserted to collect larger volumes. Water samples were filtered through 0.2 µm polyethersulfone syringe filters and collected in 15 mL plastic centrifuge tubes (two for larger samples) for subsequent analysis of pH electrical conductivity, anion and elemental concentrations, and $\delta^{2}H$ and $\delta^{18}O$ [pers. comm., 2016, *D. C. McPhail*, Emeritus Faculty, The Australian National University].

4.2. Analysis

Anion concentrations (F^-, Cl^-, Br^-, NO_3^-, SO_4^{2-} and PO_4^{3-}) of all water samples were analysed at the Research School of Earth Sciences (RSES), Australian National University (ANU), by suppressed conductivity detection using a Dionex ICS-5000 ion chromatography system fitted with an IonPac AS19 analytical column (Thermo Fisher Scientific, USA). Element concentrations (B, Na, Mg, Al, Si, K, Ca, Mn, Fe, Sr and Ba) of all water samples (except crush/leach core extracts) were analysed at RSES using a Varian Vista Pro axial inductively coupled plasma atomic emission spectrometer (ICP-AES; Varian Inc., USA) at RSES, ANU. Analytical precision was found to be better than 5% for anion and elemental analyses based on replicate analyses of calibration standards, laboratory/field replicates, and charge balance error analysis. The accuracy of Cl^-/Br^- ratios were found to be better than 5% based on repeat analysis of a seawater sample. The accuracy of elemental analyses (Na, Mg, Al, K, Ca, Mn, Fe, Sr and Ba)

were found to be better than 3% based on repeat analyses of a certified reference material (SLRS-5 river water; National Research Council Canada).

Stable water isotope ratio ($\delta^{2}H$ and $\delta^{18}O$) analyses were carried out on all water samples (except crush/leach core extracts) using cavity ring-down spectroscopy (Picarro L1102-i Isotope Analyzer; Picarro Inc., USA) at the Research School of Biology, ANU. Stable water isotope ratios were calibrated using in-house standards that are routinely checked against certified reference materials (e.g., VSMOW and SLAP). Analytical precision for stable water isotope analyses were found to be ~0.2 ‰ and ~1.0 ‰ for $\delta^{18}O$ and $\delta^{2}H$, respectively, based on repeat analyses of standards and samples.

Stable halogen isotope ratio ($\delta^{37}Cl$ and $\delta^{81}Br$) analyses were carried out on a selection of crush/leach samples (see Appendix II) at the University of Waterloo's Environmental Isotope Laboratory using the isotope ratio mass spectrometer methods described in *Shouakar-Stash et al.* [2005a] and *Shouakar-Stash et al.* [2005b]. Stable halogen isotope ratios were calibrated using in-house standards that are routinely checked against reference materials (e.g., SMOC and SMOB). Analytical precisions for stable halogen isotope analyses were found to be 0.05 – 0.20 ‰ and 0.02 – 0.27 ‰ for $\delta^{37}Cl$ and $\delta^{81}Br$, respectively, based on repeat analyses of standards and samples.

Table 9 summarises the number of samples that were analysed for the various geochemical parameters.

Table 9: Summary of the number of Lake George Basin water samples analysed for geochemical parameters.

Analysis	Number of samples
Major and minor ions/elements	144
Cl^-/Br^- ratios only	64
δ^2H and $\delta^{18}O$	86
$\delta^{37}Cl$	41
$\delta^{81}Br$	10

5. Results and discussion

See Appendix II for the tabulated hydrogeochemical results compiled as part of this study.

5.1. Basin-wide hydrogeochemical trends

5.1.1. Major ions and elements

Overall, the major ion hydrogeochemistry of Lake George Basin waters observed in this study was very similar to the results presented in *Jacobson et al.* [1991] The distribution of samples on a Piper diagram (Figure 34) indicates that all the waters within the basin had either no dominant cation or were sodium-type waters when more saline. However, two distinct evolutionary pathways were observed on the cation plot. Rainwaters evolved from more calcium-type waters towards the sodium corner. In contrast, creek waters and regional groundwaters evolved from more magnesium-type waters towards the sodium corner. This suggests that there is either a source of magnesium or a calcium sink within the lithology of the catchment.

Of these two possibilities, a magnesium source, such as chlorite dissolution, has been suggested in previous investigations [e.g., *Jacobson et al.*, 1991]. Furthermore, geochemical data for the sedimentary deposits of the Lake George Basin presented in *Abell* [1985] suggest that amphibole weathering, contained in the basin's basic volcanic intrusions, is a magnesium source. However, the low TDS of the rainwaters means that

the magnesium source (or calcium sink, e.g., mineral precipitation, ion exchange, biological uptake) would not need to be large to modify the composition of rainwater to those displayed by creek waters and groundwater in the basin.

For anion compositions, rainwater, creek water and groundwater within the Lake George Basin typically evolved from carbonate-type waters towards chloride-type but some of the rainwaters and creek waters also contained substantial sulfate. Lake water displayed an evolutionary pathway typical of evapoconcentration (i.e., the carbonate content of the lake water decreases as the water reaches saturation with respect to carbonate minerals, which leads to a subsequent increase in the chloride proportion). The lower proportion of sodium and higher proportion of sulfate for the more saline (i.e., TDS>22 g L^{-1}) lakebed porewater collected from Russells bore, compared to lake water, suggests that sodium carbonates may have also been precipitated during the evapoconcentration of the lake water (e.g., the evolutionary pathway on the right-hand side of Figure 17 in Chapter 4).

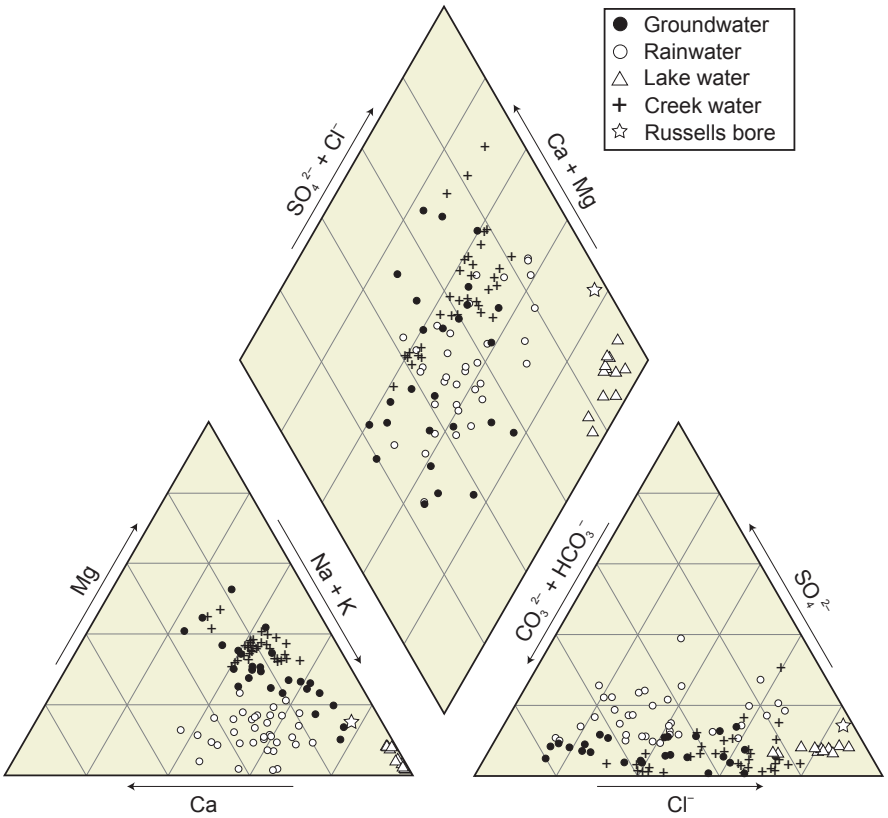

Figure 34: Piper diagram representing the major ion and elemental compositions of various water sources within the Lake George Basin.

The distinctive porewater salinity profile within the lakebed sediments presented by *Jacobson et al.* [1991] (Figure 29) was again observed for porewater extracted from the Gearys Gap core (Figure 35). The uppermost two samples show a rapid increase in salinity from the typical salinity of present-day lake water (i.e., <20 g L^{-1}). A salinity maximum of 55.1 g L^{-1} is reached at a depth only 3.2 m below the surface. Below this point salinity decreases at a rate of approximately 0.55 g L^{-1} m^{-1} to a depth of ~36 m, a lower rate of ~0.19 g L^{-1} m^{-1} between 36 and 69 m, and then at an increased rate of 0.57 g L^{-1} m^{-1} for the final 7.5 m of core. From this salinity distribution, and the approximate sediment dimensions used by *Jacobson et al.* [1991] (i.e., a mean porosity of 0.55 and 150 km^2 areal extent of sediment), an updated estimate of the total amount of dissolved salt stored within the upper 77 m of lakebed sediment is calculated as ~405 Mt. This equates to approximately 220 Mt of stored dissolved Cl^- after conversion with the

typical Cl^-/TDS mass ratio throughout the porewater profile (i.e., 0.54 with very little variation).

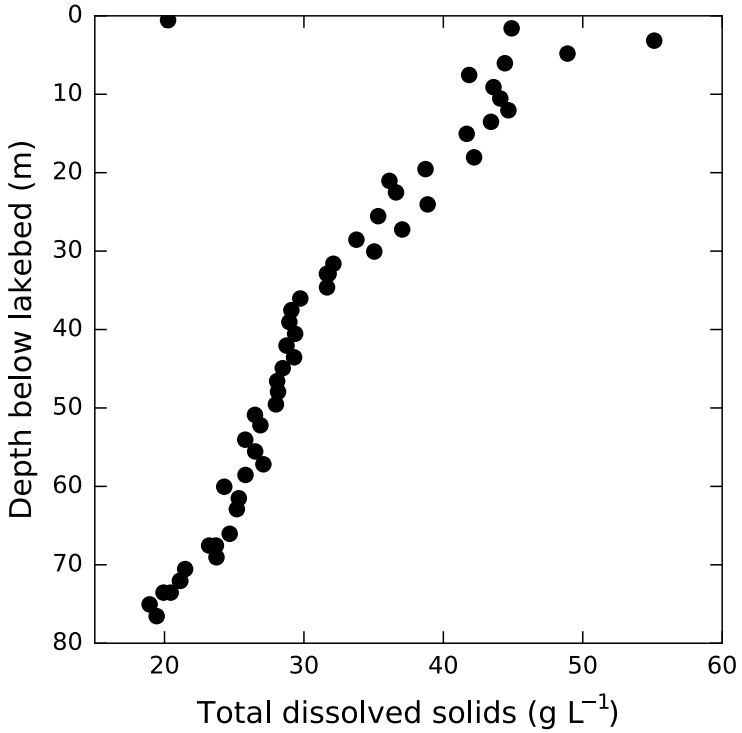

Figure 35: Total dissolved solids concentration depth profile of porewater extracted from the Gearys Gap core.

The mean atmospheric deposition rate of Cl^- in rain samples collected during this study was found to be 0.51 t km^{-2} year^{-1} (i.e., 485 t year^{-1} for the entire 950 km^2 area of the basin) based on the composite, approximately monthly, rain samples. Therefore, assuming that Cl^- behaves conservatively and all Cl^- deposited into the basin by rainfall is eventually transported to the lake sediments, the dissolved salts within the upper 77 m of lakebed sediments have taken approximately 0.45 Ma to accumulate. Although this estimate is likely to have a large amount of uncertainty associated with it (i.e., it doesn't account for variations in deposition rates over long temporal scales, and it doesn't include the salt stored within the lower ~80 m of the sedimentary sequence or the aquifers/soil surrounding the lake, or deflation of salt from the lake surface), it provides

a useful benchmark for the timescale of salt accumulation within the basin that is on the same order of magnitude as the estimated time that the sedimentary environment of the basin has been characterised by closed-drainage conditions (i.e., an environment with very little salt flushing to adjacent catchments [e.g., *Macphail et al.*, 2015; *Macphail et al.*, 2016]).

The molar ratios of the dissolved major ions and elements in porewater within the lakebed (Figure 36) also provide insights into the salt cycling dynamics and palaeohydrologic history of Lake George. The Cl^-/Na, Cl^-/SO_4^{-2} and Cl^-/Mg ratios (Figure 36a and Figure 36b, respectively) appear to show three distinct trends throughout the profile:

1. Between the ground surface and a depth of 30 m, the approximately linear increases in ratios with depth likely represent downward chemical diffusion/dispersion. The depth to which this linear increase propagates to is different for each of the three ratios – approximately 20, 30 and 10 m for the Cl^-/Na, Cl^-/SO_4^{-2} and Cl^-/Mg ratios, respectively. The differences suggest that the elements/ions reached their highest proportions at different times, because of the similar diffusion coefficients of Na, SO_4^{-2} and Mg in water [e.g., *Appelo and Postma,* 2005]. A possible explanation for the different timing of ratio patterns, considering independent sedimentary records that indicate a history of wet and dry periods [e.g., *Coventry*, 1976; *De Deckker*, 1982; *Fitzsimmons and Barrows*, 2010; *Singh et al.*, 1981], is progressive phases of precipitation/dissolution of evaporite minerals during drying of the lake (e.g., the brine progression presented in Figure 17 of Chapter 4). This is also consistent with the general increase in salinity that was observed throughout the profile (Figure 35). An alternate explanation is that the cation species may be affected by retardation (to

varying degrees) during diffusion due to cation-exchange on the surface of the clay-rich sediments. However, that does not explain the strong patterns in other anions (e.g. SO_4^{-2}), which are not as heavily influenced by that process as cations potentially are. It is also unlikely to affect ion ratios as strongly as it is observed in the Lake George profile because the porewater is brackish-saline to saline throughout the profile and dominated by Cl^--Na^+ type water. Thus, cation-exchange sites on clay mineral surfaces are likely to be saturated with Na^+ ions, and any effect of cation-exchange on ionic ratios will be minor.

The strong deviation from this trend for the Cl^-/SO_4^{-2} and Cl^-/Mg ratios in the shallowest two samples (0.6 and 1.6 m below the lakebed) may represent mixing with modern lake water, which was observed to have ranges of 18.7 – 26.0 and 20.0 – 114, respectively. This was also observed in these two samples for the Cl^-/Ca ratios, where they appear to show mixing between underlying porewater and modern lake water, which was found to have a ratio range of 61.2 – 152. However, the Cl^-/Na does not appear to behave in a similar fashion, with both samples found to have greater ratios than both the modern lake water (i.e., 0.64 – 0.97) and the underlying porewater.

2. At depths greater than 20, 30 and 10 m (for Cl^-/Na, Cl^-/SO_4^{-2} and Cl^-/Mg ratios, respectively), to 65 m below the surface, each of the Cl^-/Na, Cl^-/SO_4^{-2} and Cl^-/Mg ratios remain approximately constant at 1.3, 16 and 10, respectively. This may indicate a period of relatively stable hydrogeochemical conditions (i.e., element/ion proportions remained the same, although overall concentrations may have still been increasing).
3. Between 65 and 77 m below the surface, the Cl^-/Na, Cl^-/SO_4^{-2} and Cl^-/Mg ratios again increase linearly to the bottom of the profile. Variations in the rate of

salinity changes were observed at similar depth intervals (Figure 35) as discussed above.

These three intervals are less apparent for the Cl^-/Ca molar ratios of the lakebed porewater. However, systematic variations were still observed with ratios increasing with increasing depth at a (relatively) high rate to a depth of 15 m, then at a lower rate to a depth of 60 m, and remaining constant for the rest of the profile.

The Cl^-/K molar ratio showed no systematic trends and is quite 'noisy', unlike the other Cl^- ratios, throughout the profile (Figure 36d). Cl^-/K values did tend to cluster around ~200 with a typical variation of ±140 (1σ); however, they are not discussed further because their ambiguity suggests that they do not indicate systematic behaviour.

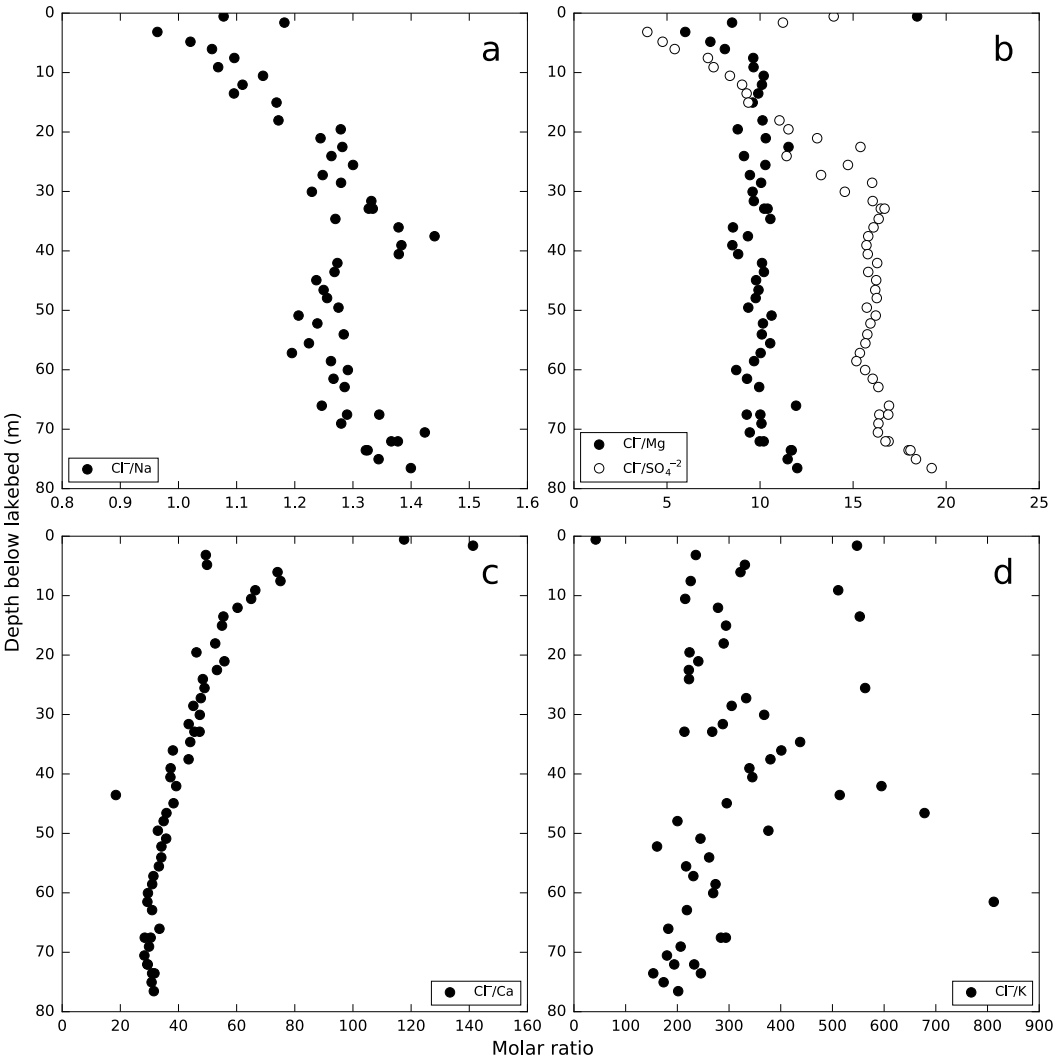

Figure 36: Major ion/element molar ratios (relative to Cl^-) depth profiles of porewater extracted from the Gearys Gap core.

5.1.2. Cl^-/Br^- ratios

The five water types (i.e., rainwater, creek water, groundwater, lake water and lakebed porewater) were observed to have distinct Cl^- and Br^- compositions (Figure 37). Rainwaters had low Cl^- concentrations (0.13 – 9.2 mg L^{-1}) and displayed the widest range of Cl^-/Br^- ratios (106 – 1 689) for the basin. Creek waters and groundwaters had Cl^- concentrations within a range of 11.3 – 732 mg L^{-1}. Creek waters had a relatively high range of Cl^-/Br^- ratios (218 – 522) compared to the groundwaters of the basin (154 – 313). Lake waters and lakebed porewater were typified by lower Cl^-/Br^- ratios (186 –

253) but were distinguished by differences in Cl^- concentrations (0.29 – 4.2 g L^{-1} and 9.2 – 12.3 g L^{-1}, respectively).

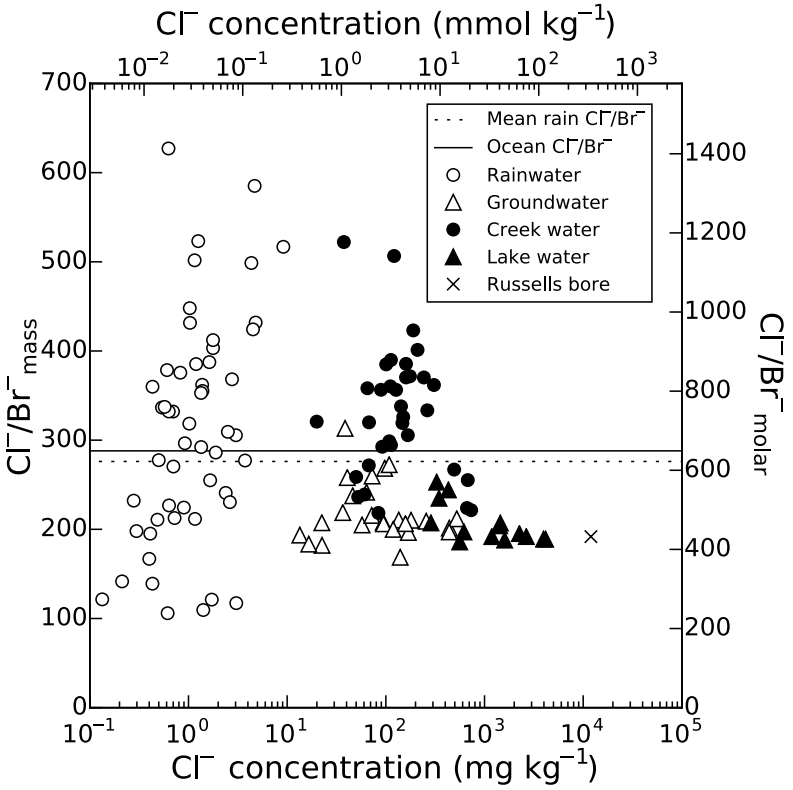

Figure 37: Cl^-/Br^- ratios as a function of chloride concentrations of various water sources within the Lake George Basin.

The mean Cl^-/Br^- ratio of rainfall (Figure 37) for the period between 1/8/2013 and 20/1/2016 was 276. This value was calculated using a precipitation weighted mean of the Cl^- and Br^- concentrations. After considering the analytical precision associated with these Cl^-/Br^- ratios (i.e., 7.1%, which is based on an analytical precision of 5% for the individual ions), the present-day rainfall ratio at Lake George is indistinguishable from that of seawater. However, the large amount of scatter associated with individual composite rain samples suggests that solutes deposited over the Lake George Basin reflect a range of sources, and that marine aerosol is not necessarily the primary source despite having a similar mean Cl^-/Br^- ratio over the long-term. The observed variation in Cl^-/Br^- ratios of Lake George rain are likely to reflect a combination of differences in

prevailing weather systems (i.e., rain systems transported from the coast versus over the continent), seasonal variations (Chapter 3 [*Short et al.*, 2017]), the proximity of Lake George to the NSW coast (i.e., a crude estimate of 88 – 102 is obtained using Equation (16) in Chapter 3; however, that equation is North America-specific and is unlikely to be applicable to other continents), and local/regional sources of additional salt (e.g., dissolution and re-deposition of dust eroded from the lake surface or dust transported from Australia's inland salt lakes). Furthermore, the years that sample collection took place were relatively dry compared to the mean (see average temperature and relative humidity recorded for the sampling periods in Appendix II), which meant that the lake was periodically dry, allowing for wind erosion from the surface. This may have resulted in some samples being influenced by salt from the surface of the lake being released into the atmosphere; however, there was no clear trend in the ratios of samples collected during the dry lake periods compared to when the lake was inundated.

Lake water and shallow lakebed porewater (i.e., Russells bore) samples consistently displayed similar Cl^-/Br^- ratios (i.e., 186 – 253 and 188 – 207, respectively) that are below the observed present-day atmospheric deposition line. The small range of Cl^-/Br^- ratios for the lake water samples, relative to the other water-types, and the similarity to lakebed porewater rather than creek water suggests that the composition of lake water is dominated by mixing with the shallow porewater of the lakebed. Furthermore, the crush/leach samples from the archived cores and porewater samples from Geary Gap core were observed to have very little variation throughout the top 77 m of lakebed sediments (Figure 38). This suggests that the lakebed Cl^-/Br^- ratio reflects the long-term (i.e., ka to Ma) mean of incoming solutes to the Lake George Basin and any short-term variations (i.e., decades to ka) have been smoothed out by mixing at the near-surface of the lake or by diffusion within the lakebed sediments.

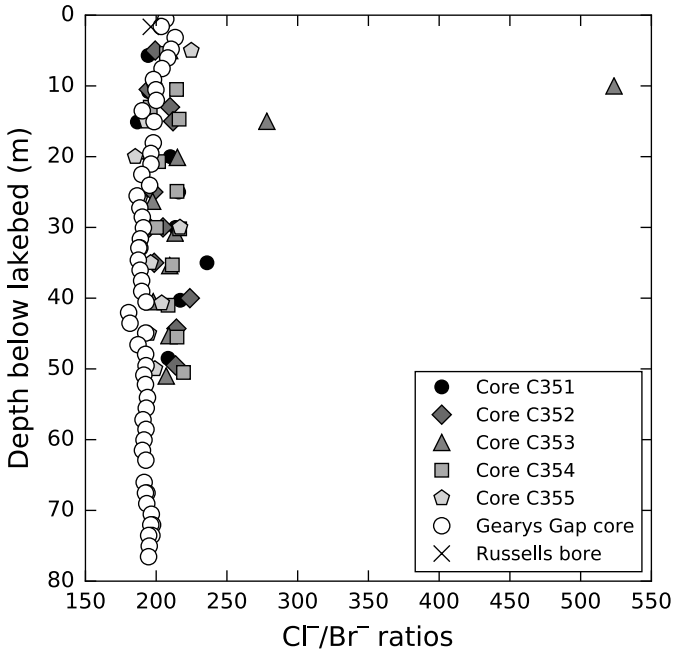

Figure 38: Cl^-/Br^- mass ratios depth profiles of the crush/leach samples obtained from the archived BMR core and for a sample collected from Russells bore.

Assuming that the mean Cl^-/Br^- ratio of the lakebed porewater *is* the long-term mean of solute inputs to the basin, it is unsurprising that this also appear to represent a lower bound for local groundwater compositions (Figure 37). Some of the sampled groundwater were observed to have intermediate Cl^-/Br^- ratios between the lakebed porewater and creek water, which is also unsurprising given that the ephemeral nature of the basin's creeks suggests that they discharge into the underlying soil and groundwater.

Most creek samples collected during this study were observed to have Cl^-/Br^- ratios elevated above that of rainfall for the same period. Only Allianoyonyiga Creek and Turallo Creek had, on average, Cl^-/Br^- ratios less than (i.e., 266 and 255, respectively) the mean rainfall composition. Butmaroo Creek, Collector Creek, Currawang Creek and Taylors Creek had, on average, Cl^-/Br^- ratios of 364, 326, 397 and 381, respectively. A possible explanation for this is the dissolution of halite (i.e.,

typical Cl^-/Br^- ratios of 5 000 – 10 000) from windborne dust, specifically dust eroded from the surface of a dry Lake George, which was observed during this study (Section 2.4 and Figure 28). The elevated ratio of creek water is unlikely to be due to groundwater discharge, which is likely to occur along some of the creek reaches, because groundwater typically has a ratio that is lower than modern rainfall.

If deposition and dissolution of dust in the basin's creeks is occurring, then the mean Cl^-/Br^- ratios of the four creeks that were observed to have elevated ratios relative to rainfall may suggest that between 16% (i.e., Collector Creek) to 25% (i.e., Taylors Creek) of Cl^- in the creek waters is due to this process. These values were calculated using Equation (6) in Chapter 2 with an assumed halite mass ratio of 5 000 and initial composition equal to mean rainfall.

5.1.3. Stable water isotopes

A total of 240 water samples from within the Lake George Basin, including rainwater, creek water, groundwater and porewater, were collected and analysed for their δ^2H and $\delta^{18}O$ compositions during this study. The results of the analyses are presented in Figure 39. The δ^2H and $\delta^{18}O$ values of the rainwater samples were used to calculate a LMWL for the Lake George Basin (blue line in Figure 39). The equation for the LMWL was determined using a precipitation amount weighted reduced major axis (RMA) regression [*Hughes and Crawford*, 2012]. The LMWL for the Lake George Basin is characterised by a slightly shallower slope (7.8) and elevated deuterium excesses (13.3) relative to the GMWL (solid black line in Figure 39). *Jacobson et al.* [1991] presented a LMWL for Canberra with a slope of 8.5 and a deuterium excess of 15.2. Unfortunately, the authors did not provide information about the sampling procedure or duration of sampling so a direct comparison will not be made.

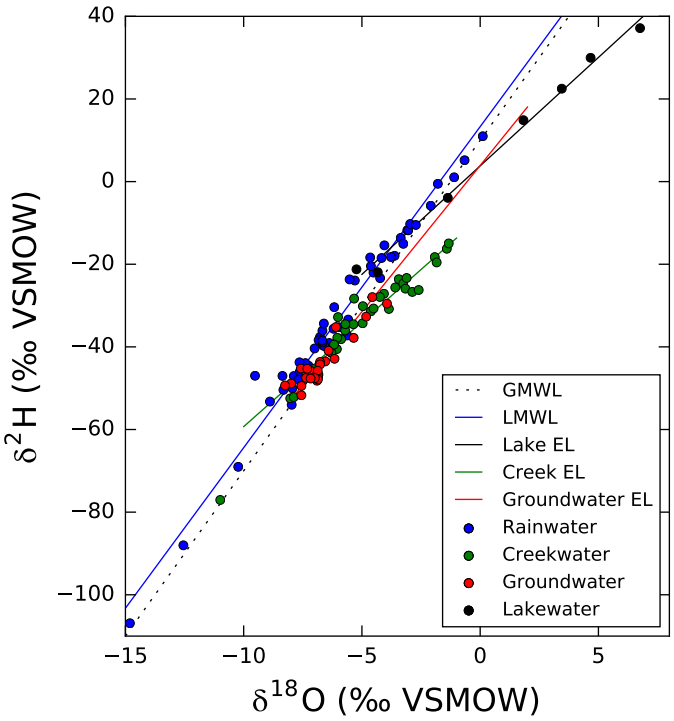

Figure 39: Stable water isotope compositions of various water sources within the Lake George Basin.

Local evaporation lines were also developed for the creek waters and Lake George surface water for the period of sampling (green and black lines, respectively, in Figure 39). The slopes of the two lines (5.1 for creek water and 5.3 for lake water) are indicative of a mean relative humidity of 25 – 75% during open-air evaporation [*Clark and Fritz*, 1997], which is consistent with the observed mean relative humidity of approximately 56% [*BoM*, 2015] for the region during that period. The slopes of the two evaporation lines were also consistent with the slope of the evaporation line (5) calculated for this region using GNIP data by *Gibson et al.* [2008]. The linear regression fitted to the groundwater (red line in Figure 39), which has a slope 7.1, suggests that groundwaters have also undergone some evaporation during or since recharge. *Jacobson et al.* [1991] also made this conclusion based on their analysis of the basin's groundwater.

The stable water isotope ratios of porewater extracted from the Gearys Gap core shows systematic variations throughout the entire profile (Figure 40). Both $\delta^{2}H$ and $\delta^{18}O$ compositions are relatively low (–25.1 and –3.81 ‰, respectively) at 0.5 m below surface, and then steadily increase (to –6.5 and –0.51 ‰, respectively) to a depth of 22.5 m. Below 22.5 m, both water isotope ratios begin to decrease again (to –16.4 and –2.4 ‰, respectively) until the deepest point sampled during the coring (i.e., ~76.5 m).

The lower values at the top of the column are consistent with modern lake water values, which were observed to be –21.2 and –5.23 ‰, respectively, in this study during a period of filling from creek runoff (i.e., June 2013). These values are different to modern rainfall values (i.e., precipitation-weighted means of –38.2 and –6.6 ‰, respectively) because creek runoff is likely to contain a proportion of groundwater and is also likely to be partially evaporated. The steady rise in stable water isotope ratios from a depth of 0.5 to 20.5 m appears, based on the linear pattern, to be due to diffusion between the isotopically 'lighter' modern lake water signature and the isotopically 'heavier' porewater [e.g., *Batlle-Aguilar et al.*, 2016; *Hendry and Wassenaar*, 2004; 2011]. Similarly, below a depth of 22.5 m, the steady decrease of stable water isotope ratios with depth also appears to be due to diffusion based on the systematic pattern. Note that the elevated $\delta^{2}H$ values at a depth of 50 – 60 m show evidence of contamination with D_2O-spiked drilling water; however, this does not appear to affect the $\delta^{18}O$ values or the element/ion concentrations discussed previously.

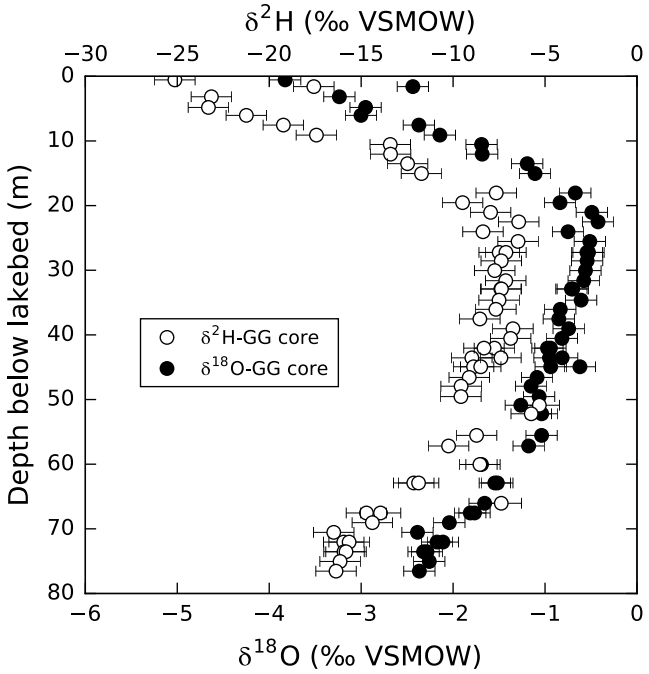

Figure 40: Stable water isotope ratio depth profiles of porewater extracted from the Gearys Gap core.

Both sections of the stable water isotope profile have similar δ^2H against $\delta^{18}O$ regression that are shallower than the modern LMWL (Figure 41). The shallow section of the stable water isotope profile has a steeper slope (5.68 ± 0.22) compared to the deeper section (5.38 ± 0.17; the four outlying samples at depths of 50.88, 52.21, 60.05 and 66.05 m were omitted because they appear to be contaminated by drilling water). These slopes are similar to the modern open-water evaporation lines for lake water and creek water discussed above (i.e., 5.3 and 5.1, respectively). The direction of change in the shallow section of the profile is inconsistent with open-air evaporation because the shallowest water (i.e., recently recharged or diffused) shows a signature of an earlier stage of an evaporation and increased evaporation is evident with increasing depth to 22.5 m. By contrast, the direction of change in the deep section suggests that the δ^2H against $\delta^{18}O$ relationship may be affected by simultaneous diffusion and progressive evaporation of an open water body at the surface. Thus, the pattern of the top section is likely to represent diffusion between the modern lake water and the previous porewater

composition, and the pattern of the bottom section is likely to represent a combination of diffusion and simultaneous evaporation.

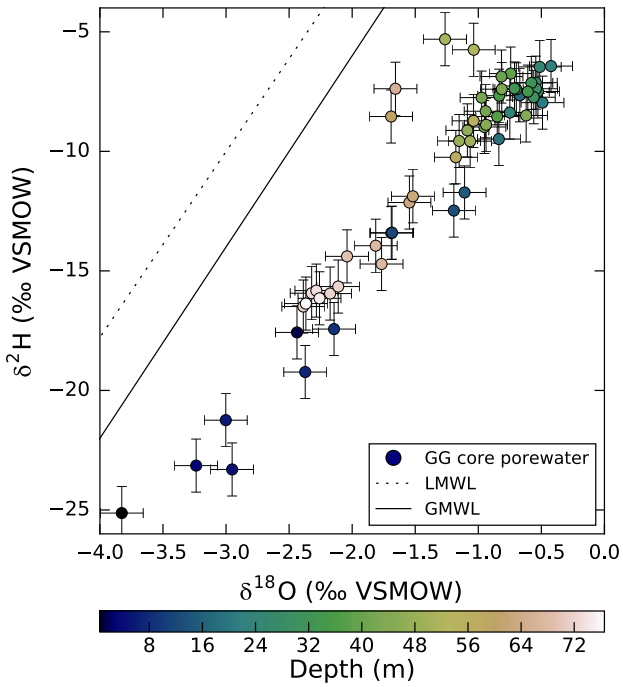

Figure 41: Stable water isotope compositions of porewater extracted from the Gearys Gap core. Colours represent the sample's depth below ground.

A possible hypothesis to explain these observations, which is consistent with the hypothesis proposed based on the trends in major ions/elements (Section 5.1.1), is a 'drying phase' followed by a 'filling phase'. The deeper isotopic pattern represents the simultaneous evaporation, possibly the mega-lake present at the end of the LGM, and diffusion between two different endmembers (i.e., the prior porewater and evaporated surface water). The shallow section represents recent diffusion between the post-LGM lake/creek/rain water isotope signature and the porewater of the shallowest ~23 m of sediment (i.e., the isotopic signature of the most evaporated stage of the prior mega-lake). However, the recent 'filling stage' has not modified the Cl^- concentrations markedly (Figure 35), which may indicate that the 'drying phase' resulted in complete or near-complete drying of the prior lake, such that the stable water isotope composition

of the subsequent shallower lake (i.e., Figure 30) dominated but still maintained a similar Cl^- concentration to the preceding lake because of the lower volume of surface water. Near-complete drying is also consistent with the trends observed for the major ion/element ratios, which suggest that evaporite mineral dissolution/precipitation occurred in the later stages of the previous lake.

However, there are deviations from the linear Cl^- concentration pattern in the shallowest 20 m of the porewater profiles presented in *Jacobson et al.* [1991] and the GG core. These, deviations, towards lower concentrations, may indicate that there were lake stands during this period of re-filling that were long enough to begin to modify the underlying porewater but they were also offset by drying that continued to allow more saline water to migrate downwards.

Finally, the tendency for both the stable water isotope composition and Cl^- concentration of porewater in the top 1 – 2 m of the profile to deviate from the typical pattern of change indicates that physical mixing between porewater and lake water is a dominant process. This may be mediated by rapid surface water infiltration through vertical cracks formed at the lake's surface during dry phases. This is supported by the hydrograph of Russells bore (data not shown), which responds rapidly to rainfall events.

5.1.4. Stable halogen isotopes

Stable halogen isotope ratios were measured on waters from around the Lake George Basin, as well as a selection of the crush/leach samples from the archived cores. A total of 12 modern water samples from the Lake George Basin were analysed for stable chlorine isotope ratios, and seven for stable bromine isotope ratios (Table 10, Figure 43 and Figure 43, Appendix II). The two composite rain samples that were

analysed show no systematic trend for positive or negative $\delta^{37}Cl$ values. The creek waters sampled from the around the basin were all observed to have positive $\delta^{37}Cl$ values; however, their $\delta^{81}Br$ values had a range of positive and negative values. The composite 2013 lake water had a negative $\delta^{37}Cl$ value but a positive $\delta^{81}Br$ value, whereas the sample from Russells Bore (i.e., porewater from only ~1.5 m below the lakebed) was observed to have both positive $\delta^{37}Cl$ and $\delta^{81}Br$ values. The groundwaters that were analysed for $\delta^{37}Cl$ were the more saline of those sampled from the Bungendore Alluvium aquifer, and all were found to have positive $\delta^{37}Cl$ values.

Table 10: Chloride and bromide concentrations, and stable isotope ratios for water samples from the Lake George Basin.

Sample ID	Water type	Cl^- (mg kg^{-1})	Br^- (μg kg^{-1})	Cl^-/Br^- (mass)	$\delta^{37}Cl$ (‰ SMOC)[1]	$\delta^{37}Br$ (‰ SMOB)[1]
LGRWCl-1[2]	Rainwater	~1	~4	~250	0.17 ± 0.11	–
LGRWCl-2[3]	Rainwater	~1	~3	~333	–0.29 ± 0.11	–
ACSW-5	Creek water	732	3 310	221	0.73 ± 0.09	1.02 ± 0.18
BCSW-8	Creek water	67.2	247	272	0.25 ± 0.05	–0.69 ± 0.20
TuCSW-6	Creek water	52.4	222	236	0.31 ± 0.06	–0.74 ± 0.20
CCSW-7	Creek water	113	383	295	0.64 ± 0.09	0.83 ± 0.26
TCSW-7	Creek water	160	432	370	0.93 ± 0.12	0.06 ± 0.01
LGSW-2013[4]	Lake water	2 340	12 300	190	–1.58 ± 0.10	0.73 ± 0.02
PMB_G	Groundwater	440	2 190	200	0.33 ± 0.10	–
PMB_LD	Groundwater	523	2 470	212	0.18 ± 0.16	–
PMB_LS	Groundwater	257	1 230	209	0.34 ± 0.12	–
Russells Bore	Porewater	11 900	62 100	192	0.23 ± 0.10	0.96 ± 0.27

[1]Analytical uncertainties represent 1σ.
[2]Composite rainwater for samples collected between 3/2/14 – 1/7/14, mixed in proportion to the rainfall depth recorded for the sample. Ionic compositions are estimated from individual sample compositions.
[3]Composite rainwater for samples collected between 4/8/14 – 3//1/14, mixed in proportion to the rainfall depth recorded for the sample. Ionic compositions are estimated from individual sample compositions.
[4]Composite lake water sample of all 2013 samples mixed in equal proportions.

The bivariate relationship between $\delta^{37}Cl$ and $\delta^{81}Br$ values, for the samples where both were measured, shows no discernible trends (Figure 42); however, sampling constraints such as volume (i.e., porewaters) and low salinity (i.e., rainwater and groundwater) means that this dataset was very small, and more sampling and analysis of stable halogen isotope ratios may begin to uncover systematic relationships.

In contrast, the relationships between the stable halogen isotope ratios (chlorine in particular) and other parameters such as halide ion concentration and Cl^-/Br^- ratios (Figure 43) displayed some patterns that are consistent with the current understanding of the fractionation processes of these isotope systems, as well as potential salt cycling mechanisms within the Lake George Basin. The $\delta^{37}Cl$ values of creek waters increase with both increasing Cl^-/Br^- ratios (Figure 43a and Figure 43c) and Cl^- concentration. This is consistent with the hypothesis presented in Section 5.1.2 – elevated Cl^-/Br^- ratios of creek water may indicate a proportion of wind-blown dust. Halite, which is likely to be the component of dust that acts to increase the Cl^-/Br^- ratios of creek water, has also been found to typically have higher $\delta^{37}Cl$ values due to the preferential partitioning of ^{37}Cl into the solid phase during halite precipitation [*Eggenkamp*, 2014]. The likely residual water in the case of the Lake George Basin, is the very shallow (i.e., the top few centimetres) lakebed porewater and lake surface water. Thus, it is also consistent that the composite lake water sample from 2013 was observed to have a lower $\delta^{37}Cl$ value relative to the creeks, such that halite precipitation and subsequent wind erosion has lowered the isotope signature. However, if this process occurs the influence on $\delta^{37}Cl$ values does not appear to propagate to the deeper porewater (i.e., the 1.5 m depth of Russells Bore intake). This is consistent with the Cl^- concentration profile of the GG core (Figure 35), where the shallowest sample at ~0.5 m depth has a markedly different (i.e., anomalously low) Cl^- concentration that does not fit with the pattern of the samples beneath it. This, as well as the ratio variations discussed in Section 5.1.1, may indicate that physical mixing of porewater and lake water suggested by *Jacobson et al.* [1991] only occurs in the top 0 – 2 m of sediment.

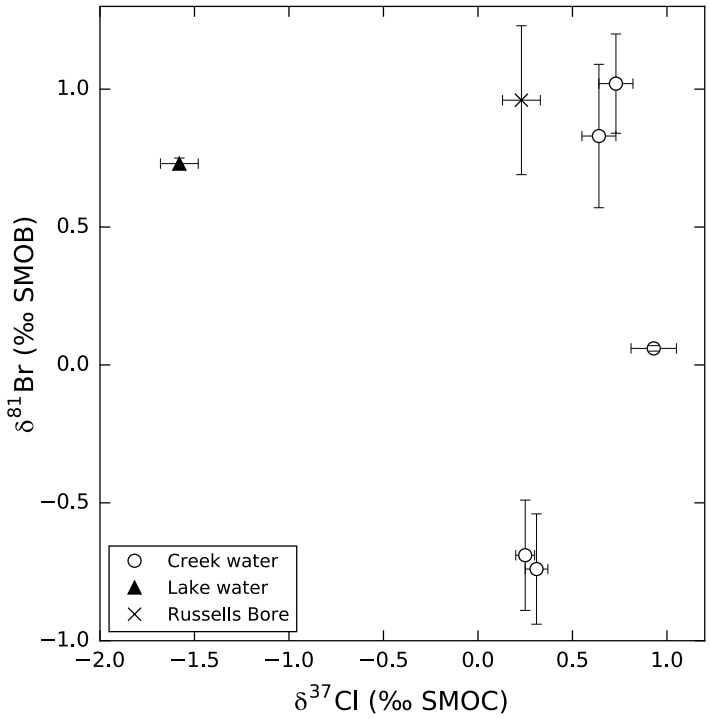

Figure 42: Stable chlorine ($\delta^{37}Cl$) and bromine ($\delta^{81}Br$) isotope ratios of creek, lake and Russells Bore water collected from the Lake George Basin between 2013 and 2015.

There is a weak positive relationship between $\delta^{81}Br$ values and Br^- concentration of creek waters; however, there is no apparent relationship with Cl^-/Br^- ratio, which (in the absence of other information or improved understanding of bromine stable isotope fractionation mechanisms) makes the potential relationship difficult to interpret. However, it has recently been found that a range of biogeochemical processes (e.g., evaporite precipitation/dissolution, biological activity/decay and photochemical induced reduction [*Eggenkamp*, 1995; 2014; *Eggenkamp et al.*, 2016; *Eggenkamp and Coleman*, 2009; *Hanlon*, 2015; *Horst et al.*, 2014]) can act upon bromine to modify its stable isotope composition. Investigation into the degree to which this fractionation occurs is still in its early days.

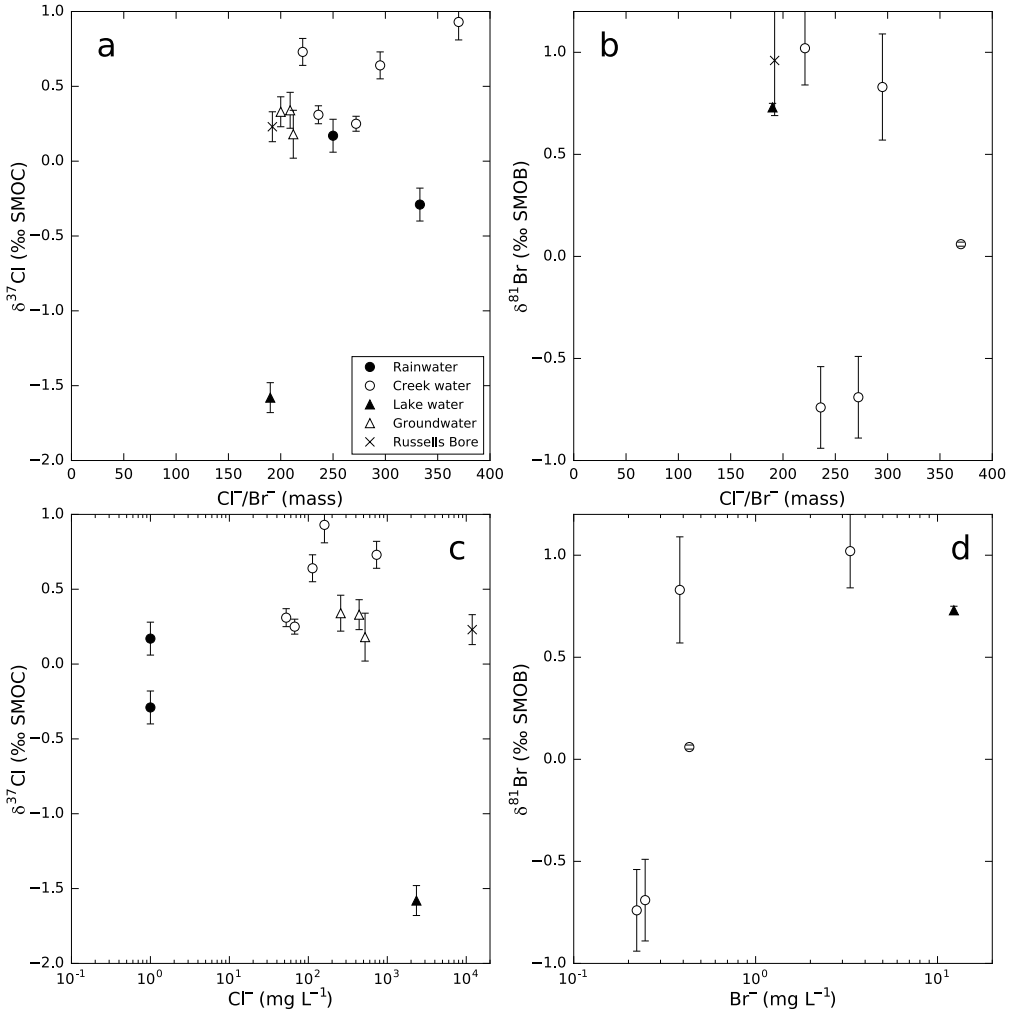

Figure 43: Stable halogen isotope ratios ($\delta^{37}Cl$ and $\delta^{81}Br$) with respect to Cl^-/Br^- ratios (a and b) and concentrations of their respective halide ions (c and d) from water samples collected from the Lake George Basin between 2013 and 2015.

Only three stable bromine isotope ratios analyses were obtained (see Appendix II) for crush/leach samples from the archived core because of sample size limitations and subsequent low total Br^- masses. These samples had a stable bromine isotope ratio range of –0.29 – +1.49 ‰, which is in the current range of observed stable bromine isotopes from other regions (i.e. –0.80 – +3.35 ‰). There is insufficient resolution to make any inferences on solute transport or geochemical reactions within the lakebed sediments.

Stable chlorine isotope ratios of the crush/leach samples from the archived cores were found to have a systematic pattern of variation throughout the vertical profile (Figure 44). Although the $\delta^{37}Cl$ data are quite 'noisy' throughout the profile, the fitted linear regressions (all with r-squared values of >0.5; Table 11) indicate that there is both a trend of decreasing $\delta^{37}Cl$ values with increasing depth and increasing distance towards the east (i.e., increasing core number corresponds to increasing distance to the west, separated by ~1 km; Figure 32). The former trend is consistent with the hypothesis presented by *Jacobson et al.* [1991] and in the previous discussion on ion/element trends and stable water isotopes that solute transport within the lakebed sediments is dominated by downward diffusion. The latter trend is one that has not been identified previously but is consistent with the data presented in *Jacobson et al.* [1991]. The Cl^- concentration of the two cores presented in *Jacobson et al.* [1991] display a systematic difference with C352 (east) having a lower overall concentration (approximately 5 – 10 g L^{-1} lower throughout the profile) compared to C354 (west). Furthermore, the GG core, which is located at a similar northing but further west (~500 m) than C354, was observed to have an even greater Cl^- concentration (approximately 5 – 10 g L^{-1} higher throughout the profile). Therefore, it appears that solutes are migrating, predominantly by diffusive processes based on $\delta^{37}Cl$ fractionation, both downwards and eastwards through the low-permeability lakebed sediments.

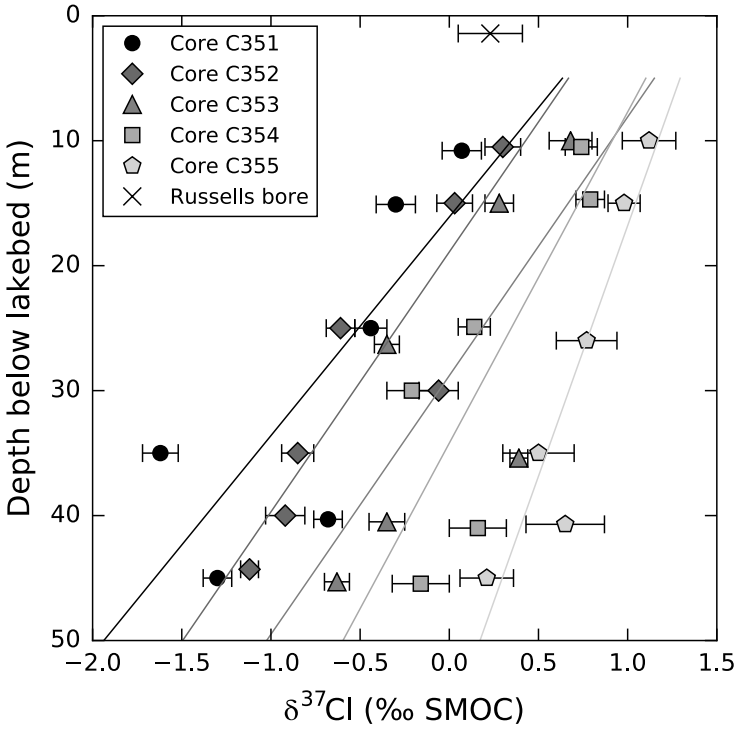

Figure 44: Stable chlorine isotope ratio ($\delta^{37}Cl$) depth profiles of the crush/leach samples obtained from the archived BMR core and for a sample collected from Russells bore. Lines are fitted linear regressions.

Table 11: Parameters calculated for the linear regressions fitted to the stable chlorine isotope ratio depths profiles (Figure 44). Regressions are in the form: $\delta^{37}Cl = a(\text{depth}) + c$.

Core	Slope, *a*	Intercept, *c*	r-squared
C351	-17.5 ± 6.4	16.1 ± 5.9	0.65
C352	-20.8 ± 4.3	18.9 ± 3.0	0.82
C353	-20.7 ± 9.0	28.8 ± 4.2	0.57
C354	-26.5 ± 9.2	34.2 ± 4.3	0.67
C355	-40.1 ± 7.5	56.9 ± 5.8	0.88

Although diffusion is likely to explain much of the vertical Cl^- concentration and vertical $\delta^{37}Cl$ trends, the horizontal trends are hard to explain by purely diffusion because of the much greater length-scale (i.e., ~5 km horizontal compared to 50 m vertical) especially if diffusion occurred on similar time-scales (i.e., if the same event is responsible for both patterns). To demonstrate this, a simple analytical solution to the one-dimensional (1D) diffusion equation was used to reproduce the observed data. In a

system where advection can be neglected (i.e., diffusion dominates), concentration changes due to diffusion as a function of time and space can be represented by Fick's second law of diffusion [*Fick*, 1855]:

$$\frac{\partial C}{\partial t} = D_e \frac{\partial^2 C}{\partial z^2} \qquad (18)$$

where C is the concentration ([amount of substance] L^{-3}), t is time, D_e is the effective diffusion coefficient ('effective' because it relates to porous media in this study; $L^2\ t^{-1}$) and z is the vertical position (L). For the condition of a fixed amount of substance being released at $x = 0$ and $t = 0$ into a column with a uniform initial concentration, Equation (18) can be solved to produce the analytical solution [e.g., *Eggenkamp*, 2014; Equation 7.6, pp. 77]:

$$C_{(x,t)} = C_i + \left(\frac{s}{\sqrt{4\pi D_e t}} exp - \frac{z^2}{4D_e t}\right) \qquad (19)$$

where $C_{(x,t)}$ is the Cl^- concentration (g L^{-1}) at a given position and time, C_i is the initial Cl^- concentration (g L^{-1}) throughout the 1D column, and s is the amount of Cl^- (g) released at t=0.

It was assumed that the initial porewater Cl^- concentration was 6 g L^{-1}, a reasonable reproduction of the vertical concentration profile of core C352 was achieved (Figure 45a) using a time of 8 000 years (i.e., consistent with the post-LGM drying of Lake George), an effective diffusion coefficient of 0.026 $m^2\ year^{-1}$ (i.e., accounting for transport in similar clay-rich porous media [*Batlle-Aguilar et al.*, 2016]), and a momentary release mass of Cl^- of 600 g (this value was modified to reproduce the observed data). This set of parameters reproduces all but the shallowest 10 m of the profile, which is likely to represent a more recent and complex (i.e., beyond the scope of

an analytical solution) modification of the porewater concentrations by mixing and diffusion with less saline modern lake water. However, this combination of parameters does not come close to achieving a reasonable fit for the horizontal profile. In fact, a period of approximately 20 000 years is needed for the concentration at 1 km from the source to be modified by only ~1% from its initial value of 5 g L^{-1}.

The simple modelling described above results in a partial fit to the observed pattern of $\delta^{37}Cl$ values (Figure 45b). That is, the shallowest 40 m of the profile approximately matches the direction and magnitude of isotopic change observed in the crush/leach samples from core C352. The deeper section deviates from the results calculated using a simple 1D representation of the system but there are only two isotope samples from this depth, so it is unclear if the results match at greater depths. The same parameters were adopted from the concentration modelling described above; however, the $\delta^{37}Cl$ values needed to be offset by +0.3 ‰ from 0 ‰ SMOC to achieve more reasonable agreement with the observed data. Interestingly, this value of +0.3 ‰ was also observed in two of the analysed groundwater samples from the Bungendore Alluvium, which may provide guidance to the long-term mean $\delta^{37}Cl$ value of incoming solutes to the basin.

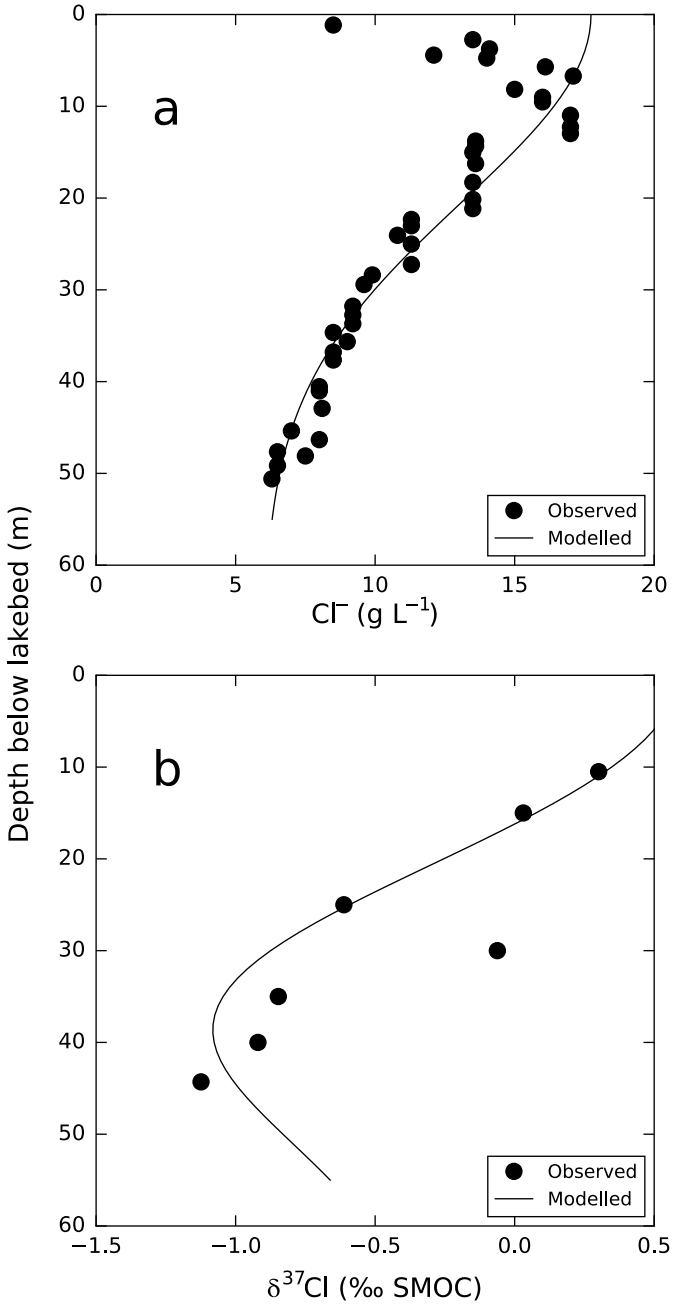

Figure 45: Observed and modelled Cl^- concentrations (a) and $\delta^{37}Cl$ values (b) of porewater and crush/leach samples, respectively, from core C352.

An equally reasonable fit can be achieved to the C354 data by only modifying the endmember concentrations for that location. A crucial point to note from the simple 1D modelling, is that to get a close fit to the observed data, both the initial values of the porewater and the source concentrations must be offset equally for the different cores.

The varying of the source concentration may be explained by progressive stages of evaporation resulting in different source concentrations at different locations. As the mega-lake reached the final stages of drying the overall concentration would have increased but the lake's footprint on the lakebed would have been decreasing, possibly focussed towards the western shore given the location of the highest salinity water. However, the seemingly equal horizontal increase Cl^- concentration with increasing western distance suggests that the horizontal pattern was present long before the event that resulted in the vertical pattern. No current palaeoenvironmental evidence exists to provide an explanation of why this pattern may exist, mostly due to these features generally being deposited post-LGM.

A recent review article *Eastoe* [2016] presented a series of hypothetical stable chlorine isotope scenarios for non-marine basins. A key finding of the review was that stable chlorine isotope can be cumulatively fractionated by simultaneous environmental processes in environments with 'vadose playas' that discharge solutes into their lakebeds (analogous to Lake George and the scenario depicted by Figure 18b in Chapter 4). The enhanced fractionation of stable chlorine isotope ratios discussed by *Eastoe* [2016] is due to multiple cycles of wetting, drying, evaporite formation and diffusion. *Eastoe* [2016] noted that their model was simplistic but was useful for highlighting that multiple processes (i.e., evaporite formation, diffusion, changes in source, biological activity, etc.) are likely to occur in field environments, which modify stable halogen isotope ratios from those predicted by ideal models that account for only individual processes separately.

Based on the data presented in this chapter, it is quite evident that stable halogen isotope variations within the Lake George Basin are worthy of further high-resolution investigation (i.e., seasonal variations, finer resolution porewater sampling, etc.). This

would attempt to address the recommendations of *Eastoe* [2016] – to carefully select field sites for further investigation of the cumulative fractionation of stable halogen isotopes by multiple simultaneous environmental processes.

In the interest of understanding local processes at Lake George, the collection of further stable water isotope ratio porewater profiles at sites along an east-west lakebed transect would also provide useful data to cross-check whether the processes leading to chlorine variations have also acted to modify water isotopes. Furthermore, Cl^- concentrations and stable halogen isotope ratios from the additional porewater profiles would also help to better constrain the pattern of horizontal salinity and isotope variations. The additional cores would only have to be a few metres deep, rather tens of metres like the GG core, to address these questions. However, obtaining $\delta^{37}Cl$ measurements from the entire length of the GG core (at ~5 m intervals) would help to address whether the simple 1D modelling results presented above also matched the lower isotope profile.

5.2. Salt cycling implications

Overall, the hydrogeochemical parameters observed in this study are broadly consistent with the salt cycling regime hypothesised in *Jacobson et al.* [1991]. The five primary water-types of the Lake George Basin described in Section 2.4 of Chapter 4 are expanded upon here based on the observations presented in this chapter:

1. Rainwaters are depleted in Mg relative to low-salinity groundwater and creek water of the basin, suggesting that Mg is dissolved into water soon after it interacts with the local geology, such as by weathering of Mg-bearing minerals (e.g., biotite, chlorite, amphibole).

The similar mean ion ratios of rainwater to seawater (i.e., Cl^-/Br^- and Cl^-/Na) and $\delta^{37}Cl$ values suggest that the atmospheric source of solutes is predominantly oceanic; however, months with much lower ion ratios may indicate that individual rain events can introduce solutes from continental sources.

2. Creek water can generally be characterised as described by *Jacobson et al.* [1991]; however, the positive relationship between elevated Cl^-/Br^- ratios and $\delta^{37}Cl$ values with increasing salinity suggests that up to 25% of the creek water Cl^- could be contributed by halite. Based on the lower Cl^-/Br^- ratios and lower $\delta^{37}Cl$ values of lake water, a potential source of this halite is *via* windborne dust eroded from salt crusts on the lakebed.

   The stable water isotope composition of creek waters indicates open water evaporation, like lake waters, but with a markedly different slope to groundwater. The progression from the non-evaporated endmember towards the most evaporated compositions coincides with high and low streamflow conditions in the creeks, respectively. Furthermore, the isotope composition of the non-evaporated endmember is similar to mean winter rainfall, which suggests that creek water is predominantly composed of direct rainfall or very recent through flow. A single tritium result for Butmaroo Creek (Appendix II), which is similar to mean rainfall, also supports this suggestion.

3. The fresh to brackish groundwaters of the alluvial plains are characterised by similar stable water isotope and major ion/element composition to creek and rain waters (except for the low proportion of Mg in rainfall). However, the distinct (relatively lower) Cl^-/Br^- ratio of groundwaters in

the alluvial plains suggests that these waters were either recharged during a time of different incoming composition (i.e., similar to the source of lakebed porewater) compared to modern rainwater, or alternatively, it could indicate that diffusion from the lakebed, which has a similar Cl^-/Br^- ratio, may have imparted its Cl^-/Br^- ratio on groundwater while not increasing its salinity markedly.

4. Lake water is characterised by brackish-saline TDS concentrations. The similar Cl^-/Br^- ratios of lake water to the underlying porewater, rather than being similar to inflowing creek water or rain, suggests that solutes are predominantly sourced by mixing between the low-salinity inflow water (i.e., direct rainfall and creek runoff) with the saline porewater stored within the underlying lakebed.

   The progressive change in stable water isotope ratios during a drying phase of the lake during 2013 indicates that increases in salinity are predominantly due to evaporation rather solute input. These progressive variations also indicate that Lake George can be considered a quasi-closed system with respect to its stable water isotope composition, such that it appears that during the period in 2013, a single source endmember was progressively evaporated to dryness with minimal variations caused by non-evaporative water losses or additional inputs from other sources.

   The low $\delta^{37}Cl$ mean value of 2013 lake water, relative to underlying porewater (i.e., Russells Bore) and creek water, may be further evidence that multiple cycles of wetting, drying and wind erosion under the modern hydrologic regime (i.e., Figure 24) have led to halite (in the form of dust)

being removed from the lake surface and redeposited in the wider catchment, and possibly into adjacent ones.

5. Lakebed porewater is most readily identified by its much greater salinity compared to most other water-types in the Lake George Basin. Near linear trends in many of the dissolved ions/elements and stable water isotopes, along with the negative fractionation of stable chlorine isotopes with depth, indicate that solute transport within the lakebed is dominated by chemical diffusion and that porewater advection is likely to be minimal. However, distinct major ion/element, and isotopic compositions of the shallowest samples (i.e., 0 – 2 m below the surface) indicate that physical mixing (i.e., through vertical cracks in the dried lakebed or by pressure driven flow), as well as diffusion, may take place with modern lake water in this zone.

Although the lakebed porewater maintains a Cl^-–Na composition throughout the profile, variations in proportions of the less predominant ions/elements were observed to have systematic variations that may elucidate parts of the complex palaeohydrologic and geochemical processes that have occurred in this basin. Furthermore, the large variations in stable water isotope ratios over the depth of the profile may provide evidence of past rainwater compositions and the timing of the evaporation of the post-LGM mega-lake. These aspects are discussed in the next section.

The observation of higher porewater salinities on the western side of the lakebed, within 2 km of the Yass River catchment headwaters (i.e., a tributary of the River Murray), should provide motivation to better understand the groundwater flow and

solute transport across the Lake George Fault. Higher water elevations and lower salinities of groundwater in this zone [e.g., *Abell*, 1985; *Jacobson et al.*, 1991] are likely to provide a buffer to migration of this salt into the Yass River catchment; however, there are no available data to rule out migration of the lakebed salt into adjacent catchments.

From a water management perspective, knowledge of the large mass of salt stored within the lakebed sediments and the direction of solute transport is useful. This information should be used to guide water management within the surrounding sub-catchments, such that hydraulic gradients (i.e., groundwater flow directions) are maintained directed towards the lake so that salinity migration into the freshwater aquifers is not artificially enhanced by groundwater flow.

5.3. Palaeohydrologic implications

Based on the patterns of multiple hydrogeochemical parameters the following three major lake phases post-LGM are proposed:

1. A period of evaporation and progressive drying of a mega-lake present at the end of the LGM. This lake was likely to contain brackish water, assuming that the concentration of the deepest porewater provides a lower limit to the initial concentration (i.e., >10 g L^{-1} as TDS). The evaporation of the ~38 m deep ancient mega-lake is likely to have occurred over a period of approximately 8 000 years based on dating of ancient shorelines (i.e., Figure 30) and simple 1D diffusion modelling of the vertical lakebed salinity profile (i.e., Figure 45).
2. A period of partial re-filling of the lake, punctuated by multiple drying phases (i.e., Figure 30). During this period water with a lower stable water

isotope composition diffused into the lakebed. However, the average salinity of lake water during this period appears to have continued to increase, based on the continuing increase in porewater salinity with decreasing depth in top 10 m of lakebed sediments. This further highlights the lower volume present during the refilling of the lake.

3. The modern ephemeral lake system. This period is characterised by the occurrence of standing water only over years to decades of above average rainfall (i.e., Figure 24). Thus, the surface water is typically brackish because the short time periods that surface water is present are not long enough for substantial amounts of salt to be re-mobilised into the water column. This water also has an average stable water isotope composition that is lower than during the LGM but has a wide range because the quasi-closed nature of the wetting and drying cycles means that they are modified predominantly by open-water evaporation.

The conceptual development of these three lake phases have been assisted by, and are consistent with, the previous palaeoenvironmental studies undertaken on the Lake George Basin. The timing and lake water level ranges are consistent with reconstructed water levels based on ancient shorelines [*Coventry*, 1976; *Fitzsimmons and Barrows*, 2010], and estimated salinities based on ostracod and pollen occurrences in the sedimentary sequence [*De Deckker*, 1982; *Singh et al.*, 1981].

6. Conclusions

The systematic variations and trends of a combination of hydrogeochemical parameters presented in this chapter have assisted in providing a clearer understanding

of a saline lake system that is important locally to water resources, and regionally for its rich palaeoenvironmental record. The findings presented in this chapter have been largely improved upon by the targeted use of Cl- and Br-based environmental tracer techniques; namely, the use of Cl^-/Br^- ratios and stable halogen isotope compositions. Although these techniques were useful in providing unique information that the other parameters could not elucidate, the other parameters also provide constraints where Cl- and Br-based methods were ambiguous or unavailable. Thus, the general findings regarding the use of Cl- and Br-based tracer techniques in the manner presented in this chapter do not stray far from the final remarks made by *Davis et al.* [1998; pp. 347-348], which are worthy of repeating (the term 'Cl^-/Br^- ratios' can be replaced more generally by Cl- and Br-based tracer techniques):

> *"The use of Cl^-/Br^- ratios is obviously not a general panacea for all intractable questions in hydrogeology. As always, no substitute exists for careful site-specific application of numerous scientific tools in an integrated approach to hydrogeologic problems. The utility of using Cl^-/Br^- ratios is so great, however, that we recommend their widespread use. Where possible, accurate bromide analyses should accompany chloride analyses in all routine as well as non-routine ground water investigations."*

The combination of environmental tracers utilised in this study have helped to broadly confirm the salt cycling processes of the Lake George Basin described by an earlier pioneering study. However, in addition to those findings, our results expand upon that knowledge by providing evidence that, in this basin, wind erosion of lakebed surface crust may provide a source of salinity to local creeks, and potentially adjacent catchments. The isotopic results presented in this chapter have also confirmed that

solute transport within the lakebed sediments of Lake George, at least in the shallowest 50 – 60 m, is predominantly controlled by chemical diffusion.

The results presented here do, however, deviate from the palaeohydrologic history described in the earlier study, in which a hypothesis of continual salt accumulation over the last 2 Ma was presented to explain the pattern of porewater salinity. The results presented in this chapter suggest that the porewater profiles of the lakebed are instead best explained by a complex hydrogeochemical evolution of an evaporating mega-lake since the LGM. Three distinct lake phases were identified, which were in broad agreement with previous palaeoenvironmental findings: (1) an initial evaporation of a post-LGM mega-lake to near- or complete-dryness over approximately 8 000 years, (2) a period of cyclic partial re-filling and drying of a lake of substantially lower volume than the mega-lake, which lasted for ~10 000 – 20 000 years, and (3) the modern configuration of an ephemeral, very shallow and brackish water lake that only sustains standing water over years to decades depending on prevailing climatic trends.

Summary

This thesis has presented findings based on theoretical analysis, large-scale monitoring and a targeted field investigation to improve the understanding of how Cl and Br can be utilised as tracers of terrestrial salt cycling, more robustly than in previous studies. Dissolved Cl and Br concentrations have been utilised for many decades as individual tracers or together as a ratio to trace geochemical processes in saline environments. More recently, the stable isotope variations of these two elements have also been found to be useful for quantifying and interpreting geochemical processes. However, both hydrogeochemical techniques need to be developed and improved by applying them in new environments and the collection of further data in well-designed studies on a local and continental scale, as well as developing quantitative methods to provide further value to their use.

Firstly, a bench-top salt dissolution experiments were used to verify a previously established quantitative mixing model that utilises Cl^-/Br^- ratios to correct Cl^-- or Br^--based tracer methods for other Cl^- sources. The results show that the model can predict the percentage of alternate salt sources accurately after analytical and endmember uncertainties are considered. Further analysis of the uncertainties and sensitivities provide scientists with a guide to which environments and scenarios the use of the mixing model would be most appropriate. The mixing model correction provides a useful and cheap method for scientists to improve their use of Cl^-- or Br^--based tracer techniques in catchment studies.

Secondly, continental-scale spatial and temporal variations in Cl^-/Br^- ratios were presented, based on the interpretation of a dataset of wet deposition compositions spanning six and half years. A recently developed imputation algorithm was applied to estimate the high proportion of censored bromide values, as well as the other eight analytes, based on the multivariate relationships of nine analytes. Cl^-/Br^- ratios of wet

deposition decrease with distance inland following a logarithmic regression. The observations provide further confidence in the findings presented in previous studies that have shown that Cl^-/Br^- ratios systematically decrease with increasing distance from the coast.

Lastly, Cl and Br tracer techniques were applied in a case study of the Lake George Basin, NSW, to trace modern salt cycling proximal to a saline lake, and to investigate how hydrogeochemical signatures can elucidate palaeohydrologic processes. The Lake George Basin was chosen as the field site because of its long, near-continuous sequence of Cenozoic lake sediments, and its complex salt cycling regime. The Cl- and Br-based tracer methods, in combination with other geochemical information, have provided a better understanding of the modern salt cycling regime within the catchment, and have also provided useful constraints on the timing of the recession of the mega-lake that existed in the basin during the last glacial maximum. This study also illustrated the utility of Cl- and Br-based tracer methods to delineate salt cycling processes in saline lake environments.

1. Recommendations

The following sections briefly outline specific recommendations that are made based on the findings of the most substantial chapters of this thesis (i.e., Chapters 2, 3 and 5), and are broadly characterised under the sub-heading ‘Quantitative use of chlorine and bromine’, ‘Near surface cycling of chlorine and bromine’, ‘Chlorine and bromine in saline lake environments’, and ‘Hydrogeochemistry of the Lake George Basin’.

1.1. Quantitative use of chlorine and bromine

The work presented in Chapter 2 illustrated the simplicity and robustness of the combined use of Cl^- and Br^- to quantify salt sources and sources of error in Cl^--based tracer methods. However, this chapter also highlighted that both the precision of the chemical analysis, as well as the uncertainty, or natural variation, in endmember compositions can dramatically limit the use of these methods. Thus, the main recommendations from this section of the thesis are two-fold:

1. Where Cl^-/Br^- ratios are being used for quantitative analysis using equations such as those presented in Chapter 2, uncertainties resulting from the chemical analysis should be accounted for. This can be achieved simply by using freely-available error propagation software, such as *uncertainties* [*Lebigot*, 2014], and yields valuable information about how reliable these techniques are for a given situation. Failure to do so could lead to misleading interpretations because the uncertainties can render these methods inadequate as quantitative tools in some situations.
2. A detailed analysis of endmember compositions (i.e., spatial and temporal variations) should always precede the application of Cl^-/Br^- ratios as a quantitative tool. If the collection of new site-specific data is unfeasible, then researchers should attempt to incorporate this uncertainty into their results in a similar fashion to the point on analytical precision above.

1.2. Near surface cycling of chlorine and bromine

The spatial and temporal analysis of wet deposition Cl^-/Br^- ratios presented in Chapter 3 demonstrates that researchers should not assume that all catchments receive atmospheric deposition with the same compositions. Cl^-/Br^- ratios of wet deposition

decrease logarithmically away from the coast, due to processes acting on large-scales (i.e., SSA transport, photochemical reactions and washout effects). This highlights the need for researchers to undertake site-specific sampling prior to applying Cl^-/Br^- ratios quantitatively. However, the systematic nature of the variations observed in these data suggest that in the absence of site-specific data (i.e., due to funding constraints, site access, *etc.*), an idealised equation may be used to provide a more reasonable estimate compared to assuming that rainfall maintains a seawater-like ratio regardless of location. The following recommendations are made regarding the future collection of continental-scale Cl^-/Br^- ratio datasets:

1. Continue to improve the detection limits of Br^- concentrations of water samples. Even at the detection limits achievable by modern methods (i.e. <0.1 ppb) some far inland sites may receive atmospheric deposition that has Br^- concentrations that are below the limits of detection. These techniques should also account for the potentially low volume of atmospheric deposition samples because of the opportunistic nature of their collection.
2. Test the predictions made by the imputation technique applied to the NADP dataset. This could be achieved by re-analysing stored samples using methods that have a lower limit of detection. However, this would potentially be affected by modification of halides during the storage period. Additionally, the continued collection and analysis of wet deposition samples by the NADP, especially as newer analysis methods with lower detection limits are adopted as they become practicable, will provide improved baseline data for interpreting the near-surface cycling of these elements.

3. Expand the network of countries undertaking large-scale atmospheric deposition sampling and analysis. The assessment of Cl^-/Br^- ratio variations presented in Chapter 3 is potentially limited by regional effects that are unique to North America. The analysis of samples, collected in a similar fashion, from other large continents would further strengthen the understanding of near-surface Cl and Br cycling.
4. Undertake additional unorthodox spatial analyses like *Davis et al.* [2004] (i.e., using low-salinity groundwater as a proxy for atmospheric deposition) to provide additional lines of evidence regarding the continental-scale transport processes of Cl and Br. Despite the seemingly crude method adopted in by *Davis et al.* [2004], their findings appear to have provided a cost-effective and accurate assessment of how Cl^-/Br^- ratios are modified over large spatial scales.
5. Collect large volume atmospheric deposition samples (i.e., to obtain sufficient mass of Cl and Br) with the aim of undertaking stable halogen isotope ratio analyses. This would help to identify whether the variations in Cl and Br cycling in atmospheric deposition are driven by physical transport mechanisms or by chemical reactions that affect their stable isotopes. It would also improve the understanding of endmember compositions when applying stable halogen isotope ratio techniques in catchment or hydrogeochemical investigations.

1.3. Chlorine and bromine in saline lake environments

The field investigation presented in Chapter 5 demonstrated the great utility of chlorine- and bromine-based tracer methods, in combination with other geochemical methods, in saline environments. However, some of the results remain ambiguous

because of gaps in the current understanding of the geochemistry of Cl and Br, especially the processes that affect stable halogen isotope ratios. The following are four key areas of future research in the pursuit of understanding the geochemistry of Cl and Br in saline lake environments:

1. The role of biological activity on how stable halogen isotope ratios are modified and if these processes modify Cl^-/Br^- ratios (i.e., do organisms preferentially remove one ion over the other?). These studies should include impacts from plant, animal and microbial species.
2. Further investigate the impact of multiple cycles of wetting-drying-leakage as outlined by *Eastoe* [2016] to determine the extent that this effect can have on observed stable halogen isotope ratios in 'vadose playas'. Additionally, the effect of wind erosion at the playa surface should be considered. The cumulative effect of processes could be further understood by undertaking complex geochemical modelling, laboratory experiments and targeted field investigations.
3. Attempts should be made to combine both Br and Cl stable isotope ratio analyses on samples collected in saline lake environments. This would continue to build the understanding of the degree to which these isotope systems are related (or unrelated) to each other.

1.4. Hydrogeochemistry of the Lake George Basin

Chapter 5 has further emphasised the rich palaeoenvironmental history that is recorded by the geologic features of the Lake George Basin. It has also highlighted that the hydrogeochemical signatures held within the porewater of the lakebed may potentially record the effects of environmental processes as effectively as other

geological features within the basin. The following recommendations with the aim of building upon the assessment presented in Chapter 5:

1. Undertake stable chlorine isotope ratio analysis on a series of porewater samples from the GG core to a depth below 60 m. This would determine whether the simple 1D modelling was sufficient for predicting stable halogen isotope ratios in the system. Accordingly, these additional data would provide useful information on the final drying phase of the post-LGM mega-lake.
2. Collect a series of shallow cores from the lakebed along and east-west transect with the purpose of obtaining porewater samples for geochemical analysis (i.e. stable halogen and water isotopes, and Cl^- concentrations). These additional datasets would help to broaden the analysis of porewater solute transport from a 1D to a 2D (potentially 3D) analysis. It would also help to investigate the hypotheses made in Chapter 5 regarding the palaeohydrologic history of Lake George, as well as its salt cycling mechanisms. These cores would only have to be a few metres, rather tens of metres like the GG core, to address these questions.
3. Undertake complex solute transport/groundwater flow modelling of the porewater within the lakebed sediments. This should be accompanied by obtaining additional data regarding the hydraulic properties (i.e., permeability, porosity and solute transport characteristics) of the lakebed sediments. This would provide researchers investigating the palaeoenvironments of Lake George with a tool to input various scenarios regarding the lake's past to, as well as water resource managers who may

want to better quantify the risk of salinisation of the local freshwater aquifers.

4. Maintain the historical monitoring at Lake George. At a bare-minimum, the hydrographic and precipitation records for Lake George should be maintained to continue the almost 200-year records that currently exist. However, studies continue to uncover the great scientific value of the Lake George Basin for environmental research, especially hydrology and climate. Thus, additional monitoring (i.e., meteorological, hydrographic, hydrogeochemical, *etc*.) would be advantageous for studying these processes in the Australian context and to build upon previous work.

References

Abell, R. S. (1985), Geology of the Lake George Basin, N.S.W.*Rep. Record 1985/4*, 115 pp, Bureau of Mineral Resources, Geology and Geophysics, Canberra, Australia.

Aitchison, J. (1982), The statistical analysis of compositional data, *Journal of the Royal Statistical Society: Series B (Methodological)*, *44*, 139-177.

Alcalá, F. J., and E. Custodio (2008a), Atmospheric chloride deposition in continental Spain, *Hydrological Processes*, *22*(18), 3636-3650, doi:10.1002/hyp.6965.

Alcalá, F. J., and E. Custodio (2008b), Using the Cl/Br ratio as a tracer to identify the origin of salinity in aquifers in Spain and Portugal, *Journal of Hydrology*, *359*(1-2), 189-207, doi:10.1016/j.jhydrol.2008.06.028.

Allen, R. G., L. S. Pereira, D. Raes, and M. Smith (1998), Crop evapotranspiration - Guidelines for computing crop water requirements*Rep.*, 333 pp, FAO Irrigation and drainage paper 56, Available at http://www.fao.org/docrep/x0490e/x0490e00.htm.

Allison, G. B., G. W. Gee, and S. W. Tyler (1994), Vadose-zone techniques for estimating groundwater recharge in arid and semiarid regions, *Soil Science Society of America Journal*, *58*(1), 6-14.

Appelo, C. A. J., and D. Postma (2005), *Geochemistry, Groundwater and Pollution*, 2nd ed., 668 pp., CRC Press, Boca Raton, USA.

Ayers, G. P., R. W. Gillett, J. M. Cainey, and A. L. Dick (1999), Chloride and bromide loss from sea-salt particles in Southern Ocean air, *Journal of Atmospheric Chemistry*, *33*(3), 299-319, doi:10.1023/A:1006120205159.

Ayers, G. P., and J. L. Gras (1983), The concentration of ammonia in Southern Ocean air, *Journal of Geophysical Research: Oceans*, *88*(C15), 10655-10659, doi:10.1029/JC088iC15p10655.

Ayers, G. P., and J. P. Ivey (1988), Precipitation composition at Cape Grim, 1977–1985, *Tellus B*, *40B*(4), 297-307, doi:10.1111/j.1600-0889.1988.tb00299.x.

Ballance, J. A., and J. R. Duncan (1985), Wind-borne transport and deposition of sea-salt in New Zealand, *New Zealand Journal of Technology*, *1*, 239-244.

Barrow, G. (2012), *'Magnificent' Lake George - The Biography*, 114 pp., Dagraja Press, Canberra.

Batlle-Aguilar, J., P. G. Cook, and G. A. Harrington (2016), Comparison of hydraulic and chemical methods for determining hydraulic conductivity and leakage rates in argillaceous aquitards, *Journal of Hydrology*, *532*, 102-121, doi:10.1016/j.jhydrol.2015.11.035.

Beavis, S. (2011), Water resources of the western catchments of Palerang Local Government Area: a report to Palerang Shire Council*Rep.*, 66 pp, Fenner School of Environment and Society, the Australian National University, Canberra, Australia.

Beekman, H. E., H. G. M. Eggenkamp, and C. A. J. Appelo (2011), An integrated modelling approach to reconstruct complex solute transport mechanisms - Cl and δ^{37}Cl in pore water of sediments from a former brackish lagoon in The Netherlands, *Applied Geochemistry*, *26*(3), 257-268, doi:10.1016/j.apgeochem.2010.11.026.

Bennetts, D. A., J. A. Webb, D. J. M. Stone, and D. M. Hill (2006), Understanding the salinisation process for groundwater in an area of south-eastern Australia, using hydrochemical and isotopic evidence, *Journal of Hydrology*, *323*(1–4), 178-192, doi:10.1016/j.jhydrol.2005.08.023.

Bentley, H. W., F. M. Phillips, S. N. Davis, M. A. Habermehl, P. L. Airey, G. E. Calf, D. Elmore, H. E. Gove, and T. Torgersen (1986), Chlorine 36 dating of very old groundwater: 1. The Great Artesian Basin, Australia, *Water Resources Research*, *22*(13), 1991-2001, doi:10.1029/WR022i013p01991.

Berglund, M., and M. E. Wieser (2011), Isotopic compositions of the elements 2009 (IUPAC technical report), *Pure and Applied Chemistry*, *83*(2), 397-410, doi:10.1351/PAC-REP-10-06-02.

Berner, E. K., and R. A. Berner (1996), *Global Environment: Water, Air, and Geochemical Cycles*, 488 pp., Prentice Hall, Upper Saddle River, USA.

Biegalski, S. R., S. Landsberger, and R. Hoff (1997), High bromine aerosol concentrations near Lake Huron from long-range transport from the Arctic during polar sunrise, *Journal of Geophysical Research Atmospheres*, *102*(19), 23337-23343.

Bird, J. R., G. E. Calf, R. F. Davie, L. K. Fifield, T. R. Ophel, W. R. Evans, J. R. Kellett, and M. A. Habermehl (1989), The role of ^{36}Cl and ^{14}C measurements in Australian groundwater studies, *Radiocarbon*, *31*, 877-883.

Birkle, P., B. M. García, and C. M. Milland Padrón (2009), Origin and evolution of formation water at the Jujo-Tecominoacán oil reservoir, Gulf of Mexico. Part 1: Chemical evolution and water-rock interaction, *Applied Geochemistry*, *24*(4), 543-554, doi:10.1016/j.apgeochem.2008.12.009.

Blackburn, G., and S. McLeod (1983), Salinity of atmospheric precipitation in the Murray-Darling Drainage division, Australia, *Australian Journal of Soil Research*, *21*(4), 411-434.

Bloch, M. R., D. Kaplan, V. Kertes, and J. Schnerb (1966), Ion separation in bursting air bubbles: an explanation for the irregular ion ratios in atmospheric precipitations, *Nature*, *209*(5025), 802-803.

Bloch, M. R., and J. Schnerb (1953), On the Cl^-/Br^--ratio and the distribution of Br-ions in liquids and solids during the evaporation of bromide-containing chloride solutions, *Bulletin of the Research Council of Israel*, *3*, 151-158.

BoM (2015), Climate Data, edited, Bureau of Meteorology, Australian Government, Canberra, Australia.

Boschetti, T., L. Toscani, O. Shouakar-Stash, P. Iacumin, G. Venturelli, C. Mucchino, and S. K. Frape (2011), Salt Waters of the Northern Apennine Foredeep Basin (Italy): Origin and Evolution, *Aquatic Geochemistry*, *17*(1), 71-108, doi:10.1007/s10498-010-9107-y.

Bowler, J. M. (1981), 30. Australian salt lakes - A palaeohydrologic approach, *Hydrobiologia*, *81-82*(1), 431-444, doi:10.1007/BF00048730.

Bowler, J. M. (1986), Spatial variability and hydrologic evolution of Australian lake basins: Analogue for pleistocene hydrologic change and evaporite formation, *Palaeogeography, Palaeoclimatology, Palaeoecology*, *54*(1-4), 21-41, doi:10.1016/0031-0182(86)90116-1.

Burrough, S. L., D. S. G. Thomas, and J. S. Singarayer (2009), Late Quaternary hydrological dynamics in the Middle Kalahari: Forcing and feedbacks, *Earth-Science Reviews*, *96*(4), 313-326, doi:10.1016/j.earscirev.2009.07.001.

Burton, G. M. (1972), Lake George, N.S.W. – Notes for sedimentologists' excursion, November, 1970*Rep. Record 1972/79*, 39 pp, Australian Bureau of Mineral Resources, Geology and Geophysics, Canberra, Australia.

Burton, G. M., and E. G. Wilson (1973), Lake George, N.S.W.: its relevance to salinity problems in agriculture*Rep. Record 1973/166*, 15 pp, Australian Bureau of Mineral Resources, Geology and Geophysics, Canberra, Australia.

Cameron, A. E., W. Herr, W. Herzog, and A. Lundén (1956), Isotopen-anreicherung beim brom durch electrolytische überführung in geschmolzenem bleibromid, *Zeitschrift für Naturforschung*, *11a*, 203-204, doi:10.1515/zna-1956-0307.

Cameron, A. E., and E. L. Lippert Jr (1955), Isotopic composition of bromine in nature, *Science*, *121*(3135), 136-137.

Carroll, D. (1962), *Rainwater as a Chemical Agent of Geologic Processes–A Review, U.S. Geological Survey Water-Supply Paper 1535–G*, 23 pp., United States Government Printing Office, Washington D.C., USA.

Cartwright, I., B. Gilfedder, and H. Hofmann (2013), Chloride imbalance in a catchment undergoing hydrological change: Upper Barwon River, southeast Australia, *Applied Geochemistry*, *31*, 187-198, doi:10.1016/j.apgeochem.2013.01.003.

Cartwright, I., S. Hall, S. Tweed, and M. Leblanc (2009), Geochemical and isotopic constraints on the interaction between saline lakes and groundwater in southeast Australia, *Hydrogeology Journal*, *17*(8), 1991-2004, doi:10.1007/s10040-009-0492-5.

Cartwright, I., T. R. Weaver, and L. K. Fifield (2006), Cl/Br ratios and environmental isotopes as indicators of recharge variability and groundwater flow: An example from the southeast Murray Basin, Australia, *Chemical Geology*, *231*(1-2), 38-56, doi:10.1016/j.chemgeo.2005.12.009.

Cartwright, I., T. R. Weaver, S. Fulton, C. Nichol, M. Reid, and X. Cheng (2004), Hydrogeochemical and isotopic constraints on the origins of dryland salinity, Murray Basin, Victoria, Australia, *Applied Geochemistry*, *19*(8), 1233-1254, doi:10.1016/j.apgeochem.2003.12.006.

Cawse, P. A. (1987), Trace and major elements in the atmosphere at rural locations in Great Britain, 1972-1981, in *Pollutant Transport and Fate in Ecosystems (Special Publication Number 6 of the British Ecological Society)*, edited by P. J. Coughtrey, M. H. Martin and M. H. Unsworth, pp. 89–112, Blackwell Scientific Publishing, Oxford, UK.

Cendón, D. I., et al. (2014), Groundwater residence tume in a dissected and weathered sandstone plateau: Kulnura-Mangrove Mountain aquifer, NSW, Australia, *Australian Journal of Earth Sciences*, *61*, 475-499, doi:10.1080/08120099.2014.893628.

Cendón, D. I., et al. (2015), Identification of sources and processes in a low-level radioactive waste site adjacent to landfills: groundwater hydrogeochemistry and isotopes, *Australian Journal of Earth Sciences*, *62*(1), 123-141, doi:10.1080/08120099.2015.975155.

Cendón, D. I., T. M. Peryt, C. Ayora, J. J. Pueyo, and C. Taberner (2004), The importance of recycling processes in the Middle Miocene Badenian evaporite basin (Carpathian foredeep): palaeoenvironmental implications, *Palaeogeography, Palaeoclimatology, Palaeoecology*, *212*(1-2), 141-158, doi:10.1016/j.palaeo.2004.05.021.

Cerling, T. E. (2014), *Archaeology and Anthropology*, 393 pp., Elsevier, Oxford, UK.

Chivas, A. R., and J. M. Bowler (1986), Introduction – the SLEADS project, *Palaeogeography, Palaeoclimatology, Palaeoecology*, *54*, 3-6.

Churchill, D. M., R. W. Galloway, and G. Singh (1978), Closed lakes and the Palaeoclimatic record, in *Climatic Change and Variability: A Southern Perspective*, edited by A. B. Pittock, L. A. Frakes, D. Jenssen, J. A. Peterson and J. W. Zillman, pp. 97-108, Cambridge University Press, Cambridge, UK.

Clark, I. D., and P. Fritz (1997), *Environmental Isotopes in Hydrogeology*, Lewis Publishers, Boca Raton, USA.

Clifford, D. A., T. J. Sorg, and G. L. Ghuyre (2011), Ion exchange and adsorption of inorganic contaminants, in *Water quality and treatment: A handbook on drinking water*, edited by J. K. Edzwald, pp. 12.11-12.67, American Water Works Association, American Society of Civil Engineers, McGraw Hill.

Cook, P. G. (2015), The role of tracers in hydrogeology, *Groundwater*, *53*, 1-2, doi:10.1111/gwat.12327.

Cook, P. G., and A. L. Herczeg (1999), *Environmental Tracers in Subsurface Hydrology*, 529 pp., Kluwer Academic Publishers, Massachusetts, USA.

Cook, P. G., G. R. Walker, and I. D. Jolly (1989), Spatial variability of groundwater recharge in a semiarid region, *Journal of Hydrology*, *111*(1–4), 195-212, doi:10.1016/0022-1694(89)90260-6.

Coventry, R. J. (1976), Abandoned shorelines and the late quaternary history of Lake George, New South Wales, *Journal of the Geological Society of Australia*, *23*(3), 249-273, doi:10.1080/00167617608728939.

Coventry, R. J., and P. H. Walker (1977), Geomorphological significance of late quaternary deposits of the Lake George Area, N.S.W, *Australian Geographer*, *13*(6), 369-376, doi:10.1080/00049187708702715.

Craig, H. (1961), Isotopic variations in meteoric waters, *Science*, *133*, 1702-1703, doi:10.1126/science.133.3465.1702.

Crosbie, R. S., D. Morrow, R. G. Cresswell, F. W. Leaney, S. Lamontagne, and M. Lefournour (2012), *New insights into the chemical and isotopic composition of rainfall across Australia*, 86 pp., CSIRO Water for a Healthy Country Flagship, Canberra, Australia.

Currell, M. J., I. Cartwright, D. C. Bradley, and D. Han (2010), Recharge history and controls on groundwater quality in the Yuncheng Basin, north China, *Journal of Hydrology*, *385*(1-4), 216-229, doi:10.1016/j.jhydrol.2010.02.022.

Dailey, K. R., K. A. Welch, and W. B. Lyons (2014), Evaluating the influence of road salt on water quality of Ohio rivers over time, *Applied Geochemistry*, *47*, 25-35, doi:10.1016/j.apgeochem.2014.05.006.

Daniel, J. S., S. Solomon, R. W. Portmann, and R. R. Garcia (1999), Stratospheric ozone destruction: The importance of bromine relative to chlorine, *Journal of Geophysical Research Atmospheres*, *104*(D19), 23871-23880.

Davis, S. N., J. T. Fabryka-Martin, and L. E. Wolfsberg (2004), Variations of bromide in potable ground water in the United States, *Ground Water*, *42*(6), 902-909, doi:10.1111/j.1745-6584.2004.t01-8-.x.

Davis, S. N., D. O. Whittemore, and J. Fabryka-Martin (1998), Uses of chloride/bromide ratios in studies of potable water, *Ground Water*, *36*(2), 338-350, doi:10.1111/j.1745-6584.1998.tb01099.x.

De Deckker, P. (1982), Late Quaternary ostracods from Lake George, New South Wales, *Alcheringa*, *6*(3-4), 305-318.

De Deckker, P. (1983), Australian salt lakes: their history, chemistry, and biota - a review, *Hydrobiologia*, *105*(1), 231-244, doi:10.1007/BF00025191.

De Deckker, P., and W. D. Williams (1982), Chemical and biological features of Tasmanian salt lakes, *Australian Journal of Marine & Freshwater Research*, *33*(6), 1127-1132.

Deocampo, D. M., and B. F. Jones (2014), Geochemistry of Saline Lakes, in *Surface And Groundwater, Weathering and Soils, Treatise on Geochemistry*, edited by J. I. Drever, pp. 437-469, Elsevier, Oxford, UK.

Desaulniers, D. E., R. S. Kaufmann, J. A. Cherry, and H. W. Bentley (1986), ^{37}Cl-^{35}Cl variations in a diffusion-controlled groundwater system, *Geochimica et Cosmochimica Acta*, *50*(8), 1757-1764, doi:10.1016/0016-7037(86)90137-7.

Dogramaci, S., G. Skrzypek, W. Dodson, and P. F. Grierson (2012), Stable isotope and hydrochemical evolution of groundwater in the semi-arid Hamersley Basin of subtropical northwest Australia, *Journal of Hydrology*, *475*, 281-293, doi:10.1016/j.jhydrol.2012.10.004.

Dossett, S. R., and V. C. Bowersox (1999), *National Trends Network site operation manual*, 99 pp., National Atmospheric Deposition Program, Champaign, USA.

Du, Y., T. Ma, J. Yang, L. Liu, H. Shan, H. Cai, C. Liu, and L. Chen (2013), A precise analytical method for bromine stable isotopes in natural waters by GasBench II-IRMS, *International Journal of Mass Spectrometry*, *338*, 50-56, doi:10.1016/j.ijms.2012.12.006.

Duce, R. A., J. W. Winchester, and T. W. Van Nahl (1965), Iodine, bromine, and chlorine in the Hawaiian marine atmosphere, *Journal of Geophysical Research*, *70*(8), 1775-1799, doi:10.1029/JZ070i008p01775.

Eastoe, C. J. (2016), Stable chlorine isotopes in arid non-marine basins: Instances and possible fractionation mechanisms, *Applied Geochemistry*, *74*, 1-12, doi:10.1016/j.apgeochem.2016.08.015.

Eastoe, C. J., A. Long, and L. P. Knauth (1999), Stable chlorine isotopes in the Palo Duro Basin, Texas: Evidence for preservation of Permian evaporite brines, *Geochimica et Cosmochimica Acta*, *63*(9), 1375-1382, doi:10.1016/S0016-7037(99)00186-6.

Eastoe, C. J., A. Long, L. S. Land, and J. R. Kyle (2001), Stable chlorine isotopes in halite and brine from the Gulf Coast Basin: brine genesis and evolution, *Chemical Geology*, *176*, 343-360, doi:10.1016/S0009-2541(00)00374-0.

Eastoe, C. J., T. M. Peryt, O. Y. Petrychenko, and D. Geisler-Cussey (2007), Stable chlorine isotopes in Phanerozoic evaporites, *Applied Geochemistry*, *22*(3), 575-588, doi:10.1016/j.apgeochem.2006.12.012.

Edmunds, W. M. (1996), Bromine geochemistry of British groundwaters, *Mineralogical Magazine*, *60*(2), 275-284.

Edwards, M., and J. A. Webb (2009), The importance of unsaturated zone biogeochemical processes in determining groundwater composition, southeastern Australia, *Hydrogeology Journal*, *17*(6), 1359-1374, doi:10.1007/s10040-009-0449-8.

Eggenkamp, H. G. M. (1995), Bromine stable isotope fractionation: Experimental determination on evaporites, in *8th EUG General Assembly*, edited, Strasbourg, France.

Eggenkamp, H. G. M. (2014), *The Geochemistry of Stable Chlorine and Bromine Isotopes*, Springer, Alphen aan Den Rijn, the Netherlands.

Eggenkamp, H. G. M. (2015), Comment on "Stable isotope fractionation of chlorine during the precipitation of single chloride minerals" by Luo, C.-G., Xiao, Y.-K., Wen, H.-J., Ma, H.-Z., Ma, Y.-Q., Zhang, Y.-l., Zhang, Y.-X. and He, M.-Y. [Applied Geochemistry 47 (2014) 141-149], *Applied Geochemistry*, *54*, 111-116, doi:10.1016/j.apgeochem.2014.11.018.

Eggenkamp, H. G. M., M. Bonifacie, M. Ader, and P. Agrinier (2016), Experimental determination of the fractionation of stable chlorine and bromine isotopes during precipitation of salts from saturated solutions, *Chemical Geology*, *433*, 46-56, doi:10.1016/j.chemgeo.2016.04.009.

Eggenkamp, H. G. M., and M. L. Coleman (2000), Rediscovery of classical methods and their application to the measurement of stable bromine isotopes in natural samples, *Chemical Geology*, *167*(3-4), 393-402, doi:10.1016/S0009-2541(99)00234-X.

Eggenkamp, H. G. M., and M. L. Coleman (2009), The effect of aqueous diffusion on the fractionation of chlorine and bromine stable isotopes, *Geochimica et Cosmochimica Acta*, *73*(12), 3539-3548, doi:10.1016/j.gca.2009.03.036.

Eggenkamp, H. G. M., R. Kreulen, and A. F. Koster Van Groos (1995), Chlorine stable isotope fractionation in evaporites, *Geochimica et Cosmochimica Acta*, *59*(24), 5169-5175, doi:10.1016/0016-7037(95)00353-3.

Eiler, J. M., et al. (2014), Frontiers of stable isotope geoscience, *Chemical Geology*, *372*, 119-143, doi:10.1016/j.chemgeo.2014.02.006.

Ellison, S. L. R., and A. Williams (2012), *Eurachem/CITAC guide CG 4: Quantifying uncertainty in analytical measurement*, 3rd ed., 133 pp., Available from www.eurachem.org.

EPA (2016), Protection of Stratospheric Ozone: The 2016 Critical Use Exemption From the Phaseout of Methyl Bromide, Final Rule (US Environmental Protection Authority), *Federal Register*, *80*(CFR 82), 61985-61993.

Epstein, S., and T. Mayeda (1953), Variation of O^{18} content of waters from natural sources, *Geochimica et Cosmochimica Acta*, *4*(5), 213-224.

Eugster, H. P., and B. F. Jones (1979), Behavior of major solutes during closed basin-lakes brine evolution, *American Journal of Science*, *279*(6), 609-631.

Eyles, N., and M. Meriano (2010), Road-impacted sediment and water in a Lake Ontario watershed and lagoon, City of Pickering, Ontario, Canada: An example of urban basin analysis, *Sedimentary Geology*, *224*(1–4), 15-28, doi:10.1016/j.sedgeo.2009.12.004.

Eyles, N., M. Meriano, and P. Chow-Fraser (2013), Impacts of European settlement (1840–present) in a Great Lake watershed and lagoon: Frenchman's Bay, Lake Ontario, Canada, *Environ Earth Sci*, *68*(8), 2211-2228, doi:10.1007/s12665-012-1904-8.

Fan, T., and O. B. Toon (2011), Modeling sea-salt aerosol in a coupled climate and sectional microphysical model: mass, optical depth and number concentration, *Atmospheric Chemistry and Physics*, *11*(9), 4587-4610, doi:10.5194/acp-11-4587-2011.

Farrance, I., and R. Frenkel (2012), Uncertainty of measurement: a review of the rules for calculating uncertainty components through functional relationships, *The Clinical Biochemist Reviews*, *33*(2), 49-75.

Feth, J. H. (1981), *Chloride in Natural Continental Water – A Review*, *U.S. Geological Survey Water-Supply Paper 2176*, 36 pp., United States Geological Survey, Washington DC, USA.

Fick, A. (1855), Über Diffusion, *Annalen der Physik*, *170*(1), 59-86, doi:10.1002/andp.18551700105.

Fitzsimmons, K. E., and T. T. Barrows (2010), Holocene hydrologic variability in temperate southeastern Australia: An example from Lake George, New South Wales, *Holocene*, *20*(4), 585-597, doi:10.1177/0959683609356589.

Flury, M., and A. Papritz (1993), Bromide in the natural environment: Occurrence and toxicity, *Journal of Environmental Quality*, *22*(4), 747-758, doi:10.2134/jeq1993.00472425002200040017x.

Frape, S. K., O. Shouakar-Stash, T. Pačes, and R. Stotler (2007), Geochemical and isotopic characteristics of the waters from crystalline and sedimentary structures of the Bohemian Massif, paper presented at Water-Rock Interaction - Proceedings of the 12th International Symposium on Water-Rock Interaction, WRI-12.

Friedman, I., G. I. Smith, and K. G. Hardcastle (1976), Studies of quaternary saline lakes-II. Isotopic and compositional changes during desiccation of the brines in Owens Lake, California, 1969-1971, *Geochimica et Cosmochimica Acta*, *40*(5), 501-511, doi:10.1016/0016-7037(76)90218-0.

Gallant, A. J. E., and J. Gergis (2011), An experimental streamflow reconstruction for the River Murray, Australia, 1783–1988, *Water Resources Research*, *47*(12), W00G04, doi:10.1029/2010WR009832.

Galvão, J. A., M. Mathiensen, M. Oetterer, Y. Moliner-Martínez, R. A. Gonzalez-Fuenzalida, M. Muñoz-Ortuño, R. Herráez-Hernández, J. Verdú-Andrés, C. Molins-Leguaand, and P. Falcó (2013), Determination of Ammonia in Water Samples, in *Handbook of Water Analysis*, edited by L. M. L. Nollet and L. S. P. De Gelder, pp. 249-281, CRC Press, Amsterdam, the Netherlands.

García-Veigas, J., L. Rosell, I. Zak, E. Playà, C. Ayora, and A. Starinsky (2009), Evidence of potash salt formation in the Pliocene Sedom Lagoon (Dead Sea Rift, Israel), *Chemical Geology*, *265*(3–4), 499-511, doi:10.1016/j.chemgeo.2009.05.013.

Gartman, N. (2014), *Quality Assurance Report National Atmospheric Deposition Program 2013*, 38 pp., National Atmospheric Deposition Program, Champaign, USA.

Gasser, G., M. Rona, A. Voloshenko, R. Shelkov, N. Tal, I. Pankratov, S. Elhanany, and O. Lev (2010), Quantitative evaluation of tracers for quantification of wastewater

contamination of potable water sources, *Environmental Science & Technology*, *44*(10), 3919-3925, doi:10.1021/es100604c.

Gat, J. R., and R. Gonfiantini (1981), *Stable Isotope Hydrology: Deuterium and Oxygen-18 in the Water Cycle*, 339 pp., International Atomic Energy Agency, Vienna, Austria.

Gelman, F., and L. Halicz (2011), High-precision isotope ratio analysis of inorganic bromide by continuous flow MC-ICPMS, *International Journal of Mass Spectrometry*, *307*(1-3), 211-213, doi:10.1016/j.ijms.2011.01.003.

Ghassemi, F., A. J. Jakeman, and H. A. Nix (1995), *Salinisation of Land and Water Resources: Human Causes, Extent, Management and Case Studies*, 1st ed., University of New South Wales Press, Sydney.

Gibson, J. J., S. J. Birks, and T. W. D. Edwards (2008), Global prediction of δA and δ^{2}H- δ^{18}O evaporation slopes for lakes and soil water accounting for seasonality, *Global Biogeochemical Cycles*, *22*(2), doi:10.1029/2007GB002997.

Gleeson, T., K. M. Befus, S. Jasechko, E. Luijendijk, and M. B. Cardenas (2015), The global volume and distribution of modern groundwater, *Nature Geoscience*, *9*, 161-167, doi:10.1038/ngeo2590.

Godon, A., N. Jendrzejewski, H. G. M. Eggenkamp, D. A. Banks, M. Ader, M. L. Coleman, and F. Pineau (2004), A cross-calibration of chlorine isotopic measurements and suitability of seawater as the international reference material, *Chemical Geology*, *207*(1-2), 1-12, doi:10.1016/j.chemgeo.2003.11.019.

Graedel, T. E., and W. C. Keene (1996), The budget and cycle of Earth's natural chlorine, *Pure and Applied Chemistry*, *68*(9), 1689-1697.

Groen, J., J. Velstra, and A. G. C. A. Meesters (2000), Salinization processes in paleowaters in coastal sediments of Suriname: Evidence from δ^{37}Cl analysis and diffusion modelling, *Journal of Hydrology*, *234*(1-2), 1-20, doi:10.1016/S0022-1694(00)00235-3.

Gröning, M., H. O. Lutz, Z. Roller-Lutz, M. Kralik, L. Gourcy, and L. Pöltenstein (2012), A simple rain collector preventing water re-evaporation dedicated for δ^{18}O and δ^{2}H analysis of cumulative precipitation samples, *Journal of Hydrology*, *448-449*, 195-200, doi:10.1016/j.jhydrol.2012.04.041.

Guelle, W., M. Schulz, Y. Balkanski, and F. Dentener (2001), Influence of the source formulation on modeling the atmospheric global distribution of sea salt aerosol, *Journal of Geophysical Research Atmospheres*, *106*(D21), 27509-27524, doi:10.1029/2001JD900249.

Haas, P. M. (1991), Policy responses to stratospheric ozone depletion, *Global Environmental Change*, *1*(3), 224-234, doi:10.1016/0959-3780(91)90044-T.

Hahnenberger, M., and K. Nicoll (2012), Meteorological characteristics of dust storm events in the eastern Great Basin of Utah, U.S.A, *Atmospheric Environment*, *60*, 601-612, doi:10.1016/j.atmosenv.2012.06.029.

Hanlon, C. (2015), A Characterization of Bromine and Chlorine Stable Isotopes in the Sand Hills Region of Nebraska, USA, 99 pp, University of Waterloo, Waterloo, Canada.

Harriss, R. C., and H. H. Williams (1969), Specific-ion electrode measurements on Br, Cl and F in atmospheric precipitation, *Journal of Applied Meteorology*, *8*(2), 299-301, doi:10.1175/1520-0450(1969)008<0299:SIEMOB>2.0.CO;2.

Haynes, W. M. (2015), *CRC Handbook of Chemistry and Physics*, 96th ed., 2677 pp., Apple Academic Press Inc., Oakville, Canada.

Healy, R. (2010), *Estimating Groundwater Recharge*, 245 pp., Cambridge University Press, Cambridge, UK.

Hendry, M. J., and L. I. Wassenaar (2004), Transport and geochemical controls on the distribution of solutes and stable isotopes in a thick clay-rich till aquitard, Canada, *Isotopes in Environmental and Health Studies*, *40*(1), 3-19, doi:10.1080/10256010310001644942.

Hendry, M. J., and L. I. Wassenaar (2011), Millennial-scale diffusive migration of solutes in thick clay-rich aquitards: Evidence from multiple environmental tracers, *Hydrogeology Journal*, *19*(1), 259-270, doi:10.1007/s10040-010-0647-4.

Herczeg, A. L., S. S. Dogramaci, and F. W. J. Leaney (2001), Origin of dissolved salts in a large, semi-arid groundwater system: Murray Basin, Australia, *Marine and Freshwater Research*, *52*(1), 41-52, doi:10.1071/MF00040.

Herczeg, A. L., and W. M. Edmunds (1999), Inorganic Ions as Tracers, in *Environmental Tracers in Subsurface Hydrology*, edited by P. G. Cook and A. L. Herczeg, pp. 31-77, Kluwer Academic Publishers, Massachusetts, USA.

Herczeg, A. L., and F. W. Leaney (2011), Review: Environmental tracers in arid-zone hydrology, *Hydrogeology Journal*, *19*(1), 17-29, doi:10.1007/s10040-010-0652-7.

Hofmann, H., and I. Cartwright (2013), Using hydrogeochemistry to understand inter-aquifer mixing in the on-shore part of the Gippsland Basin, southeast Australia, *Applied Geochemistry*, *33*, 84-103, doi:10.1016/j.apgeochem.2013.02.004.

Holser, W. T. (1966), Bromide geochemistry of salt rocks, in *Marine Evaporites: Origin, Diagenesis and Geochemistry*, edited by D. W. Kirkland, pp. 333-360, Dowden, Hutchinson & Ross Inc., California, USA.

Holser, W. T. (1970), Bromide geochemistry of some non-marine salt deposits in the Southern Great Basin, *Mineral Society of America Special Papers*, *3*, 307-319.

Horner, K. N. (2013), New environmental tracer methods for quantifying solute sources in semi-arid alluvial aquifers, The Australian National University, Canberra, Australia.

Horner, K. N., M. A. Short, and D. C. McPhail (2017), Chloride and bromide sources in water: Quantitative model use and uncertainty, *Journal of Hydrology*, *549*, 571-580, doi:10.1016/j.jhydrol.2017.04.028.

Horst, A., H. Holmstrand, P. Andersson, B. F. Thornton, A. Wishkerman, F. Keppler, and T. Gustafsson (2014), Stable bromine isotopic composition of methyl bromide released from plant matter, *Geochimica et Cosmochimica Acta*, *125*, 186-195, doi:10.1016/j.gca.2013.10.016.

Hughes, C. E., and J. Crawford (2012), A new precipitation weighted method for determining the meteoric water line for hydrological applications demonstrated using Australian and global GNIP data, *Journal of Hydrology*, *464-465*, 344-351, doi:10.1016/j.jhydrol.2012.07.029.

Hutton, J. T. (1976), Chloride in Rainwater in Relation to Distance from Ocean, *Search*, *7*, 207-208.

Hydroilex (2005), Lake George Groundwater Sustainability Investigation*Rep.*, 39 pp, Bungendore, Australia.

Jacobi, H. W., D. Voisin, J. L. Jaffrezo, J. Cozic, and T. A. Douglas (2012), Chemical composition of the snowpack during the OASIS spring campaign 2009 at Barrow, Alaska, *Journal of Geophysical Research: Atmospheres*, *117*(D14), D00R13, doi:10.1029/2011JD016654.

Jacobson, G., J. Jankowski, and R. S. Abell (1991), Groundwater and surface water interaction at Lake George, New South Wales, *BMA Journal of Australian Geology & Geophysics*, *12*, 852-858.

Jacobson, G., and A. W. Schuett (1979), Water levels, balance, and chemistry of Lake George, *BMR Journal*, *4*, 25-32.

Jambon, A., B. Déruelle, G. Dreibus, and F. Pineau (1995), Chlorine and bromine abundance in MORB: the contrasting behaviour of the Mid-Atlantic Ridge and East Pacific Rise and implications for chlorine geodynamic cycle, *Chemical Geology*, *126*(2), 101-117, doi:10.1016/0009-2541(95)00112-4.

Jennings, J. (1981), The rise and fall of Lake George (New South Wales, Australia), *Geographical Magazine*, *53*(13), 852-858.

Jochum, K. P., and J. Enzweiler (2014), Reference Materials in Geochemical and Environmental Research, in *Analytical Geochemistry/Inorganic INSTR. Analysis, Treatise on Geochemistry*, edited by W. F. McDonough, pp. 43-70, Elsevier, Oxford, UK.

Johnson, J. D., J. R. Graney, R. C. Capo, and B. W. Stewart (2015), Identification and quantification of regional brine and road salt sources in watersheds along the New York/Pennsylvania border, USA, *Applied Geochemistry*, *60*, 37-50, doi:10.1016/j.apgeochem.2014.08.002.

Jones, B. F., D. L. Naftz, R. J. Spencer, and C. G. Oviatt (2009), Geochemical Evolution of Great Salt Lake, Utah, USA, *Aquatic Geochemistry*, *15*(1-2), 95-121, doi:10.1007/s10498-008-9047-y.

Junge, C. E., and R. T. Werby (1958), The concentration of chloride, sodium, potassium, calcium, and sulfate in rain water over the United States, *Journal of Meteorology*, *15*(5), 417-425, doi:10.1175/1520-0469(1958)015<0417:TCOCSP>2.0.CO;2.

Jungwirth, P., and D. J. Tobias (2002), Ions at the air/water interface, *The Journal of Physical Chemistry B*, *106*(25), 6361-6373, doi:10.1021/jp020242g.

Katz, B. G., S. M. Eberts, and L. J. Kauffman (2011), Using Cl/Br ratios and other indicators to assess potential impacts on groundwater quality from septic systems: A review and examples from principal aquifers in the United States, *Journal of Hydrology*, *397*(3-4), 151-166, doi:10.1016/j.jhydrol.2010.11.017.

Kaufmann, R., A. Long, H. Bentley, and S. Davis (1984), Natural chlorine isotope variations, *Nature*, *309*(5966), 338-340.

Kaushal, S. S., P. M. Groffman, G. E. Likens, K. T. Belt, W. P. Stack, V. R. Kelly, L. E. Band, and G. T. Fisher (2005), Increased salinization of fresh water in the northeastern United States, *Proceedings of the National Academy of Sciences of the United States of America*, *102*(38), 13517-13520.

Keene, W. C., et al. (1999), Composite global emissions of reactive chlorine from anthropogenic and natural sources: Reactive Chlorine Emissions Inventory, *Journal of Geophysical Research: Atmospheres*, *104*(D7), 8429-8440, doi:10.1029/1998JD100084.

Kelly, V. R., G. M. Lovett, K. C. Weathers, S. E. G. Findlay, D. L. Strayer, D. J. Burns, and G. E. Likens (2008), Long-term sodium chloride retention in a rural watershed: legacy effects of road salt on streamwater concentration, *Environmental Science & Technology*, *42*(2), 410-415, doi:10.1021/es071391l.

Kendall, C., and J. J. McDonnell (1998), *Isotope Tracers in Catchment Hydrology*, 839 pp., Elsevier, Amsterdam, the Netherlands.

Keywood, M. D., A. R. Chivas, L. K. Fifield, R. G. Cresswell, and G. P. Ayers (1997), The accession of chloride to the western half of the Australian continent, *Australian Journal of Soil Research*, *35*(5), 1177-1189, doi:10.1071/S97001.

Kharaka, Y. K., and J. S. Hanor (2014), Deep Fluids in Sedimentary Basins, in *Surface And Groundwater, Weathering and Soils, Treatise on Geochemistry*, edited by J. I. Drever, pp. 471-515, Elsevier, Oxford, UK, doi:10.1016/B978-0-08-095975-7.00516-7.

Kim, Y., K. S. Lee, D. C. Koh, D. H. Lee, S. G. Lee, W. B. Park, G. W. Koh, and N. C. Woo (2003), Hydrogeochemical and isotopic evidence of groundwater salinization in a coastal aquifer: A case study in Jeju volcanic island, Korea, *Journal of Hydrology*, *270*(3-4), 282-294, doi:10.1016/S0022-1694(02)00307-4.

Kohfeld, K. E., R. M. Graham, A. M. de Boer, L. C. Sime, E. W. Wolff, C. Le Quéré, and L. Bopp (2013), Southern Hemisphere westerly wind changes during the Last

Glacial Maximum: paleo-data analysis, *Quaternary Science Reviews, 68*, 76-95, doi:10.1016/j.quascirev.2013.01.017.

Lamb, D., and J. Van Bowersox (2000), The national atmospheric deposition program: an overview, *Atmospheric Environment, 34*(11), 1661-1663, doi:10.1016/S1352-2310(99)00425-2.

Lavastre, V., N. Jendrzejewski, P. Agrinier, M. Javoy, and M. Evrard (2005), Chlorine transfer out of a very low permeability clay sequence (Paris Basin, France): ^{35}Cl and ^{37}Cl evidence, *Geochimica et Cosmochimica Acta, 69*(21), 4949-4961, doi:10.1016/j.gca.2005.04.025.

Lebigot, E. O. (2014), *uncertainties*: a Python package for calculations with uncertainties, edited, Available at http://pythonhosted.org/uncertainties/.

Lenahan, M. J., K. L. Bristow, and P. de Caritat (2011), Detecting induced correlations in hydrochemistry, *Chemical Geology, 284*(1–2), 182-192, doi:10.1016/j.chemgeo.2011.02.018.

Li, X., A. Zhou, Y. Liu, T. Ma, C. Liu, L. Liu, and J. Yang (2012), Stable isotope geochemistry of dissolved chloride in relation to hydrogeology of the strongly exploited Quaternary aquifers, North China Plain, *Applied Geochemistry, 27*(10), 2031-2041, doi:10.1016/j.apgeochem.2012.05.013.

Liljestrand, H. M., and J. J. Morgan (1981), Spatial variations of acid precipitation in southern California, *Environmental Science and Technology, 15*(3), 333-339.

Lim, W. H., M. L. Roderick, M. T. Hobbins, S. C. Wong, and G. D. Farquhar (2013), The energy balance of a US Class A evaporation pan, *Agricultural and Forest Meteorology, 182-183*, 314-331, doi:10.1016/j.agrformet.2013.07.001.

Lindsay, S. S., and M. J. Baedecker (1993), Determination of aqueous sulfide in contaminated and natural water using the methylene blue method, in *Regional Ground Water Quality*, edited by W. A. Alley, pp. 349-356, Van Nostrand Reinhold, New York, USA.

Liu, D., J. Abuduwaili, J. Lei, and G. Wu (2011), Deposition rate and chemical composition of the aeolian dust from a bare saline playa, Ebinur Lake, Xinjiang, China, *Water Air Soil Pollut, 218*(1-4), 175-184, doi:10.1007/s11270-010-0633-4.

Lollar, B. S. (2014), *Environmental Geochemistry*, 605 pp., Elsevier, Oxford, UK.

Love, A. J., A. L. Herczeg, L. Sampson, R. G. Cresswell, and L. K. Fifield (2000), Sources of chloride and implications for ^{36}Cl dating of old groundwater, Southwestern Great Artesian Basin, Australia, *Water Resources Research, 36*(6), 1561-1574, doi:10.1029/2000WR900019.

Lundén, A., and A. Lodding (1960), Isotopenanreicherung bei brom durch electrolytische überführung in geschmolzenem zinkbromid, *Zeitschrift für Naturforschung, 15a*, 320-322, doi:10.1515/zna-1960-0407.

Luo, C. G., Y. Xiao, H. Wen, H. Ma, Y. Ma, Y. Zhang, Y. Zhang, and M. He (2014), Stable isotope fractionation of chlorine during the precipitation of single chloride minerals, *Applied Geochemistry*, *47*, 141-149, doi:10.1016/j.apgeochem.2014.06.005.

Luo, C. G., Y. K. Xiao, H. Z. Ma, Y. Q. Ma, Y. L. Zhang, and M. Y. He (2012), Stable isotope fractionation of chlorine during evaporation of brine from a saline lake, *Chinese Science Bulletin*, *57*(15), 1833-1843, doi:10.1007/s11434-012-4994-5.

Luo, C. G., Y. K. Xiao, H. J. Wen, H. Z. Ma, Y. Q. Ma, Y. L. Zhang, and M. Y. He (2015), Reply to the comment on the paper stable isotope fractionation of chlorine during the precipitation of single chloride minerals, *Applied Geochemistry*, *54*, 117-118, doi:10.1016/j.apgeochem.2014.11.026.

Lyons, W. B., S. W. Tyler, H. E. Gaudette, and D. T. Long (1995), The use of strontium isotopes in determining groundwater mixing and brine fingering in a playa spring zone, Lake Tyrrell, Australia, *Journal of Hydrology*, *167*(1-4), 225-239.

Mackenzie, F. T. (2014), *Sediments, Diagenesis and Sedimentary Rocks*, 656 pp., Elsevier, Oxford, UK.

MacKinnon, G., A. B. MacKenzie, G. T. Cook, I. D. Pulford, H. J. Duncan, and E. M. Scott (2011), Spatial and temporal variations in Pb concentrations and isotopic composition in road dust, farmland soil and vegetation in proximity to roads since cessation of use of leaded petrol in the UK, *Science of the Total Environment*, *409*(23), 5010-5019, doi:10.1016/j.scitotenv.2011.08.010.

Macphail, M., L. K. Fifield, B. Pillans, M. Davies, and G. Hope (2015), Lake George revisited: New evidence for the origin and evolution of a large closed lake, Southern Tablelands, NSW, Australia, *Australian Journal of Earth Sciences*, *62*(7), 853-871, doi:10.1080/08120099.2015.1108365.

Macphail, M., L. K. Fifield, B. Pillans, and G. Hope (2016), Lake George revisited: new evidence for the origin and evolution of a large closed lake, Southern Tablelands, NSW, Australia. 2: earliest Pleistocene (Gelasian) environments, *Australian Journal of Earth Sciences*, 1-16, doi:10.1080/08120099.2016.1212399.

Macumber, P. G. (1991), *Interaction between groundwater and surface systems in northern Victoria*, 352 pp., Department of Conservation and Environment, Victorian Government, Melbourne, Australia.

Mahalinganathan, K., M. Thamban, C. M. Laluraj, and B. L. Redkar (2012), Relation between surface topography and sea-salt snow chemistry from Princess Elizabeth Land, East Antarctica, *Cryosphere*, *6*(2), 505-515, doi:10.5194/tc-6-505-2012.

Manö, S., and M. O. Andreae (1994), Emission of methyl bromidefrom biomass burning, *Science*, *263*(5151), 1255-1257, doi:10.1126/science.263.5151.1255.

Mason, A. J. (1995), Investigation of the sand resources of the Lake George Basin*Rep. Record 1995/32*, 30 pp, Geological Survey of New South Wales, Sydney, Australia.

Mazurek, M., et al. (2011), Natural tracer profiles across argillaceous formations, *Applied Geochemistry*, *26*(7), 1035-1064, doi:10.1016/j.apgeochem.2011.03.124.

McArthur, J. M., P. K. Sikdar, M. A. Hoque, and U. Ghosal (2012), Waste-water impacts on groundwater: Cl/Br ratios and implications for arsenic pollution of groundwater in the Bengal Basin and Red River Basin, Vietnam, *Science of the Total Environment*, *437*, 390-402, doi:10.1016/j.scitotenv.2012.07.068.

McCaffrey, M. A., B. Lazar, and H. D. Holland (1987), The evaporation path of seawater and the coprecipitation of Br^- and K^+ with halite, *Journal of Sedimentary Petrology*, *57*(5), 928-937, doi:10.1306/212F8CAB-2B24-11D7-8648000102C1865D.

McElroy, M. B., R. J. Salawitch, S. C. Wofsy, and J. A. Logan (1986), Reductions of Antarctic ozone due to synergistic interactions of chlorine and bromine, *Nature*, *321*(6072), 759-762.

McEwan Mason, J. R. S. (1991), The late Cainozoic magnetostratigraphy and preliminary palynology of Lake George, New South Wales, in *The Cainozoic in Australia: A Reappraisal of the Evidence*, edited by M. A. J. Williams, P. De Deckker and A. P. Kershaw, pp. 195-209, Geological Society of Australia, Sydney, Australia.

McInnis, D., S. Silliman, M. Boukari, N. Yalo, S. Orou-Pete, C. Fertenbaugh, K. Sarre, and H. Fayomi (2013), Combined application of electrical resistivity and shallow groundwater sampling to assess salinity in a shallow coastal aquifer in Benin, West Africa, *Journal of Hydrology*, *505*, 335-345, doi:10.1016/j.jhydrol.2013.10.014.

McMahon, T. A., M. C. Peel, L. Lowe, R. Srikanthan, and T. R. McVicar (2013), Estimating actual, potential, reference crop and pan evaporation using standard meteorological data: A pragmatic synthesis, *Hydrology and Earth System Sciences*, *17*(4), 1331-1363, doi:10.5194/hess-17-1331-2013.

Mernagh, T. P. (2013), A review of Australian salt lakes and assessment of their potential for strategic resources*Rep. Record 2013/39*, 251 pp, Geoscience Australia, Australian Government, Canberra, Australia.

Mernagh, T. P., E. N. Bastrakov, S. Jaireth, P. de Caritat, P. M. English, and J. D. A. Clarke (2016), A review of Australian salt lakes and associated mineral systems, *Australian Journal of Earth Sciences*, 1-27, doi:10.1080/08120099.2016.1149517.

Middleton, N. J., and D. S. G. Thomas (1997), *World Atlas of Desertification*, 2nd ed., 182 pp., A Hodder Arnold Publication, London, UK.

Millero, F. J. (2014), Physico-Chemical Controls on Seawater, in *The Oceans and Marine Geochemistry, Treatise on Geochemistry*, edited by M. J. Mottl and H. Elderfield, pp. 1-18, Elsevier, Oxford, UK.

Molina, M. J., and F. S. Rowland (1974), Stratospheric sink for chlorofluoromethanes: chlorine atomc-atalysed destruction of ozone, *Nature*, *249*(5460), 810-812.

Montzka, S. A., J. H. Butler, J. W. Elkins, T. M. Thompson, A. D. Clarke, and L. T. Lock (1999), Present and future trends in the atmospheric burden of ozone-depleting halogens, *Nature*, *398*(6729), 690-694, doi:10.1038/19499.

Moretto, R. (1988), Observations on the incorporation of trace elements in halite of Oligocene salt beds, Bourg-en-Bresse Basin, France, *Geochimica et Cosmochimica Acta*, *52*(12), 2809-2814, doi:0.1016/0016-7037(88)90148-2.

Mullaney, J. R., D. L. Lorenz, and A. D. Arnston (2009), *Chloride in groundwater and surface water in areas underlain by the glacial aquifer system, northern United States, U.S. Geological Survey Scientific Investigations Report 2009-5086*, 54 pp., U.S. Department of the Interior, Washington D.C.

NADP (2013), *National Atmospheric Deposition Program 2012 Annual Summary*, 28 pp., National Atmospheric Deposition Program, Champaign, USA.

NADP (2016), *NADP Network Quality Assurance Plan*, 29 pp., National Atmospheric Deposition Program, Champaign, USA.

Neal, C., C. J. Smith, J. Walls, P. Billingham, S. Hill, and M. Neal (1990), Comments on the hydrochemical regulation of the halogen elements in rainfall, stemflow, throughfall and stream waters at an acidic forested area in mid-wales, *Science of the Total Environment*, *91*, 1-11, doi:10.1016/0048-9697(90)90284-2.

Neal, M., C. Neal, H. Wickham, and S. Harman (2007), Determination of bromide, chloride, fluoride, nitrate and sulphate by ion chromatography: Comparisons of methodologies for rainfall, cloud water and river waters at the Plynlimon catchments of mid-Wales, *Hydrology and Earth System Sciences*, *11*(1), 294-300, doi:10.5194/hess-11-294-2007.

Nimz, G. J. (1998), Lithogenic and Cosmogenic Tracers in Catchment Hydrology, in *Isotope Tracers in Catchment Hydrology*, edited by C. Kendall and J. J. McDonnell, pp. 247-289, Elsevier, Amsterdam, the Netherlands.

NOAA (2015), Regional Climate Maps: USA, edited, National Oceanic and Atmospheric Administration, United States Government, Washigton D.C., USA.

Noakes, L. C. (1951), Notes on fluctuations of water level at Lake George*Rep. Record 1951/17*, 6 pp, Bureau of Mineral Resources, Geology and Geophysics, Canberra, Australia.

Palarea-Albaladejo, J., and J. A. Martín-Fernández (2015), zCompositions - R package for multivariate imputation of left-censored data under a compositional approach, *Chemometrics and Intelligent Laboratory Systems*, *143*, 85-96, doi:10.1016/j.chemolab.2015.02.019.

Panno, S. V., K. C. Hackley, H. H. Hwang, S. E. Greenberg, I. G. Krapac, S. Landsberger, and D. J. O'Kelly (2006), Characterization and identification of Na-Cl sources in ground water, *Ground Water*, *44*(2), 176-187, doi:10.1111/j.1745-6584.2005.00127.x.

Park, J., C. M. Bethke, T. Torgersen, and T. M. Johnson (2002), Transport modeling applied to the interpretation of groundwater ^{36}Cl age, *Water Resources Research*, *38*(5), 1043, doi:10.1029/2001WR000399.

Parkhurst, D. L., and C. A. J. Appelo (2013), Description of Input and Examples for PHREEQC Version 3—A Computer Program for Speciation, Batch-Reaction, One-Dimensional Transport, and Inverse Geochemical Calculations*Rep.*, 519 pp, U.S. Geological Survey, available at http://pubs.usgs.gov/tm/06/a43/pdf/tm6-A43.pdf.

Pawlowsky-Glahn, V., and A. Buccianti (2011), *Compositional Data Analysis: Theory and Applications*, 400 pp., John Wiley & Sons, New York, USA.

Peel, M. C., B. L. Finlayson, and T. A. McMahon (2007), Updated world map of the Köppen-Geiger climate classification, *Hydrology and Earth System Sciences*, *11*(5), 1633-1644.

Perera, N., B. Gharabaghi, and K. Howard (2013), Groundwater chloride response in the Highland Creek watershed due to road salt application: A re-assessment after 20 years, *Journal of Hydrology*, *479*, 159-168, doi:10.1016/j.jhydrol.2012.11.057.

Peryt, T. M., H. Tomassi-Morawiec, G. Czapowski, S. P. Hryniv, J. J. Pueyo, C. J. Eastoe, and S. Vovnyuk (2005), Polyhalite occurrence in the Werra (Zechstein, upper Permian) peribaltic basin of Poland and Russia: Evaporite facies constraints, *Carbonates Evaporites*, *20*(2), 182-194, doi:10.1007/BF03175461.

Petrides, B., I. Cartwright, and T. R. Weaver (2006), The evolution of groundwater in the Tyrrell catchment, south-central Murray Basin, Victoria, Australia, *Hydrogeology Journal*, *14*(8), 1522-1543, doi:10.1007/s10040-006-0057-9.

Phillips, F. M. (2013), Chlorine-36 Dating of Old Groundwater, in *Isotope Methods for Dating Old Groundwater*, edited, pp. 125-152, International Atomic Energy Agency, Vienna, Austria.

Prospero, J. M., P. Ginoux, O. Torres, S. E. Nicholson, and T. E. Gill (2002), Environmental characterization of global sources of atmospheric soil dust identified with the Nimbus 7 total ozone mapping spectrometer (TOMS) absorbing aerosol product, *Reviews of Geophysics*, *40*(1), 2-1-2-31, doi:10.1029/2000RG000095.

Quinby-Hunt, M. S., and K. K. Turekian (1983), Distribution of elements in sea water, *Eos, Transactions American Geophysical Union*, *64*(14), 130-130, doi:10.1029/EO064i014p00130.

Rebeix, R., et al. (2014), Chlorine transport processes through a 2000 m aquifer/aquitard system, *Marine and Petroleum Geology*, *53*, 102-116, doi:10.1016/j.marpetgeo.2013.12.013.

Reynolds, R. L., J. C. Yount, M. Reheis, H. Goldstein, P. Chavez, R. Fulton, J. Whitney, C. Fuller, and R. M. Forester (2007), Dust emission from wet and dry playas in the Mojave Desert, USA, *Earth Surface Processes and Landforms*, *32*(12), 1811-1827, doi:10.1002/esp.1515.

Rhew, R. C., M. E. Whelan, and D. H. Min (2014), Large methyl halide emissions from south Texas salt marshes, *Biogeosciences*, *11*(22), 6427-6434, doi:10.5194/bg-11-6427-2014.

Richard, A., D. A. Banks, J. Mercadier, M. C. Boiron, M. Cuney, and M. Cathelineau (2011), An evaporated seawater origin for the ore-forming brines in unconformity-related uranium deposits (Athabasca Basin, Canada): Cl/Br and δ^{37}Cl analysis of fluid inclusions, *Geochimica et Cosmochimica Acta*, *75*(10), 2792-2810, doi:10.1016/j.gca.2011.02.026.

Rosen, M. R. (1994), The importance of groundwater in playas: A review of playa classifications and the sedimentology and hydrology of playas, in *Special Paper of the Geological Society of America*, edited, pp. 1-18, doi:10.1130/SPE289-p1.

Rudnick, R. L., and S. Gao (2014), Composition of the Continental Crust, in *The Crust, Treatise on Geochemistry*, edited by R. L. Rudnick, pp. 1-51, Elsevier, Oxford, UK.

Russell, H. C. (1877), *Climate of New South Wales: descriptive, historical, and tabular*, 190 pp., Charles Potter, Acting Government Printer, Sydney, Australia.

Russell, H. C. (1886), Notes upon floods in Lake George, *Journal and Proceedings of the Royal Society of New South Wales, 20*, 241-260.

Saiz-Lopez, A., and R. von Glasow (2012), Reactive halogen chemistry in the troposphere, *Chemical Society Reviews*, *41*(19), 6448-6472, doi:10.1039/C2CS35208G.

Sander, R., et al. (2003), Inorganic bromine in the marine boundary layer: a critical review, *Atmospheric Chemistry and Physics*, *3*(5), 1301-1336, doi:10.5194/acp-3-1301-2003.

Scanlon, B. R. (2000), Uncertainties in estimating water fluxes and residence times using environmental tracers in an arid unsaturated zone, *Water Resources Research*, *36*(2), 395-409.

Scanlon, B. R., R. W. Healy, and P. G. Cook (2002), Choosing appropriate techniques for quantifying groundwater recharge, *Hydrogeology Journal*, *10*(1), 18-39, doi:10.1007/s10040-001-0176-2.

Scanlon, B. R., R. C. Reedy, and J. A. Tachovsky (2007), Semiarid unsaturated zone chloride profiles: Archives of past land use change impacts on water resources in the southern High Plains, United States, *Water Resources Research*, *43*(6), W06423, doi:10.1029/2006WR005769.

Scanlon, B. R., D. A. Stonestrom, R. C. Reedy, F. W. Leaney, J. Gates, and R. G. Cresswell (2009), Inventories and mobilization of unsaturated zone sulfate, fluoride, and chloride related to land use change in semiarid regions, southwestern United States and Australia, *Water Resources Research*, *45*(7), W00A18, doi:10.1029/2008WR006963.

Scheiber, L., C. Ayora, E. Vázquez-Suñé, D. I. Cendón, A. Soler, E. Custodio, and J. C. Baquero (2015), Recent and old groundwater in the Niebla-Posadas regional aquifer (southern Spain): Implications for its management, *Journal of Hydrology*, *523*, 624-635, doi:10.1016/j.jhydrol.2015.01.076.

Seinfeld, J. H., and S. N. Pandis (2006), *Atmospheric Chemistry and Physics: From Air Pollution to Climate Change*, 1203 pp., John Wiley and Sons, Inc., Hoboken, USA.

Shaw, S., R. Marjerison, D. Bouldin, J. Parlange, and M. Walter (2012), Simple model of changes in stream chloride levels attributable to road salt applications, *Journal of Environmental Engineering*, *138*(1), 112-118, doi:10.1061/(ASCE)EE.1943-7870.0000458.

Shiga, Y., R. S. B. Greene, K. M. Scott, and E. Stelcer (2011), Recognising terrestrially-derived salt (NaCl) in SE Australian dust, *Aeolian Research*, *2*(4), 215-220, doi:10.1016/j.aeolia.2011.02.003.

Short, M. A., P. de Caritat, and D. C. McPhail (2017), Continental-scale variation in chloride/bromide ratios of wet deposition, *Science of The Total Environment*, *574*, 1533-1543, doi:10.1016/j.scitotenv.2016.08.161.

Shouakar-Stash, O. (2008), Evaluation of Stable Chlorine and Bromine Isotopes in Sedimentary Formation Fluids, 355 pp, University of Waterloo, Waterloo, Canada.

Shouakar-Stash, O., S. V. Alexeev, S. K. Frape, L. P. Alexeeva, and R. J. Drimmie (2007), Geochemistry and stable isotopic signatures, including chlorine and bromine isotopes, of the deep groundwaters of the Siberian Platform, Russia, *Applied Geochemistry*, *22*(3), 589-605, doi:10.1016/j.apgeochem.2006.12.005.

Shouakar-Stash, O., R. J. Drimmie, and S. K. Frape (2005a), Determination of inorganic chlorine stable isotopes by continuous flow isotope ratio mass spectrometry, *Rapid Communications in Mass Spectrometry*, *19*(2), 121-127, doi:10.1002/rcm.1762.

Shouakar-Stash, O., S. K. Frape, and R. J. Drimmie (2005b), Determination of bromine stable isotopes using continuous-flow isotope ratio mass spectrometry, *Analytical Chemistry*, *77*(13), 4027-4033, doi:10.1021/ac048318n.

Sie, P. M. J., and S. K. Frape (2002), Evaluation of the groundwaters from the Stripa mine using stable chlorine isotopes, *Chemical Geology*, *182*(2-4), 565-582, doi:10.1016/S0009-2541(01)00340-0.

Siemann, M. G., and M. Schramm (2000), Thermodynamic modelling of the Br partition between aqueous solutions and halite, *Geochimica et Cosmochimica Acta*, *64*(10), 1681-1693, doi:10.1016/S0016-7037(99)00385-3.

Sim, L. L., J. A. Davis, and J. M. Chambers (2006), Ecological regime shifts in salinised wetland systems. II. Factors affecting the dominance of benthic microbial communities, *Hydrobiologia*, *573*(1), 109-131, doi:10.1007/s10750-006-0268-z.

Simpson, W. R., L. Alvarez-Aviles, T. A. Douglas, M. Sturm, and F. Domine (2005), Halogens in the coastal snow pack near Barrow, Alaska: Evidence for active bromine air-snow chemistry during springtime, *Geophysical Research Letters*, *32*(4), L04811, doi:10.1029/2004GL021748.

Simpson, W. R., et al. (2007), Halogens and their role in polar boundary-layer ozone depletion, *Atmospheric Chemistry and Physics*, *7*(16), 4375-4418, doi:10.5194/acp-7-4375-2007.

Singh, G., and E. A. Geissler (1985), Late Cainozoic history of vegetation, fire, lake levels and climate, at Lake George, New South Wales, Australia, *Philosophical*

Transactions of the Royal Society of London. Series B, Biological Sciences, *311*(1151), 379-447, doi:10.2307/2398672.

Singh, G., N. D. Opdyke, and J. M. Bowler (1981), Late Cainozoic stratigraphy, palaeomagnetic chronology and vegetational history from Lake George, NSW, Australia, *Journal Geological Society of Australia*, *28*(3-4), 435-452.

Skrzypek, G., S. Dogramaci, and P. F. Grierson (2013), Geochemical and hydrological processes controlling groundwater salinity of a large inland wetland of northwest Australia, *Chemical Geology*, *357*, 164-177, doi:10.1016/j.chemgeo.2013.08.035.

Sollars, C. J., C. J. Peters, and R. Perry (1982), Bromide in urban runoff - water quality considerations, paper presented at Effects of Waste Disposal on Groundwater and Surface Water, International Association of Hydrological Sciences Publication No. 139, Exeter, UK, July.

Stallard, R. F., and J. M. Edmond (1981), Geochemistry of the Amazon. 1. Precipitation chemistry and the marine contribution to the dissolved load at the time of peak discharge, *Journal of Geophysical Research*, *86*(C10), 9844-9858, doi:10.1029/JC086iC10p09844.

Stigter, T. Y., A. M. M. Carvalho Dill, and L. Ribeiro (2011), Major issues regarding the efficiency of monitoring programs for nitrate contaminated groundwater, *Environmental Science & Technology*, *45*(20), 8674-8682, doi:10.1021/es201798g.

Stone, A. E. C., and W. M. Edmunds (2016), Unsaturated zone hydrostratigraphies: a novel archive of past climates in dryland continental regions, *Earth Science Reviews*, *157*, 121-144, doi:10.1016/j.earscirev.2016.03.007.

Stotler, R. L., S. K. Frape, and O. Shouakar-Stash (2010), An isotopic survey of δ^{81}Br and δ^{37}Cl of dissolved halides in the Canadian and Fennoscandian Shields, *Chemical Geology*, *274*(1-2), 38-55, doi:10.1016/j.chemgeo.2010.03.014.

Stutz, J., R. Ackermann, J. D. Fast, and L. Barrie (2002), Atmospheric reactive chlorine and bromine at the Great Salt Lake, Utah, *Geophysical Research Letters*, *29*(10), 18-11-18-14, doi:10.1029/2002GL014812.

Taberner, C., D. I. Cendón, J. J. Pueyo, and C. Ayora (2000), The use of environmental markers to distinguish marine vs. continental deposition and to quantify the significance of recycling in evaporite basins, *Sedimentary Geology*, *137*(3-4), 213-240, doi:10.1016/S0037-0738(00)00105-6.

Taylor, T. G. (1907), The Lake George Senkungsfeld: a study of the evolution of lakes George and Bathurst, N.S.W, *Proceedings of the Linnaean Society of New South Wales*, *32*, 325- 345.

Tiffany, M. A., J. W. Winchester, and R. H. Loucks (1969), Natural and pollution sources of iodine, bromine, and chlorine in Great Lakes, *Journal of the Water Pollution Control Federation*, *41*(7), 1319-1329.

Torgersen, T., P. De Deckker, A. R. Chivas, and J. M. Bowler (1986), Salt Lakes: a discussion of processes influencing palaeoenvironmental interpretation and

recommendations for future study, *Palaeogeography, Palaeoclimatology, Palaeoecology*, *54*(1-4), 7-19, doi:10.1016/0031-0182(86)90115-X.

Torgersen, T., M. A. Habermehl, F. M. Phillips, D. Elmore, P. Kubik, G. B. Jones, T. Hemmick, and H. E. Gove (1991), Chlorine 36 dating of very old groundwater: 3. Further studies in the Great Artesian Basin, Australia, *Water Resources Research*, *27*(12), 3201-3213, doi:10.1029/91WR02078.

Tyler, S. W., J. B. Chapman, S. H. Conrad, D. P. Hammermeister, D. O. Blout, J. J. Miller, M. J. Sully, and J. M. Ginanni (1996), Soil-water flux in the Southern Great Basin, United States: Temporal and spatial variations over the last 120,000 years, *Water Resources Research*, *32*(6), 1481-1499, doi:10.1029/96WR00564.

USGS (2012), Shuttle Radar Topography Mission, edited, United States Department of the Interior, Washington DC, USA.

Valyashko, M. G. (1956), Geochemistry of bromine in the processes of salt deposition and the use of bromine content as a genetic and prospecting criterion, *Geokhimiya*, *6*, 570-589.

Vengosh, A. (2014), Salinization and Saline Environments, in *Environmental Geochemistry, Treatise on Geochemistry*, edited by B. S. Lollar, pp. 325-378, Elsevier, Oxford, UK.

Vengosh, A., and I. Pankratov (1998), Chloride/bromide and chloride/fluoride ratios of domestic sewage effluents and associated contaminated ground water, *Ground Water*, *36*(5), 815-824.

Vet, R., et al. (2014), A global assessment of precipitation chemistry and deposition of sulfur, nitrogen, sea salt, base cations, organic acids, acidity and pH, and phosphorus, *Atmospheric Environment*, *93*, 3-100, doi:10.1016/j.atmosenv.2013.10.060.

Virkkula, A., M. Aurela, R. Hillamo, T. Mäkelä, T. Pakkanen, V.-M. Kerminen, W. Maenhaut, F. François, and J. Cafmeyer (1999), Chemical composition of atmospheric aerosol in the European subarctic: Contribution of the Kola Peninsula smelter areas, central Europe, and the Arctic Ocean, *Journal of Geophysical Research: Atmospheres*, *104*(D19), 23681-23696, doi:10.1029/1999JD900426.

Vogt, R., P. J. Crutzen, and R. Sander (1996), A mechanism for halogen release from sea-salt aerosol in the remote marine boundary layer, *Nature*, *383*(6598), 327-330.

von Glasow, R., and P. J. Crutzen (2014), Tropospheric Halogen Chemistry, in *The Atmosphere, Treatise on Geochemistry*, edited by R. Keeling and L. Russel, pp. 19-69, Elsevier, Oxford, UK.

Wang, W., X. Liu, L. Zhao, D. Guo, X. Tian, and F. Adams (2006), Effectiveness of leaded petrol phase-out in Tianjin, China based on the aerosol lead concentration and isotope abundance ratio, *Science of the Total Environment*, *364*(1-3), 175-187, doi:10.1016/j.scitotenv.2005.07.002.

Warren, J. K. (2010), Evaporites through time: Tectonic, climatic and eustatic controls in marine and nonmarine deposits, *Earth-Science Reviews*, *98*(3–4), 217-268, doi:10.1016/j.earscirev.2009.11.004.

Warren, J. K. (2014), Geochemistry of Evaporite Ores in an Earth-Scale Climatic and Tectonic Framework, in *Geochemistry of Mineral Deposits*, edited by S. D. Scott, pp. 569-593, Elsevier, Oxford, UK, doi:10.1016/B978-0-08-095975-7.01125-6.

Wetherbee, G. A., and R. A. Martin (2014), *U.S. Geological Survey External Quality-Assurance Project Report for the National Atmospheric Deposition Program/National Trends Network and Mercury Deposition Network, 2011-12, NADP QA Report 2014-01*, 62 pp., National Atmospheric Deposition Program, Champaign, USA.

Wetherbee, G. A., R. A. Martin, M. F. Rhodes, and T. A. Chesney (2014), External Quality-Assurance Project for the National Atmospheric Deposition Program/National Trends Network and Mercury Deposition Network, 2009-2010*Rep.*, 53 pp, U.S. Geological Survey Scientific Investigations Report 2013–5147.

Wetherbee, G. A., M. J. Shaw, N. E. Latysh, C. M. B. Lehmann, and J. E. Rothert (2010), Comparison of precipitation chemistry measurements obtained by the Canadian Air and Precipitation Monitoring Network and National Atmospheric Deposition Program for the period 1995-2004, *Environmental Monitoring and Assessment*, *164*(1-4), 111-132, doi:10.1007/s10661-009-0879-8.

Williams, W. D. (1981), 1. Inland salt lakes: An introduction, *Hydrobiologia*, *81-82*(1), 1-14, doi:10.1007/BF00048701.

Williams, W. D. (2002), Environmental threats to salt lakes and the likely status of inland saline ecosystems in 2025, *Environmental Conservation*, *29*(2), 154-167, doi:10.1017/S0376892902000103.

Xiao, Y. K., W. G. Liu, H. P. Qi, and C. G. Zhang (1993), A new method for the high precision isotopic measurement of bromine by thermal ionization mass spectrometry, *International Journal of Mass Spectrometry and Ion Processes*, *123*(2), 117-123, doi:10.1016/0168-1176(93)87005-D.

Yamanaka, M., S. H. Bottrell, J. Wu, Y. Kumagai, K. Mori, and H. Satake (2014), Chlorine stable isotope evidence for salinization processes of confined groundwater in southwestern Nobi Plain aquifer system, central Japan, *Journal of Hydrology*, *519*(PA), 295-306, doi:10.1016/j.jhydrol.2014.07.022.

Yohai, V. J. (1987), High breakdown-point and high efficiency robust estimates for regression, *The Annals of Statistics*, *15*(2), 642-656, doi:10.2307/2241331.

Zakon, Y., L. Halicz, and F. Gelman (2014), Isotope analysis of sulfur, bromine, and chlorine in individual anionic species by ion chromatography/multicollector-ICPMS, *Analytical Chemistry*, *86*(13), 6495-6500, doi:10.1021/ac5010025.

Zhang, M., S. K. Frape, A. J. Love, A. L. Herczeg, B. E. Lehmann, U. Beyerle, and R. Purtschert (2007), Chlorine stable isotope studies of old groundwater, southwestern Great Artesian Basin, Australia, *Applied Geochemistry*, *22*(3), 557-574, doi:10.1016/j.apgeochem.2006.12.004.

Zhou, M. Y., S. J. Yang, F. P. Parungo, and J. M. Harris (1990), Chemistry of marine aerosols over the western Pacific Ocean, *Journal of Geophysical Research*, *95*(D2), 1779-1787.

Zhu, C., J. R. Winterle, and E. I. Love (2003), Late Pleistocene and Holocene groundwater recharge from the chloride mass balance method and chlorine-36 data, *Water Resources Research*, *39*(7), SBH41-SBH415, doi:10.1029/2003WR001987.

Zlotnik, V. A., J. B. Ong, J. D. Lenters, J. Schmieder, and S. C. Fritz (2012), Quantification of salt dust pathways from a groundwater-fed lake: Implications for solute budgets and dust emission rates, *Journal of Geophysical Research: Earth Surface*, *117*(F2), F02014, doi:10.1029/2011JF002107.

Appendix I

NADP wet deposition collection site summary statistics

1. Collection site details

Site code	Site name	Latitude (DD)	Longitude (DD)	Elevation (m)	Orthogonal inland distance (km)	Number of samples	Censoring (%)								
							Ca	Mg	K	Na	NH_4^+	NO_3^{2-}	Cl^-	SO_4^{2-}	Br^-
AK01	Poker Creek	65.155	–147.491	230	409	203	14.3	25.6	8.9	15.3	46.8	3.9	2.0	0.0	95.6
AK02	Juneau	58.514	–134.784	25	2	209	25.4	12.9	2.4	0.5	59.3	0.0	0.0	0.0	78.5
AK03	Denali National Park - Mt. McKinley	63.723	–148.968	661	243	205	19.0	26.8	21.5	19.5	58.0	5.9	5.4	0.0	93.7
AK06	Gates of the Arctic National Park - Bettles	66.906	–151.683	630	343	178	8.4	17.4	13.5	11.2	45.5	3.4	1.7	0.0	89.9
AK97	Katmai National Park - King Salmon	58.679	–156.666	50	23	194	10.3	5.2	1.0	0.5	25.8	0.5	0.0	0.0	75.8
AL02	Delta Elementary	30.791	–87.850	66	18	27	0.0	0.0	0.0	0.0	3.7	0.0	0.0	0.0	77.8
AL03	Centreville	32.903	–87.250	135	257	177	2.8	3.4	0.6	0.6	0.6	0.0	0.0	0.0	75.1
AL10	Black Belt Research and Extension Center	32.458	–87.242	58	208	245	2.0	2.4	0.8	0.0	2.4	0.0	0.0	0.0	73.1
AL19	Birmingham	33.553	–86.815	200	341	107	0.0	0.0	0.0	0.0	0.9	0.0	0.0	0.0	77.6
AL24	Bay Road	30.475	–88.141	6	4	23	0.0	0.0	0.0	0.0	0.0	0.0	0.0	0.0	56.5
AL99	Sand Mountain Research and Extension Center	34.289	–85.970	349	441	240	4.6	4.2	0.8	1.3	0.4	0.0	0.4	0.0	85.4
AR02	Warren 2WSW	33.605	–92.097	76	420	201	1.5	1.5	0.0	0.5	1.5	0.0	0.0	0.0	69.7
AR03	Caddo Valley	34.180	–93.099	71	513	201	1.0	2.5	0.0	0.0	2.5	0.0	0.0	0.0	73.1
AR16	Buffalo National River - Buffalo Point	36.084	–92.587	311	698	212	0.9	3.8	0.0	1.9	1.4	0.0	0.5	0.0	81.1
AR27	Fayetteville	36.101	–94.174	381	740	227	0.9	3.1	0.4	0.0	0.4	0.0	0.4	0.0	78.4
AZ03	Grand Canyon National Park - Hopi Point	36.059	–112.184	2071	542	153	0.7	0.7	1.3	3.3	0.7	0.0	0.7	0.0	71.9
AZ06	Organ Pipe Cactus National Monument	31.949	–112.802	501	93	96	2.1	3.1	3.1	1.0	3.1	0.0	0.0	0.0	31.3
AZ97	Petrified Forest National Park - Rainbow Forest	34.822	–109.893	1707	513	144	0.0	4.9	0.7	1.4	0.0	0.0	0.0	0.0	67.4
AZ98	Chiricahua	32.010	–109.389	1570	357	158	0.6	2.5	0.0	0.6	1.9	0.0	0.0	0.0	70.9
AZ99	Oliver Knoll	33.071	–109.866	1176	369	127	0.0	4.7	0.8	1.6	0.8	0.0	0.0	0.0	59.8
BC22	Haul Road Station	54.029	–128.702	10	57	129	4.7	10.1	1.6	0.0	14.7	0.0	0.0	0.0	80.6
BC23	Lakelse Lake	54.377	–128.578	111	4	92	25.0	29.3	5.4	4.3	67.4	0.0	1.1	0.0	92.4
BC24	Port Edward	54.223	–130.270	80	2	71	7.0	4.2	1.4	0.0	42.3	0.0	0.0	0.0	63.4
CA28	Kings River Experimental Watershed	37.059	–119.182	2000	222	131	8.4	9.9	1.5	2.3	8.4	0.0	1.5	0.0	87.0
CA42	Tanbark Flat	34.207	–117.762	853	62	104	1.0	0.0	0.0	0.0	0.0	0.0	0.0	0.0	54.8
CA45	Hopland	39.005	–123.086	253	47	140	4.3	4.3	0.0	0.7	7.1	0.0	0.0	0.0	72.1
CA50	Sagehen Creek	39.432	–120.240	1931	231	95	9.5	24.2	6.3	4.2	23.2	0.0	3.2	0.0	89.5
CA66	Pinnacles National Monument - Bear Valley	36.483	–121.157	317	59	104	4.8	5.8	1.9	0.0	9.6	1.0	0.0	0.0	78.8
CA67	Joshua Tree National Park - Black Rock	34.070	–116.389	1239	133	70	4.3	10.0	5.7	4.3	4.3	0.0	0.0	0.0	65.7
CA75	Sequoia National Park - Giant Forest	36.566	–118.778	1921	232	108	3.7	8.3	0.9	2.8	4.6	0.0	0.9	0.0	80.6
CA76	Montague	41.766	–122.480	799	129	156	5.8	12.2	2.6	2.6	3.8	0.6	0.0	0.0	91.0
CA88	Davis	38.536	–121.776	18	67	110	2.7	0.9	0.0	0.0	0.0	0.0	0.0	0.0	71.8
CA94	Converse Flats	34.194	–116.913	1724	110	127	6.3	6.3	3.1	3.1	2.4	0.0	0.0	0.0	70.9

Appendix I – NADP wet deposition collection site summary statistics

Site code	Site name	Latitude (DD)	Longitude (DD)	Elevation (m)	Orthogonal inland distance (km)	Number of samples	Censoring (%)								
							Ca	Mg	K	Na	NH_4^+	NO_3^{2-}	Cl^-	SO_4^{2-}	Br^-
CA96	Lassen Volcanic National Park - Manzanita Lake	40.539	–121.577	1754	204	158	12.0	15.2	7.0	5.7	18.4	0.6	1.3	0.0	89.9
CA99	Yosemite National Park - Hodgdon Meadow	37.796	–119.858	1393	184	135	10.4	11.1	4.4	3.0	8.1	0.7	0.7	0.0	80.7
CO00	Alamosa	37.442	–105.868	2285	965	146	0.7	3.4	0.7	0.0	2.1	0.0	0.7	0.0	67.8
CO01	Las Animas Fish Hatchery	38.118	–103.316	1226	1178	143	0.0	0.0	0.0	0.7	0.0	0.0	0.0	0.0	76.2
CO02	Niwot Saddle	40.055	–105.589	3520	1218	212	1.4	3.8	2.4	2.4	4.2	0.0	1.9	0.0	81.1
CO08	Four Mile Park	39.403	–107.345	2502	1070	246	0.8	2.8	0.0	2.8	2.8	0.8	0.8	0.0	83.3
CO09	Kawaneechee Meadow	40.827	–105.829	2633	1279	127	3.1	12.6	1.6	4.7	3.1	0.0	0.0	0.0	85.8
CO10	Gothic	38.956	–106.986	2915	1041	195	1.5	7.7	6.2	2.6	4.6	0.0	2.1	0.0	80.0
CO15	Sand Spring	40.508	–107.703	1998	1168	214	1.4	2.8	6.1	0.9	3.3	0.0	0.0	0.0	69.6
CO19	Rocky Mountain National Park - Beaver Meadows	40.364	–105.581	2477	1248	228	1.8	4.8	2.6	2.6	3.9	0.0	2.2	0.0	76.8
CO21	Manitou	39.101	–105.093	2362	1154	198	0.5	3.0	1.5	1.5	2.0	0.0	0.5	0.0	80.8
CO22	Pawnee	40.806	–104.756	1641	1327	165	0.0	4.8	1.8	2.4	0.0	0.0	0.0	0.0	76.4
CO89	Rocky Mountain National Park - Loch Vale	40.290	–105.660	3159	1236	186	1.6	12.4	1.6	2.7	1.6	0.0	1.6	0.0	81.7
CO90	Niwot Ridge - Southeast	40.037	–105.544	3015	1218	220	1.8	8.2	2.3	4.1	2.3	0.0	0.9	0.0	80.9
CO91	Wolf Creek Pass	37.469	–106.787	3287	917	234	3.4	7.7	1.7	3.0	0.9	0.0	0.4	0.0	78.2
CO92	Sunlight Peak	39.426	–107.380	3218	1067	236	1.3	3.0	0.4	3.0	2.1	0.0	0.4	0.0	84.7
CO93	Buffalo Pass - Dry Lake	40.535	–106.781	2538	1210	236	1.7	5.5	2.1	3.8	1.3	0.0	0.4	0.0	82.2
CO94	Sugarloaf	39.994	–105.480	2524	1218	223	1.8	4.9	0.4	1.8	1.3	0.0	0.0	0.0	85.7
CO96	Molas Pass	37.750	–107.689	3248	896	218	1.4	3.7	1.8	1.4	8.3	0.5	0.0	0.0	86.2
CO97	Buffalo Pass - Summit Lake	40.538	–106.677	3234	1213	241	2.9	7.1	3.7	2.9	2.1	0.0	1.2	0.0	86.3
CO98	Rocky Mountain National Park - Loch Vale	40.288	–105.663	3159	1236	235	1.7	9.4	3.4	3.8	0.9	0.0	2.1	0.0	86.4
CO99	Mesa Verde National Park - Chapin Mesa	37.198	–108.491	2162	800	178	0.0	1.1	2.2	1.1	2.2	0.0	0.0	0.0	73.6
CT15	Abington	41.840	–72.010	209	47	259	5.8	6.2	0.8	0.0	0.8	0.0	0.0	0.0	81.5
FL03	Bradford Forest	29.975	–82.198	44	84	210	1.9	0.0	0.0	0.0	5.7	0.0	0.0	0.0	54.8
FL05	Chassahowitzka National Wildlife Refuge	28.749	–82.555	3	9	241	0.8	0.0	0.4	0.0	2.9	0.0	0.0	0.0	50.2
FL11	Everglades National Park - Research Center	25.390	–80.680	2	22	244	0.4	0.0	0.0	0.0	2.5	0.4	0.0	0.0	28.7
FL14	Quincy	30.549	–84.600	60	60	237	1.7	0.4	0.0	0.4	5.5	0.4	0.0	0.0	61.6
FL23	Sumatra	30.111	–84.990	14	39	256	7.0	1.2	0.4	0.4	5.1	0.0	0.0	0.0	66.0
FL32	Orlando	28.593	–81.190	21	38	184	0.0	0.0	0.0	0.0	3.3	0.0	0.0	0.0	46.7
FL41	Verna Well Field	27.380	–82.283	25	28	223	0.9	0.4	0.0	0.0	0.4	0.0	0.0	0.0	47.1
FL96	Pensacola	30.550	–87.375	45	22	117	4.3	0.9	0.0	0.0	2.6	0.0	0.9	0.0	53.0
FL99	Kennedy Space Center	28.543	–80.644	2	4	232	0.0	0.0	0.0	0.0	5.2	0.0	0.0	0.0	30.6
GA09	Okefenokee National Wildlife Refuge	30.740	–82.128	45	65	250	2.0	1.2	1.2	0.0	8.0	0.0	0.0	0.0	66.4
GA20	Bellville	32.085	–81.937	54	77	269	5.2	2.6	0.7	0.0	0.4	0.0	0.0	0.0	68.8
GA33	Sapelo Island	31.396	–81.281	3	1	202	1.0	0.0	0.0	0.0	5.4	0.0	0.0	0.0	34.2
GA41	Georgia Station	33.181	–84.810	267	354	228	7.9	2.6	0.4	0.0	1.8	0.4	0.0	0.0	77.2
GA99	Chula	31.522	–83.548	108	170	238	2.9	2.1	0.8	0.0	0.0	0.0	0.0	0.0	78.6
IA08	Big Springs Fish Hatchery	42.910	–91.470	229	1378	269	0.0	0.0	0.0	1.5	0.4	0.0	0.4	0.0	90.7
IA23	McNay Research Center	40.963	–93.393	320	1295	229	0.0	0.4	0.9	1.3	0.0	0.0	0.4	0.0	86.0

Site code	Site name	Latitude (DD)	Longitude (DD)	Elevation (m)	Orthogonal inland distance (km)	Number of samples	Censoring (%)								
							Ca	Mg	K	Na	NH_4^+	NO_3^{2-}	Cl^-	SO_4^{2-}	Br^-
ID02	Priest River Experimental Forest	48.352	–116.840	726	389	211	6.6	10.9	1.9	2.4	2.4	0.0	0.0	0.0	92.4
ID03	Craters of the Moon National Monument	43.461	–113.555	1807	803	160	2.5	10.6	8.8	5.0	1.9	0.6	1.3	0.0	76.9
ID11	Reynolds Creek	43.205	–116.750	1200	576	157	1.3	8.3	2.5	1.3	3.8	0.0	1.3	0.0	69.4
IL11	Bondville	40.053	–88.372	212	921	276	0.7	2.9	1.1	1.4	0.0	0.0	0.4	0.0	87.7
IL18	Shabbona	41.841	–88.851	265	1047	252	0.4	0.4	1.2	1.2	0.4	0.0	0.4	0.0	86.5
IL46	Alhambra	38.869	–89.622	164	965	248	0.0	2.8	0.4	0.8	0.4	0.0	0.0	0.0	87.5
IL63	Dixon Springs Agricultural Center	37.436	–88.672	161	786	238	0.4	2.1	0.0	0.4	0.4	0.0	0.0	0.0	76.5
IL78	Monmouth	40.933	–90.723	229	1121	249	0.0	0.4	0.0	0.8	0.0	0.0	0.0	0.0	89.2
IL95	–	40.053	–88.372	212	921	9	0.0	0.0	11.1	11.1	11.1	0.0	0.0	0.0	88.9
IN20	Roush Lake	40.840	–85.464	244	714	261	0.4	0.4	0.0	1.1	0.4	0.0	0.0	0.0	86.2
IN22	Southwest Purdue Agriculture Center	38.741	–87.486	134	836	253	0.4	1.2	0.0	1.2	0.4	0.0	0.0	0.0	83.4
IN34	Indiana Dunes National Lakeshore	41.632	–87.088	208	887	290	0.3	0.3	0.0	0.3	0.0	0.0	0.0	0.0	83.1
IN41	Agronomy Center for Research and Extension	40.475	–86.992	215	819	271	0.0	1.1	0.4	0.7	0.0	0.0	0.0	0.0	86.7
KS07	Farlington Fish Hatchery	37.651	–94.804	281	929	240	0.0	0.8	0.0	0.4	0.4	0.0	0.4	0.0	79.6
KS31	Konza Prairie	39.102	–96.609	350	1121	232	0.0	1.7	0.4	2.2	0.0	0.4	0.0	0.0	79.3
KS32	Lake Scott State Park	38.672	–100.916	863	1175	167	0.0	0.6	0.0	0.0	0.0	0.0	0.0	0.0	80.2
KS97	Kickapoo Tribe - Powhattan	39.760	–95.636	367	1124	4	0.0	0.0	0.0	0.0	0.0	0.0	0.0	0.0	75.0
KY03	Mackville	37.705	–85.049	293	647	278	0.7	4.7	0.4	0.7	0.4	0.0	0.4	0.0	86.3
KY10	Mammoth Cave National Park - Houchin Meadow	37.132	–86.148	236	740	237	3.0	3.8	0.0	0.8	0.8	0.0	0.0	0.0	87.8
KY19	Cannons Lane	38.232	–85.673	177	694	242	0.8	0.8	0.0	0.8	0.4	0.0	0.0	0.0	86.4
KY22	Lilley Cornett Woods	37.078	–82.994	335	498	281	1.8	5.3	0.4	0.7	1.1	0.0	0.4	0.0	88.3
KY35	Clark State Fish Hatchery	38.118	–83.547	204	515	196	0.5	2.6	0.0	0.5	0.5	0.0	0.0	0.0	87.8
KY99	Mulberry Flat	36.903	–88.012	110	716	222	2.7	4.5	0.5	1.4	0.5	0.0	0.0	0.0	83.8
LA12	Iberia Research Station	29.931	–91.717	6	20	90	0.0	1.1	0.0	0.0	4.4	0.0	0.0	0.0	51.1
LA30	Southeast Research Station	30.782	–90.202	77	46	234	3.4	1.3	0.4	0.0	2.6	0.0	0.0	0.0	56.0
MA01	North Atlantic Coastal Lab	41.976	–70.024	57	1	237	0.0	0.0	0.0	0.0	4.2	0.0	0.0	0.0	39.2
MA08	Quabbin Reservoir	42.393	–72.344	306	103	279	6.1	7.2	0.7	0.0	3.2	0.0	0.0	0.0	82.4
MA13	East	42.385	–71.215	190	14	53	0.0	0.0	1.9	0.0	1.9	0.0	0.0	0.0	62.3
MA14	Nantucket	41.290	–70.175	16	1	59	0.0	0.0	0.0	0.0	3.4	0.0	0.0	0.0	28.8
MA22	Boston University	42.350	–71.104	32	12	21	0.0	0.0	0.0	0.0	4.8	0.0	0.0	0.0	81.0
MD07	Catoctin Mountain Park	39.647	–77.485	471	83	165	0.6	1.8	0.0	0.0	0.0	0.0	0.0	0.0	88.5
MD08	Piney Reservoir	39.705	–79.012	769	201	267	2.6	9.4	1.1	1.1	1.1	0.0	0.0	0.0	89.5
MD13	Wye	38.913	–76.153	6	0	264	5.3	3.4	0.0	0.0	0.0	0.0	0.0	0.0	68.6
MD15	Smith Island	37.993	–76.035	2	1	269	3.0	0.0	0.0	0.0	1.1	0.0	0.0	0.0	53.2
MD18	Assateague Island National Seashore - Woodcock	38.251	–75.159	0	1	246	4.1	0.0	0.4	0.0	2.0	0.0	0.0	0.0	54.9
MD99	Beltsville	39.028	–76.817	46	24	251	3.6	5.2	0.4	0.4	0.8	0.0	0.0	0.0	74.5
ME00	Caribou	46.868	–68.013	191	155	251	4.8	10.4	0.4	1.2	6.4	0.0	0.0	0.0	85.7
ME02	Bridgton	44.108	–70.729	222	58	265	9.8	11.7	3.0	0.4	4.2	0.0	0.0	0.0	90.9
ME04	Carrabassett Valley	45.003	–70.212	259	112	210	8.6	12.9	2.4	0.5	6.2	0.0	1.0	0.0	92.4

Site code	Site name	Latitude (DD)	Longitude (DD)	Elevation (m)	Orthogonal inland distance (km)	Number of samples	Censoring (%)								
							Ca	Mg	K	Na	NH_4^+	NO_3^{2-}	Cl^-	SO_4^{2-}	Br^-
ME08	Gilead	44.400	–71.010	212	97	201	7.0	11.4	1.0	1.0	5.5	1.0	1.0	0.0	84.1
ME09	Greenville Station	45.489	–69.665	322	119	289	7.3	12.5	2.1	4.5	6.9	0.3	0.7	0.0	88.9
ME94	Indian Township	45.244	–67.631	101	35	90	14.4	8.9	3.3	0.0	4.4	0.0	0.0	0.0	87.8
ME96	Casco Bay-Wolfe's Neck Farm	43.833	–70.065	15	1	247	4.5	3.2	0.8	0.0	5.3	0.0	0.0	0.0	74.9
ME98	Acadia National Park - McFarland Hill	44.377	–68.261	150	4	278	6.1	2.2	0.7	0.0	6.5	0.0	0.0	0.0	69.1
MI09	Douglas Lake	45.561	–84.678	238	734	288	0.3	2.4	1.0	3.5	1.7	0.0	0.7	0.0	89.9
MI26	Kellogg Biological Station	42.410	–85.393	288	788	268	0.4	1.1	0.0	1.1	0.4	0.0	0.0	0.0	90.3
MI48	Seney National Wildlife Refuge - Headquarters	46.289	–85.950	220	698	271	1.1	5.2	2.6	0.7	1.5	0.0	0.7	0.0	87.1
MI51	Unionville	43.614	–83.360	201	748	256	0.8	2.7	1.6	2.7	0.4	0.0	0.4	0.0	88.3
MI52	Ann Arbor	42.416	–83.902	267	703	265	0.4	0.8	0.0	1.9	0.0	0.0	0.4	0.0	87.2
MI53	Wellston	44.224	–85.819	292	912	263	0.8	1.9	0.0	2.3	0.8	0.0	0.0	0.0	92.4
MI98	Raco	46.372	–84.746	272	643	188	0.5	1.1	0.0	1.6	1.1	0.0	0.0	0.0	89.4
MI99	Chassell	47.105	–88.552	296	737	263	0.8	3.0	0.0	4.2	3.0	0.8	0.8	0.0	84.4
MN01	Cedar Creek	45.402	–93.203	280	1121	249	0.0	2.8	0.8	2.8	0.4	0.0	0.0	0.0	88.8
MN08	Hovland	47.847	–89.965	224	759	248	0.8	4.4	0.8	5.6	1.2	0.0	1.2	0.0	86.7
MN16	Marcell Experimental Forest	47.531	–93.469	431	983	263	0.4	3.0	0.0	4.6	2.3	0.4	0.4	0.0	91.6
MN18	Fernberg	47.946	–91.496	524	842	256	0.8	3.5	2.3	5.5	1.2	0.0	1.2	0.0	84.4
MN23	Camp Ripley	46.249	–94.497	410	1129	244	0.0	1.6	0.4	2.5	0.4	0.0	0.0	0.0	89.8
MN27	Lamberton	44.237	–95.301	367	1327	217	0.0	0.5	0.0	1.4	0.5	0.0	0.0	0.0	88.9
MN28	Grindstone Lake	46.122	–93.000	350	1049	237	1.3	3.8	0.4	4.2	0.4	0.0	0.0	0.0	93.2
MN32	Voyageurs National Park - Sullivan Bay	48.413	–92.831	421	886	247	2.4	5.7	2.8	7.7	2.0	0.0	0.8	0.0	89.9
MN99	Wolf Ridge	47.384	–91.207	361	862	253	2.4	5.1	1.2	6.7	2.0	0.8	0.4	0.0	88.1
MO03	Ashland Wildlife Area	38.754	–92.199	257	997	237	0.0	1.3	0.0	0.8	0.4	0.0	0.0	0.0	82.3
MO05	University Forest	36.911	–90.319	165	754	234	0.4	1.3	0.0	0.4	0.4	0.0	0.4	0.0	81.6
MS10	Clinton	32.307	–90.319	86	223	178	2.2	1.1	0.0	0.6	2.2	0.0	0.0	0.0	75.8
MS12	Grand Bay NERR	30.429	–88.428	2	7	176	1.7	1.7	0.0	0.0	0.6	0.0	0.0	0.0	53.4
MS19	Newton	32.327	–89.209	134	221	251	4.4	4.8	0.0	0.4	2.0	0.0	0.0	0.0	69.7
MS30	Coffeeville	34.003	–89.799	134	419	210	2.4	3.3	0.5	0.0	2.9	0.0	0.0	0.0	81.9
MT00	Little Bighorn Battlefield National Monument	45.570	–107.438	962	1099	220	1.4	3.6	0.9	0.0	0.5	0.0	0.5	0.0	79.5
MT05	Glacier National Park - Fire Weather Station	48.510	–113.997	964	588	247	6.5	14.6	2.4	1.6	3.6	0.4	0.8	0.0	90.3
MT07	Clancy	46.485	–112.065	1448	734	235	0.9	6.8	0.9	5.5	3.4	0.4	1.3	0.0	88.1
MT96	Poplar River	48.315	–105.144	640	1208	131	0.8	1.5	2.3	3.1	0.8	0.0	0.8	0.0	71.8
MT97	Lost Trail Pass	45.692	–113.968	2401	629	209	11.5	21.1	1.9	5.3	12.4	0.5	1.0	0.0	90.9
MT98	Havre - Northern Agricultural Research Center	48.501	–109.798	819	884	193	0.0	0.5	1.0	3.1	0.0	0.0	0.5	0.0	88.6
NC03	Lewiston	36.133	–77.171	22	38	270	3.3	1.5	0.0	0.0	1.1	0.0	0.4	0.0	73.7
NC06	Beaufort	34.885	–76.621	2	8	244	2.5	0.8	0.4	0.0	2.5	0.0	0.0	0.0	50.0
NC17	University Research Farm	36.067	–79.734	238	265	35	0.0	2.9	0.0	0.0	2.9	0.0	0.0	0.0	77.1
NC25	Coweeta	35.061	–83.431	686	377	282	9.6	12.1	1.4	2.1	3.2	0.0	0.4	0.0	83.0
NC29	Hofmann Forest	34.825	–77.323	14	24	274	1.1	0.7	0.7	0.0	2.9	0.0	0.0	0.0	58.8

Site code	Site name	Latitude (DD)	Longitude (DD)	Elevation (m)	Orthogonal inland distance (km)	Number of samples	Censoring (%)								
							Ca	Mg	K	Na	NH_4^+	NO_3^{2-}	Cl^-	SO_4^{2-}	Br^-
NC34	Piedmont Research Station	35.697	–80.623	219	286	253	6.3	5.5	0.0	0.0	0.0	0.0	0.0	0.0	80.6
NC35	Clinton Crops Research Station	35.026	–78.278	41	94	264	4.5	2.3	0.0	0.0	0.4	0.0	0.0	0.0	67.8
NC36	Jordan Creek	34.971	–79.528	132	161	269	5.2	2.6	0.0	0.0	1.1	0.0	0.0	0.0	79.6
NC41	Finley Farm	35.729	–78.680	120	148	284	6.0	2.8	0.4	0.0	0.0	0.0	0.0	0.0	78.9
NC45	Mt. Mitchell	35.735	–82.286	1987	383	248	16.9	19.8	2.4	6.9	4.4	0.0	2.0	0.0	88.7
ND00	Theodore Roosevelt National Park - Painted Canyon	46.895	–103.378	863	1342	210	0.5	2.4	1.4	0.0	1.0	0.0	0.0	0.0	87.6
ND08	Icelandic State Park	48.782	–97.755	306	1002	186	0.0	0.0	0.0	2.2	0.5	0.0	0.0	0.0	87.6
ND11	Woodworth	47.125	–99.238	578	1218	166	0.0	0.0	0.0	0.0	0.0	0.0	0.0	0.0	82.5
NE15	Mead	41.153	–96.491	352	1330	214	0.0	1.4	0.0	0.0	0.0	0.0	0.0	0.0	82.2
NE99	North Platte Agricultural Experiment Station	41.059	–100.746	919	1419	186	0.0	0.5	0.5	0.5	0.0	0.0	0.0	0.0	78.5
NH02	Hubbard Brook	43.943	–71.703	250	112	273	7.7	13.6	0.4	1.8	5.1	0.7	0.0	0.0	87.9
NJ00	Edwin B. Forsythe National Wildlife Refuge	39.473	–74.437	2	2	229	3.1	0.9	0.0	0.0	0.4	0.0	0.0	0.0	55.5
NJ39	Cattus Island County Park	39.989	–74.134	1	0	108	6.5	0.0	0.9	0.0	0.9	0.0	0.0	0.0	41.7
NJ99	Washington Crossing	40.315	–74.854	72	50	260	3.1	3.5	0.0	0.0	0.8	0.0	0.0	0.0	77.3
NM01	Gila Cliff Dwellings National Monument	33.220	–108.235	1772	500	78	0.0	0.0	0.0	0.0	3.8	0.0	0.0	0.0	61.5
NM07	Bandelier National Monument	35.779	–106.266	1997	808	169	0.6	5.3	1.2	4.7	1.8	0.0	0.0	0.0	75.1
NM08	Mayhill	32.910	–105.471	2022	716	134	0.0	0.7	0.7	1.5	0.7	0.0	0.0	0.0	70.9
NM12	Capulin Volcano National Monument	36.779	–103.981	2190	1032	82	0.0	1.2	1.2	0.0	2.4	1.2	0.0	0.0	62.2
NV03	Smith Valley	38.799	–119.257	1501	263	114	2.6	11.4	0.9	2.6	0.0	0.0	2.6	0.0	82.5
NV05	Great Basin National Park - Lehman Caves	39.005	–114.217	2066	671	170	0.6	1.8	0.0	1.8	1.8	0.0	0.0	0.0	62.4
NY01	Alfred	42.228	–77.802	697	340	258	0.4	4.3	0.4	1.9	0.8	0.0	0.0	0.0	89.5
NY06	Bronx	40.868	–73.878	68	5	103	1.0	0.0	0.0	0.0	0.0	0.0	0.0	0.0	62.1
NY08	Aurora Research Farm	42.734	–76.660	249	312	272	2.2	6.3	1.1	2.2	0.0	0.0	0.4	0.0	89.3
NY10	Chautauqua	42.299	–79.396	488	418	233	0.0	0.9	0.0	0.4	0.9	0.0	0.0	0.0	89.7
NY20	Huntington Wildlife	43.973	–74.223	500	292	304	7.2	11.5	2.3	4.6	2.3	0.3	0.3	0.0	92.8
NY22	Akwesasne Mohawk - Fort Covington	44.923	–74.481	70	325	246	1.2	3.7	0.0	2.4	0.4	0.0	0.4	0.0	92.3
NY28	Piseco Lake	43.434	–74.500	519	288	123	5.7	13.0	1.6	4.9	2.4	0.0	0.0	0.0	93.5
NY29	Moss Lake	43.787	–74.843	566	323	231	1.3	8.2	0.0	0.4	2.6	0.0	0.4	0.0	89.2
NY43	Rochester	43.146	–77.548	136	396	96	0.0	0.0	0.0	1.0	1.0	0.0	0.0	0.0	85.4
NY52	Bennett Bridge	43.528	–75.949	247	349	190	2.6	7.9	0.0	2.6	1.6	0.0	0.0	0.0	84.7
NY59	Wanakena	44.146	–74.903	468	343	130	1.5	10.0	0.0	6.9	0.8	0.0	0.0	0.0	90.0
NY68	Biscuit Brook	41.994	–74.503	634	135	286	2.1	7.0	0.3	0.0	1.4	0.0	0.3	0.0	88.8
NY92	Amherst	42.993	–78.772	183	453	88	0.0	0.0	0.0	0.0	2.3	1.1	0.0	0.0	79.5
NY93	Paul Smith's	44.434	–74.246	498	313	118	2.5	6.8	0.0	4.2	0.8	0.0	0.0	0.0	89.8
NY94	Nick's Lake	43.683	–74.983	525	310	1	0.0	0.0	0.0	0.0	0.0	0.0	0.0	0.0	0.0
NY96	Cedar Beach - Southold	41.035	–72.389	1	7	247	0.4	0.0	0.0	0.0	1.6	0.0	0.0	0.0	38.5
NY98	Whiteface Mountain	44.393	–73.859	610	282	300	2.7	10.3	0.7	6.3	1.3	0.0	0.0	0.0	92.0
NY99	West Point	41.351	–74.048	211	52	247	1.6	2.8	0.4	0.4	2.4	0.4	0.0	0.0	85.0
OH09	Oxford	39.531	–84.724	284	617	216	0.0	1.4	0.0	1.4	0.5	0.0	0.0	0.0	85.6

Appendix I – NADP wet deposition collection site summary statistics

Site code	Site name	Latitude (DD)	Longitude (DD)	Elevation (m)	Orthogonal inland distance (km)	Number of samples	Censoring (%)								
							Ca	Mg	K	Na	NH_4^+	NO_3^{2-}	Cl^-	SO_4^{2-}	Br^-
OH15	Lykens	40.550	–82.998	303	519	60	0.0	0.0	0.0	1.7	0.0	0.0	0.0	0.0	88.3
OH17	Delaware	40.356	–83.066	285	516	269	0.7	2.6	0.4	1.9	0.4	0.0	0.0	0.0	90.3
OH49	Caldwell	39.793	–81.531	276	376	279	0.0	1.4	0.4	1.8	0.4	0.0	0.4	0.0	84.6
OH54	Deer Creek State Park	39.636	–83.261	267	504	251	1.6	3.2	0.0	2.4	0.8	0.0	0.0	0.0	86.1
OH71	Wooster	40.781	–81.920	308	453	276	0.4	1.4	0.4	1.4	0.4	0.0	0.0	0.0	88.0
OK00	Salt Plains National Wildlife Refuge	36.805	–98.201	345	874	191	0.0	0.0	0.0	0.0	0.0	0.0	0.0	0.0	73.8
OK17	Kessler Farm Field Laboratory	34.980	–97.521	331	655	142	0.0	0.7	0.0	0.0	0.0	0.0	0.0	0.0	71.8
OK29	Goodwell Research Station	36.591	–101.618	999	1001	154	0.0	1.3	0.0	0.0	0.0	0.0	0.0	0.0	77.3
OK99	Stilwell	35.751	–94.670	299	643	3	0.0	0.0	0.0	0.0	0.0	0.0	0.0	0.0	66.7
OR09	Silver Lake Ranger Station	43.119	–121.059	1338	250	98	3.1	8.2	2.0	5.1	9.2	3.1	0.0	0.0	92.9
OR10	H. J. Andrews Experimental Forest	44.212	–122.256	443	140	237	20.3	14.3	3.0	1.7	29.5	0.0	0.4	0.0	83.5
OR18	Starkey Experimental Forest	45.225	–118.513	1254	403	210	7.6	19.0	8.6	4.3	14.8	1.4	0.5	0.0	89.5
OR97	Hyslop Farm	44.635	–123.190	69	66	217	8.3	4.6	0.5	0.0	0.5	0.0	0.0	0.0	77.0
PA00	Arendtsville	39.923	–77.308	269	96	249	1.6	4.8	0.0	0.4	0.0	0.0	0.0	0.0	88.4
PA02	Crooked Creek Lake	40.713	–79.514	294	289	159	0.6	6.9	0.0	0.0	3.1	0.6	0.0	0.0	73.6
PA13	Allegheny Portage Railroad National Historic Site	40.457	–78.560	739	211	158	0.0	0.0	0.0	0.0	0.6	0.6	0.0	0.0	65.8
PA15	Penn State	40.788	–77.946	393	210	266	1.9	6.8	0.0	0.4	0.0	0.0	0.0	0.0	88.3
PA18	Young Woman's Creek	41.414	–77.680	272	255	254	0.0	5.1	0.0	2.0	2.4	0.0	0.0	0.0	85.0
PA21	Goddard State Park	41.427	–80.145	385	380	164	0.0	3.0	0.0	0.0	1.2	0.0	0.0	0.0	76.2
PA29	Kane Experimental Forest	41.598	–78.768	618	324	284	2.5	8.5	1.1	2.8	1.8	0.0	0.4	0.0	89.8
PA30	Erie	42.156	–80.113	177	442	162	0.0	1.2	0.0	0.0	0.0	0.0	0.0	0.0	66.7
PA42	Leading Ridge	40.658	–77.940	287	197	258	0.4	3.1	0.8	1.2	0.0	0.0	0.0	0.0	82.9
PA47	Millersville	39.991	–76.386	84	58	209	1.4	3.3	0.0	0.5	0.0	0.0	0.0	0.0	81.3
PA52	Little Pine State Park	41.364	–77.356	228	237	182	1.6	5.5	0.0	2.2	2.2	0.5	0.0	0.0	78.6
PA60	Valley Forge	40.117	–75.883	46	51	176	1.7	2.3	0.0	0.0	0.6	0.0	0.0	0.0	69.9
PA71	Little Buffalo State Park	40.460	–77.169	155	140	164	0.6	3.0	0.0	0.6	0.0	0.0	0.0	0.0	75.0
PA72	Milford	41.327	–74.820	212	90	210	2.9	4.8	0.0	0.5	0.5	0.0	0.0	0.0	84.3
PA83	Laurel Hill State Park	39.987	–79.254	594	229	161	1.2	7.5	0.0	0.0	1.2	0.0	0.0	0.0	79.5
PA90	Hills Creek State Park	41.804	–77.190	476	274	183	1.1	5.5	0.0	1.6	2.2	0.0	0.0	0.0	84.2
PA98	Frances Slocum State Park	41.345	–75.890	370	159	154	0.0	7.1	0.0	1.3	0.6	0.0	0.0	0.0	75.3
PR20	El Verde	18.321	–65.820	380	10	306	0.7	0.0	0.0	0.0	24.2	0.0	0.0	0.0	24.8
SC03	Savannah River	33.245	–81.651	90	115	157	3.8	3.2	0.0	0.0	1.3	0.0	0.0	0.0	69.4
SC05	Cape Romain National Wildlife Refuge	32.943	–79.659	1	0	234	0.4	0.0	0.4	0.0	5.6	0.4	0.0	0.0	45.7
SC06	Santee National Wildlife Refuge	33.539	–80.435	24	92	215	2.3	1.9	0.0	0.0	3.3	0.5	0.0	0.0	64.2
SD04	Wind Cave National Park - Elk Mountain	43.558	–103.484	1292	1456	211	0.0	0.9	1.4	1.9	0.5	0.0	0.0	0.0	82.5
SD08	Cottonwood	43.946	–101.855	733	1552	159	0.6	0.6	1.3	2.5	0.0	0.0	0.6	0.0	85.5
SD99	Huron Well Field	44.335	–98.292	398	1496	185	0.0	1.1	0.5	0.0	0.0	0.0	0.5	0.0	82.2
SK20	Cactus Lake	52.022	–109.862	790	971	126	0.0	0.0	0.0	0.8	0.8	0.0	0.0	0.0	81.7
SK21	Hudson Bay	52.840	–102.380	367	756	128	0.0	3.1	0.0	2.3	0.8	0.0	0.0	0.0	78.9

Site code	Site name	Latitude (DD)	Longitude (DD)	Elevation (m)	Orthogonal inland distance (km)	Number of samples	Censoring (%)								
							Ca	Mg	K	Na	NH_4^+	NO_3^{2-}	Cl^-	SO_4^{2-}	Br^-
TN00	Walker Branch Watershed	35.961	–84.287	341	509	94	0.0	0.0	0.0	0.0	1.1	0.0	0.0	0.0	91.5
TN04	Speedwell	36.470	–83.827	384	544	277	3.2	6.1	0.4	1.1	0.4	0.0	0.0	0.0	87.0
TN11	Great Smoky Mountains National Park - Elkmont	35.665	–83.590	640	447	276	5.1	14.1	0.0	3.3	2.5	0.0	0.0	0.0	89.9
TN14	Hatchie National Wildlife Refuge	35.469	–89.171	117	565	191	2.6	5.2	0.0	0.5	1.6	0.0	0.5	0.0	88.0
TX02	Muleshoe National Wildlife Refuge	33.956	–102.776	1144	827	77	1.3	1.3	0.0	0.0	1.3	0.0	0.0	0.0	59.7
TX03	Beeville	28.467	–97.707	82	67	174	0.0	0.0	0.0	0.0	0.0	0.0	0.0	0.0	38.5
TX04	Big Bend National Park - K-Bar	29.303	–103.178	1056	561	122	1.6	9.0	1.6	1.6	0.8	0.0	0.8	0.0	63.1
TX10	Attwater Prairie Chicken National Wildlife Refuge	29.661	–96.259	54	117	176	0.0	0.0	0.0	0.0	0.6	0.0	0.0	0.0	43.8
TX16	Sonora	30.261	–100.555	696	401	181	0.6	2.2	0.6	0.0	0.6	0.0	0.0	0.0	60.2
TX21	Longview	32.379	–94.712	103	292	224	1.3	2.2	0.0	0.0	1.8	0.0	0.0	0.0	65.6
TX22	Guadalupe Mountains National Park Frijole Ranger Station	31.907	–104.805	1705	707	148	0.7	1.4	2.0	0.7	1.4	0.7	0.0	0.0	61.5
TX43	Cañónceta	34.880	–101.665	1057	850	151	0.7	2.0	0.7	2.0	0.0	0.0	0.7	0.0	70.9
TX56	L.B.J. National Grasslands	33.392	–97.640	312	493	190	0.5	2.6	0.0	0.5	0.5	0.0	0.0	0.0	69.5
UT01	Logan	41.666	–111.891	1370	954	201	0.0	0.0	0.0	0.0	0.0	0.0	0.0	0.0	46.3
UT08	Murphy Ridge	41.359	–111.048	2146	986	87	0.0	0.0	1.1	1.1	1.1	0.0	0.0	0.0	69.0
UT09	Canyonlands National Park - Island in the Sky	38.458	–109.821	1797	896	169	0.6	3.6	2.4	2.4	1.8	0.0	0.0	0.0	79.3
UT98	Green River	39.000	–110.174	1256	917	125	0.0	1.6	0.8	0.8	0.0	0.0	0.0	0.0	81.6
UT99	Bryce Canyon National Park - Repeater Hill	37.619	–112.173	2477	679	164	1.2	1.8	1.2	3.7	3.0	0.0	0.0	0.0	75.6
VA00	Charlottesville	38.040	–78.543	172	106	262	3.8	6.1	0.0	0.4	1.1	0.0	0.0	0.0	76.0
VA10	Mason Neck	38.629	–77.205	6	1	4	0.0	0.0	0.0	0.0	0.0	0.0	0.0	0.0	75.0
VA13	Horton's Station	37.329	–80.558	916	297	275	4.4	7.3	0.4	3.6	4.4	0.4	0.0	0.0	88.7
VA24	Prince Edward	37.165	–78.307	150	112	263	6.5	6.5	0.0	0.0	1.5	0.0	0.0	0.0	84.4
VA27	James Madison University Farm	38.303	–78.818	336	131	1	0.0	0.0	0.0	0.0	0.0	0.0	0.0	0.0	0.0
VA28	Shenandoah National Park - Big Meadows	38.523	–78.435	1072	91	263	9.5	12.2	2.7	2.7	2.3	0.0	0.8	0.0	90.9
VA98	Harcum	37.531	–76.493	13	7	92	0.0	0.0	0.0	0.0	4.3	0.0	0.0	0.0	80.4
VA99	Natural Bridge Station	37.627	–79.513	282	203	243	7.4	11.9	0.4	2.1	2.9	0.0	0.0	0.0	84.4
VI01	Virgin Islands National Park - Lind Point	18.336	–64.796	56	0	250	0.0	0.0	0.0	0.0	14.8	0.0	0.0	0.0	12.4
VT01	Bennington	42.876	–73.163	305	178	247	0.4	0.8	0.0	0.4	4.0	0.0	0.0	0.0	93.9
VT99	Underhill	44.528	–72.868	399	230	285	1.4	4.9	0.4	4.6	1.8	0.4	0.0	0.0	92.3
WA14	Olympic National Park - Hoh Ranger Station	47.860	–123.933	182	36	213	12.2	6.1	0.9	0.0	45.1	0.9	0.0	0.0	62.4
WA19	North Cascades National Park - Marblemount Ranger Station	48.540	–121.446	124	69	238	14.3	10.1	1.7	0.0	23.1	0.0	0.0	0.0	84.5
WA21	La Grande	46.835	–122.287	617	42	227	11.9	6.2	0.0	0.0	20.7	0.9	0.0	0.0	79.7
WA24	Palouse Conservation Farm	46.761	–117.185	766	374	225	1.3	7.1	1.3	1.3	0.9	0.0	0.0	0.0	89.3
WA98	Columbia River Gorge	45.569	–122.210	233	117	224	8.9	5.4	0.4	0.4	0.4	0.0	0.0	0.0	74.1
WA99	Mount Rainier National Park-Tahoma Woods	46.758	–122.124	424	57	206	14.6	9.7	0.0	0.5	24.8	0.0	0.0	0.0	84.0
WI08	Brule River	46.747	–91.606	207	944	60	0.0	0.0	0.0	6.7	1.7	0.0	0.0	0.0	91.7
WI09	Popple River	45.796	–88.399	421	836	151	0.7	7.9	0.7	0.7	0.7	0.0	0.0	0.0	92.1
WI10	Potawatomi	45.565	–88.808	570	878	265	0.4	4.2	0.4	5.7	1.1	0.4	1.1	0.0	89.8
WI25	Suring	45.052	–88.373	262	902	193	1.0	4.7	0.5	1.0	0.0	0.0	0.0	0.0	88.1

Appendix I – NADP wet deposition collection site summary statistics

Site code	Site name	Latitude (DD)	Longitude (DD)	Elevation (m)	Orthogonal inland distance (km)	Number of samples	Censoring (%)								
							Ca	Mg	K	Na	NH_4^+	NO_3^{2-}	Cl^-	SO_4^{2-}	Br^-
WI28	Lake Dubay	44.707	–89.772	385	1007	173	1.2	5.8	0.6	0.0	1.2	0.0	0.0	0.0	83.2
WI31	Devil's Lake	43.435	–89.680	389	1132	65	0.0	0.0	0.0	4.6	0.0	0.0	0.0	0.0	81.5
WI35	Perkinstown	45.206	–90.598	472	1007	261	0.8	5.4	0.8	4.6	0.4	0.0	1.1	0.0	90.0
WI36	Trout Lake	46.051	–89.654	509	880	263	1.9	4.2	0.0	5.7	1.1	0.4	0.0	0.0	89.7
WI37	Spooner	45.823	–91.874	331	1017	238	0.4	2.5	0.4	5.0	0.0	0.0	0.0	0.0	89.9
WI98	Wildcat Mountain	43.702	–90.569	386	1138	166	0.0	1.8	1.8	0.6	0.0	0.6	0.0	0.0	88.0
WI99	Lake Geneva	42.579	–88.501	288	1049	178	0.0	1.7	0.0	0.0	0.0	0.0	0.0	0.0	90.4
WV04	Babcock State Park	37.980	–80.953	753	323	163	1.8	3.7	0.0	1.8	0.6	0.0	0.0	0.0	90.8
WV05	Cedar Creek State Park	38.879	–80.848	210	311	229	2.2	8.3	0.0	3.5	1.7	0.0	0.0	0.0	90.0
WV18	Parsons	39.090	–79.662	505	216	292	2.1	4.8	0.0	2.1	0.7	0.0	0.0	0.0	87.0
WY00	Snowy Range	41.376	–106.260	3269	1395	262	1.9	6.9	6.1	4.6	5.0	0.8	1.1	0.0	79.4
WY02	Sinks Canyon	42.734	–108.850	2164	1145	192	1.6	7.8	4.7	7.8	2.1	0.0	3.1	0.0	76.6
WY06	Pinedale	42.929	–109.788	2388	1067	175	2.9	10.3	10.3	6.3	5.7	0.6	0.6	0.0	63.4
WY08	Yellowstone National Park - Tower Falls	44.917	–110.420	1912	910	251	2.8	10.8	5.2	6.4	1.6	0.0	1.2	0.0	78.9
WY94	Grand Tetons National Park	43.833	–110.701	2107	950	143	0.7	3.5	1.4	2.8	0.7	0.0	0.0	0.0	81.8
WY95	Brooklyn Lake	41.365	–106.241	3181	1395	269	1.5	8.2	3.7	5.2	6.3	0.4	0.4	0.0	81.4
WY97	South Pass City	42.494	–108.832	2524	1157	153	1.3	7.2	2.6	3.3	3.3	0.0	0.7	0.0	73.9
WY98	Gypsum Creek	43.223	–109.992	2428	1031	196	4.1	9.2	9.2	4.1	4.6	0.0	2.6	0.0	69.4
WY99	Newcastle	43.873	–104.192	1466	1404	205	0.0	2.9	3.4	1.0	2.4	0.0	0.5	0.0	80.0

2. Chloride and bromide summaries

Site code	Measured only					Imputed (*lrEM* method)				
	Median concentration (mg L^{-1})		Mean weekly wet deposition (kg ha^{-1})		Mean weekly wet deposition	Median concentration (mg L^{-1})		Mean weekly wet deposition (kg ha^{-1})		Mean weekly wet deposition
	Cl^-	Br^-	Cl^-	Br^-	Cl^-/ Br^- (mass)	Cl^-	Br^-	Cl^-	Br^-	Cl^-/ Br^- (mass)
AK01	0.0270	0.0061	0.0037	0.0006	7	0.0270	0.0007	0.0037	0.0001	38
AK02	0.1680	0.0034	0.0859	0.0013	67	0.1680	0.0012	0.0859	0.0006	150
AK03	0.0240	0.0047	0.0028	0.0005	5	0.0240	0.0005	0.0027	0.0001	34
AK06	0.0340	0.0079	0.0036	0.0006	6	0.0340	0.0007	0.0035	0.0001	27
AK97	0.2525	0.0042	0.1038	0.0012	86	0.2525	0.0017	0.1038	0.0004	238
AL02	0.3750	0.0051	0.1806	0.0009	198	0.3750	0.0034	0.1806	0.0011	158
AL03	0.1870	0.0038	0.0970	0.0013	75	0.1870	0.0031	0.0970	0.0010	95
AL10	0.2040	0.0041	0.0814	0.0012	66	0.2040	0.0031	0.0814	0.0009	94
AL19	0.1710	0.0035	0.0851	0.0011	80	0.1710	0.0034	0.0851	0.0010	83
AL24	0.6980	0.0081	0.5054	0.0045	113	0.6980	0.0044	0.5054	0.0028	181
AL99	0.1130	0.0043	0.0487	0.0011	46	0.1125	0.0026	0.0485	0.0008	57
AR02	0.2140	0.0046	0.0818	0.0010	82	0.2140	0.0034	0.0818	0.0010	83
AR03	0.1740	0.0039	0.0818	0.0014	57	0.1740	0.0033	0.0818	0.0012	71
AR16	0.1010	0.0048	0.0334	0.0011	29	0.1005	0.0030	0.0333	0.0007	45
AR27	0.1175	0.0038	0.0450	0.0010	44	0.1150	0.0031	0.0449	0.0008	59
AZ03	0.1165	0.0085	0.0163	0.0009	17	0.1160	0.0031	0.0163	0.0005	34
AZ06	0.4475	0.0079	0.0720	0.0006	111	0.4475	0.0060	0.0720	0.0006	124
AZ97	0.1500	0.0063	0.0106	0.0004	30	0.1500	0.0037	0.0106	0.0002	44
AZ98	0.0965	0.0069	0.0158	0.0006	24	0.0965	0.0032	0.0158	0.0004	37
AZ99	0.1430	0.0070	0.0118	0.0004	29	0.1430	0.0038	0.0118	0.0003	41
BC22	0.2230	0.0029	0.2089	0.0020	106	0.2230	0.0015	0.2089	0.0010	207
BC23	0.0560	0.0027	0.0288	0.0005	57	0.0555	0.0008	0.0285	0.0003	109
BC24	0.4630	0.0031	0.3127	0.0020	160	0.4630	0.0023	0.3127	0.0012	257
CA28	0.0740	0.0058	0.0229	0.0088	3	0.0740	0.0016	0.0225	0.0014	16
CA42	0.5255	0.0061	0.1813	0.0013	140	0.5255	0.0042	0.1813	0.0009	201
CA45	0.2895	0.0045	0.1629	0.0016	102	0.2895	0.0019	0.1629	0.0007	221
CA50	0.0310	0.0108	0.0094	0.0017	6	0.0300	0.0007	0.0092	0.0003	30
CA66	0.2700	0.0042	0.0639	0.0005	126	0.2700	0.0019	0.0639	0.0003	227
CA67	0.1520	0.0064	0.0226	0.0003	84	0.1520	0.0020	0.0226	0.0002	105
CA75	0.0870	0.0062	0.0270	0.0004	66	0.0835	0.0016	0.0268	0.0004	69
CA76	0.0445	0.0067	0.0049	0.0004	14	0.0445	0.0009	0.0049	0.0001	42
CA88	0.2790	0.0056	0.1003	0.0012	82	0.2790	0.0027	0.1003	0.0006	170
CA94	0.1780	0.0071	0.0424	0.0009	47	0.1780	0.0024	0.0424	0.0004	97
CA96	0.0495	0.0070	0.0167	0.0003	49	0.0490	0.0008	0.0165	0.0002	69
CA99	0.0790	0.0042	0.0382	0.0007	55	0.0780	0.0017	0.0379	0.0005	83
CO00	0.0630	0.0065	0.0037	0.0003	11	0.0625	0.0024	0.0037	0.0002	22
CO01	0.0700	0.0062	0.0071	0.0006	12	0.0700	0.0033	0.0071	0.0003	21
CO02	0.0495	0.0064	0.0053	0.0011	5	0.0490	0.0021	0.0052	0.0004	14
CO08	0.0445	0.0066	0.0065	0.0005	12	0.0440	0.0019	0.0065	0.0003	23
CO09	0.0420	0.0037	0.0051	0.0004	11	0.0420	0.0016	0.0051	0.0002	24
CO10	0.0440	0.0067	0.0066	0.0007	9	0.0430	0.0018	0.0065	0.0003	22
CO15	0.0535	0.0076	0.0043	0.0006	8	0.0535	0.0024	0.0043	0.0002	18
CO19	0.0500	0.0071	0.0055	0.0006	9	0.0490	0.0020	0.0054	0.0003	19
CO21	0.0600	0.0079	0.0065	0.0009	7	0.0590	0.0032	0.0065	0.0004	17
CO22	0.0600	0.0070	0.0065	0.0004	15	0.0600	0.0030	0.0065	0.0003	22
CO89	0.0360	0.0051	0.0056	0.0006	9	0.0345	0.0017	0.0055	0.0003	19
CO90	0.0370	0.0057	0.0063	0.0014	5	0.0365	0.0018	0.0062	0.0005	14
CO91	0.0470	0.0069	0.0108	0.0009	12	0.0465	0.0020	0.0108	0.0005	22
CO92	0.0370	0.0063	0.0054	0.0005	10	0.0370	0.0014	0.0054	0.0002	23
CO93	0.0360	0.0063	0.0053	0.0119	0	0.0360	0.0017	0.0052	0.0023	2
CO94	0.0480	0.0052	0.0058	0.0008	7	0.0480	0.0022	0.0058	0.0003	18
CO96	0.0480	0.0051	0.0081	0.0009	9	0.0480	0.0017	0.0081	0.0003	24
CO97	0.0370	0.0049	0.0051	0.0009	6	0.0370	0.0017	0.0051	0.0003	18
CO98	0.0390	0.0065	0.0059	0.0011	5	0.0380	0.0017	0.0058	0.0003	17
CO99	0.0830	0.0067	0.0084	0.0005	17	0.0830	0.0032	0.0084	0.0003	28
CT15	0.1770	0.0051	0.0709	0.0013	56	0.1770	0.0030	0.0709	0.0007	104
FL03	0.3625	0.0045	0.1251	0.0011	113	0.3625	0.0034	0.1251	0.0011	116
FL05	0.6530	0.0055	0.2116	0.0013	165	0.6530	0.0040	0.2116	0.0013	166
FL11	0.9720	0.0067	0.3060	0.0019	161	0.9720	0.0054	0.3060	0.0017	178
FL14	0.3430	0.0045	0.1270	0.0012	102	0.3430	0.0035	0.1270	0.0011	120
FL23	0.4120	0.0044	0.1703	0.0019	89	0.4120	0.0034	0.1703	0.0013	135
FL32	0.4985	0.0059	0.1933	0.0014	134	0.4985	0.0041	0.1933	0.0014	142
FL41	0.5600	0.0050	0.1825	0.0014	129	0.5600	0.0040	0.1825	0.0013	142
FL96	0.4755	0.0043	0.2798	0.0022	128	0.4700	0.0039	0.2774	0.0015	183
FL99	0.9185	0.0070	0.3645	0.0019	191	0.9185	0.0052	0.3645	0.0017	219
GA09	0.2975	0.0047	0.1168	0.0013	89	0.2975	0.0033	0.1168	0.0010	122
GA20	0.2720	0.0044	0.0800	0.0009	90	0.2720	0.0033	0.0800	0.0008	106

Appendix I – NADP wet deposition collection site summary statistics

Site code	Measured only					Imputed (*lrEM* method)				
	Median concentration (mg L^{-1})		Mean weekly wet deposition (kg ha^{-1})		Mean weekly wet deposition	Median concentration (mg L^{-1})		Mean weekly wet deposition (kg ha^{-1})		Mean weekly wet deposition
	Cl^-	Br^-	Cl^-	Br^-	Cl^-/ Br^- (mass)	Cl^-	Br^-	Cl^-	Br^-	Cl^-/ Br^- (mass)
GA33	1.1565	0.0074	0.3846	0.0020	194	1.1565	0.0055	0.3846	0.0016	237
GA41	0.1500	0.0034	0.0531	0.0010	54	0.1500	0.0028	0.0531	0.0008	70
GA99	0.2265	0.0043	0.0761	0.0009	87	0.2265	0.0028	0.0761	0.0008	100
IA08	0.0655	0.0049	0.0164	0.0010	16	0.0650	0.0033	0.0163	0.0006	25
IA23	0.0770	0.0046	0.0197	0.0013	15	0.0770	0.0033	0.0196	0.0007	27
ID02	0.0390	0.0078	0.0092	0.0008	12	0.0390	0.0012	0.0092	0.0002	38
ID03	0.0650	0.0064	0.0087	0.0004	23	0.0650	0.0016	0.0086	0.0002	51
ID11	0.0570	0.0068	0.0075	0.0003	25	0.0570	0.0016	0.0074	0.0002	42
IL11	0.0830	0.0053	0.0192	0.0011	18	0.0815	0.0033	0.0191	0.0006	31
IL18	0.0780	0.0068	0.0159	0.0012	14	0.0780	0.0036	0.0158	0.0006	25
IL46	0.0830	0.0046	0.0260	0.0011	24	0.0830	0.0031	0.0260	0.0007	36
IL63	0.1000	0.0054	0.0406	0.0018	23	0.1000	0.0032	0.0406	0.0010	40
IL78	0.0710	0.0040	0.0194	0.0009	21	0.0710	0.0030	0.0194	0.0006	30
IL95	0.0850	–	0.0173	–	–	0.0850	0.0023	0.0173	0.0003	67
IN20	0.0800	0.0043	0.0192	0.0020	10	0.0800	0.0034	0.0192	0.0008	24
IN22	0.0890	0.0049	0.0311	0.0021	15	0.0890	0.0034	0.0311	0.0010	30
IN34	0.1110	0.0045	0.0281	0.0009	31	0.1110	0.0039	0.0281	0.0008	36
IN41	0.0770	0.0041	0.0187	0.0013	14	0.0770	0.0033	0.0187	0.0007	28
KS07	0.1120	0.0048	0.0365	0.0011	34	0.1115	0.0032	0.0363	0.0008	44
KS31	0.0735	0.0050	0.0201	0.0013	16	0.0735	0.0030	0.0201	0.0007	30
KS32	0.0580	0.0042	0.0105	0.0013	8	0.0580	0.0028	0.0105	0.0006	19
KS97	0.1165	–	0.0256	–	–	0.1165	0.0018	0.0256	0.0004	68
KY03	0.0770	0.0052	0.0308	0.0027	12	0.0765	0.0029	0.0307	0.0010	31
KY10	0.0760	0.0035	0.0357	0.0010	36	0.0760	0.0027	0.0357	0.0008	47
KY19	0.1080	0.0036	0.0384	0.0032	12	0.1080	0.0033	0.0384	0.0011	34
KY22	0.0585	0.0043	0.0190	0.0021	9	0.0580	0.0025	0.0189	0.0008	24
KY35	0.0720	0.0059	0.0250	0.0017	14	0.0720	0.0032	0.0250	0.0009	29
KY99	0.0910	0.0037	0.0421	0.0022	19	0.0910	0.0028	0.0421	0.0010	43
LA12	0.4475	0.0052	0.2233	0.0019	117	0.4475	0.0041	0.2233	0.0017	131
LA30	0.3225	0.0049	0.1648	0.0016	102	0.3225	0.0036	0.1648	0.0014	120
MA01	1.4510	0.0081	0.5235	0.0027	196	1.4510	0.0047	0.5235	0.0019	274
MA08	0.1110	0.0045	0.0410	0.0014	30	0.1110	0.0026	0.0410	0.0007	63
MA13	0.3210	0.0080	0.2660	0.0027	100	0.3210	0.0036	0.2660	0.0015	180
MA14	1.6720	0.0074	0.9027	0.0041	219	1.6720	0.0060	0.9027	0.0031	289
MA22	0.4170	0.0066	0.1349	0.0019	73	0.4170	0.0027	0.1349	0.0007	197
MD07	0.0890	0.0068	0.0453	0.0022	20	0.0890	0.0032	0.0453	0.0009	50
MD08	0.0660	0.0065	0.0161	0.0018	9	0.0660	0.0026	0.0161	0.0006	28
MD13	0.2590	0.0051	0.0761	0.0010	75	0.2590	0.0035	0.0761	0.0008	101
MD15	0.8300	0.0064	0.2664	0.0015	177	0.8300	0.0043	0.2664	0.0011	234
MD18	0.7415	0.0084	0.2821	0.0020	142	0.7415	0.0043	0.2821	0.0013	222
MD99	0.1430	0.0049	0.0480	0.0011	44	0.1430	0.0033	0.0480	0.0008	64
ME00	0.0620	0.0054	0.0197	0.0011	17	0.0620	0.0016	0.0197	0.0005	44
ME02	0.0770	0.0059	0.0569	0.0017	33	0.0770	0.0020	0.0569	0.0006	103
ME04	0.0585	0.0062	0.0373	0.0010	38	0.0580	0.0017	0.0370	0.0005	80
ME08	0.0540	0.0053	0.0464	0.0017	27	0.0530	0.0021	0.0460	0.0007	69
ME09	0.0560	0.0077	0.0284	0.0015	19	0.0560	0.0017	0.0282	0.0005	57
ME94	0.1450	0.0032	0.0457	0.0006	82	0.1450	0.0017	0.0457	0.0004	128
ME96	0.3180	0.0063	0.1466	0.0017	85	0.3180	0.0032	0.1466	0.0008	177
ME98	0.3650	0.0060	0.1700	0.0018	94	0.3650	0.0029	0.1700	0.0009	185
MI09	0.0475	0.0073	0.0086	0.0012	7	0.0470	0.0027	0.0085	0.0005	18
MI26	0.0685	0.0064	0.0151	0.0013	12	0.0685	0.0034	0.0151	0.0006	24
MI48	0.0430	0.0038	0.0063	0.0006	10	0.0430	0.0023	0.0063	0.0004	17
MI51	0.0550	0.0049	0.0096	0.0014	7	0.0550	0.0031	0.0095	0.0005	18
MI52	0.0700	0.0055	0.0142	0.0015	10	0.0700	0.0034	0.0142	0.0006	22
MI53	0.0550	0.0102	0.0124	0.0020	6	0.0550	0.0030	0.0124	0.0006	20
MI98	0.0425	0.0064	0.0089	0.0008	11	0.0425	0.0026	0.0089	0.0004	20
MI99	0.0470	0.0070	0.0075	0.0013	6	0.0470	0.0023	0.0075	0.0005	16
MN01	0.0630	0.0056	0.0112	0.0011	10	0.0630	0.0027	0.0112	0.0005	21
MN08	0.0390	0.0043	0.0060	0.0010	6	0.0390	0.0024	0.0060	0.0004	14
MN16	0.0330	0.0051	0.0053	0.0007	8	0.0330	0.0021	0.0053	0.0003	16
MN18	0.0350	0.0052	0.0040	0.0004	9	0.0350	0.0019	0.0040	0.0003	15
MN23	0.0480	0.0065	0.0084	0.0008	11	0.0480	0.0027	0.0084	0.0005	18
MN27	0.0640	0.0047	0.0158	0.0006	27	0.0640	0.0032	0.0158	0.0005	33
MN28	0.0380	0.0042	0.0071	0.0013	5	0.0380	0.0022	0.0071	0.0005	16
MN32	0.0280	0.0062	0.0049	0.0010	5	0.0280	0.0017	0.0049	0.0004	14
MN99	0.0390	0.0070	0.0061	0.0007	9	0.0390	0.0024	0.0061	0.0004	15
MO03	0.0890	0.0049	0.0286	0.0019	15	0.0890	0.0031	0.0286	0.0009	32
MO05	0.1130	0.0043	0.0539	0.0025	22	0.1130	0.0032	0.0536	0.0011	47
MS10	0.2240	0.0043	0.0813	0.0015	54	0.2240	0.0034	0.0813	0.0010	82

Appendix I – NADP wet deposition collection site summary statistics

Site code	Measured only					Imputed (*lrEM* method)				
	Median concentration (mg L^{-1})		Mean weekly wet deposition (kg ha^{-1})		Mean weekly wet deposition	Median concentration (mg L^{-1})		Mean weekly wet deposition (kg ha^{-1})		Mean weekly wet deposition
	Cl^-	Br^-	Cl^-	Br^-	Cl^-/ Br^- (mass)	Cl^-	Br^-	Cl^-	Br^-	Cl^-/ Br^- (mass)
MS12	0.6780	0.0057	0.3490	0.0025	137	0.6780	0.0042	0.3490	0.0019	184
MS19	0.1780	0.0037	0.0837	0.0014	60	0.1780	0.0028	0.0837	0.0010	86
MS30	0.1550	0.0042	0.0585	0.0013	46	0.1550	0.0032	0.0585	0.0009	69
MT00	0.0490	0.0095	0.0039	0.0022	2	0.0485	0.0019	0.0039	0.0006	7
MT05	0.0290	0.0056	0.0051	0.0010	5	0.0290	0.0011	0.0051	0.0002	21
MT07	0.0345	0.0088	0.0046	0.0004	10	0.0330	0.0014	0.0045	0.0002	26
MT96	0.0475	0.0096	0.0052	0.0006	9	0.0470	0.0028	0.0052	0.0004	14
MT97	0.0270	0.0038	0.0059	0.0007	8	0.0270	0.0007	0.0059	0.0002	35
MT98	0.0400	0.0089	0.0039	0.0004	9	0.0400	0.0021	0.0039	0.0002	19
NC03	0.2670	0.0046	0.0930	0.0010	93	0.2665	0.0034	0.0927	0.0007	128
NC06	1.0665	0.0065	0.4204	0.0026	159	1.0665	0.0044	0.4204	0.0018	239
NC17	0.1540	0.0032	0.1419	0.0043	33	0.1540	0.0023	0.1419	0.0014	102
NC25	0.0870	0.0046	0.0487	0.0016	31	0.0870	0.0025	0.0485	0.0008	59
NC29	0.4710	0.0060	0.2104	0.0016	133	0.4710	0.0039	0.2104	0.0012	182
NC34	0.1280	0.0045	0.0426	0.0014	30	0.1280	0.0034	0.0426	0.0008	54
NC35	0.3060	0.0044	0.0899	0.0010	95	0.3060	0.0034	0.0899	0.0007	124
NC36	0.1780	0.0049	0.0783	0.0014	58	0.1780	0.0032	0.0783	0.0008	100
NC41	0.1740	0.0041	0.0617	0.0012	51	0.1740	0.0029	0.0617	0.0007	89
NC45	0.0440	0.0050	0.0236	0.0019	13	0.0430	0.0016	0.0232	0.0006	37
ND00	0.0505	0.0062	0.0053	0.0005	11	0.0505	0.0021	0.0053	0.0002	23
ND08	0.0470	0.0107	0.0052	0.0011	5	0.0470	0.0029	0.0052	0.0004	13
ND11	0.0525	0.0063	0.0050	0.0005	10	0.0525	0.0031	0.0050	0.0003	16
NE15	0.0620	0.0067	0.0173	0.0008	23	0.0620	0.0029	0.0173	0.0006	28
NE99	0.0640	0.0056	0.0089	0.0044	2	0.0640	0.0031	0.0089	0.0012	7
NH02	0.0660	0.0041	0.0270	0.0009	31	0.0660	0.0022	0.0270	0.0005	49
NJ00	0.7750	0.0063	0.3747	0.0024	157	0.7750	0.0043	0.3747	0.0015	251
NJ39	0.7185	0.0057	0.5686	0.0031	181	0.7185	0.0042	0.5686	0.0021	274
NJ99	0.1980	0.0044	0.0813	0.0011	73	0.1980	0.0034	0.0813	0.0008	99
NM01	0.0875	0.0083	0.0104	0.0006	16	0.0875	0.0034	0.0104	0.0004	25
NM07	0.0680	0.0080	0.0062	0.0006	10	0.0680	0.0024	0.0062	0.0003	21
NM08	0.0705	0.0050	0.0154	0.0009	17	0.0705	0.0027	0.0154	0.0006	27
NM12	0.0790	0.0093	0.0137	0.0007	21	0.0790	0.0036	0.0137	0.0004	35
NV03	0.0610	0.0075	0.0054	0.0004	15	0.0560	0.0013	0.0053	0.0001	42
NV05	0.1235	0.0090	0.0134	0.0011	12	0.1235	0.0035	0.0134	0.0006	24
NY01	0.0510	0.0093	0.0116	0.0022	5	0.0510	0.0027	0.0116	0.0007	18
NY06	0.6270	0.0042	0.2533	0.0016	154	0.6270	0.0040	0.2533	0.0011	226
NY08	0.0560	0.0058	0.0106	0.0012	9	0.0560	0.0028	0.0106	0.0005	21
NY10	0.0630	0.0048	0.0222	0.0008	27	0.0630	0.0034	0.0222	0.0009	26
NY20	0.0370	0.0048	0.0094	0.0009	11	0.0370	0.0018	0.0093	0.0004	23
NY22	0.0430	0.0040	0.0086	0.0013	7	0.0430	0.0025	0.0086	0.0005	18
NY28	0.0530	0.0036	0.0220	0.0010	22	0.0530	0.0024	0.0220	0.0005	41
NY29	0.0410	0.0075	0.0139	0.0012	11	0.0410	0.0023	0.0139	0.0006	22
NY43	0.1215	0.0031	0.1001	0.0005	204	0.1215	0.0037	0.1001	0.0006	166
NY52	0.0540	0.0052	0.0175	0.0007	25	0.0540	0.0029	0.0175	0.0006	28
NY59	0.0460	0.0033	0.0145	0.0008	18	0.0460	0.0024	0.0145	0.0005	28
NY68	0.0700	0.0053	0.0335	0.0019	17	0.0700	0.0026	0.0334	0.0008	42
NY92	0.1330	0.0033	0.0728	0.0005	146	0.1330	0.0039	0.0728	0.0006	115
NY93	0.0550	0.0031	0.0153	0.0007	22	0.0550	0.0023	0.0153	0.0005	30
NY94	0.0190	–	0.0044	–	–	0.0190	0.0015	0.0044	0.0003	13
NY96	1.9900	0.0108	0.6059	0.0028	213	1.9900	0.0056	0.6059	0.0020	297
NY98	0.0350	0.0059	0.0105	0.0011	9	0.0350	0.0021	0.0105	0.0005	20
NY99	0.1390	0.0045	0.0777	0.0019	41	0.1390	0.0034	0.0777	0.0010	79
OH09	0.0910	0.0042	0.0339	0.0016	21	0.0910	0.0036	0.0339	0.0008	41
OH15	0.0550	0.0079	0.0100	0.0003	38	0.0550	0.0033	0.0100	0.0005	19
OH17	0.0690	0.0070	0.0189	0.0022	9	0.0690	0.0033	0.0189	0.0008	24
OH49	0.0985	0.0060	0.0248	0.0018	13	0.0980	0.0038	0.0247	0.0009	27
OH54	0.0670	0.0041	0.0182	0.0007	26	0.0670	0.0032	0.0182	0.0006	29
OH71	0.0820	0.0068	0.0206	0.0018	11	0.0820	0.0035	0.0206	0.0007	28
OK00	0.1680	0.0058	0.0428	0.0009	49	0.1680	0.0037	0.0428	0.0007	63
OK17	0.1855	0.0054	0.0575	0.0014	41	0.1855	0.0039	0.0575	0.0010	56
OK29	0.1360	0.0061	0.0319	0.0006	53	0.1360	0.0036	0.0319	0.0004	80
OK99	0.1190	–	0.0714	–	–	0.1190	0.0028	0.0714	0.0015	48
OR09	0.0390	0.0062	0.0031	0.0001	22	0.0390	0.0012	0.0031	0.0001	38
OR10	0.1255	0.0042	0.1288	0.0019	66	0.1220	0.0011	0.1283	0.0007	185
OR18	0.0340	0.0050	0.0054	0.0004	14	0.0335	0.0008	0.0054	0.0001	36
OR97	0.2950	0.0044	0.1358	0.0015	93	0.2950	0.0016	0.1358	0.0006	245
PA00	0.1140	0.0054	0.0440	0.0013	35	0.1140	0.0032	0.0440	0.0007	60
PA02	0.0870	0.0036	0.0220	0.0008	28	0.0870	0.0035	0.0220	0.0007	32
PA13	0.2400	0.0044	0.0562	0.0007	80	0.2400	0.0041	0.0562	0.0008	67

Appendix I – NADP wet deposition collection site summary statistics

Site code	Measured only					Imputed (*lrEM* method)				
	Median concentration (mg L^{-1})		Mean weekly wet deposition (kg ha^{-1})		Mean weekly wet deposition	Median concentration (mg L^{-1})		Mean weekly wet deposition (kg ha^{-1})		Mean weekly wet deposition
	Cl^-	Br^-	Cl^-	Br^-	Cl^-/ Br^- (mass)	Cl^-	Br^-	Cl^-	Br^-	Cl^-/ Br^- (mass)
PA15	0.0835	0.0037	0.0202	0.0008	24	0.0835	0.0032	0.0202	0.0006	32
PA18	0.0820	0.0036	0.0226	0.0011	21	0.0820	0.0033	0.0226	0.0007	32
PA21	0.1005	0.0038	0.0237	0.0009	25	0.1005	0.0036	0.0237	0.0007	33
PA29	0.0480	0.0041	0.0143	0.0013	11	0.0480	0.0027	0.0143	0.0006	23
PA30	0.1540	0.0044	0.0319	0.0007	43	0.1540	0.0041	0.0319	0.0008	41
PA42	0.1125	0.0045	0.0258	0.0008	31	0.1125	0.0034	0.0258	0.0006	40
PA47	0.1420	0.0050	0.0502	0.0011	44	0.1420	0.0034	0.0502	0.0008	65
PA52	0.0990	0.0041	0.0224	0.0008	29	0.0990	0.0033	0.0224	0.0006	36
PA60	0.2920	0.0045	0.0967	0.0010	92	0.2920	0.0037	0.0967	0.0008	114
PA71	0.1515	0.0038	0.0438	0.0009	47	0.1515	0.0036	0.0438	0.0007	61
PA72	0.1360	0.0052	0.0558	0.0021	27	0.1360	0.0033	0.0558	0.0010	57
PA83	0.0880	0.0033	0.0245	0.0009	27	0.0880	0.0032	0.0245	0.0007	34
PA90	0.0700	0.0038	0.0173	0.0007	25	0.0700	0.0031	0.0173	0.0005	33
PA98	0.1050	0.0037	0.0226	0.0006	38	0.1050	0.0027	0.0226	0.0005	49
PR20	2.2395	0.0092	1.4210	0.0054	263	2.2395	0.0075	1.4210	0.0047	305
SC03	0.2290	0.0042	0.0812	0.0008	97	0.2290	0.0031	0.0812	0.0007	111
SC05	0.7860	0.0065	0.2768	0.0019	147	0.7860	0.0044	0.2768	0.0015	191
SC06	0.2300	0.0047	0.0879	0.0010	90	0.2300	0.0035	0.0879	0.0009	95
SD04	0.0510	0.0056	0.0066	0.0004	16	0.0510	0.0022	0.0066	0.0003	21
SD08	0.0490	0.0058	0.0063	0.0008	8	0.0490	0.0026	0.0062	0.0004	18
SD99	0.0630	0.0057	0.0094	0.0010	10	0.0620	0.0620	0.0094	0.0005	19
SK20	0.0640	0.0054	0.0063	0.0007	9	0.0640	0.0640	0.0063	0.0003	19
SK21	0.0415	0.0039	0.0034	0.0002	15	0.0415	0.0415	0.0034	0.0002	15
TN00	0.0915	0.0093	0.0406	0.0027	15	0.0915	0.0915	0.0406	0.0010	39
TN04	0.0810	0.0040	0.0314	0.0015	21	0.0810	0.0810	0.0314	0.0007	43
TN11	0.0595	0.0033	0.0231	0.0011	21	0.0595	0.0595	0.0231	0.0007	32
TN14	0.1025	0.0060	0.0473	0.0026	18	0.1020	0.1020	0.0470	0.0010	48
TX02	0.1170	0.0052	0.0224	0.0009	25	0.1170	0.1170	0.0224	0.0006	36
TX03	0.9495	0.0077	0.1785	0.0033	54	0.9495	0.9495	0.1785	0.0023	77
TX04	0.0950	0.0067	0.0080	0.0004	18	0.0950	0.0950	0.0080	0.0003	28
TX10	0.7000	0.0065	0.1931	0.0013	152	0.7000	0.7000	0.1931	0.0012	164
TX16	0.2180	0.0052	0.0338	0.0007	47	0.2180	0.2180	0.0338	0.0005	62
TX21	0.2675	0.0044	0.0857	0.0012	70	0.2675	0.2675	0.0857	0.0009	90
TX22	0.0970	0.0062	0.0172	0.0005	34	0.0970	0.0970	0.0172	0.0004	39
TX43	0.0870	0.0052	0.0182	0.0007	27	0.0870	0.0870	0.0181	0.0005	37
TX56	0.1570	0.0048	0.0626	0.0011	55	0.1570	0.1570	0.0626	0.0009	73
UT01	0.3960	0.0081	0.0903	0.0006	141	0.3960	0.3960	0.0903	0.0005	193
UT08	0.0910	0.0096	0.0110	0.0005	22	0.0910	0.0910	0.0110	0.0002	45
UT09	0.0790	0.0081	0.0062	0.0004	15	0.0790	0.0790	0.0062	0.0002	26
UT98	0.1030	0.0090	0.0062	0.0004	16	0.1030	0.1030	0.0062	0.0002	29
UT99	0.0740	0.0079	0.0088	0.0007	13	0.0740	0.0740	0.0088	0.0003	27
VA00	0.1070	0.0062	0.0491	0.0012	42	0.1070	0.1070	0.0491	0.0008	64
VA10	0.1405	0.0328	0.0581	0.0001	520	0.1405	0.1405	0.0581	0.0008	75
VA13	0.0700	0.0059	0.0164	0.0012	13	0.0700	0.0700	0.0164	0.0006	28
VA24	0.0960	0.0042	0.0445	0.0009	47	0.0960	0.0960	0.0445	0.0006	76
VA27	0.0880	0.0026	0.0036	0.0001	34	0.0880	0.0880	0.0036	0.0001	34
VA28	0.0560	0.0064	0.0278	0.0044	6	0.0550	0.0550	0.0276	0.0008	33
VA98	0.3620	0.0074	0.1956	0.0041	48	0.3620	0.3620	0.1956	0.0015	127
VA99	0.0650	0.0044	0.0239	0.0010	23	0.0650	0.0650	0.0239	0.0006	41
VI01	3.4625	0.0124	0.6860	0.0026	268	3.4625	3.4625	0.6860	0.0024	287
VT01	0.0730	0.0048	0.0238	0.0034	7	0.0730	0.0730	0.0238	0.0008	30
VT99	0.0390	0.0056	0.0131	0.0014	9	0.0390	0.0390	0.0131	0.0006	24
WA14	0.3960	0.0052	0.7825	0.0063	125	0.3960	0.3960	0.7825	0.0029	272
WA19	0.1145	0.0036	0.1005	0.0016	61	0.1145	0.1145	0.1005	0.0007	134
WA21	0.2040	0.0038	0.0709	0.0009	82	0.2040	0.2040	0.0709	0.0005	157
WA24	0.0580	0.0045	0.0082	0.0003	25	0.0580	0.0580	0.0082	0.0002	45
WA98	0.2265	0.0039	0.1193	0.0013	91	0.2265	0.2265	0.1193	0.0007	162
WA99	0.1870	0.0035	0.1247	0.0013	99	0.1870	0.1870	0.1247	0.0006	216
WI08	0.0485	0.0026	0.0084	0.0001	88	0.0485	0.0485	0.0084	0.0004	24
WI09	0.0460	0.0060	0.0064	0.0009	7	0.0460	0.0460	0.0064	0.0004	18
WI10	0.0360	0.0054	0.0062	0.0012	5	0.0350	0.0350	0.0061	0.0004	15
WI25	0.0470	0.0114	0.0083	0.0010	9	0.0470	0.0470	0.0083	0.0005	17
WI28	0.0440	0.0056	0.0094	0.0013	7	0.0440	0.0440	0.0094	0.0006	16
WI31	0.0570	0.0034	0.0135	0.0007	19	0.0570	0.0570	0.0135	0.0005	25
WI35	0.0395	0.0045	0.0080	0.0010	8	0.0390	0.0390	0.0079	0.0005	16
WI36	0.0400	0.0042	0.0072	0.0008	9	0.0400	0.0400	0.0072	0.0004	19
WI37	0.0480	0.0043	0.0095	0.0010	10	0.0480	0.0480	0.0095	0.0005	20
WI98	0.0460	0.0065	0.0103	0.0015	7	0.0460	0.0460	0.0103	0.0006	18
WI99	0.0680	0.0078	0.0165	0.0012	14	0.0680	0.0680	0.0165	0.0007	24

Appendix I – NADP wet deposition collection site summary statistics

Site code	Measured only					Imputed (*lrEM* method)				
	Median concentration (mg L^{-1})		Mean weekly wet deposition (kg ha^{-1})		Mean weekly wet deposition	Median concentration (mg L^{-1})		Mean weekly wet deposition (kg ha^{-1})		Mean weekly wet deposition
	Cl^-	Br^-	Cl^-	Br^-	Cl^-/ Br^- (mass)	Cl^-	Br^-	Cl^-	Br^-	Cl^-/ Br^- (mass)
WV04	0.0570	0.0052	0.0165	0.0014	12	0.0570	0.0570	0.0165	0.0007	24
WV05	0.0590	0.0034	0.0177	0.0007	24	0.0590	0.0590	0.0177	0.0006	28
WV18	0.0590	0.0068	0.0155	0.0023	7	0.0590	0.0590	0.0155	0.0008	19
WY00	0.0460	0.0087	0.0041	0.0008	5	0.0445	0.0445	0.0041	0.0003	16
WY02	0.0340	0.0081	0.0051	0.0006	9	0.0325	0.0325	0.0049	0.0002	20
WY06	0.0625	0.0087	0.0057	0.0007	9	0.0620	0.0620	0.0057	0.0003	19
WY08	0.0495	0.0055	0.0060	0.0003	19	0.0490	0.0490	0.0059	0.0002	36
WY94	0.0970	0.0041	0.0131	0.0003	38	0.0970	0.0970	0.0131	0.0002	55
WY95	0.0390	0.0063	0.0049	0.0007	7	0.0390	0.0014	0.0049	0.0003	19
WY97	0.0485	0.0059	0.0063	0.0006	10	0.0480	0.0018	0.0062	0.0003	23
WY98	0.0560	0.0090	0.0058	0.0006	9	0.0530	0.0018	0.0056	0.0003	21
WY99	0.0505	0.0059	0.0055	0.0005	10	0.0500	0.0022	0.0055	0.0003	19

Appendix II

Lake George Basin hydrogeochemical data

1. *Rainwater*

a. *Site ID key*

Site ID prefix	Description	Latitude (DD)	Longitude (DD)
RPRW	Rocky Point rainwater sampling point	–35.009	149.462
BRW	Bungendore Post Office rainwater sampling point	–35.235	149.445
WRW	Winderadeen Homestead rainwater sampling point	–34.940	149.427
LGRW	Lake George rainwater – a mixture of the three sampling points for element/ion and stable water isotope analyses		
LGRWT	Lake George rainwater tritium – a mixture of the three sampling points for tritium analyses		
LGRWCl	Lake George rainwater chlorine – a mixture of the three sampling points for stable chlorine isotope analyses		

b. *Field parameters and major elements/ions (μg kg^{-1})*

Site ID	Date	Rainfall (mm)	Temp.[1] (°C)	Temp.[2] (°C)	Humidity[3] (°C)	pH	HCO_3^-	H_2CO_3	Ca	Mg	Na	K	SO_4^{2-}	Cl^-	Si	NH_4^+	NO_3^{2-}	NO_2^-	PO_4^{3-}	Br^-	F^-
RPRW-1	2/09/2013	18.6	17.0	8.4	70.2	6.67	–	–	376	211	1 752	339	1 450	3 048	275	–	702	517	258	26	16
BRW-1	2/09/2013	26.4	18.0	8.4	70.2	6.06	–	–	882	236	959	426	1 356	1 412	502	–	685	6 001	469	13	16
WRW-1	2/09/2013	31.6	17.2	8.4	70.2	5.77	–	–	320	113	975	135	969	1 721	311	–	542	2 527	<1	14	15
RPRW-2	1/10/2013	56.1	19.0	12.7	72.7	5.83	–	–	165	53	420	120	557	723	241	–	381	3 192	57	3	16
BRW-2	1/10/2013	85.6	18.0	12.7	72.7	5.91	1 300	4 000	249	61	231	139	519	485	233	232	269	168	26	2	14
WRW-2	1/10/2013	53.0	18.0	12.7	72.7	5.56	–	–	185	50	325	116	588	635	250	–	419	92	<1	3	11
RPRW-3	28/10/2013	11.6	18.0	13.9	64.5	6.13	1 600	3 000	563	225	1 920	204	1 092	3 024	409	386	932	224	<1	10	6
BRW-3	28/10/2013	12.4	–	13.9	64.5	7.51	–	–	–	–	–	–	1 300	3 742	–	–	68	63	<1	14	20
WRW-3	28/10/2013	18.0	–	13.9	64.5	6.90	–	–	–	–	–	–	1 716	2 628	–	–	167	21	<1	11	15
RPRW-4	2/12/2013	68.0	15.7	15.4	67.4	6.34	600	700	290	130	791	116	752	1 164	127	90	459	349	283	6	3
WRW-4	2/12/2013	74.8	13.8	15.4	67.4	5.65	–	–	175	49	419	220	634	1 019	118	–	441	38	<1	3	22
RPRW-5	6/01/2014	10.9	22.1	19.7	62.2	6.82	–	–	548	267	1 680	331	1 568	2 506	868	–	1 602	3 607	130	8	37
BRW-5	6/01/2014	22.0	22.1	19.7	62.2	6.50	–	–	475	136	1 573	834	352	1 154	1 367	–	2 743	11	170	2	6
WRW-5	6/01/2014	18.9	23.0	19.7	62.2	6.07	–	–	566	142	582	409	980	1 182	809	–	1 051	15	129	1	23
RPRW-6	3/02/2014	6.7	26.5	22.9	55.9	7.03	–	–	–	–	–	–	6 619	9 148	–	–	2 706	345	4 120	18	40
BRW-6	3/02/2014	8.2	26.5	22.9	55.9	7.03	–	–	–	–	–	–	2 770	4 338	–	–	1 231	190	1 304	9	27
WRW-6	3/02/2014	8.0	26.5	22.9	55.9	7.03	–	–	–	–	–	–	2 323	2 762	–	–	2 070	260	246	8	32
LGRW-1[4]	3/02/2014	7.6	26.5	22.9	55.9	7.03	10 500	2 100	1 630	535	2 960	1 481	3 513	4 507	1 462	2 743	2 564	4 006	1 673	11	26
RPRW-7	3/03/2014	76.4	20.1	20.1	68.2	6.25	4 500	6 000	451	183	1 076	230	1 120	1 707	220	1 442	1 242	1 672	2	6	22

Site ID	Date	Rainfall (mm)	Temp.[1] (°C)	Temp.[2] (°C)	Humidity[3] (°C)	pH	HCO_3^-	H_2CO_3	Ca	Mg	Na	K	SO_4^{2-}	Cl^-	Si	NH_4^+	NO_3^{2-}	NO_2^-	PO_4^{3-}	Br^-	F^-
RPRW-7t	3/03/2014	76.4	18.0	20.1	68.2	6.42	4 100	3 900	382	131	678	176	1 053	1 376	223	1 288	714	118	166	4	23
BRW-7	3/03/2014	75.8	21.4	20.1	68.2	6.37	9 800	9 800	458	112	809	459	1 575	1 627	185	2 911	739	93	482	4	13
WRW-7	3/03/2014	147.0	18.3	20.1	68.2	5.73	1 300	6 000	283	42	385	139	874	1 888	<100	464	776	58	74	7	23
RPRW-8	31/03/2014	88.6	15.5	18.3	80.4	5.96	600	1 800	247	48	309	70	495	566	<100	206	501	23	<1	3	11
RPRW-8t	31/03/2014	88.6	15.8	18.3	80.4	5.83	1 700	6 500	343	51	310	66	542	410	<100	399	448	6	69	2	4
BRW-8	31/03/2014	77.0	14.4	18.3	80.4	6.46	2 300	2 100	317	48	208	112	823	431	123	631	418	54	98	3	9
WRW-8	31/03/2014	141.0	17.6	18.3	80.4	6.16	300	600	162	17	183	19	354	212	<100	193	389	4	<1	2	2
RPRW-9	12/05/2014	79.8	16.0	13.1	83.4	5.44	1 000	9 200	153	29	306	25	403	500	<100	335	360	<1	1	2	3
BRW-9	12/05/2014	90.8	17.6	13.1	83.4	5.91	1 100	3 300	221	15	212	43	280	279	124	258	246	<1	8	1	2
WRW-9	12/05/2014	91.0	14.0	13.1	83.4	5.54	900	6 500	153	26	218	24	327	297	<100	232	282	<1	11	2	2
RPRW-10	2/06/2014	25.4	16.4	11.8	86.5	5.34	1 000	11 800	191	41	348	112	555	614	121	296	537	17	10	6	5
BRW-10	2/06/2014	29.3	16.5	11.8	86.5	5.93	2 300	6 800	391	90	764	280	377	898	172	167	374	14	<1	4	7
WRW-10	2/06/2014	27.0	15.6	11.8	86.5	6.20	1 800	2 900	225	27	347	228	450	573	<100	515	467	27	<1	2	16
RPRW-11	1/07/2014	37.7	13.8	7.8	92.4	6.17	900	1 600	141	41	522	101	249	1 036	<100	258	227	<1	<1	2	2
BRW-11	1/07/2014	57.2	14.0	7.8	92.4	6.07	1 300	1 300	242	39	390	118	189	627	<100	155	117	2	<1	1	1
WRW-11	1/07/2014	66.8	13.7	7.8	92.4	5.99	600	1 500	142	26	419	49	229	703	<100	90	147	<1	<1	3	1
RPRW-12	4/08/2014	9.9	–	6.6	88.9	–	–	–	–	–	–	–	1 178	2 384	–	–	845	50	<1	10	42
BRW-12	4/08/2014	16.6	14.6	6.6	88.9	6.42	2 600	2 500	529	127	732	179	621	1 344	217	438	411	38	<1	5	4
WRW-12	4/08/2014	27.2	13.8	6.6	88.9	6.73	2 300	1 100	223	60	623	116	488	1 195	<100	657	399	5	<1	3	3
RPRW-13	1/09/2014	42.8	10.8	8.0	85.5	6.89	1 100	400	146	19	292	113	218	606	<100	296	192	<1	<1	2	2
BRW-13	1/09/2014	51.2	10.0	8.0	85.5	5.99	1 000	2 900	255	33	254	118	267	539	<100	167	215	2	<1	2	2
WRW-13	1/09/2014	61.3	10.8	8.0	85.5	5.93	800	2 600	99	25	210	71	160	432	<100	180	135	<1	<1	1	2
RPRW-14	8/10/2014	36.1	13.1	11.9	78.8	6.58	6 200	4 300	378	224	1 047	781	1 233	1 774	143	2 473	435	2 189	550	4	4
BRW-14	8/10/2014	41.5	13.8	11.9	78.8	5.86	1 600	5 900	519	136	543	464	444	1 385	260	116	249	19	<1	4	4
WRW-14	8/10/2014	56.5	15.7	11.9	78.8	6.32	8 100	9 800	367	109	541	516	888	919	168	2 395	327	18	747	3	2
RPRW-15	3/11/2014	29.6	17.5	15.4	70.3	6.02	2 200	5 200	262	76	401	191	340	697	151	528	258	8	<1	2	2
BRW-15	3/11/2014	38.0	17.1	15.4	70.3	6.27	1 900	6 500	344	118	377	557	272	826	270	219	176	15	106	2	2
WRW-15	3/11/2014	31.1	16.5	15.4	70.3	6.02	3 200	7 700	306	83	477	229	421	1 030	219	889	320	3	39	2	2
RPRW-16	1/12/2014	37.5	21.7	19.3	66.5	6.92	8 300	2 400	393	246	811	845	1 710	1 657	211	2 885	776	51	1 650	7	6
WRW-16	1/12/2014	36.6	22.5	19.3	66.5	6.35	4 400	4 500	391	142	663	460	721	1 772	236	1 442	753	10	294	4	5
RPRW-18	9/02/2015	23.7	18.2	19.4	75.1	5.18	500	7 500	214	101	481	153	462	1 256	199	142	244	<1	90	2	3
BRW-18	9/02/2015	67.5	18.2	19.4	75.1	5.85	5 100	17 600	208	66	233	238	523	631	158	1 507	265	4	185	2	2
WRW-18	9/02/2015	54.6	18.2	19.4	75.1	6.4	6 300	6 100	564	258	472	875	1 900	1 341	198	3 786	674	2 255	1 365	4	3
RPRW-19	23/03/2015	35.0	16.8	19.8	74.0	6.01	1 900	4 800	1 067	416	2 337	600	2 032	4 794	403	1 391	1 585	1 189	283	11	15
BRW-19	23/03/2015	20.8	13.8	19.8	74.0	6.18	1 430	2 430	1 509	560	1 214	1 467	2 971	4 681	953	6 371	200	5 000	2 224	8	18
WRW-20	22/07/2015	110.0	14.6	6.6	89.7	6.41	211	213	226	66	234	124	266	401	147	489	286	21	99	2	1

[1]Field temperature of sample
[2]Average atmospheric temperature recorded at Rocky Point over sampling period
[2]Average atmospheric relative humidity recorded at Rocky Point over sampling period
[4]Mixed samples from the three separate sites mixed in proportion to rainfall amounts

c. Trace elements (μg kg^{-1})

Site ID	Date	Latitude (DD)	Longitude (DD)	Fe	Li	B	Al	V	Cr	Mn	Co	Ni	Cu	Zn	As	Rb	Sr	Mo	Sn	Ba	Pb	U
RPRW-1	2/09/2013	–35.009	149.462	<10	<0.1	4.9	44.5	<0.5	<1.0	5.6	<1.0	<0.5	2.5	33.5	0.2	0.2	2.5	<1.0	1.7	1.9	0.3	<0.1
BRW-1	2/09/2013	–35.235	149.445	26.7	<0.1	6.2	60.9	<0.5	<1.0	16.5	<1.0	<0.5	2.1	61.8	0.1	0.4	3.5	<1.0	6.0	7.9	0.6	<0.1
WRW-1	2/09/2013	–34.940	149.427	16.0	<0.1	4.0	41.7	<0.5	<1.0	5.1	<1.0	<0.5	<1.0	24.0	<0.1	0.2	2.1	<1.0	1.6	1.9	0.2	<0.1
RPRW-2	1/10/2013	–35.009	149.462	12.0	<0.1	2.6	46.8	<0.5	<1.0	2.9	<1.0	<0.5	4.7	14.5	<0.1	0.1	1.2	<1.0	1.2	1.2	0.4	<0.1
BRW-2	1/10/2013	–35.235	149.445	10.2	<0.1	2.7	45.8	<0.5	<1	4.6	<1	<0.5	3.4	11.1	<0.1	0.2	1.4	<1	2.5	2.6	0.3	<0.1
WRW-2	1/10/2013	–34.940	149.427	12.6	<0.1	2.9	48.2	<0.5	<1	4.0	<1	<0.5	<1	6.0	<0.1	0.1	1.3	<1	1.3	1.1	0.2	<0.1
RPRW-3	28/10/2013	–35.009	149.462	<10	<0.1	3.5	12.7	<0.5	<1	14.4	<1	<0.5	<1	17.8	0.1	0.2	4.1	<1	3.4	5.5	<0.1	<0.1
RPRW-4	2/12/2013	–35.009	149.462	<10	<0.1	1.5	17.5	<0.5	<1	<0.5	<1	<0.5	<1	2.0	<0.1	<0.1	2.2	<1	<1	0.8	<0.1	<0.1
WRW-4	2/12/2013	–34.940	149.427	<10	<0.1	1.5	11.9	<0.5	<1	5.8	<1	<0.5	<1	6.7	<0.1	0.1	0.9	<1	<1	0.8	0.1	<0.1
RPRW-5	6/01/2014	–35.009	149.462	<10	<0.1	4.9	20.1	<0.5	<1	4.0	<1	<0.5	<1	3.8	1.1	0.2	3.2	<1	1.2	1.5	0.1	<0.1
BRW-5	6/01/2014	–35.235	149.445	<10	<0.1	3.9	13.3	<0.5	<1	5.9	<1	<0.5	1.3	15.5	<0.1	0.5	2.4	<1	2.0	3.9	0.2	<0.1
WRW-5	6/01/2014	–34.940	149.427	<10	<0.1	3.4	11.8	<0.5	<1	39.1	<1	<0.5	1.6	21.4	<0.1	0.3	2.6	<1	1.4	2.2	0.1	<0.1
LGRW-1[1]	3/02/2014	–	–	<10	<0.1	12.0	54.6	<0.5	<1	27.2	<1	<0.5	8.3	29.6	0.3	0.9	9.6	<1	2.6	5.9	0.2	<0.1
RPRW-7	3/03/2014	–35.009	149.462	<10	<0.1	5.1	47.2	<0.5	<1	3.9	<1	<0.5	<1	9.0	0.1	0.2	3.2	<1	<1	1.4	0.2	<0.1
RPRW-7t	3/03/2014	–35.009	149.462	<10	<0.1	4.2	49.6	<0.5	<1	5.9	<1	<0.5	<1	27.6	<0.1	0.1	2.3	<1	5.1	24.1	0.1	<0.1
BRW-7	3/03/2014	–35.235	149.445	<10	<0.1	4.4	47.2	<0.5	<1	<0.5	<1	<0.5	3.5	13.4	<0.1	0.3	2.3	<1	1.1	4.4	0.3	<0.1
WRW-7	3/03/2014	–34.940	149.427	<10	<0.1	4.1	45.6	<0.5	<1	8.4	<1	<0.5	<1	14.5	<0.1	0.2	1.7	<1	<1	1.8	0.1	<0.1
RPRW-8	31/03/2014	–35.009	149.462	15.1	<0.1	4.1	49.5	<0.5	<1	3.1	<1	<0.5	<1	6.9	<0.1	<0.1	1.5	<1	<1	1.0	0.1	<0.1
RPRW-8t	31/03/2014	–35.009	149.462	11.3	<0.1	4.6	57.0	<0.5	<1	2.7	<1	<0.5	<1	15.7	<0.1	<0.1	1.6	<1	<1	13.7	0.1	<0.1
BRW-8	31/03/2014	–35.235	149.445	<10	<0.1	4.0	40.1	<0.5	<1	1.6	<1	<0.5	<1	8.9	<0.1	<0.1	1.7	<1	<1	2.7	0.4	<0.1
WRW-8	31/03/2014	–34.940	149.427	<10	<0.1	3.3	43.6	<0.5	<1	1.7	<1	<0.5	<1	8.7	<0.1	<0.1	1.0	<1	1.0	0.7	0.1	<0.1
RPRW-9	12/05/2014	–35.009	149.462	<10	<0.1	3.3	49.3	<0.5	<1	2.7	<1	<0.5	1.2	6.1	1.1	<0.1	0.9	<1	<1	1.2	0.4	<0.1
BRW-9	12/05/2014	–35.235	149.445	<10	<0.1	2.7	31.4	<0.5	<1	2.1	<1	<0.5	<1	5.9	<0.1	0.1	1.0	<1	2.3	1.6	0.2	<0.1
WRW-9	12/05/2014	–34.940	149.427	<10	<0.1	2.3	20.3	<0.5	<1	1.3	<1	<0.5	<1	5.4	<0.1	<0.1	0.8	<1	<1	1.7	0.3	<0.1
RPRW-10	2/06/2014	–35.009	149.462	<10	<0.1	3.8	60.4	<0.5	<1	2.6	<1	<0.5	<1	12.0	1.1	0.2	1.2	<1	<1	0.9	0.1	<0.1
BRW-10	2/06/2014	–35.235	149.445	<10	<0.1	4.5	66.5	<0.5	<1	1.8	<1	<0.5	1.1	15.5	0.1	0.2	2.2	<1	<1	2.4	0.5	<0.1
WRW-10	2/06/2014	–34.940	149.427	<10	<0.1	3.2	61.0	<0.5	<1	1.5	<1	<0.5	1.4	11.5	<0.1	0.2	1.2	<1	<1	0.8	0.3	<0.1
RPRW-11	1/07/2014	–35.009	149.462	<10	<0.1	2.5	41.6	<0.5	<1	1.5	<1	<0.5	<1	8.2	1.0	0.1	0.9	<1	<1	0.8	<0.1	<0.1
BRW-11	1/07/2014	–35.235	149.445	<10	<0.1	3.0	45.6	<0.5	<1	2.3	<1	<0.5	<1	11.3	1.1	0.1	1.2	<1	<1	2.2	0.1	<0.1
WRW-11	1/07/2014	–34.940	149.427	<10	<0.1	1.8	40.3	<0.5	<1	1.0	<1	<0.5	<1	8.4	<0.1	0.1	0.9	<1	<1	0.7	0.1	<0.1
BRW-12	4/08/2014	–35.235	149.445	<10	<0.1	4.8	49.1	<0.5	<1	3.7	<1	<0.5	1.4	32.2	1.1	0.2	2.7	<1	<1	4.5	0.6	<0.1
WRW-12	4/08/2014	–34.940	149.427	<10	<0.1	3.3	50.7	<0.5	<1	2.1	<1	<0.5	<1	151.2	<0.1	0.1	1.5	<1	<1	1.1	0.1	<0.1
RPRW-13	1/09/2014	–35.009	149.462	<10	<0.1	2.5	41.4	<0.5	<1	1.2	<1	<0.5	<1	11.3	1.0	0.1	0.8	<1	<1	3.9	<0.1	<0.1
BRW-13	1/09/2014	–35.235	149.445	<10	<0.1	2.8	39.8	<0.5	<1	3.0	<1	<0.5	<1	15.7	1.1	0.1	1.3	<1	<1	3.3	0.1	<0.1
WRW-13	1/09/2014	–34.940	149.427	<10	<0.1	1.5	39.8	<0.5	<1	2.9	<1	<0.5	2.2	20.4	0.1	0.1	0.7	<1	<1	0.7	0.2	<0.1
RPRW-14	8/10/2014	–35.009	149.462	<10	<0.1	4.9	70.6	<0.5	<1	3.8	<1	<0.5	1.1	6.9	<0.1	0.2	2.2	<1	<1	0.6	0.2	<0.1
BRW-14	8/10/2014	–35.235	149.445	<10	<0.1	6.3	75.2	<0.5	<1	10.8	<1	<0.5	8.8	24.1	1.1	0.4	2.6	<1	<1	4.4	0.2	<0.1
WRW-14	8/10/2014	–34.940	149.427	<10	<0.1	5.3	76.6	<0.5	<1	6.4	<1	<0.5	1.1	11.3	<0.1	0.4	1.9	<1	<1	1.2	0.2	<0.1

Site ID	Date	Latitude (DD)	Longitude (DD)	Fe	Li	B	Al	V	Cr	Mn	Co	Ni	Cu	Zn	As	Rb	Sr	Mo	Sn	Ba	Pb	U
RPRW-15	3/11/2014	–35.009	149.462	<10	<0.1	2.3	43.3	<0.5	<1	2.3	<1	<0.5	<1	4.1	<0.1	0.1	1.4	<1	<1	0.7	<0.1	<0.1
BRW-15	3/11/2014	–35.235	149.445	<10	<0.1	4.1	48.7	<0.5	<1	3.6	<1	<0.5	<1	9.8	1.1	0.4	2.0	<1	<1	2.0	0.2	<0.1
WRW-15	3/11/2014	–34.940	149.427	<10	<0.1	2.5	42.5	<0.5	<1	6.8	<1	<0.5	<1	8.5	<0.1	0.2	1.3	<1	<1	1.2	<0.1	<0.1
RPRW-16	1/12/2014	–35.009	149.462	<10	<0.1	2.6	24.1	6.1	2.3	123.9	<1	<0.5	<1	5.0	<0.1	0.4	2.3	<1	<0.4	1.2	<0.1	<0.1
WRW-16	1/12/2014	–34.940	149.427	11.0	<0.1	3.0	19.7	0.7	<1	18.2	<1	<0.5	<1	14.7	0.8	0.4	2.3	<1	<0.4	1.8	<0.1	<0.1
RPRW-18	9/02/2015	–35.009	149.462	<10	<0.1	1.4	10.0	<0.5	0.0	7.2	<1	<0.5	34.6	18.4	<0.1	<0.1	1.2	<1	<0.4	0.9	0.2	<0.1
BRW-18	9/02/2015	–35.235	149.445	<10	<0.1	1.9	20.7	<0.5	<1	4.8	<1	<0.5	5.7	23.8	0.3	0.1	1.1	<1	0.4	2.3	0.4	<0.1
WRW-18	9/02/2015	–34.940	149.427	<10	<0.1	3.0	14.1	<0.5	<1	22.2	<1	<0.5	19.3	662.2	0.9	0.6	2.2	<1	1.0	2.8	0.3	<0.1
RPRW-19	23/03/2015	–35.009	149.462	<10	<0.1	4.1	15.3	0.7	0.2	19.0	<1	<0.5	<1	22.6	0.9	0.3	6.2	<1	<0.4	2.3	<0.1	<0.1
BRW-19	23/03/2015	–35.235	149.445	12.3	<0.1	8.2	20.4	<0.5	<1	10.6	<1	<0.5	4.0	22.3	0.2	0.8	6.6	<1	0.4	5.3	0.6	<0.1
WRW-20	22/07/2015	–34.940	149.427	<10	<0.1	1.6	10.8	<0.5	<1	15.4	<1	<0.5	6.1	33.3	0.8	0.1	1.3	<1	5.4	1.2	<0.1	<0.1
RPRW-21	20/01/2016	–35.009	149.462	<10	<0.1	3.2	23.3	<0.5	0.1	13.2	<1	<0.5	20.8	57.7	0.8	0.5	8.7	<1	2.4	5.2	0.4	<0.1
BRW-21	20/01/2016	–35.235	149.445	<10	<0.1	4.6	24.2	<0.5	<1	1.9	<1	<0.5	6.0	30.8	<0.1	0.5	3.4	<1	2.2	5.4	0.2	<0.1
WRW-21	20/01/2016	–34.940	149.427	<10	<0.1	3.7	15.7	<0.5	<1	1.7	<1	0.7	26.5	22.2	0.9	0.6	2.3	<1	10.0	1.8	0.2	<0.1

[1]Mixed samples from the three separate sites mixed in proportion to rainfall amounts

d. Isotopes

Site ID	Collection dates	Latitude (DD)	Longitude (DD)	Rainfall (mm)	Mean temperature (°C)	$\delta^{2}H$ (‰ VSMOW)[1]	$\delta^{18}O$ (‰ VSMOW)[2]	$\delta^{37}Cl$ (‰ SMOC)[3]	^{3}H activity (TU ± 1σ)
RPRW-1	1/8/2013 – 2/09/2013	–35.009	149.462	18.6	8.4	–18.0	–3.62	–	–
BRW-1	1/8/2013 – 2/09/2013	–35.235	149.445	26.4	8.4	–22.0	–4.51	–	–
WRW-1	1/8/2013 – 2/09/2013	–34.940	149.427	31.6	8.4	–18.3	–3.77	–	–
LGRWT-1[4]	1/8/2013 – 2/09/2013	–	–	25.5	8.4	–19.4	–3.96	–	5.41 ± 0.26
RPRW-2	2/09/2013 – 1/10/2013	–35.009	149.462	56.1	12.7	–47.1	–7.88	–	–
BRW-2	2/09/2013 – 1/10/2013	–35.235	149.445	85.6	12.7	–47.0	–8.36	–	–
WRW-2	2/09/2013 – 1/10/2013	–34.940	149.427	53.0	12.7	–38.4	–6.83	–	–
LGRWT-2[4]	2/09/2013 – 1/10/2013	–	–	64.9	12.7	–44.2	–7.69	–	4.01 ± 0.19
RPRW-3	1/10/2013 – 28/10/2013	–35.009	149.462	11.6	13.9	1.0	–1.10	–	–
BRW-3	1/10/2013 – 28/10/2013	–35.235	149.445	12.4	13.9	11.0	0.11	–	–
WRW-3	1/10/2013 – 28/10/2013	–34.940	149.427	18.0	13.9	5.2	–0.66	–	–
RPRW-4	28/10/2013 – 2/12/2013	–35.009	149.462	68.0	15.4	–39.3	–6.57	–	3.77 ± 0.19
WRW-4	28/10/2013 – 2/12/2013	–34.940	149.427	74.8	15.4	–38.9	–6.66	–	–
RPRW-5	2/12/2013 – 6/01/2014	–35.009	149.462	10.9	19.7	–0.5	–1.79	–	–
BRW-5	2/12/2013 – 6/01/2014	–35.235	149.445	22.0	19.7	–15.4	–4.05	–	–
WRW-5	2/12/2013 – 6/01/2014	–34.940	149.427	18.9	19.7	–10.3	–2.96	–	–
RPRW-6	6/01/2014 – 3/02/2014	–35.009	149.462	6.7	22.9	–37.2	–5.62	–	–
BRW-6	6/01/2014 – 3/02/2014	–35.235	149.445	8.2	22.9	–54.0	–7.97	–	–
WRW-6	6/01/2014 – 3/02/2014	–34.940	149.427	8.0	22.9	–33.4	–5.58	–	–

Site ID	Collection dates	Latitude (DD)	Longitude (DD)	Rainfall (mm)	Mean temperature (°C)	$\delta^{2}H$ (‰ VSMOW)[1]	$\delta^{18}O$ (‰ VSMOW)[2]	$\delta^{37}Cl$ (‰ SMOC)[3]	^{3}H activity (TU ± 1σ)
LGRWT-3[4]	6/01/2014 – 3/02/2014	–	–	7.6	22.1	–39.1	–6.61	–	4.49 ± 0.23
RPRW-7	3/02/2014 – 3/03/2014	–35.009	149.462	76.4	20.1	–11.2	–1.26	–	–
RPRW-7t	3/02/2014 – 3/03/2014	–35.009	149.462	76.4	20.1	–39.7	–6.63	–	3.50 ± 0.20
BRW-7	3/02/2014 – 3/03/2014	–35.235	149.445	75.8	20.1	–40.4	–7.00	–	–
WRW-7	3/02/2014 – 3/03/2014	–34.940	149.427	147.0	20.1	–30.9	–4.65	–	–
RPRW-8	3/03/2014 – 31/03/2014	–35.009	149.462	88.6	18.3	–31.9	–6.04	–	–
RPRW-8t	3/03/2014 – 31/03/2014	–35.009	149.462	88.6	18.3	–38.5	–6.76	–	2.70 ± 0.10
BRW-8	3/03/2014 – 31/03/2014	–35.235	149.445	77.0	18.3	–44.6	–7.26	–	–
WRW-8	3/03/2014 – 31/03/2014	–34.940	149.427	141.0	18.3	–38.5	–6.68	–	–
RPRW-9	31/03/2014 – 12/05/2014	–35.009	149.462	79.8	13.1	–50.0	–7.94	–	2.50 ± 0.10
BRW-9	31/03/2014 – 12/05/2014	–35.235	149.445	90.8	13.1	–45.9	–7.62	–	–
WRW-9	31/03/2014 – 12/05/2014	–34.940	149.427	91.0	13.1	–43.9	–7.39	–	–
RPRW-10	12/05/2014 – 2/06/2014	–35.009	149.462	25.4	11.8	–37.6	–6.77	–	3.10 ± 0.20
BRW-10	12/05/2014 – 2/06/2014	–35.235	149.445	29.3	11.8	–36.1	–6.67	–	–
WRW-10	12/05/2014 – 2/06/2014	–34.940	149.427	27.0	11.8	–34.4	–6.61	–	–
RPRW-11	2/06/2014 – 1/07/2014	–35.009	149.462	37.7	7.7	–47.0	–9.52	–	2.85 ± 0.14
BRW-11	2/06/2014 – 1/07/2014	–35.235	149.445	57.2	7.7	–50.4	–8.32	–	–
WRW-11	2/06/2014 – 1/07/2014	–34.940	149.427	66.8	7.7	–43.7	–7.64	–	–
LGRWCl-1[4]	3/02/2014 – 1/07/2014	–	–	370.3	14.2	–	–	0.17	–
RPRW-12	1/07/2014 – 4/08/2014	–35.009	149.462	9.9	6.6	–23.9	–5.30	–	–
BRW-12	1/07/2014 – 4/08/2014	–35.235	149.445	16.6	6.6	–23.7	–5.52	–	–
WRW-12	1/07/2014 – 4/08/2014	–34.940	149.427	27.2	6.6	–30.4	–6.17	–	–
LGRWT-4[4]	1/07/2014 – 4/08/2014	–	–	21.9	6.6	–	–	–	3.50 ± 0.18
RPRW-13	4/08/2014 – 1/09/2014	–35.009	149.462	42.8	7.6	–88.0	–12.55	–	3.13 ± 0.15
BRW-13	4/08/2014 – 1/09/2014	–35.235	149.445	51.2	7.6	–69.0	–10.23	–	–
WRW-13	4/08/2014 – 1/09/2014	–34.940	149.427	61.3	7.6	–106.9	–14.81	–	–
RPRW-14	1/09/2014 – 8/10/2014	–35.009	149.462	36.1	11.3	–18.4	–4.65	–	4.4 ± 0.19
BRW-14	1/09/2014 – 8/10/2014	–35.235	149.445	41.5	11.3	–15.1	–3.25	–	–
WRW-14	1/09/2014 – 8/10/2014	–34.940	149.427	56.5	11.3	–20.5	–4.62	–	–
RPRW-15	8/10/2014 – 3/11/2014	–35.009	149.462	29.6	15.4	–35.6	–6.20	–	3.24 ± 0.15
BRW-15	8/10/2014 – 3/11/2014	–35.235	149.445	38.0	15.4	–48.0	–7.69	–	–
WRW-15	8/10/2014 – 3/11/2014	–34.940	149.427	31.1	15.4	–35.3	–5.97	–	–
LGRWCl-2[4]	4/08/2014 – 3/11/2014	–	–	129.4	11.4	–	–	–0.29	–
RPRW-16	3/11/2014 – 1/12/2014	–35.009	149.462	37.5	19.3	–13.6	–3.36	–	–
WRW-16	3/11/2014 – 1/12/2014	–34.940	149.427	36.6	19.3	–10.5	–2.72	–	–
LGRWT-16[4]	3/11/2014 – 1/12/2014	–	–	37.0	19.3	–	–	–	4.14 ± 0.18
RPRW-18	12/01/2015 – 9/02/2015	–35.009	149.462	23.7	19.4	–39.1	–6.38	–	–
BRW-18	12/01/2015 – 9/02/2015	–35.235	149.445	67.5	19.4	–39.8	–6.58	–	–
WRW-18	12/01/2015 – 9/02/2015	–34.940	149.427	54.6	19.4	–23.4	–4.23	–	–
LGRWT-18[4]	12/01/2015 – 9/02/2015	–	–	61.1	19.4	–	–	–	2.70 ± 0.12

Site ID	Collection dates	Latitude (DD)	Longitude (DD)	Rainfall (mm)	Mean temperature (°C)	$\delta^{2}H$ (‰ VSMOW)[1]	$\delta^{18}O$ (‰ VSMOW)[2]	$\delta^{37}Cl$ (‰ SMOC)[3]	^{3}H activity (TU ± 1σ)
RPRW-19	9/02/2015 – 23/03/2015	–35.009	149.462	35.0	19.8	–11.8	–3.08	–	–
BRW-19	9/02/2015 – 23/03/2015	–35.235	149.445	20.8	19.8	–11.8	–3.04	–	–
WRW-20	21/5/2015 – 22/07/2015	–34.940	149.427	110.0	6.6	–53.2	–8.89	–	2.06 ± 0.09
EV01	3/04/2014 – 5/04/2014	–35.101	149.375	38.0	15.6	–50.52	–7.00	–	–

[1]Mean analytical precision was ±1.1 ‰ (1σ)
[2]Mean analytical precision was ±0.17 ‰ (1σ)
[3]Mean analytical precision was ±0.11 ‰ (1σ)
[4]Mixed samples from the three separate sites mixed in proportion to rainfall amounts

2. Creek water

a. Site ID key

Site ID prefix	Description
ACSW	Allianoyonyiga Creek
BCSW	Butmaroo Creek
CCSW	Collector Creek
CuCSW	Currawang Creek
TCSW	Taylors Creek
TuCSW	Turallo Creek

a. Field parameters and major elements/ions

Site ID	Date	Latitude (DD)	Longitude (DD)	Temp. (°C)[1]	pH	Eh (mV)	TDS[2] (mg kg^{-1})	O_2 (mg L^{-1})	HCO_3^- (mg L^{-1})	Ca	Mg	Na	K	SO_4^{2-}	Cl^-	Si	NO_3^-	PO_4^{3-}	Br^-	F^-
										(mg kg^{-1})							(µg kg^{-1})			
BCSW-1	14/8/2013	–35.183	149.439	12.0	8.45	131	483	11.03	161	22.0	29.5	88.2	3.33	33.2	142	2.27	450	<10	422	288
BCSW-2	14/8/2013	–35.204	149.484	13.0	8.13	113	427	9.86	176	25.5	28.3	61.0	2.57	16.4	113	3.44	594	<10	289	262
CCSW-1	2/9/2013	–34.939	149.430	15.3	7.24	343	265	7.59	59.9	16.3	19.6	36.8	6.28	19.9	101	3.34	1251	37	262	114
TCSW-1	2/9/2013	–35.114	149.484	15.2	7.48	192	657	8.85	177	29.2	41.6	125	2.35	9.17	263	7.48	226	<20	789	371
ACSW-1	1/10/2013	–35.248	149.536	17.4	7.29	–	948	7.29	263	78.0	78.3	90.4	1.14	117	307	10.8	281	<20	849	142
TuCSW-1	2/10/2013	–35.248	149.437	13.1	7.36	–	283	4.75	143	20.4	15.4	35.3	3.07	5.79	50.0	9.08	817	83	193	150
TuCSW-2[3]	2/10/2013	–35.248	149.437	13.1	7.36	–	270	4.75	135	16.9	15.4	34.4	3.38	5.60	50.1	7.81	832	102	195	153
BCSW-3	9/1/2014	–35.204	149.484	19.8	7.25	–65	421	3.74	206	26.5	26.1	58.5	3.18	0.287	91.9	7.42	154	<10	314	338
CCSW-2	9/1/2014	–34.939	149.430	20.3	7.43	112	384	6.99	87.8	27.0	27.9	58.0	5.69	8.83	167	<1.5	426	<10	547	164
TCSW-2	9/1/2014	–35.112	149.522	19.8	7.66	–13	424	6.98	138	22.1	26.4	75.7	1.44	2.65	150	6.76	197	<10	460	446
TuCSW-3	9/1/2014	–35.246	149.433	19.2	7.17	–89	432	6.05	222	32.6	23.6	55.1	3.28	0.104	84.1	9.79	143	<10	385	234
CCSW-3	21/2/2014	–34.939	149.430	20.6	7.59	205	355	5.98	89.7	23.5	24.3	51.9	6.18	9.42	147	1.75	109	70	461	157
CuCSW-1	21/2/2014	–34.955	149.456	15.7	6.53	95	579	0.66	84.9	51.2	46.2	59.8	6.02	129	189	9.39	1 231	117	448	108
TCSW-3	21/2/2014	–35.112	149.522	25.6	7.38	111	333	6.16	110	16.9	20.0	58.5	2.30	7.60	111	5.12	954	65	309	391

Site ID	Date	Latitude (DD)	Longitude (DD)	Temp. (°C)[1]	pH	Eh (mV)	TDS[2] (mg kg^{-1})	O_2 (mg L^{-1})	HCO_3^- (mg L^{-1})	Ca	Mg	Na	K	SO_4^{2-}	Cl^-	Si	NO_3^-	PO_4^{3-}	Br^-	F^-
										(mg kg^{-1})							(µg kg^{-1})			
BCSW-4[4]	5/6/2014	–35.205	149.495	12.5	7.84	290	447	10.18	136	15.3	28.6	91.4	4.60	7.28	160	2.08	316	29	415	382
BCSW-5	5/6/2014	–35.204	149.484	10.6	7.64	290	328	7.67	125	16.2	21.6	51.6	3.41	18.8	89.3	2.80	<10	<10	251	248
ACSW-2	4/8/2014	–35.042	149.528	8.9	7.62	340	2 152	6.1	681	99.7	163	349	3.08	169	676	6.33	<60	<50	2 650	472
BCSW-6	4/8/2014	–35.204	149.484	6.5	7.9	300	459	9	179	23.2	31.4	71.7	3.18	20.8	127	2.31	107	<10	357	263
CCSW-4	4/8/2014	–34.939	149.430	9.4	7.32	366	204	6.1	59.0	13.0	14.3	30.9	3.66	8.86	67.5	4.25	1980	32	211	108
CuCSW-2	4/8/2014	–34.955	149.456	6.0	7.21	360	621	4.8	128	46.3	57.0	68.0	1.33	71.7	243	4.24	388	<20	656	81
TCSW-4	4/8/2014	–35.112	149.522	7.7	7.64	300	461	7.4	90.2	20.2	31.7	90.1	1.51	11.8	209	4.91	363	<20	522	302
TuCSW-4	4/8/2014	–35.246	149.433	6.6	7.44	320	298	6.6	149	18.6	16.3	39.1	2.88	4.43	60.9	6.39	<10	<10	255	164
ACSW-3	1/9/2014	–35.042	149.528	11.4	7.95	290	1 888	–	732	86.6	133	264	3.08	165	492	8.47	434	81	1 844	516
BCSW-7	1/9/2014	–35.204	149.484	12.0	7.73	270	198	–	95.2	9.8	12.3	26.6	2.03	8.10	37.5	5.59	123	16	72	200
CCSW-5	1/9/2014	–34.939	149.430	12.8	7.49	300	194	–	55.0	13.0	14.7	28.2	4.17	10.1	65.0	3.01	626	85	182	136
TCSW-5	1/9/2014	–35.112	149.522	10.9	7.64	290	295	–	70.4	11.1	21.2	54.2	1.35	10.1	121	4.59	192	<10	239	229
TuCSW-5	1/9/2014	–35.246	149.433	10.9	7.4	300	144	–	80.1	8.0	6.97	15.2	2.24	3.18	19.9	7.18	726	84	62	116
ACSW-4	3/11/2014	–35.042	149.528	17.2	7.96	215	2 242	–	826	112	160	364	2.85	100	664	8.93	802	<70	2 966	571
CCSW-6	3/11/2014	–34.939	149.430	18.7	7.71	230	303	4.45	91.2	21.9	21.9	45.1	3.32	9.85	108	0.54	153	52	363	159
TCSW-6	3/11/2014	–35.112	149.522	21.2	7.39	215	436	6.92	115	22.2	28.4	82.2	0.98	5.10	175	5.74	<10	40	472	319
ACSW-5	13/11/2014	–35.042	149.528	18.4	8.22	190	2 347	4.55	833	97.0	170	388	3.56	110	732	8.66	<70	<70	3 308	584
BCSW-8	13/11/2014	–35.204	149.484	21.4	7.28	210	345	1.77	178	21.7	21.1	47.7	3.40	0.225	67.2	4.63	108	<10	247	302
TuCSW-6	13/11/2014	–35.246	149.433	21.8	7.32	230	282	4.57	144	22.5	15.0	36.0	2.25	1.89	52.4	7.06	<10	<10	222	174
CCSW-7	1/12/2014	–34.939	149.430	22.5	8.36	–20	323	4.8	104	22.9	23.1	48.2	3.33	6.97	113	0.61	<10	48	383	166
TCSW-7	1/12/2014	–35.112	149.522	20.9	7.73	–10	394	3.9	104	20.4	24.3	73.0	1.38	3.31	160	5.72	192	<10	432	315

[1]Field temperature
[2]Total dissolved solids
[3]Field duplicate of TuCSW-1
[4]Collected from Dry Creek, a tributary of Butmaroo Creek

b. Trace elements (µg kg^{-1})

Site ID	Date	Latitude (DD)	Longitude (DD)	Fe	Li	B	Al	V	Cr	Mn	Co	Ni	Cu	Zn	As	Rb	Sr	Mo	Ba	Pb	U
BCSW-1	14/08/2013	–35.183	149.439	135	<0.1	14.5	38	<0.5	6.0	23	<1	1.1	6.3	12.0	0.6	0.8	159	<1	38.1	0.3	0.8
BCSW-2	14/08/2013	–35.204	149.484	1 096	<0.1	6.1	85	<0.5	5.4	21	<1	1.1	2.8	7.7	0.6	0.8	134	<1	36.2	0.4	1.2
CCSW-1	2/09/2013	–34.939	149.430	725	0.2	9.5	28	1.0	2.1	45	<1	1.7	5.3	13.5	0.7	2.3	99	<1	49.3	0.8	0.1
TCSW-1	2/09/2013	–35.114	149.484	23	0.4	10.2	19	<0.5	9.5	20	<1	0.8	2.8	11.3	0.8	1.1	248	<1	72.4	0.2	0.9
ACSW-1	1/10/2013	–35.248	149.536	<50	<0.1	7.6	26	<0.5	10.0	4	<1	2.0	8.1	18.9	0.8	1.3	247	<1	55.4	0.5	0.3
TuCSW-1	2/10/2013	–35.248	149.437	1255	0.5	10.5	124	0.8	3.3	217	<1	1.7	12.8	43.6	0.9	1.4	103	<1	35.5	0.9	0.5
TuCSW-2[1]	2/10/2013	–35.248	149.437	794	0.5	10.3	99	0.7	3.2	219	<1	1.7	8.6	29.4	0.9	1.4	105	<1	35.1	0.6	0.5
BCSW-3	9/01/2014	–35.204	149.484	173	0.2	10.6	<10	<0.5	4.1	414	<1	0.8	9.7	23.5	0.8	1.0	145	<1	58.7	0.2	0.3
CCSW-2	9/01/2014	–34.939	149.430	121	0.5	11.9	<10	<0.5	6.0	24	<1	1.3	4.8	13.9	1.0	2.7	176	<1	61.5	0.3	0.2
TCSW-2	9/01/2014	–35.112	149.522	<30	<0.1	10.6	<10	<0.5	6.6	121	<1	0.8	3.6	9.4	0.7	1.3	163	<1	60.2	<0.1	0.4

Site ID	Date	Latitude (DD)	Longitude (DD)	Fe	Li	B	Al	V	Cr	Mn	Co	Ni	Cu	Zn	As	Rb	Sr	Mo	Ba	Pb	U
TuCSW-3	9/01/2014	–35.246	149.433	241	0.3	7.4	<10	<0.5	4.0	1 370	1.1	0.8	6.3	22.4	1.1	1.6	162	<1	42.0	0.3	0.2
CCSW-3	21/02/2014	–34.939	149.430	163	0.4	13.4	<10	<0.5	5.1	32	<1	1.2	1.5	4.9	0.9	2.9	142	<1	49.9	0.1	0.1
CuCSW-1	21/02/2014	–34.955	149.456	3 209	1.0	10.4	<10	<0.5	7.7	1 560	21.6	5.3	2.5	49.0	1.2	3.8	289	<1	111.7	0.2	0.1
TCSW-3	21/02/2014	–35.112	149.522	504	0.5	13.6	164	<0.5	5.6	137	<1	1.2	1.9	4.7	0.6	1.8	133	<1	52.7	0.3	0.4
BCSW-4[2]	5/06/2014	–35.205	149.495	42	<0.1	13.5	80	<0.5	3.4	62	1.1	1.1	6.7	4.7	1.8	0.9	143	<1	82.0	0.2	1.3
BCSW-5	5/06/2014	–35.204	149.484	726	<0.1	11.0	69	0.5	1.9	14	<1	1.0	2.3	4.0	1.6	0.8	102	<1	42.1	0.3	0.4
ACSW-2	4/08/2014	–35.042	149.528	<50	<0.1	13.6	158	1.3	7.7	196	1.7	3.2	5.4	9.1	3.9	0.7	550	<1	68.7	0.3	20.3
BCSW-6	4/08/2014	–35.204	149.484	136	<0.1	7.8	61	0.3	1.9	10	<1	0.9	1.3	3.0	1.5	0.7	140	<1	43.2	0.1	1.5
CCSW-4	4/08/2014	–34.939	149.430	686	0.3	10.2	568	1.1	1.8	26	<1	1.4	5.7	6.1	0.6	1.8	88	<1	41.1	0.4	0.1
CuCSW-2	4/08/2014	–34.955	149.456	63	0.2	8.9	62	<0.5	3.2	104	1.3	1.1	2.1	5.7	1.6	0.9	248	<1	77.3	<0.1	0.1
TCSW-4	4/08/2014	–35.112	149.522	90	0.2	8.2	63	<0.5	2.9	201	1.1	0.8	0.9	3.6	1.2	1.0	178	<1	88.6	<0.1	0.2
TuCSW-4	4/08/2014	–35.246	149.433	70	0.1	9.3	54	<0.5	1.1	293	<1	0.7	0.7	3.0	0.5	1.1	111	<1	39.5	<0.1	0.2
ACSW-3	1/09/2014	–35.042	149.528	<50	<0.1	13.5	122	1.6	6.2	23	1.3	2.2	3.9	7.6	3.3	1.3	475	<1	74.9	0.2	7.7
BCSW-7	1/09/2014	–35.204	149.484	778	<0.1	10.2	1 051	2.1	2.3	25	<1	1.8	2.8	4.0	1.6	1.3	59	<1	26.0	0.7	0.8
CCSW-5	1/09/2014	–34.939	149.430	536	0.2	10.5	294	1.0	1.7	50	<1	1.5	3.0	4.1	0.7	1.8	85	<1	41.7	0.3	0.2
TCSW-5	1/09/2014	–35.112	149.522	449	0.1	8.8	255	0.5	2.2	39	<1	1.2	2.3	3.4	0.5	1.1	110	<1	58.2	0.3	0.5
TuCSW-5	1/09/2014	–35.246	149.433	956	0.2	9.3	411	1.3	1.7	63	<1	1.8	5.7	4.6	0.6	0.9	43	<1	22.1	0.6	0.6
ACSW-4	3/11/2014	–35.042	149.528	<40	<0.1	15.4	117	1.7	7.8	245	2.2	4.2	5.2	7.2	4.4	1.0	591	1.2	78.4	0.2	15.9
CCSW-6	3/11/2014	–34.939	149.430	456	0.1	10.5	48	<0.5	1.5	38	<1	1.2	3.2	2.8	0.8	1.6	119	<1	47.3	0.2	0.1
TCSW-6	3/11/2014	–35.112	149.522	<10	0.2	8.7	43	<0.5	2.5	437	<1	0.9	1.4	3.5	0.6	0.9	166	<1	91.1	<0.1	0.2
ACSW-5	13/11/2014	–35.042	149.528	<40	<0.1	12.5	54	2.8	<1	71	<1	3.1	10.8	7.2	3.2	1.2	760	1.7	101.2	0.1	17.1
BCSW-8	13/11/2014	–35.204	149.484	294	<0.1	15.1	73	0.5	1.3	110	<1	1.0	2.5	3.0	2.0	1.1	110	<1	50.8	0.1	0.3
TuCSW-6	13/11/2014	–35.246	149.433	422	0.2	11.2	58	<0.5	1.2	668	1.1	0.8	3.3	2.8	1.7	1.5	105	<1	23.9	0.1	0.2
CCSW-7	1/12/2014	–34.939	149.430	360	<0.1	10.5	14	0.8	<1	16	<1	0.9	<1	2.7	1.0	1.8	157	<1	54.2	0.1	0.1
TCSW-7	1/12/2014	–35.112	149.522	<10	0.2	9.1	–	<0.5	3.1	416	<1	0.9	<1	4.0	0.9	1.5	180	<1	95.9	<0.1	<0.1

[1]Field duplicate of TuCSW-1
[2]Collected from Dry Creek, a tributary of Butmaroo Creek

c. Isotopes

Site ID	Date	Latitude (DD)	Longitude (DD)	$\delta^{2}H$ (‰ VSMOW)[1]	$\delta^{18}O$ (‰ VSMOW)[2]	$\delta^{37}Cl$ (‰ SMOC ± 1σ)	$\delta^{81}Br$ (‰ SMOB ± 1σ)	^{3}H activity (TU ± 1σ)
BCSW-1	14/08/2013	–35.183	149.439	–38.1	–5.88	–	–	3.27 ± 0.16
BCSW-2	14/08/2013	–35.204	149.484	–37.8	–6.04	–	–	–
CCSW-1	2/09/2013	–34.939	149.430	–32.8	–6.01	–	–	–
TCSW-1	2/09/2013	–35.114	149.484	–41.4	–6.30	–	–	–
ACSW-1	1/10/2013	–35.248	149.536	–40.5	–6.06	–	–	–
TuCSW-1	2/10/2013	–35.248	149.437	–43.9	–6.94	–	–	–
TuCSW-2	2/10/2013	–35.248	149.437	–46.7	–6.84	–	–	–

Site ID	Date	Latitude (DD)	Longitude (DD)	$\delta^{2}H$ (‰ VSMOW)[1]	$\delta^{18}O$ (‰ VSMOW)[2]	$\delta^{37}Cl$ (‰ SMOC ± 1σ)	$\delta^{81}Br$ (‰ SMOB ± 1σ)	^{3}H activity (TU ± 1σ)
BCSW-3	9/01/2014	–35.204	149.484	–16.2	–1.41	–	–	–
CCSW-2	9/01/2014	–34.939	149.430	–15.0	–1.33	–	–	–
TCSW-2	9/01/2014	–35.112	149.522	–26.7	–2.87	–	–	–
TuCSW-3	9/01/2014	–35.246	149.433	–30.8	–3.86	–	–	–
CCSW-3	21/02/2014	–34.939	149.430	–19.6	–1.84	–	–	–
CuCSW-1	21/02/2014	–34.955	149.456	–39.4	–6.18	–	–	–
TCSW-3	21/02/2014	–35.112	149.522	–26.2	–2.60	–	–	–
BCSW-4[3]	5/06/2014	–35.205	149.495	–23.6	–3.44	–	–	–
BCSW-5	5/06/2014	–35.204	149.484	–27.1	–4.07	–	–	–
ACSW-2	4/08/2014	–35.042	149.528	–34.5	–5.36	–	–	–
BCSW-6	4/08/2014	–35.204	149.484	–27.9	–4.24	–	–	–
CCSW-4	4/08/2014	–34.939	149.430	–28.3	–5.33	–	–	–
CuCSW-2	4/08/2014	–34.955	149.456	–34.5	–5.70	–	–	–
TCSW-4	4/08/2014	–35.112	149.522	–30.2	–4.96	–	–	–
TuCSW-4	4/08/2014	–35.246	149.433	–36.0	–5.71	–	–	–
ACSW-3	1/09/2014	–35.042	149.528	–41.4	–6.29	–	–	–
BCSW-7	1/09/2014	–35.204	149.484	–52.5	–8.03	–	–	–
CCSW-5	1/09/2014	–34.939	149.430	–77.0	–10.99	–	–	–
TCSW-5	1/09/2014	–35.112	149.522	–45.4	–7.06	–	–	–
TuCSW-5	1/09/2014	–35.246	149.433	–52.2	–7.88	–	–	–
ACSW-4	3/11/2014	–35.042	149.528	–25.6	–3.59	–	–	–
CCSW-6	3/11/2014	–34.939	149.430	–34.3	–4.97	–	–	–
TCSW-6	3/11/2014	–35.112	149.522	–31.4	–4.62	–	–	–
ACSW-5	13/11/2014	–35.042	149.528	–18.3	–1.92	0.73 ± 0.09	1.02 ± 0.18	–
BCSW-8	13/11/2014	–35.204	149.484	–24.7	–3.25	0.25 ± 0.05	–0.69 ± 0.20	–
TuCSW-6	13/11/2014	–35.246	149.433	–30.7	–4.51	0.31 ± 0.06	–0.74 ± 0.20	–
CCSW-7	1/12/2014	–34.939	149.430	–25.9	–3.16	0.64 ± 0.09	0.83 ± 0.26	–
TCSW-7	1/12/2014	–35.112	149.522	–23.3	–3.11	0.93 ± 0.12	0.06 ± 0.01	–

[1]Mean analytical precision was ±1.1 ‰ (1σ)
[2]Mean analytical precision was ±0.17 ‰ (1σ)
[3]Collected from Dry Creek, a tributary of Butmaroo Creek

3. *Lake water*

a. *Field parameters and major elements/ions (mg kg^{-1} unless otherwise stated)*

Site ID	Date	Latitude (DD)	Longitude (DD)	Temp. (°C)[1]	pH	Eh (mV)	TDS[2]	O_2 (mg L^{-1})	HCO_3^-	CO_3^{2-}	Ca	Mg	Na	K	SO_4^{2-}	Cl^-	Si	NO_3^-	PO_4^{3-}	Br^-	F^-
LGSW-1	20/05/2013	–35.089	149.465	12.4	9.57	262	8 217	6.3	377	228	53.9	136	2 871	22.1	469	4 026	0.88	7.36	1.23	21.3	1.14
LGSW-2	20/05/2013	–35.091	149.464	12.5	9.41	252	8 541	6.8	521	223	56.4	140	2 971	17.9	479	4 102	0.88	4.35	1.02	21.4	1.17
LGSW-3	20/05/2013	–35.092	149.464	12.2	9.42	227	8 239	6.5	500	213	53.5	132	2 870	16.8	462	3 963	0.88	3.80	1.08	21.0	1.12
LGSW-4	25/06/2013	–35.089	149.465	10.7	9.25	302	1 164	9.9	90	11	6.32	10.4	411	4.55	66.7	560	<0.5	0.38	0.59	3.01	0.52
LGSW-5	1/08/2013	–35.089	149.465	14.4	8.99	–	2 551	10.7	265	26	17.9	37.4	866	6.66	138	1 186	<0.5	1.21	0.29	6.18	0.50
LGSW-6	2/09/2013	–35.089	149.465	20.1	9.11	179	3 335	10.3	265	42	25.6	51.2	1 140	8.55	193	1 598	<0.5	1.47	0.42	8.50	0.64
LGSW-7	1/10/2013	–35.089	149.465	13.5	8.98	–	4 666	9.1	357	44	37.5	76.7	1 585	10.9	279	2 258	0.59	2.41	0.59	11.6	0.87
LGSW-8	28/10/2013	–35.089	149.465	18.6	9.31	–	5 092	–	147	44	40.2	82.9	1 769	12.5	328	2 652	0.68	<0.2	0.74	13.8	0.98
LGSW-9	2/12/2013	–35.089	149.465	31.1	9.86	355	8 595	9.9	246	380	42.7	142	3 065	20.0	511	4 158	0.87	3.84	0.79	22.0	1.17
LGSW-10	2/06/2014	–35.089	149.465	14.8	9.31	300	1 363	14.9	134	19	4.61	4.91	491	5.57	81.0	618	<2.5	0.41	<0.04	3.14	0.73
LGSW-11	1/07/2014	–35.089	149.465	11.0	8.78	280	1 135	–	236	9	5.31	4.19	387	4.53	55.5	430	<4.0	0.41	<0.04	1.76	0.53
LGSW-12	4/08/2014	–35.089	149.465	14.6	9.09	290	3 296	9.9	408	53	17.2	28.3	1 145	10.7	205	1 420	<4.5	1.23	0.35	6.96	0.85
LGSW-13	1/09/2014	–35.089	149.465	15.1	9.22	290	874	–	156	16	6.38	7.20	294	5.22	40.9	346	<1.5	0.27	0.10	1.47	0.41
LGSW-14	8/10/2014	–35.089	149.465	26.3	9.52	–	2 903	5.7	114	43	11.2	19.6	1 058	11.5	190	1 446	<1.5	1.37	<0.1	6.98	0.93
LGSW-15	12/01/2015	–35.089	149.465	21.9	9.73	170	599	2.3	91	31	2.67	1.73	260	3.20	39.7	286	2.18	<0.02	0.36	1.38	0.90
LGSW-16	22/07/2015	–35.089	149.465	19.9	9.21	–	710	8.9	241	27	3.16	2.83	333	3.28	34.1	327	3.26	0.58	0.14	1.29	0.73

[1]Field temperature
[2]Total dissolved solids

b. *Trace elements (μg kg^{-1})*

Site ID	Date	Latitude (DD)	Longitude (DD)	Fe	Li	B	Al	V	Cr	Mn	Co	Ni	Cu	Zn	As	Rb	Sr	Mo	Sn	Ba	Pb	U
LGSW-1	20/05/2013	–35.089	149.465	297	<1	816	455	43.4	39.1	8.3	<10	5.6	23.6	13.5	25.6	2.0	863	22.9	<10	161	<1	15.9
LGSW-2	20/05/2013	–35.091	149.464	<10	<1	809	163	41.8	78.7	<5	<10	<5	19.7	17.8	26.0	1.2	838	22.3	<10	150	<1	8.0
LGSW-3	20/05/2013	–35.092	149.464	<10	<1	754	141	39.0	57.0	12.6	<10	<5	14.0	13.5	25.4	1.2	801	21.0	<10	148	<1	6.9
LGSW-4	25/06/2013	–35.089	149.465	<10	0.6	362	128	30.6	7.9	1.7	<2	1.9	8.9	5.1	8.5	0.6	101	4.3	<2	21	0.3	3.1
LGSW-5	1/08/2013	–35.089	149.465	<10	<0.5	303	66	16.2	<5	<2.5	<5	<2.5	10.3	8.1	8.1	0.6	260	6.7	<5	44	<0.5	3.7
LGSW-6	2/09/2013	–35.089	149.465	<10	2.6	479	218	28.0	<10	<5	<10	<5	18.0	13.0	9.9	1.4	432	11.7	<10	79	1.3	6.2
LGSW-7	1/10/2013	–35.089	149.465	<10	3.0	590	182	33.1	<10	<5	<10	<5	16.5	14.8	14.3	1.5	743	15.2	<10	122	1.2	8.0
LGSW-8	28/10/2013	–35.089	149.465	<10	3.1	699	186	42.9	<10	<5	<10	<5	15.5	10.3	16.1	1.7	731	17.4	<10	130	1.0	9.1
LGSW-9	2/12/2013	–35.089	149.465	<10	4.0	1022	138	45.9	11.0	<5	<10	<5	16.7	12.0	24.7	1.9	914	24.5	<10	156	1.1	11.3
LGSW-10	2/06/2014	–35.089	149.465	<10	0.6	362	152	32.9	7.6	2.1	<2	1.2	8.8	4.5	6.5	0.5	68	5.8	<2	15	0.2	6.0
LGSW-11	1/07/2014	–35.089	149.465	<10	0.7	247	144	18.2	5.7	2.6	<2	2.1	16.0	10.8	6.1	0.6	63	4.2	<2	14	0.6	4.0
LGSW-12	4/08/2014	–35.089	149.465	<10	1.5	382	74	31.8	1.5	0.9	<1	4.0	14.6	4.5	10.5	0.7	324	15.0	<5	58	0.2	17.2

LGSW-13	1/09/2014	–35.089	149.465	80	0.7	187	296	25.6	3.5	1.9	<2	1.6	9.3	3.5	3.0	0.6	83	3.3	<2	13	0.4	2.5
LGSW-14	8/10/2014	–35.089	149.465	<15	1.5	567	477	71.7	13.9	<2.5	<5	<2.5	15.2	5.1	8.4	1.4	217	15.4	<5	42	0.7	8.4
LGSW-15	12/01/2015	–35.089	149.465	<4	0.2	446	32	<0.5	<1	0.9	<1	1.0	11.6	2.1	10.4	0.4	36	3.5	<0.5	5	<0.1	2.8
LGSW-16	22/07/2015	–35.089	149.465	<4	0.2	296	42	<0.5	<1	3.0	<1	1.7	23.3	1.7	9.0	0.3	40	3.2	<0.5	7	0.1	6.8

c. Isotopes

Site ID	Date	Latitude (DD)	Longitude (DD)	$\delta^{2}H$ (‰ VSMOW)[1]	$\delta^{18}O$ (‰ VSMOW)[2]	$\delta^{37}Cl$ (‰ SMOC ± 1σ)	$\delta^{81}Br$ (‰ SMOB ± 1σ)	^{3}H activity (TU ± 1σ)
LGSW-1	20/05/2013	–35.089	149.465	21.3	3.29	–	–	–
LGSW-2	20/05/2013	–35.091	149.464	23.5	3.38	–	–	–
LGSW-3	20/05/2013	–35.092	149.464	22.5	3.45	–	–	–
LGSW-4	25/06/2013	–35.089	149.465	–21.2	–5.23	–	–	–
LGSW-5	1/08/2013	–35.089	149.465	–21.9	–4.33	–	–	3.73 ± 0.18
LGSW-6	2/09/2013	–35.089	149.465	–3.9	–1.37	–	–	–
LGSW-7	1/10/2013	–35.089	149.465	14.9	1.83	–	–	–
LGSW-8	28/10/2013	–35.089	149.465	29.9	4.67	–	–	–
LGSW-9	2/12/2013	–35.089	149.465	37.1	6.76	–	–	–
LGSW-2013[3]	Jun – Dec 2013	–35.089	149.465	–	–	–1.58 ± 0.10	0.73 ± 0.02	–
LGSW-10	2/06/2014	–35.089	149.465	–30.2	–5.88	–	–	–
LGSW-11	1/07/2014	–35.089	149.465	–19.3	–4.10	–	–	–
LGSW-12	4/08/2014	–35.089	149.465	7.6	0.05	–	–	–
LGSW-13	1/09/2014	–35.089	149.465	–38.9	–5.26	–	–	–
LGSW-14	8/10/2014	–35.089	149.465	38.3	5.28	–	–	–
LGSW-15	12/01/2015	–35.089	149.465	–49.6	–6.66	–	–	–
LGSW-16	22/07/2015	–35.089	149.465	–27.6	–4.44	–	–	–

[1]Mean analytical precision was ±1.1 ‰ (1σ)
[2]Mean analytical precision was ±0.17 ‰ (1σ)
[3]Mixture, in equal parts, of the 2013 samples for stable halogen isotope analyses

4. Groundwater

a. Field parameters and sample details

Site ID	Date	Latitude (DD)	Longitude (DD)	Intake interval (m BGS[1])	Standing water level (m AHD[2])	Temp. (°C)[3]	pH	EC (µS cm^{-1})[4]	TDS[5] (mg kg^{-1})	Eh (mV)	O_2 (mg L^{-1})	S^{2-} (µg L^{-1})[6]	Fe^{2+} (mg L^{-1})[6]
GW085100	21/1/2014	–35.250	149.428	20–24	685.295	16.7	6.74	648	466	–	2.00	3	<0.01
GW085100	22/11/2014	–35.250	149.428	20–24	684.835	15.2	6.93	657	436	190	1.50	<1	0.02
GW085101	24/10/2013	–35.245	149.425	39–45	680.040	12.4	7.28	413	333	235	3.68	36	0.16
GW085101	25/11/2014	–35.245	149.425	39–45	669.655	20.6	6.87	417	316	110	2.33	9	<0.01
GW085102	24/10/2013	–35.245	149.425	48–54	680.260	15.6	7.21	523	421	253	2.31	4	0.44
GW085102	25/11/2014	–35.245	149.425	48–54	665.896	19.4	7.16	516	410	130	1.45	9	0.04
GW085103	24/10/2013	–35.245	149.425	8–11	684.370	15.2	7.18	954	760	192	0.27	4	0.44
GW085103	25/11/2014	–35.245	149.425	8–11	684.342	15.7	7.25	983	742	30	0.35	<1	0.11
GW085104	30/1/2014	–35.267	149.431	24–29	691.428	16.2	7.41	291	213	120	6.19	3	<0.01
GW085104[7]	30/1/2014	–35.267	149.431	24–30	691.428	16.2	7.41	291	226	120	6.19	4	<0.01
GW085104	24/11/2014	–35.267	149.431	24–30	691.418	17.0	7.56	294	216	150	3.96	3	0.01
GW085105	30/1/2014	–35.267	149.431	3–5	691.466	17.7	6.53	499	352	–	3.43	<1	<0.01
GW085105	24/11/2014	–35.267	149.431	3–5	691.446	15.0	6.87	388	267	170	3.36	<1	<0.01
PMB_AD	21/1/2014	–35.245	149.437	11–17	684.144	19.7	6.08	727	428	120	0.20	<1	2.27
PMB_AD	24/11/2014	–35.245	149.437	11–17	684.234	16.9	6.48	738	437	60	0.18	2	2.30
PMB_AS	21/1/2014	–35.245	149.437	7–10	685.020	17.1	6.44	981	656	100	0.20	22	2.33
PMB_AS	24/11/2014	–35.245	149.437	7–10	685.080	15.6	6.55	922	624	–200	0.08	10	2.33
PMB_BD	2/10/2013	–35.243	149.443	51–60	685.980	16.1	6.77	502	320	23.1	0.12	4	0.25
PMB_BD[7]	2/10/2013	–35.243	149.443	51–60	685.980	16.1	6.77	502	324	23.1	0.12	4	0.25
PMB_BD	26/11/2014	–35.243	149.443	51–60	685.433	18.5	6.71	482	302	–150	0.19	2	0.44
PMB_BS	21/1/2014	–35.243	149.443	15–18	686.089	16.9	6.17	706	481	57	3.88	2	0.03
PMB_BS	26/11/2014	–35.243	149.443	15–18	686.064	16.0	6.14	710	450	–50	3.23	6	0.01
PMB_C	28/1/2014	–35.241	149.418	9–18	686.176	18.1	7.31	635	512	–100	0.05	29	0.04
PMB_C	21/11/2014	–35.241	149.418	9–18	685.847	16.0	7.32	650	503	–30	1.05	13	0.03
PMB_D	28/1/2014	–35.260	149.437	11–14	688.982	15.2	7.35	206	173	195	8.80	17	<0.01
PMB_D	21/11/2014	–35.260	149.437	11–14	689.062	15.4	7.30	221	174	230	6.75	23	0.02
PMB_E	30/1/2014	–35.273	149.428	12–18	692.708	15.6	7.07	424	293	25	3.35	6	0.02
PMB_E	22/11/2014	–35.273	149.428	12–18	692.797	15.6	7.13	407	272	260	3.20	6	0.03
PMB_FD	23/1/2014	–35.205	149.495	46–58	686.690	16.7	6.82	469	363	–140	0.00	5	0.02
PMB_FD	26/11/2014	–35.205	149.495	46–58	687.020	21.8	6.85	486	363	–140	0.65	<1	0.02
PMB_FS	23/1/2014	–35.205	149.495	15–18	686.862	19.8	6.27	557	375	–110	0.30	17	1.73
PMB_FS	26/11/2014	–35.205	149.495	15–18	687.062	16.0	6.24	546	341	–210	0.08	19	1.55
PMB_G	23/1/2014	–35.206	149.503	28–40	689.671	16.5	6.61	1 978	1 289	–160	0.00	3	0.04
PMB_G	26/11/2014	–35.206	149.503	28–40	689.433	18.4	6.72	1 991	1 252	60	0.27	36	0.05
PMB_G[7]	26/11/2014	–35.206	149.503	28–40	689.433	18.4	6.72	1 991	1 252	60	0.27	36	0.05

Site ID	Date	Latitude (DD)	Longitude (DD)	Intake interval (m BGS[1])	Standing water level (m AHD[2])	Temp. (°C)[3]	pH	EC (µS cm^{-1})[4]	TDS[5] (mg kg^{-1})	Eh (mV)	O_2 (mg L^{-1})	S^{2-} (µg L^{-1})[6]	Fe^{2+} (mg L^{-1})[6]
PMB_KD	5/2/2014	–35.220	149.423	22–31	679.220	15.3	7.20	744	557	–60	0.09	10	0.31
PMB_KD	27/11/2014	–35.220	149.423	22–31	679.460	15.8	7.26	708	538	–130	0.27	5	0.37
PMB_KS	27/11/2014	–35.220	149.423	5–8	679.704	13.6	7.64	836	489	–200	0.50	4	2.20
PMB_LD	5/2/2014	–35.221	149.438	15–18	681.137	16.0	6.73	2 689	1 757	–80	0.07	47	0.09
PMB_LD	27/11/2014	–35.221	149.438	15–18	681.022	15.6	6.76	2 580	1 666	40	0.12	19	0.02
PMB_LS	5/2/2014	–35.221	149.438	7–10	681.131	14.9	7.21	1 702	1 203	–125	0.00	7	0.04
PMB_LS	27/11/2014	–35.221	149.438	7–10	681.011	15.1	7.23	1 658	1 176	40	0.48	4	0.02
PMB_M	28/1/2014	–35.250	149.451	15–18	690.294	20.1	6.33	213	163	–150	0.14	7	0.04
PMB_M	20/11/2014	–35.250	149.451	15–18	690.511	15.7	6.12	199	161	210	0.58	13	0.07
Harrys bore	31/3/2014	–35.174	149.492	–	–	17.0	7.57	1 222	835	240	8.00	–	–
Dominics bore	23/1/2014	–35.205	149.486	–	–	14.8	6.59	518	347	–20	1.52	19	1.56
GW020910[8]	23/1/2014	–35.195	149.487	–	–	20.4	7.30	486	375	81	–	–	–
GW052310[9]	20/5/2013	–35.092	149.496	18–40	–	17.2	8.18	1 147	894	290	3.30	–	–
Winderadeen bore	12/5/2014	–34.976	149.390	–	–	13.2	7.74	2 039	1 465	200	6.59	67	0.58
Russells bore 1	21/2/2014	–35.089	149.462	1.42	671.838	25.3	7.67	34400	24264	90	–	–	–
Russells bore 2	3/3/2014	–35.089	149.462	1.42	671.794	23.2	7.73	32700	23669	275	6.21	–	–
Russells bore 3	31/3/2014	–35.089	149.462	1.42	672.111	19.4	7.55	37300	24328	300	6.42	–	–
Russells bore 4	12/5/2014	–35.089	149.462	1.42	672.508	14	7.90	34700	23855	5	8.14	–	–
Russells bore 5	2/6/2014	–35.089	149.462	1.42	672.475	13.9	7.92	33400	22643	360	9.76	–	–
Russells bore 6	1/7/2014	–35.089	149.462	1.42	673.137	16.3	7.94	43300	22455	370	–	–	–
Russells bore 7	4/8/2014	–35.089	149.462	1.42	673.115	12.5	7.79	27000	22628	350	4.00	–	–
Russells bore 8	1/9/2014	–35.089	149.462	1.42	673.205	9.7	7.77	30100	22445	330	–	–	–
Russells bore 9	8/10/2014	–35.089	149.462	1.42	673.114	13.6	7.92	33000	22181	200	2.92	–	–
Russells bore 10	3/11/2014	–35.089	149.462	1.42	672.516	18.4	8.00	27980	20559	210	2.48	–	–
Russells bore 11	1/12/2014	–35.089	149.462	1.42	672.352	21.5	8.01	31200	18845	130	3.64	–	–
Russells bore 12	9/2/2015	–35.089	149.462	1.42	673.004	18.2	7.67	34700	22915	236	3.96	–	–
Russells bore 13	21/05/2015	–35.089	149.462	1.42	672.515	14.5	8.16	35500	23269	510	8.41	–	–

[1]Below ground surface
[2]Australian height datum
[3]Field temperature
[4]Electrical conductivity
[5]Total dissolved solids
[6]Determined using a portable spectrophotometer
[7]Field duplicate
[8]Osbournes bore
[9]Keatleys bore

b. Major ions/elements (mg kg^{-1} unless otherwise stated)

Site ID	Date	Latitude (DD)	Longitude (DD)	HCO_3^- (mg L^{-1})	Ca	Mg	Na	K	Si	SO_4^{2-}	Cl^-	Br^-	F^-	NO_3^-	PO_4^{3-}
GW085100	21/1/2014	–35.250	149.428	201	41.0	38.5	42.8	0.775	13.1	19.5	106	0.408	0.265	2.63	<0.01
GW085100	22/11/2014	–35.250	149.428	187	37.3	34.4	42.3	0.748	12.2	20.4	97.3	0.363	0.276	2.96	<0.01
GW085101	24/10/2013	–35.245	149.425	204	25.4	16.4	41.7	0.610	4.27	17.4	22.2	0.111	0.607	0.105	0.023
GW085101	25/11/2014	–35.245	149.425	185	25.3	15.7	43.5	0.584	4.00	17.9	22.5	0.108	0.625	0.329	0.030
GW085102	24/10/2013	–35.245	149.425	248	33.5	17.2	56.9	0.716	4.44	21.7	37.8	0.170	0.662	<0.01	0.018
GW085102	25/11/2014	–35.245	149.425	238	32.7	16.4	58.2	0.737	4.23	21.8	36.6	0.167	0.678	<0.01	0.057
GW085103	24/10/2013	–35.245	149.425	395	40.9	29.2	133	1.34	11.6	57.5	90.1	0.410	0.358	0.172	<0.01
GW085103	25/11/2014	–35.245	149.425	368	43.8	29.5	130	1.43	11.3	62.3	94.3	0.454	0.439	0.434	<0.01
GW085104	30/1/2014	–35.267	149.431	117	12.1	8.76	36.1	0.692	5.58	9.36	22.1	0.131	0.697	0.485	0.045
GW085104[1]	30/1/2014	–35.267	149.431	126	12.6	9.11	37.5	0.723	5.81	9.72	23.3	0.132	0.721	0.270	0.038
GW085104	24/11/2014	–35.267	149.431	117	12.3	8.64	39.0	0.811	5.64	9.46	22.6	0.124	0.708	0.167	<0.01
GW085105	30/1/2014	–35.267	149.431	147	27.4	22.1	39.6	0.430	10.5	26.4	73.5	0.394	0.220	4.30	<0.01
GW085105	24/11/2014	–35.267	149.431	120	17.2	13.2	42.4	0.410	9.34	17.0	46.1	0.194	0.264	0.898	<0.01
PMB_AD	21/1/2014	–35.245	149.437	96	32.2	28.2	58.7	2.07	20.7	18.1	169	0.840	0.100	0.163	<0.01
PMB_AD	24/11/2014	–35.245	149.437	105	31.4	26.9	60.5	2.12	20.5	16.9	169	0.861	0.107	0.120	<0.01
PMB_AS	21/1/2014	–35.245	149.437	231	43.1	35.2	106	1.59	16.1	51.6	162	0.760	0.089	4.62	<0.01
PMB_AS	24/11/2014	–35.245	149.437	245	39.0	31.0	104	1.48	15.3	45.7	135	0.642	0.101	4.63	<0.01
PMB_BD	2/10/2013	–35.243	149.443	106	15.6	19.2	48.3	2.49	15.0	13.1	99.0	0.472	0.190	0.119	<0.01
PMB_BD[1]	2/10/2013	–35.243	149.443	106	16.3	20.2	50.0	2.63	15.8	13.0	98.4	0.479	0.188	0.618	<0.01
PMB_BD	26/11/2014	–35.243	149.443	96	19.3	17.7	46.7	2.18	12.9	11.4	94.6	0.459	0.167	<0.01	<0.01
PMB_BS	21/1/2014	–35.243	149.443	135	32.8	25.0	70.8	1.00	18.2	40.5	124	0.619	0.038	32.8	<0.01
PMB_BS	26/11/2014	–35.243	149.443	112	31.5	23.1	71.9	1.01	17.2	38.7	119	0.594	0.038	34.0	0.023
PMB_C	28/1/2014	–35.241	149.418	294	15.6	20.2	106	1.35	8.20	28.6	36.7	0.124	0.957	<0.01	<0.01
PMB_C	21/11/2014	–35.241	149.418	286	18.0	18.2	101	1.14	8.83	29.4	38.6	0.123	1.02	<0.01	0.025
PMB_D	28/1/2014	–35.260	149.437	103	9.33	8.02	22.8	1.02	5.78	4.97	11.3	0.061	0.919	5.52	<0.01
PMB_D	21/11/2014	–35.260	149.437	98	11.3	7.70	23.3	0.952	6.30	4.97	13.4	0.069	0.909	7.26	<0.01
PMB_E	30/1/2014	–35.273	149.428	113	20.2	15.8	43.3	0.998	8.96	10.4	71.2	0.326	0.469	8.66	<0.01
PMB_E	22/11/2014	–35.273	149.428	108	18.4	13.9	42.9	0.976	8.75	13.9	57.4	0.280	0.503	6.89	<0.01
PMB_FD	23/1/2014	–35.205	149.495	167	21.5	14.6	57.6	1.98	24.6	10.3	65.3	0.267	0.287	0.136	<0.01
PMB_FD	26/11/2014	–35.205	149.495	170	21.7	14.1	58.5	1.99	22.4	9.74	63.7	0.264	0.274	0.332	0.054
PMB_FS	23/1/2014	–35.205	149.495	119	15.1	17.7	73.9	0.856	17.7	10.2	118	0.407	0.193	0.116	<0.01
PMB_FS	26/11/2014	–35.205	149.495	102	16.7	15.4	65.0	0.785	20.8	9.55	108	0.397	0.174	0.126	<0.02
PMB_G	23/1/2014	–35.206	149.503	384	75.2	132	137	3.69	13.4	74.7	465	2.30	0.376	0.333	<0.03
PMB_G	26/11/2014	–35.206	149.503	373	85.9	126	135	3.37	14.5	71.0	440	2.18	0.425	0.378	<0.03
PMB_G[1]	26/11/2014	–35.206	149.503	373	85.9	126	135	3.38	14.4	71.2	440	2.20	0.423	0.352	<0.03
PMB_KD	5/2/2014	–35.220	149.423	285	39.3	25.4	78.9	1.51	13.2	38.8	73.8	0.346	0.275	0.191	<0.01
PMB_KD	27/11/2014	–35.220	149.423	267	38.0	24.1	81.0	1.60	12.8	40.7	71.9	0.334	0.394	0.114	<0.01
PMB_KS	27/11/2014	–35.220	149.423	160	54.0	38.1	40.6	1.44	2.63	0.105	180	0.857	0.277	0.266	<0.01

Site ID	Date	Latitude (DD)	Longitude (DD)	HCO_3^- (mg L^{-1})	Ca	Mg	Na	K	Si	SO_4^{2-}	Cl^-	Br^-	F^-	NO_3^-	PO_4^{3-}
PMB_LD	5/2/2014	–35.221	149.438	482	87.6	87.7	341	5.12	14.7	184	550	2.64	0.342	0.926	<0.04
PMB_LD	27/11/2014	–35.221	149.438	445	79.9	79.7	338	4.99	13.3	177	523	2.47	0.443	1.63	<0.04
PMB_LS	5/2/2014	–35.221	149.438	488	31.7	40.6	269	2.06	16.7	91.6	253	1.25	1.65	6.43	0.049
PMB_LS	27/11/2014	–35.221	149.438	467	29.8	38.5	272	2.04	15.9	85.0	257	1.23	1.72	5.84	<0.02
PMB_M	28/1/2014	–35.250	149.451	74	6.38	10.8	20.2	1.32	12.7	7.62	14.2	0.092	0.220	15.7	0.026
PMB_M	20/11/2014	–35.250	149.451	46	7.11	11.3	17.5	1.04	12.2	13.0	16.5	0.090	0.136	36.7	0.027
Harrys bore	31/3/2014	–35.174	149.492	397	32.3	36.2	169	1.27	15.4	20.5	158	0.766	0.911	2.92	<0.01
Dominics bore	23/1/2014	–35.205	149.486	145	21.6	18.4	40.4	1.04	19.4	12.7	72.6	0.280	0.134	0.134	<0.01
GW020910[2]	23/1/2014	–35.195	149.487	193	12.1	16.1	71.2	0.435	18.6	15.5	40.7	0.158	0.665	6.18	0.039
GW052310[3]	20/5/2013	–35.092	149.496	426	22.6	19.4	201	2.30	17.1	21.9	140	0.829	0.772	40.8	0.172
Winderadeen bore	12/5/2014	–34.976	149.390	564	41.2	26.8	370	3.46	11.4	0.136	439	2.23	4.33	0.231	<0.02
Russells bore 1	21/2/2014	–35.089	149.462	722	195	906	7 452	31.6	1.14	2 862	11 978	62.4	2.0	27.1	<1
Russells bore 2	3/3/2014	–35.089	149.462	501	182	927	7 173	29.8	1.16	2 836	11 895	62.6	2.0	32.6	<1
Russells bore 3	31/3/2014	–35.089	149.462	460	170	947	7 353	29.5	1.17	2 949	12 306	65.2	2.0	19.3	<1
Russells bore 4	12/5/2014	–35.089	149.462	748	194	858	7 179	29.0	1.11	2 796	11 933	62.1	2.1	29.3	<1
Russells bore 5	2/6/2014	–35.089	149.462	396	167	883	6 955	26.4	1.05	2 672	11 428	59.1	2.0	32.0	<1
Russells bore 6	1/7/2014	–35.089	149.462	341	163	870	6 758	25.5	0.991	2 684	11 498	57.2	1.9	33.7	<1
Russells bore 7	4/8/2014	–35.089	149.462	516	165	877	6 759	24.4	0.883	2 674	11 496	57.0	1.9	36.5	<1
Russells bore 8	1/9/2014	–35.089	149.462	434	168	876	6 803	24.6	0.831	2 657	11 363	56.2	1.9	40.3	<1
Russells bore 9	8/10/2014	–35.089	149.462	524	192	785	6 672	25.9	0.853	2 640	11 220	55.5	1.9	41.9	<1
Russells bore 10	3/11/2014	–35.089	149.462	611	177	601	6 229	25.0	0.784	2 521	10 290	50.4	1.8	29.1	<1
Russells bore 11	1/12/2014	–35.089	149.462	555	176	699	5 712	25.5	0.865	2 335	9 208	44.5	1.8	64.1	<1
Russells bore 12	9/2/2015	–35.089	149.462	476	186	821	6 999	28.6	1.06	2 740	11 553	61.2	2.0	24.6	<1
Russells bore 13	21/05/2015	–35.089	149.462	490	180	830	7 026	28.4	1.08	2 799	11 807	63.0	2.0	23.9	<1

[1]Field duplicate
[2]Osbournes bore
[3]Keatleys bore

c. Trace elements (μg kg^{-1})

Site ID	Date	Latitude (DD)	Longitude (DD)	Fe	Li	B	Al	V	Cr	Mn	Co	Ni	Cu	Zn	As	Rb	Sr	Mo	Sn	Ba	Pb	U
GW085100	21/1/2014	–35.250	149.428	<30	0.9	8	<10	0.6	5	<0.5	<1	0.5	<1	2	0.3	0.4	238	<1	<1	27	0.1	0.3
GW085100	22/11/2014	–35.250	149.428	<10	0.7	11	–	0.6	1	0.5	<1	3.5	<1	3	0.4	0.4	279	<1	<0.4	34	<0.1	0.3
GW085101	24/10/2013	–35.245	149.425	<20	1.1	16	22	3.3	1	<0.5	<1	1.1	2	24	0.3	1.8	144	<1	<1	13	0.2	0.2
GW085101	25/11/2014	–35.245	149.425	<10	0.7	14	–	3.1	<1	0.7	<1	1.1	<1	15	0.4	1.8	169	<1	<0.4	15	<0.1	<0.1
GW085102	24/10/2013	–35.245	149.425	<20	4.4	16	21	0.5	<1	0.7	<1	0.7	<1	5	0.3	2.1	213	<1	<1	13	0.1	0.3
GW085102	25/11/2014	–35.245	149.425	<10	3.7	14	–	<0.5	<1	0.9	<1	6.7	<1	8	0.4	2.1	225	<1	<0.4	15	<0.1	0.2
GW085103	24/10/2013	–35.245	149.425	418	0.8	14	22	1.3	4	43	1	1.0	<1	9	1.6	0.2	267	<1	<1	101	0.2	3.0
GW085103	25/11/2014	–35.245	149.425	<20	0.7	13	–	1.7	1	21	1	1.1	1	7	1.3	0.1	343	<1	<0.4	138	<0.1	2.9

Site ID	Date	Latitude (DD)	Longitude (DD)	Fe	Li	B	Al	V	Cr	Mn	Co	Ni	Cu	Zn	As	Rb	Sr	Mo	Sn	Ba	Pb	U
GW085104	30/1/2014	–35.267	149.431	<10	1.0	16	51	<0.5	1	0.6	<1	<0.5	<1	<0.5	0.1	0.3	106	<1	<1	5	0.1	0.2
GW085104[1]	30/1/2014	–35.267	149.431	<10	1.0	16	47	<0.5	1	0.6	<1	<0.5	<1	<0.5	0.1	0.3	109	<1	<1	5	0.1	0.2
GW085104	24/11/2014	–35.267	149.431	<10	0.7	15	–	<0.5	<1	0.7	<1	<0.5	<1	5	0.3	0.2	131	<1	<0.4	8	<0.1	<0.1
GW085105	30/1/2014	–35.267	149.431	<10	0.6	18	54	<0.5	3	<0.5	<1	<0.5	<1	3	0.3	0.2	251	<1	<1	72	0.1	<0.1
GW085105	24/11/2014	–35.267	149.431	<10	0.3	15	–	<0.5	<1	0.4	<1	<0.5	<1	3	1.0	<0.1	170	<1	<0.4	57	<0.1	<0.1
PMB_AD	21/1/2014	–35.245	149.437	2 694	2.0	13	37	<0.5	8	7 105	31	5.9	1	32	1.0	0.2	216	<1	<1	460	0.2	0.1
PMB_AD	24/11/2014	–35.245	149.437	2 669	1.8	14	–	<0.5	3	6 625	<1	7.3	2	46	1.9	0.2	253	<1	<0.4	629	<0.1	<0.1
PMB_AS	21/1/2014	–35.245	149.437	3 896	1.0	7	36	<0.5	6	709	6	2.8	<1	7	2.1	0.3	253	<1	<1	151	0.8	0.7
PMB_AS	24/11/2014	–35.245	149.437	2 603	0.9	7	–	0.8	3	693	7	3.3	<1	8	3.2	0.3	279	<1	<0.4	194	<0.1	1.0
PMB_BD	2/10/2013	–35.243	149.443	215	0.4	15	20	<0.5	4	1 099	2	0.9	<1	5	0.8	1.2	108	<1	<1	73	0.1	0.1
PMB_BD[1]	2/10/2013	–35.243	149.443	213	0.4	14	20	<0.5	4	1 067	2	0.9	<1	5	0.8	1.1	105	<1	<1	72	0.1	0.1
PMB_BD	26/11/2014	–35.243	149.443	407	0.2	15	–	<0.5	2	1 686	2	7.1	<1	19	1.9	0.9	147	<1	<0.4	179	<0.1	<0.1
PMB_BS	21/1/2014	–35.243	149.443	<10	1.1	4	<10	<0.5	5	0.8	<1	1.2	<1	5	0.3	0.3	210	<1	<1	118	<0.1	0.1
PMB_BS	26/11/2014	–35.243	149.443	<10	1.0	5	–	0.8	3	0.9	<1	1.1	<1	7	1.3	0.3	243	<1	<0.4	146	<0.1	<0.1
PMB_C	28/1/2014	–35.241	149.418	<10	0.5	22	36	0.7	1	36	<1	<0.5	<1	3	0.1	0.2	176	<1	<1	34	0.1	0.8
PMB_C	21/11/2014	–35.241	149.418	<20	0.4	24	–	1.2	1	44	<1	<0.5	<1	3	1.0	0.2	200	<1	<0.4	45	<0.1	0.8
PMB_D	28/1/2014	–35.260	149.437	<10	<0.1	25	44	<0.5	1	<0.5	<1	<0.5	<1	1	0.1	0.4	93	<1	<1	12	<0.1	0.1
PMB_D	21/11/2014	–35.260	149.437	<10	0.0	21	–	<0.5	1	0.4	<1	<0.5	<1	1	0.8	0.3	75	<1	<0.4	11	<0.1	<0.1
PMB_E	30/1/2014	–35.273	149.428	<10	0.4	19	42	<0.5	3	<0.5	<1	<0.5	<1	2	0.2	0.4	205	<1	<1	29	<0.1	0.2
PMB_E	22/11/2014	–35.273	149.428	<10	0.6	17	–	<0.5	1	0.7	<1	<0.5	<1	1	0.2	0.3	197	<1	<0.4	28	<0.1	0.1
PMB_FD	23/1/2014	–35.205	149.495	<10	0.4	30	37	0.7	3	864	<1	1.0	<1	3	0.4	1.1	140	<1	<1	85	0.1	0.5
PMB_FD	26/11/2014	–35.205	149.495	<10	0.3	27	–	0.5	1	767	<1	1.8	<1	15	0.5	1.0	158	<1	<0.4	72	<0.1	0.4
PMB_FS	23/1/2014	–35.205	149.495	1 671	0.6	9	39	<0.5	6	246	1	1.7	<1	18	1.3	0.4	130	<1	<1	142	0.1	<0.1
PMB_FS	26/11/2014	–35.205	149.495	1 752	0.6	8	–	<0.5	2	255	2	1.1	<1	8	1.6	0.5	129	<1	<0.4	152	<0.1	<0.1
PMB_G	23/1/2014	–35.206	149.503	<10	0.8	15	39	<0.5	16	1 175	1	1.6	<1	6	1.4	2.9	595	<1	<1	143	0.1	3.5
PMB_G	26/11/2014	–35.206	149.503	<20	0.8	13	–	<0.5	7	1 384	2	3.0	2	22	1.5	3.3	714	<1	<0.4	180	0.2	4.0
PMB_G[1]	26/11/2014	–35.206	149.503	<20	0.8	13	–	<0.5	7	1 368	2	2.9	2	22	1.5	3.3	712	<1	<0.4	177	0.2	3.7
PMB_KD	5/2/2014	–35.220	149.423	163	0.4	21	39	<0.5	4	149	<1	1.8	1	16	4.0	0.3	309	<1	<1	138	0.1	0.3
PMB_KD	27/11/2014	–35.220	149.423	313	0.6	16	–	<0.5	2	144	<1	3.9	<1	10	4.4	0.3	319	<1	<0.4	122	<0.1	0.3
PMB_KS	27/11/2014	–35.220	149.423	9 971	0.1	4	–	<0.5	2	1 001	<1	0.9	<1	13	2.1	0.6	419	<1	<0.4	119	<0.1	<0.1
PMB_LD	5/2/2014	–35.221	149.438	<10	0.7	44	47	<0.5	17	913	3	1.9	1	11	1.5	0.2	518	<1	<1	82	<0.1	4.7
PMB_LD	27/11/2014	–35.221	149.438	<40	0.7	50	12	0.9	<1	1 091	4	1.3	1	6	1.8	0.3	721	<1	<0.4	119	<0.1	4.8
PMB_LS	5/2/2014	–35.221	149.438	<10	0.8	21	35	6.2	6	47	<1	1.0	<1	2	1.3	0.1	231	1	<1	34	<0.1	6.0
PMB_LS	27/11/2014	–35.221	149.438	<40	0.7	21	11	7.4	<1	52	<1	1.6	<1	3	2.0	0.1	303	2	<0.4	46	<0.1	5.3
PMB_M	28/1/2014	–35.250	149.451	22	0.6	12	63	<0.5	1	421	<1	1.5	3	22	0.3	0.4	61	<1	<1	11	0.2	0.1
PMB_M	20/11/2014	–35.250	149.451	<10	0.7	9	48	<0.5	<1	372	<1	0.9	2	5	0.4	0.3	74	<1	<0.4	13	<0.1	<0.1
Harrys bore	31/3/2014	–35.174	149.492	30	0.8	22	30	2.5	8	20	<1	0.9	3	4	0.6	0.3	258	1	<1	61	0.1	9.6
Dominics bore	23/1/2014	–35.205	149.486	15 000	0.3	11	38	<0.5	4	522	<1	<0.5	191	5	0.5	0.5	139	<1	<1	88	0.1	<0.1
GW020910[2]	23/1/2014	–35.195	149.487	<10	0.5	6	65	2.1	1	<0.5	<1	2.6	193	41	0.4	0.2	74	<1	<1	28	1.2	1.1
GW052310[3]	20/5/2013	–35.092	149.496	270	1.8	51	17	5.7	7	2	<1	0.5	11	26	0.9	0.3	182	<1	<1	31	1.1	3.6

Site ID	Date	Latitude (DD)	Longitude (DD)	Fe	Li	B	Al	V	Cr	Mn	Co	Ni	Cu	Zn	As	Rb	Sr	Mo	Sn	Ba	Pb	U
Winderadeen bore	12/5/2014	–34.976	149.390	480	<0.1	157	35	<0.5	2	18	<1	0.7	<1	12	1.8	3.0	1 594	<1	<1	434	<0.1	<0.1
Russells bore 1	21/2/2014	–35.089	149.462	<1 000	4.9	1 121	77	26	36	127	<10	191	63	43	53	4	6 632	50	<5	92	<1	16
Russells bore 2	3/3/2014	–35.089	149.462	<1 000	4.1	1 226	85	24	41	138	<10	344	321	50	53	4	7 040	41	<5	100	<1	22
Russells bore 3	31/3/2014	–35.089	149.462	<1 000	3.6	1 127	73	16	35	231	<10	227	<10	47	46	3	6 545	40	<5	63	<1	23
Russells bore 4	12/5/2014	–35.089	149.462	<1 000	3.0	1 066	91	11	38	92	<10	91	<10	38	47	3	6 452	39	<5	61	<1	20
Russells bore 5	2/6/2014	–35.089	149.462	<1 000	2.9	995	55	12	42	106	<10	73	<10	41	48	3	6 599	37	<5	56	<1	20
Russells bore 6	1/7/2014	–35.089	149.462	<1 000	2.7	953	69	12	40	71	<10	59	1 970	75	57	3	6 867	42	<5	64	4.5	19
Russells bore 7	4/8/2014	–35.089	149.462	<1 000	2.0	815	75	13	35	27	<10	26	1 030	35	48	2	6 315	35	<5	43	<1	20
Russells bore 8	1/9/2014	–35.089	149.462	<1 000	1.8	775	64	15	35	32	<10	18	973	31	47	2	5 964	35	<5	38	<1	20
Russells bore 9	8/10/2014	–35.089	149.462	<1 000	3.3	781	93	14	<10	43	<10	–	396	27	40	2	6 497	37	<5	44	<1	18
Russells bore 10	3/11/2014	–35.089	149.462	<1 000	3.3	767	187	28	<10	18	<10	–	621	31	44	2	5 201	33	<5	45	<1	16
Russells bore 11	1/12/2014	–35.089	149.462	2 364	3.7	873	26	20	<10	37	<10	–	<10	38	43	3	6 071	39	<5	43	<1	18
Russells bore 12	9/2/2015	–35.089	149.462	<1 000	4.3	987	13	10	<10	107	<10	–	<10	24	37	2	6 339	41	<5	41	<1	17
Russells bore 13	21/05/2015	–35.089	149.462	<1 000	4.6	1 012	23	5	<10	69	<10	–	1 764	27	37	3	6 849	48	<5	41	<1	16

[1]Field duplicate
[2]Osbournes bore
[3]Keatleys bore

d. Isotopes

Site ID	Date	Latitude (DD)	Longitude (DD)	$\delta^{2}H$ (‰ VSMOW)[1]	$\delta^{18}O$ (‰ VSMOW)[2]	$\delta^{13}C$ (‰ VPDB)[3]	^{14}C (% modern carbon ± 1σ)	$\delta^{37}Cl$ (‰ SMOC ± 1σ)	$\delta^{81}Br$ (‰ SMOB± 1σ)	^{3}H activity (TU ± 1σ)
GW085100	21/1/2014	–35.250	149.428	–43.5	–6.55	–12.0	97.94 ± 0.31	–	–	–
GW085100	22/11/2014	–35.250	149.428	–42.7	–6.41	–	–	–	–	0.82 ± 0.05
GW085101	24/10/2013	–35.245	149.425	–46.3	–7.35	–10.5	30.42 ± 0.31	–	–	–
GW085101	25/11/2014	–35.245	149.425	–47.0	–7.26	–	–	–	–	–
GW085102	24/10/2013	–35.245	149.425	–47.5	–7.36	–11.4	17.11 ± 0.31	–	–	–
GW085102	25/11/2014	–35.245	149.425	–47.2	–7.23	–	–	–	–	–
GW085103	24/10/2013	–35.245	149.425	–45.2	–7.58	–9.9	90.03 ± 0.31	–	–	2.18 ± 0.10
GW085103	25/11/2014	–35.245	149.425	–47.4	–7.34	–	–	–	–	–
GW085104	30/1/2014	–35.267	149.431	–48.9	–7.99	–8.9	35.72 ± 0.31	–	–	–
GW085104[4]	30/1/2014	–35.267	149.431	–52.7	–7.88	–	–	–	–	–
GW085104	24/11/2014	–35.267	149.431	–52.4	–7.77	–	–	–	–	–
GW085105	30/1/2014	–35.267	149.431	–43.7	–6.77	–13.6	102.3 ± 0.47	–	–	1.23 ± 0.06
GW085105	24/11/2014	–35.267	149.431	–43.0	–6.60	–	–	–	–	–
PMB_AD	21/1/2014	–35.245	149.437	–47.1	–6.85	–11.4	89.12 ± 0.31	–	–	–
PMB_AD	24/11/2014	–35.245	149.437	–45.6	–6.87	–	–	–	–	–
PMB_AS	21/1/2014	–35.245	149.437	–40.9	–6.41	–12.1	100.8 ± 0.31	–	–	1.40 ± 0.07
PMB_AS	24/11/2014	–35.245	149.437	–39.4	–6.14	–	–	–	–	–
PMB_BD	2/10/2013	–35.243	149.443	–48.2	–6.90	–14.6	47.3 ± 0.31	–	–	–

Site ID	Date	Latitude (DD)	Longitude (DD)	$\delta^{2}H$ (‰ VSMOW)[1]	$\delta^{18}O$ (‰ VSMOW)[2]	$\delta^{13}C$ (‰ VPDB)[3]	^{14}C (% modern carbon ± 1σ)	$\delta^{37}Cl$ (‰ SMOC ± 1σ)	$\delta^{81}Br$ (‰ SMOB± 1σ)	^{3}H activity (TU ± 1σ)
PMB_BD[4]	2/10/2013	–35.243	149.443	–43.6	–6.99	–14.3	–	–	–	–
PMB_BD	26/11/2014	–35.243	149.443	–46.8	–7.19	–	–	–	–	–
PMB_BS	21/1/2014	–35.243	149.443	–45.6	–7.25	–12.0	100.7 ± 0.31	–	–	1.14 ± 0.06
PMB_BS	26/11/2014	–35.243	149.443	–46.2	–7.05	–	–	–	–	–
PMB_C	28/1/2014	–35.241	149.418	–45.6	–7.21	–11.8	12.34 ± 0.31	–	–	–
PMB_C	21/11/2014	–35.241	149.418	–46.0	–7.29	–	–	–	–	0.26 ± 0.03
PMB_D	28/1/2014	–35.260	149.437	–35.2	–6.10	–10.4	82.64 ± 0.31	–	–	4.38 ± 0.19
PMB_D	21/11/2014	–35.260	149.437	–35.5	–5.99	–	–	–	–	–
PMB_E	30/1/2014	–35.273	149.428	–44.2	–6.77	–9.6	84.03 ± 0.31	–	–	1.34 ± 0.07
PMB_E	22/11/2014	–35.273	149.428	–42.4	–6.39	–	–	–	–	–
PMB_FD	23/1/2014	–35.205	149.495	–45.8	–6.87	–15.9	46.6 ± 0.37	–	–	–
PMB_FD	26/11/2014	–35.205	149.495	–44.7	–6.78	–	–	–	–	–
PMB_FS	23/1/2014	–35.205	149.495	–42.9	–6.16	–14.0	96.85 ± 0.32	–	–	1.16 ± 0.06
PMB_FS	26/11/2014	–35.205	149.495	–41.7	–6.22	–	–	–	–	–
PMB_G	23/1/2014	–35.206	149.503	–51.7	–7.56	–12.9	86.27 ± 0.31	–	–	3.11 ± 0.14
PMB_G	26/11/2014	–35.206	149.503	–50.4	–7.63	–	–	0.33 ± 0.10	–	–
PMB_G[4]	26/11/2014	–35.206	149.503	–51.0	–7.54	–	–	–	–	–
PMB_KD	5/2/2014	–35.220	149.423	–47.9	–6.86	–12.5	12.68 ± 0.31	–	–	–
PMB_KD	27/11/2014	–35.220	149.423	–46.3	–7.07	–	–	–	–	–
PMB_KS	27/11/2014	–35.220	149.423	–32.7	–4.82	–	–	–	–	–
PMB_LD	5/2/2014	–35.221	149.438	–49.5	–7.56	–11.4	84.53 ± 0.31	–	–	–
PMB_LD	27/11/2014	–35.221	149.438	–49.2	–7.39	–	–	0.18 ± 0.16	–	–
PMB_LS	5/2/2014	–35.221	149.438	–47.6	–6.99	–14.2	94.63 ± 0.31	–	–	<0.15
PMB_LS	27/11/2014	–35.221	149.438	–47.2	–7.04	–	–	0.34 ± 0.12	–	–
PMB_M	28/1/2014	–35.250	149.451	–45.3	–7.31	–17.2	87.71 ± 0.31	–	–	6.12 ± 0.27
PMB_M	20/11/2014	–35.250	149.451	–42.7	–6.78	–	–	–	–	–
Harrys bore	31/3/2014	–35.174	149.492	–28.0	–4.56	–	–	–	–	–
Dominics bore	23/1/2014	–35.205	149.486	–29.5	–3.94	–	–	–	–	–
GW020910[5]	23/1/2014	–35.195	149.487	–47.7	–7.17	–	–	–	–	–
GW052310[6]	20/5/2013	–35.092	149.496	–37.8	–5.35	–	–	–	–	–
Winderadeen bore	12/5/2014	–34.976	149.390	–49.3	–8.25	–	–	–	–	–
Russells bore 1	21/2/2014	–35.089	149.462	–8.6	–0.60	–	–	–	–	–
Russells bore 2	3/3/2014	–35.089	149.462	–7.0	–0.62	–	–	–	–	–
Russells bore 3	31/3/2014	–35.089	149.462	–5.8	–0.72	–	–	–	–	–
Russells bore 4	12/5/2014	–35.089	149.462	–6.5	–0.57	–	–	0.23 ± 0.10	0.96 ± 0.27	–
Russells bore 5	2/6/2014	–35.089	149.462	–8.3	–0.42	–	–	–	–	–
Russells bore 6	1/7/2014	–35.089	149.462	–7.0	–0.72	–	–	–	–	–
Russells bore 7	4/8/2014	–35.089	149.462	–6.3	–0.66	–	–	–	–	–
Russells bore 8	1/9/2014	–35.089	149.462	–7.5	–0.63	–	–	–	–	–
Russells bore 9	8/10/2014	–35.089	149.462	–7.1	–0.57	–	–	–	–	–

Site ID	Date	Latitude (DD)	Longitude (DD)	$\delta^{2}H$ (‰ VSMOW)[1]	$\delta^{18}O$ (‰ VSMOW)[2]	$\delta^{13}C$ (‰ VPDB)[3]	^{14}C (% modern carbon ± 1σ)	$\delta^{37}Cl$ (‰ SMOC ± 1σ)	$\delta^{81}Br$ (‰ SMOB± 1σ)	^{3}H activity (TU ± 1σ)
Russells bore 10	3/11/2014	–35.089	149.462	–6.1	–0.78	–	–	–	–	–
Russells bore 11	1/12/2014	–35.089	149.462	–6.5	–0.75	–	–	–	–	–
Russells bore 12	9/2/2015	–35.089	149.462	–6.1	–0.73	–	–	–	–	–
Russells bore 13	21/05/2015	–35.089	149.462	–5.8	–0.66	–	–	–	–	–

[1]Mean analytical precision was ±1.1 ‰ (1σ)
[2]Mean analytical precision was ±0.17 ‰ (1σ)
[3]Mean analytical precision was ±0.36 ‰ (1σ)
[4]Field duplicate
[5]Osbournes bore
[6]Keatleys bore

5. *Gearys Gap porewater*

a. Field parameters and major elements/ions (mg kg^{-1})

Sample depth (m)[1]	Temp. (°C)[2]	pH	TDS	Cl^-	SO_4^{2-}	Br^-	F^-	NO_3^-	PO_4^{3-}	Na	Mg	Ca	K	Sr
0.56	23.7	8.36	20 255	10 805	2 098	52.2	4.2	bdl	bdl	6 502	402	104	283	2.6
1.60	25.5	8.11	44 897	23 779	5 738	116.8	6.5	41.1	bdl	13 045	1 919	190	48	12
3.17	25.0	8.34	55 125	21 966	15 101	102.9	4.5	18.2	bdl	14 782	2 518	503	103	16
4.82	22.5	7.63	48 904	20 992	11 941	99.7	3.7	bdl	bdl	13 339	1 963	476	70	13
6.05	24.4	7.83	44 414	19 976	10 001	96.0	3.1	13.7	bdl	12 249	1 689	305	68	9.8
7.55	25.6	7.77	41 852	20 261	7 627	99.3	2.6	16.2	bdl	11 989	1 442	305	99	8.6
9.10	19.7	7.73	43 597	21 114	7 626	106.6	2.1	12.5	bdl	12 818	1 500	359	46	9.2
10.55	25.0	7.84	44 084	22 198	7 178	111.1	3.2	20.5	bdl	12 569	1 493	386	114	9.3
12.05	24.5	7.80	44 667	22 545	6 762	112.7	bdl	21.9	bdl	13 170	1 530	423	89	9.4
13.52	20.0	7.71	43 417	21 904	6 397	115.2	1.8	10.7	bdl	12 968	1 516	447	44	9.6
15.05	24.9	8.20	41 676	21 412	6 190	107.9	3.7	18.9	bdl	11 883	1 528	440	80	9.8
18.05	24.5	8.19	42 204	22 244	5 458	112.4	bdl	bdl	bdl	12 309	1 505	478	85	9.8
19.55	24.4	8.07	38 721	20 860	4 904	106.3	bdl	20.8	bdl	10 577	1 625	511	103	10
21.05	24.9	8.04	36 133	19 782	4 102	100.8	bdl	19.6	bdl	10 310	1 316	401	91	9.3
22.52	24.8	7.80	36 606	20 632	3 632	108.7	bdl	15.5	bdl	10 439	1 227	438	102	8.1
24.05	25.4	8.11	38 875	20 891	4 955	106.9	bdl	22.5	bdl	10 727	1 568	488	104	9.7
25.55	22.8	7.90	35 325	19 832	3 650	106.3	bdl	12.7	bdl	9 893	1 322	458	39	8.4
27.25	24.1	8.01	37 049	20 246	4 132	107.4	bdl	15.0	bdl	10 521	1 468	480	67	9.3
28.55	23.9	8.22	33 764	18 970	3 208	99.7	2.3	19.6	bdl	9 615	1 293	475	69	8.1
30.06	24.1	8.09	35 045	19 267	3 587	100.9	bdl	21.2	bdl	10 164	1 376	460	58	8.7
31.62	24.1	8.16	32 113	18 212	3 074	96.5	bdl	15.6	bdl	8 869	1 292	473	70	8.2
32.90	24.4	8.18	31 650	18 015	2 961	95.6	bdl	16.1	bdl	8 804	1 208	448	93	7.6
32.90	24.5	8.22	31 771	18 173	2 951	96.8	bdl	bdl	bdl	8 834	1 198	435	75	7.4
34.63	22.7	7.89	31 656	17 822	2 949	95.1	bdl	16.9	bdl	9 102	1 158	457	45	7.5
36.05	24.4	8.10	29 739	16 914	2 847	89.7	bdl	14.2	bdl	7 958	1 357	502	47	8.4
37.54	24.8	8.02	29 099	16 813	2 881	88.6	bdl	16.8	bdl	7 570	1 233	437	49	7.8
39.05	24.0	8.02	28 956	16 430	2 833	86.6	2.8	16.5	bdl	7 702	1 323	498	53	8.3
40.55	24.7	8.20	29 368	16 679	2 863	86.5	bdl	27.9	bdl	7 845	1 296	506	53	8.2
42.05	24.8	7.34	28 753	16 147	2 685	89.4	1.0	7.0	bdl	8 224	1 095	465	30	7.4
43.55	23.6	7.80	29 294	16 092	2 758	88.7	1.3	6.6	bdl	8 228	1 081	985	35	16
44.93	24.2	7.72	28 479	15 820	2 640	82.1	bdl	bdl	bdl	8 294	1 108	467	59	7.4
46.58	22.0	7.27	28 079	15 641	2 618	83.6	bdl	9.8	bdl	8 118	1 081	493	25	7.5
47.94	24.3	7.86	28 141	15 650	2 606	81.3	bdl	17.7	bdl	8 084	1 099	507	86	7.6
49.55	24.1	8.23	27 992	15 560	2 679	80.7	bdl	29.4	bdl	7 914	1 139	535	46	8.0
50.88	24.3	8.10	26 488	14 616	2 442	76.4	bdl	16.1	bdl	7 857	944	462	66	6.7
52.21	24.2	8.17	26 880	14 858	2 527	77.2	bdl	21.3	12.2	7 778	1 003	492	102	7.0
54.05	24.2	8.03	25 790	14 405	2 476	74.3	bdl	22.0	11.8	7 275	978	478	61	6.9
55.55	24.7	8.08	26 502	14 603	2 527	75.7	2.2	17.3	12.1	7 735	949	496	74	7.1
57.19	24.2	8.04	27 092	14 759	2 603	77.4	2.0	13.6	7.9	8 009	1 009	532	70	7.5
58.55	24.5	7.98	25 809	14 252	2 545	73.9	2.3	16.2	bdl	7 323	1 010	520	57	7.5
60.05	24.4	7.84	24 284	13 460	2 331	70.3	2.2	13.8	8.4	6 760	1 058	516	55	7.5
61.52	22.3	7.82	25 330	14 061	2 373	73.9	1.9	13.0	bdl	7 200	1 037	542	19	7.9
62.91	24.6	8.00	25 188	14 082	2 333	73.1	2.8	20.0	10.2	7 103	970	515	71	7.5
66.05	24.6	8.24	24 675	13 823	2 213	72.2	2.9	18.7	bdl	7 192	794	467	84	6.4
67.55	24.7	8.13	23 687	13 208	2 181	68.2	2.3	17.8	9.4	6 641	975	526	50	7.6
67.55	24.2	7.99	23 199	13 184	2 115	68.5	bdl	15.0	8.2	6 356	902	490	51	7.0
69.05	24.1	7.93	23 727	13 246	2 194	68.5	2.6	14.4	7.6	6 712	901	501	71	7.2
70.55	24.4	8.05	21 478	12 275	2 036	62.4	3.5	30.3	13.0	5 592	891	491	75	7.1
72.05	24.1	7.96	21 132	12 060	1 933	61.1	2.6	18.5	10.4	5 679	828	463	69	6.7
72.05	24.4	7.98	21 104	12 022	1 946	61.3	2.9	18.0	8.9	5 708	808	464	57	6.7
73.55	25.7	8.05	20 444	11 664	1 758	59.2	2.9	21.5	13.9	5 721	686	426	84	6.1
73.55	24.5	8.43	19 930	11 414	1 711	58.6	2.5	16.3	9.7	5 586	669	407	51	5.9
75.05	25.0	7.98	18 931	10 877	1 604	55.8	2.2	12.1	7.5	5 248	649	400	69	5.7
76.55	24.8	7.86	19 436	11 355	1 601	58.3	bdl	22.4	13.2	5 262	649	407	62	5.9

[1]Depth below the lakebed
[1]Temperature recorded in the laboratory

b. Trace elements (μg kg^{-1})

Sample depth (m)[1]	Al	As	B	Ba	Cu	Fe	Li	Mn	U	Zn
0.56	283	47	870	64	104	310	81	283	79	325
1.60	401	84	1 318	47	190	416	143	48	77	201
3.17	566	79	1 258	57	503	751	713	103	629	349
4.82	271	80	1 199	31	476	393	628	70	37	187
6.05	544	81	578	40	305	379	498	68	8	140
7.55	459	73	864	28	305	283	489	99	25	77
9.10	453	78	878	55	359	357	540	46	4	199
10.55	402	78	732	33	386	336	543	114	7	128
12.05	431	79	850	30	423	390	590	89	2	128
13.52	449	87	771	47	447	383	637	44	9	145
15.05	425	52	299	40	440	404	459	80	11	130
18.05	468	64	270	36	478	289	395	85	4	57
19.55	399	64	572	58	511	543	625	103	4	205
21.05	463	79	232	48	401	411	539	91	96	77
22.52	434	72	440	53	438	362	556	102	1	107
24.05	302	58	413	41	488	295	490	104	3	65
25.55	375	59	335	44	458	320	405	39	2	111
27.25	348	61	310	55	480	388	410	67	10	141
28.55	418	73	324	112	475	352	593	69	3	202
30.06	359	80	241	63	460	365	619	58	8	132
31.62	354	63	254	68	473	707	644	70	11	107
32.90	300	72	242	61	448	239	569	93	2	56
32.90	266	75	204	49	435	243	513	75	2	50
34.63	265	68	215	143	457	379	555	45	2	199
36.05	346	62	262	68	502	268	615	47	3	142
37.54	405	64	188	61	437	399	584	49	3	142
39.05	223	60	212	50	498	323	619	53	3	185
40.55	408	59	280	48	506	277	700	53	bdl	174
42.05	165	50	228	87	465	364	400	30	8	143
43.55	279	49	124	73	985	304	485	35	11	90
44.93	312	43	153	69	467	258	446	59	3	92
46.58	118	45	208	68	493	264	456	25	bdl	128
47.94	383	42	214	69	507	328	599	86	bdl	148
49.55	254	43	261	98	535	222	486	46	3	54
50.88	541	41	161	103	462	188	527	66	6	73
52.21	351	40	197	74	492	204	499	102	9	43
54.05	225	51	168	163	478	222	620	61	13	81
55.55	429	55	189	132	496	339	701	74	4	106
57.19	252	55	158	131	532	376	641	70	5	119
58.55	165	53	118	92	520	614	606	57	3	139
60.05	243	54	112	96	516	458	620	55	4	128
61.52	178	22	17	85	542	188	79	19	7	121
62.91	119	60	111	61	515	219	468	71	14	77
66.05	109	37	142	126	467	272	427	84	55	55
67.55	74	35	147	101	526	204	457	50	3	108
67.55	118	44	48	95	490	175	600	51	2	59
69.05	228	45	92	59	501	204	577	71	11	64
70.55	144	44	158	68	491	613	591	75	24	259
72.05	153	48	102	98	463	180	514	69	7	66
72.05	120	32	160	81	464	297	bdl	57	7	95
73.55	108	32	115	110	426	190	bdl	84	6	57
73.55	130	33	37	63	407	143	bdl	51	5	37
75.05	112	33	75	60	400	153	bdl	69	1	49
76.55	99	30	100	79	407	164	bdl	62	bdl	55

[1]Depth below the lakebed

c. Isotopes

Sample depth (m)[1]	δ^2H (‰ VSMOW)[2]	$\delta^{18}O$ (‰ VSMOW)[3]
0.56	–25.13	–3.83
1.60	–17.57	–2.44
3.17	–23.14	–3.24
4.82	–23.31	–2.95
6.05	–21.24	–3.00
7.55	–19.23	–2.37
9.10	–17.43	–2.14
10.55	–13.42	–1.69
12.05	–13.40	–1.68
13.52	–12.48	–1.19
15.05	–11.72	–1.11
18.05	–7.65	–0.67
19.55	–9.49	–0.84
21.05	–7.96	–0.49
22.52	–6.43	–0.42
24.05	–8.38	–0.75
25.55	–6.47	–0.51
27.25	–7.49	–0.53
27.25	–7.13	–0.54
28.55	–7.38	–0.54
30.06	–7.74	–0.56
31.62	–7.14	–0.58
32.90	–7.40	–0.70
32.90	–7.37	–0.71
34.63	–7.50	–0.61
36.05	–7.67	–0.83
37.54	–8.54	–0.85
39.05	–6.75	–0.74
40.55	–6.87	–0.82
42.05	–7.75	–0.97
42.05	–8.32	–0.94
43.55	–8.98	–0.95
43.55	–7.40	–0.81
44.93	–8.89	–0.94
44.93	–8.50	–0.62
46.58	–9.12	–1.09
47.94	–9.57	–1.15
49.55	–9.57	–1.06
50.88	–5.31	–1.26
52.21	–5.75	–1.04
55.55	–8.72	–1.04
57.19	–10.25	–1.18
60.05	–8.54	–1.69
62.91	–12.14	–1.55
62.91	–11.88	–1.52
66.05	–7.38	–1.66
67.55	–13.95	–1.81
67.55	–14.71	–1.77
69.05	–14.39	–2.04
70.55	–16.49	–2.39
72.05	–15.95	–2.17
72.05	–15.65	–2.11
73.55	–15.93	–2.32
73.55	–15.82	–2.28
75.05	–16.15	–2.26
76.55	–16.37	–2.37

[1]Depth below the lakebed
[2]Mean analytical precision was ±1.1 ‰ (1σ)
[3]Mean analytical precision was ±0.17 ‰ (1σ)

6. Archived BMR core crush/leach samples

Sample ID[1]	Latitude (DD)	Longitude (DD)	pH @ 25°C	EC[2] @ 25°C (µS cm^{-1})	Cl^- (mg kg^{-1})	Br^- (mg kg^{-1})	Cl^-/Br^- (mass)	$\delta^{37}Cl$ (‰ SMOC ± 1σ)	$\delta^{81}Br$ (‰ SMOB ± 1σ)
C351-5.7	–35.100	149.413	8.05	18 150	4 441	22.9	194	–	–
C351-10.8	–35.100	149.413	7.91	17 900	4 718	24.3	195	0.07 ± 0.11	–
C351-15.1	–35.100	149.413	7.59	14 050	3 079	16.5	187	–0.30 ± 0.11	–
C351-20.0	–35.100	149.413	8.13	11 950	2 602	12.4	210	–	–
C351-25.0	–35.100	149.413	8.17	6 850	1 528	7.08	216	–0.44 ± 0.09	–
C351-30.0	–35.100	149.413	7.87	13 000	3 079	14.4	214	–	–
C351-35.0	–35.100	149.413	7.58	12 800	2 201	9.33	236	–1.62 ± 0.10	–
C351-40.3	–35.100	149.413	8.01	4 700	1 070	4.93	217	–0.68 ± 0.08	–
C351-45.0	–35.100	149.413	7.85	4 100	940	4.39	214	–1.30 ± 0.08	–
C351-48.5	–35.100	149.413	7.72	3 950	1 026	4.92	208	–	–
C352-5.0	–35.099	149.413	7.94	11 700	2 543	12.8	199	–	–
C352-10.5	–35.099	149.413	7.96	17 500	4 363	22.4	195	0.30 ± 0.10	–
C352-13.0	–35.099	149.413	8.08	17 450	3 319	15.8	210	–	–
C352-15.0	–35.099	149.413	7.71	15 450	2 609	12.3	212	0.03 ± 0.10	–
C352-20.3	–35.099	149.413	7.71	15 100	3 686	18.7	197	–	–
C352-25.0	–35.099	149.413	7.84	10 550	2 835	14.3	198	–0.61 ± 0.08	–
C352-30.0a	–35.099	149.413	7.9	17 700	3 056	15.7	195	–0.06 ± 0.11	0.65 ± 0.07
C352-30.0b	–35.099	149.413	7.99	12 900	3 107	15.2	205	–	–
C352-35.0	–35.099	149.413	7.92	10 300	2 687	13.5	199	–0.85 ± 0.09	–
C352-40.0	–35.099	149.413	7.60	15 850	2 888	12.9	224	–0.92 ± 0.11	–
C352-44.3	–35.099	149.413	7.65	4 600	1 005	4.69	214	–1.12 ± 0.05	–
C352-49.5	–35.099	149.413	7.81	4 500	942	4.41	214	–	–
C353-5.0	–35.097	149.402	7.97	25 700	4 667	22.3	209	–	–
C353-10.0	–35.097	149.402	7.74	25 450	4 633	8.85	524	0.68 ± 0.12	–
C353-15.0	–35.097	149.402	7.77	22 700	3 975	14.3	278	0.28 ± 0.08	–
C353-20.1	–35.097	149.402	7.99	11 025	2 118	9.85	215	–	–
C353-26.3	–35.097	149.402	7.89	9 450	2 333	11.8	197	–0.35 ± 0.07	–
C353-30.8	–35.097	149.402	3.88	21 100	2 884	13.5	213	–	–
C353-35.4	–35.097	149.402	7.53	16 350	2 208	10.5	210	0.39 ± 0.05	–
C353-40.5	–35.097	149.402	8.03	9 890	2 535	12.8	198	–0.35 ± 0.10	–
C353-45.3	–35.097	149.402	7.66	18 350	3 366	16.1	209	–0.63 ± 0.07	–
C353-51.0	–35.097	149.402	7.89	4 810	887	4.28	207	–	–
C354-5.4	–35.095	149.391	7.97	16 300	4 310	20.8	207	–	–
C354-10.5	–35.095	149.391	3.84	30 750	4 719	22.0	214	0.74 ± 0.09	–
C354-13.0	–35.095	149.391	8.00	34 850	8 274	42.3	196	–	1.49 ± 0.06
C354-14.7	–35.095	149.391	3.75	36 250	5 759	26.6	216	0.79 ± 0.08	–
C354-20.7	–35.095	149.391	7.29	14 500	3 720	18.4	202	–	–

Sample ID[1]	Latitude (DD)	Longitude (DD)	pH @ 25°C	EC[2] @ 25°C (µS cm^{-1})	Cl^- (mg kg^{-1})	Br^- (mg kg^{-1})	Cl^-/Br^- (mass)	$\delta^{37}Cl$ (‰ SMOC ± 1σ)	$\delta^{81}Br$ (‰ SMOB ± 1σ)
C354-24.9	–35.095	149.391	7.43	20 000	4 768	22.2	215	0.14 ± 0.09	–
C354-30.0	–35.095	149.391	7.79	15 250	3 713	18.6	200	–0.21 ± 0.14	–0.29 ± 0.03
C354-30.2	–35.095	149.391	3.93	31 750	6 087	28.1	217	–	–
C354-35.3	–35.095	149.391	6.83	10 300	2 651	12.5	211	–	–
C354-41.0	–35.095	149.391	7.62	13 850	3 660	17.6	208	0.16 ± 0.16	–
C354-45.5	–35.095	149.391	7.66	13 400	3 226	15.0	215	–0.16 ± 0.016	–
C354-50.5	–35.095	149.391	6.47	23 050	4 231	19.3	219	–	–
C355-5.0	–35.093	149.380	7.16	19 300	3 106	13.8	225	–	–
C355-10.0	–35.093	149.380	7.33	33 950	6 863	34.6	199	1.12 ± 0.15	–
C355-15.0	–35.093	149.380	6.73	23 300	6 020	31.2	193	0.98 ± 0.09	–
C355-20.0	–35.093	149.380	7.38	34 400	8 797	47.5	185	–	–
C355-26.0	–35.093	149.380	7.44	32 050	7 633	40.5	188	0.77 ± 0.17	–
C355-30.0	–35.093	149.380	3.80	38 800	6 231	28.7	217	–	–
C355-35.0	–35.093	149.380	7.11	15 550	3 783	19.3	196	0.50 ± 0.20	–
C355-40.7	–35.093	149.380	4.27	38 250	8 001	39.2	204	0.65 ± 0.22	–
C355-45.0	–35.093	149.380	6.23	10 100	2 554	13.1	195	0.21 ± 0.15	–
C355-50.0	–35.093	149.380	6.60	9 450	2 382	12.0	199	–	–

[1]Prefix represents the core number; suffix represents the mid-section of the core depth where the samples were collected from
[2]Electrical conductivity

The Treachery of the Long Form

Impossible to encounter a lengthy example of journalism without also conceiving of the tedious hours dedicated to its composition.

The long form represents an attack on leisure, both the reader's and the author's.

–Carson Cistulli, *The New Enthusiast*, 2015